

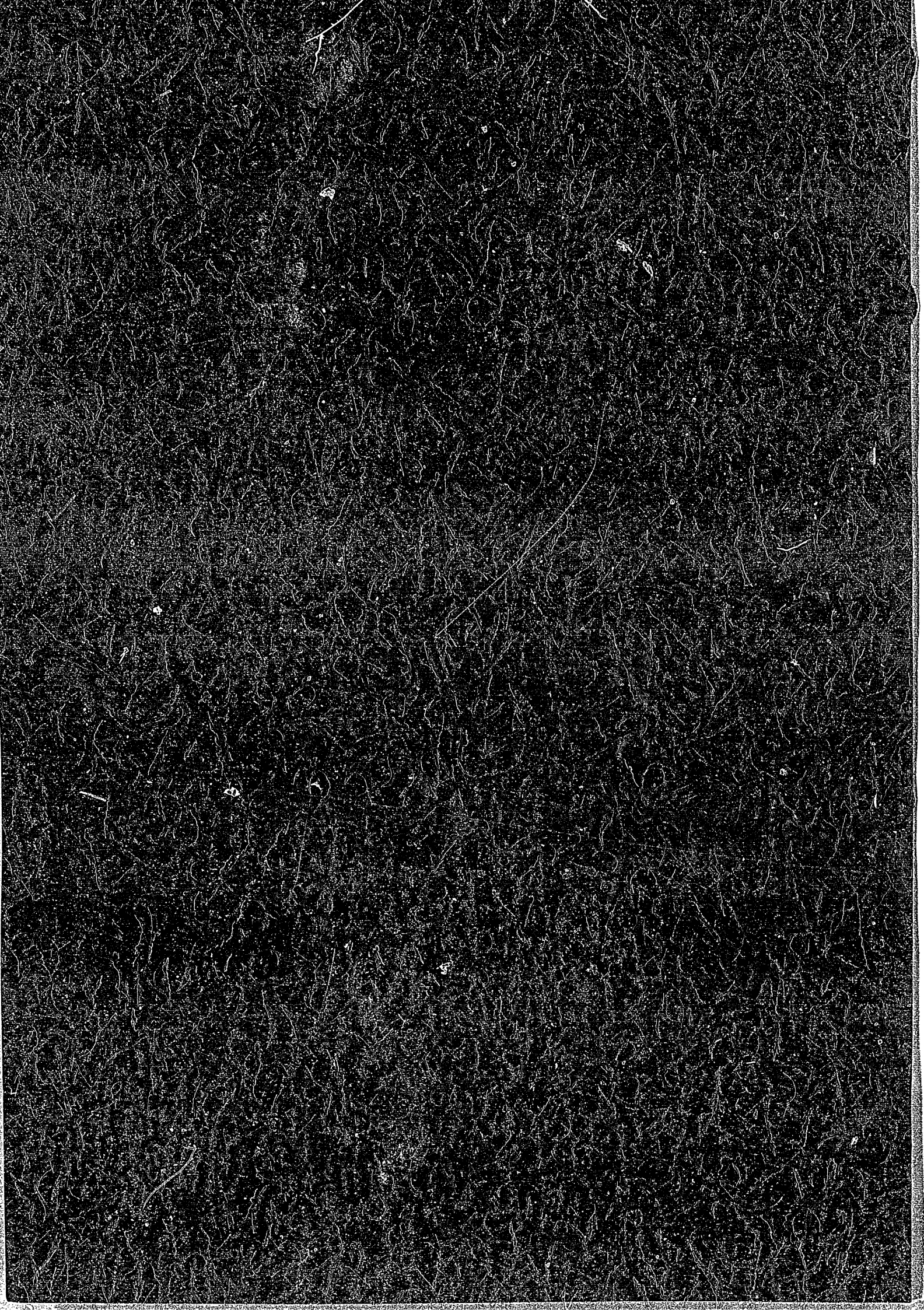
IPPJ-AM-35

PROCEEDINGS OF WORKSHOP
ON
SYNERGISTIC EFFECTS IN SURFACE PHENOMENA
RELATED TO PLASMA-WALL INTERACTIONS

EDITED BY
N. ITOH, K. KAMADA AND H. TAWARA

INSTITUTE OF PLASMA PHYSICS
NAGOYA UNIVERSITY

NAGOYA, JAPAN



PROCEEDINGS
OF
WORKSHOP ON SYNERGISTIC EFFECTS IN SURFACE PHENOMENA
RELATED TO PLASMA-WALL INTERACTIONS
INSTITUTE OF PLASMA PHYSICS
NAGOYA UNIVERSITY
MAY 21 – 23, 1984

Edited by
Noriaki ITOH, Kohji KAMADA and Hiroyuki TAWARA

Institute of Plasma Physics, Nagoya University
Chikusa-ku, Nagoya 464, Japan

October 1984

This document is prepared as a preprint of compilation of atomic data for fusion research sponsored fully or partly by the IPP/Nagoya University. This is intended for future publication in a journal or will be included in a data book after some evaluations or rearrangements of its contents. This document should not be referred without the agreement of the authors. Enquiries about copyright and reproduction should be addressed to Research Information Center, IPP/Nagoya University, Nagoya, Japan.

Foreword

Plasma-wall interaction in fusion machines is considered to be one of the most important topics in nuclear fusion studies. A great deal of experimental and theoretical studies have been carried out to meet data needs and explore phenomena that may cause serious effects in the design of fusion machines. A substantial parts of experimental studies, however, are designed so that they reveal a specific feature of particle-surface interaction under a well-characterized condition. The phenomena that occur in a fusion machine are by no means so simple; Varieties of processes are effective concurrently on the wall. This is the reason why the synergistic effects are to be investigated.

This Workshop, held at Institute of Plasma Physics, Nagoya University, is a satellite meeting of the 6th International Conference on Plasma Surface Interactions in Controlled Fusion Devices held at Nagoya University. The idea of having this satellite meeting, which emphasizes the fundamental surface phenomena related to plasma-surface interaction, was raised by Professor A. Miyahara. The organization of the Workshop has started March 1983. The suggestion of having the word of "synergistic effects" in the title came from the Oak Ridge group. Since the topic of the Workshop is new and not well defined, we decided to invite a few scientists to give review talks and not to call for contributed papers to allow ample time for discussion. We asked the chairmen of sessions a great burden: to guide discussion, to suggest commentators, to give a summary talk and to write a summary paper.

Thanks to the invited speakers, chairmen and all participants, the Workshop was kept to be active and exciting from the beginning to the end. Even without any scheduled contributed papers, all session chairmen had to

cut a certain amount of discussions which ranged from the meaning of the word "synergism" to physics of the surface processes. We thank to all members of the International and Organizing Committees for their helpful suggestions and cooperation. We also acknowledge the support by the Research Information Center, Institute of Plasma Physics, Nagoya University. Financial support was provided by Ministry of Education, Science and Culture.

The proceedings include the invited papers and summary reports. The names of scientists who gave comments may be found in the summary papers. We hope that the proceedings give an overview of the synergistic effects in surface phenomena related to the plasma wall interaction.

August 31, 1984

Noriaki Itoh

Kohji Kamada

Co-Chairmen of the Workshop on
the Synergistic Effects in
Surface Phenomena Related to
Plasma-Wall Interaction.

Contents

R. A. Langley, D. Manos and J. Roth, Synergistic Effects in Fusion Machines – Session Summary	1
R. Behrisch and J. B. Roberto, Plasma Surface Interaction Processes and Possible Synergisms	11
S. Imoto, Synergisms in Hydrogen Recycling – Session Summary	15
B. L. Doyle and D. K. Brice, Steady State Hydrogen Transport in Solids	25
J. Bohdansky and J. Roth, Synergisms in Surface Erosion – Session Summary	74
O. Auciello, A. A. Haasz and P. C. Stangeby, Synergism in Materials Erosion Due to Multispecies Impact	96
W. O. Hofer, Synergistic Effects Related to Surface Composition – Session Summary	176
D. M. Gruen, A. R. Krauss and M. J. Pellin, Effects of Monolayer Coverages on Substrate Sputtering Yields	193
A. R. Krauss, A. B. DeWald, D. M. Gruen and N. Q. Lam, Synergistic Sputtering Properties of Binary Alloys	220
Program	255
List of Participants	256

International Committee

J. Bohdansky (Garching)
P. Deschamps (Fontenay aux
Roses)
B. L. Doyle (Sandia)
D. M. Gruen (Argonne)
W. O. Hofer (Jülich)
G. M. McCracken (Culham)
A. Miyahara (Nagoya)
J. B. Roberto (Oak Ridge)
E. W. Thomas (Georgia)

Organizing Committee

S. Imoto (Osaka)
S. Ishino (Tokyo)
N. Itoh (Nagoya)
K. Kamada (Nagoya)
K. Morita (Nagoya)
S. Morozumi (Sendai)
K. Muraoka (Fukuoka)
M. Okada (Tsukuba)
Y. Obata (Tokai)
R. Shimizu (Osaka)
H. Shimizu (Tsukuba)
H. Tawara (Nagoya)
T. Yamashina (Sapporo)
K. Watanabe (Toyama)

SYNERGISTIC EFFECTS IN FUSION MACHINES - SESSION SUMMARY

R. A. Langley,^{*} D. Manos,⁺ and J. Roth^z

The opening session consisted of a review talk by Dr. R. Behrisch,¹⁾ followed by talks given by Drs. D. Manos²⁾ and J. Roth³⁾. The complete text of Dr. Behrisch's paper is printed elsewhere⁴⁾, and only a short synopsis is given here. The two presentations by Drs. Manos and Roth were the only documented observations of possible synergistic effects in fusion machines in the area of plasma-wall interactions; synopses of both talks are presented.

The session opened with a discussion of the definition of synergism. Dr. Behrisch offered a working definition of synergism as it applies to fusion: "Synergisms refer to phenomena where the combined effect of independent processes is significantly different from the individual effects considered separately." Extensive discussion followed, and a consensus was reached on the following points:

1. Definitions of synergism derived from other fields do not necessarily apply here.
2. Many phenomena that in the past have been considered "synergistic" have been found not to be, once sufficient understanding has been attained. There was a contingent thought that once phenomena are completely understood, there will probably be no synergistic effects.

^{*} Oak Ridge National Laboratory, Oak Ridge, TN 37830, U.S.A. (operated by Martin Marietta Energy Systems, Inc., under contract DE-AC05-84OR21400 with the U.S. Department of Energy).

⁺ Princeton Plasma Physics Laboratory, Princeton, NJ 08544, U.S.A.

^z Max Planck Institute of Plasma Physics, D-8046 Garching/Munich, Federal Republic of Germany.

3. We have the opportunity to define the word through our use of it, and we should be careful in its use.
4. The proposed working definition was sufficient for the present.

Dr. Behrisch's talk reviewed areas in which synergistic effects might be expected to occur and provided an estimated order for each of the effects. Anticipated causal agents are:

- reactive ions,
- temperature,
- radiation damage,
- multiple particle fluxes,
- surface modification and
- external stresses.

The areas included are:

- particle deposition,
- erosion,
- segregation and
- diffusion.

He concluded that (1) the poor correlation between measurements in the plasma boundary and in the first wall of plasma experiments could be greatly improved by considering synergistic effects; (2) surface composition and structure are essential parameters in synergisms; and (3) synergistic effects have been observed in recycling, wall erosion, and melt layer stability.

Evidence for enhanced erosion on a graphite probe cap during rf heating of the Princeton Large Torus (PLT) was presented by Dr. Manos. This presentation reviewed material reported earlier at the 30th National Symposium of the American Vacuum Society. A detailed account is available in the literature⁵⁾.

A probe cap made of graphite was exposed to 460 PLT discharges that were rf-heated. On removal, a number of features were evident, including arc tracks, cracking, discoloration, deposition of metal, and -- most

significantly -- patterned erosion (see Fig. 1). The final feature is the emphasis of this report. The erosion appears as a crescent-shaped beveling of the cap, approximately 1.5 cm^2 in area, along the intersection of the forward face (parallel to the B field) and the cylindrical side wall (perpendicular to the B field), as shown in Fig. 2.

Furthermore, the site of the bevel is elevated approximately 50° to 60° from the direction of the B field. It was determined that approximately 60 mg of carbon was eroded within the crescent-shaped zone.

Thermal calculations, based on the heat flux deposited in the cap and measured by sensing elements contained behind small apertures, indicate that the maximum temperature was low enough that no more than $4 \times 10^{-5} \text{ } \mu\text{g}/\text{cm}^2 \cdot \text{s}$ (a total over the 460 exposures of $<0.03 \mu\text{g}$) could have been removed by evaporation. Spalling is not evident and was not expected⁶⁾ at the low observed power levels.

Sputtering by the thermal plasma, using the known yields of Roth et al.,⁷⁾ could at most account for only 1 mg, approximately a factor of 50 too low. The heat flux during rf heating is known to be dominated by H^+ ions with $E \approx 50\text{-}100 \text{ eV}$ generated by the auxiliary heating. This flux could have been responsible for only 1 μg of removal. These facts suggest that an enhancement of the thermal plasma erosion rate by fast ion bombardment was responsible for the large quantity removed. To test this hypothesis, Manos and his colleagues calculated the orbits of the known distribution of fast ion velocities (v_{\perp} , v_{\parallel} , E) measured independently⁸⁾ (see Fig. 2). The points of impact of these orbits on the probe cap were mapped and compared to the observed pattern of erosion. These were in good agreement, supporting the contention that the erosion is directly related to the fast ion bombardment, although it could not have been caused by direct fast ion sputtering because of the low flux. He emphasized that the location of the damage is quite far removed from the anticipated maximum particle

or energy loading from the thermal plasma.

It was therefore concluded that fast ion enhancement of the erosion of graphite by the thermal plasma, which is well known in laboratory systems^{9,10)}, is likely to have been responsible for these tokamak observations.

Dr. Roth summarized erosion of graphite in the ASDEX divertor and simultaneous deposition of impurities both with and without neutral beam injection (NBI) heating¹¹⁾. Erosion yields for graphite exposed to particle beams are shown in Fig. 3 as a function of temperature. Around 900 K for energetic hydrogen bombardment or around 500 K for thermal atomic hydrogen, a chemical reaction occurs to form CH₄ or CH₃, respectively. The yield due to thermal hydrogen can be enhanced by a factor of 100 due to simultaneous energetic ion bombardment as demonstrated in Fig. 3 with coincident Ar bombardment and can reach values on the order of 5×10^{-3} . Above 1200 K, the erosion yield for energetic ions increases significantly, reaching values a factor of up to 50 higher at 2000 K than at room temperature. This increase in yield is due to radiation-enhanced sublimation of graphite¹⁰⁾.

In Fig. 4 the time dependence of the erosion of graphite strips in the ASDEX divertor is shown, simultaneous with the deposition of impurities for a series of identical deuterium discharges with NBI. The strips were exposed to the divertor plasma in the position of the separatrix perpendicular to the magnetic field lines. The flux of hydrogen ions with $E > 200$ eV is on the order of 2.6×10^{18} cm⁻².s at the separatrix position, while the flux of low-energy hydrogen ions resulting from the 10-eV divertor plasma is about one order of magnitude higher. The erosion and deposition were determined from the shift of a previously implanted ¹³C marker in the graphite strips.

Before and during NBI there is drastic erosion of carbon; in other phases of the discharge, deposition dominates. The erosion during NBI reaches values of $> 2 \times$

10^{17} C atoms/cm²·s. If energetic ions were responsible, the required sputtering should be on the order of 0.1. This is in agreement with the erosion data for most temperatures above 500 K. The surface temperature of the strips, which have low thermal capacity, may exceed 1200 K. If the erosion were due to low-energy hydrogen ions, possibly enhanced by the simultaneously impinging ion flux, then a yield on the order of 10^{-2} would be required. This yield can only be reached in a very narrow temperature interval at 800 K. Thus, it seems probable that the erosion is due to the energetic hydrogen ion flux that results from radiation-enhanced sublimation at temperatures above 1200 K.

It must be noted that the ion fluxes at the divertor plates are a factor of 10 lower due to the grazing angle of incidence of the magnetic field lines; the plates do not reach temperatures greater than 400 K. The erosion observed at the carbon probe is therefore not representative for the divertor plates.

The discussion on synergism demonstrated that the definition is still somewhat nebulous. The two experimental results presented in the session can be considered to demonstrate synergistic effects until a more specific definition is forthcoming and until a more complete understanding of the physical processes is reached.

References

Entries 1 to 3 give speakers and titles of the contributions presented at the session. Most of the non-invited presentations 2 to 3 will be published in the Proceedings of the 6th Int. Conf. on Plasma-Surface Interactions, and appear in the Journal of Nuclear Materials, North-Holland, Amsterdam 1984.

1. R. Behrish "Synergistic Effects in Plasma-Surface Interaction" (invited)
2. D. Manos "Erosion of Graphite Probe in PLT under RF-Heated Discharge"
3. J. Roth "Graphite Erosion Measurement in ASDEX"
4. J. B. Roberto and R. Behrisch, presented at the 6th Conference on Plasma Surface Interactions, Nagoya, Japan, May 1984.
5. D. Manos, T. Bennett, R. Budny, S. Cohen, S. Kilpartrick and J. Timberlake, J. Vac. Sci. Technol., in press
6. G. M. McCracken and P. E. Stott, Nucl. Fusion 19, 889 (1979)
7. J. B. Roberto, J. Bohdansky, W. O. Ottenberger, Max-Planck-Institut fur Plasmaphysik Report IPP-9/26 (1979)
8. D. M. Manos et al., presented at the 6th Conference on Plasma Surface Interactions, Nagoya, Japan, May 1984.
9. E. Vietzke, K. Flaskamp and V. Philipps, J. Nucl. Mater. 111 & 112, 763 (1982)
10. J. Roth, J. Roberto and K. Wilson, J. Nucl. Mater. 123, 1447 (1984)
11. J. B. Roberto, J. Roth, E. Taglauer and O. W. Holland, presented at the 6th Conference on Plasma Surface Interactions, Nagoya, Japan, May 1984.

#83X0943

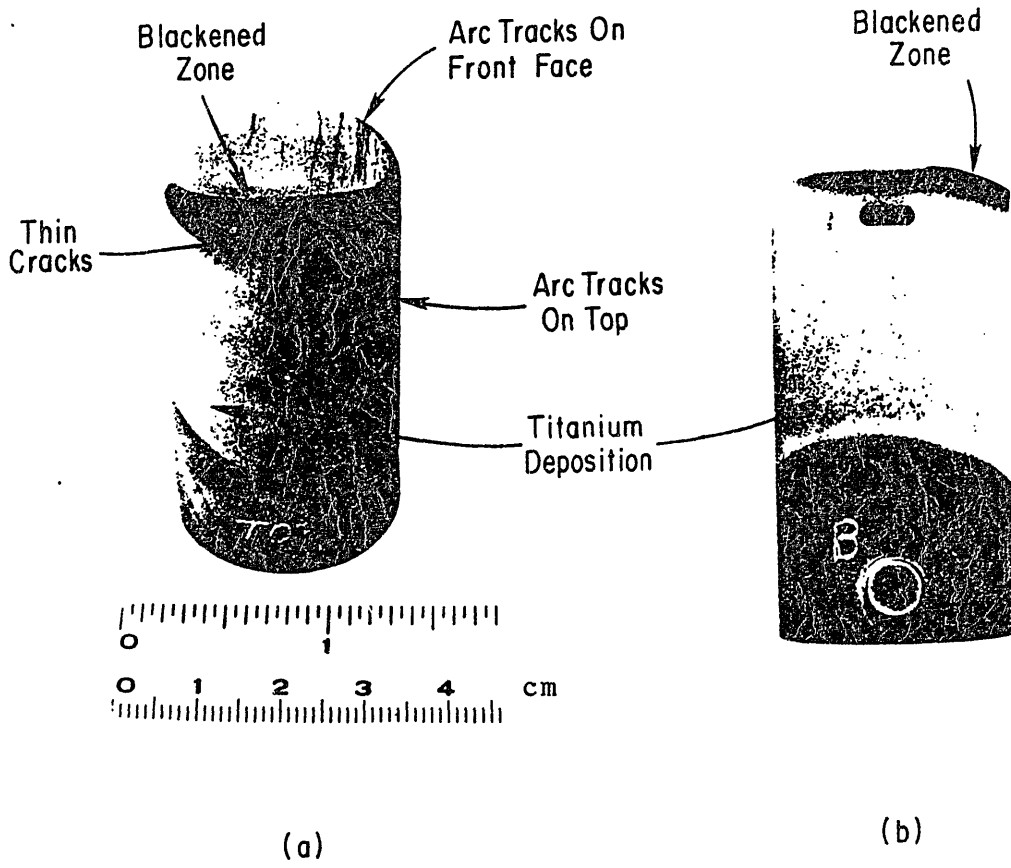


Fig. 1

83X0946

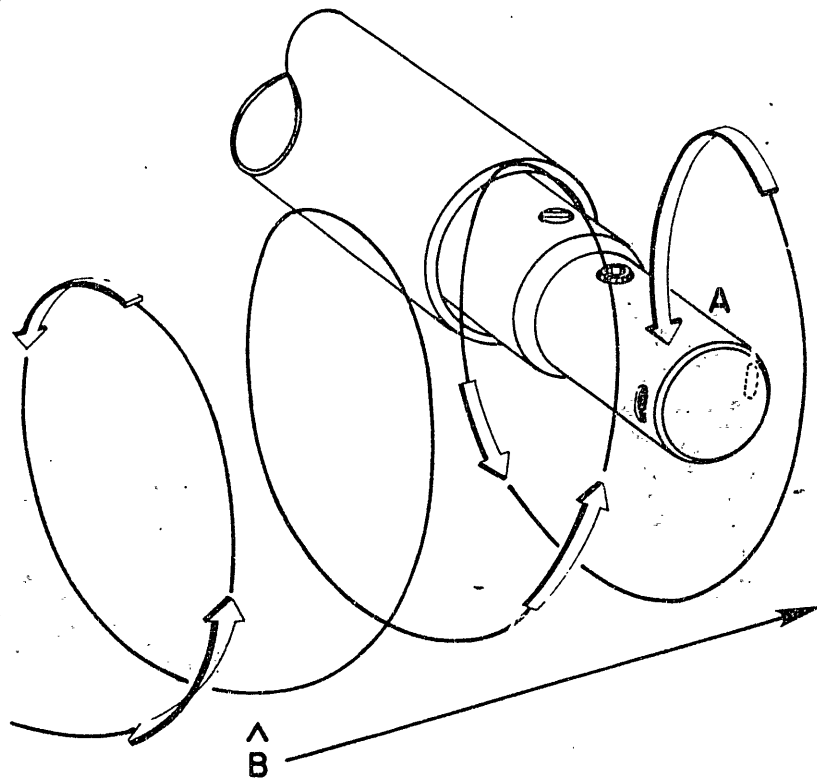


Fig. 2

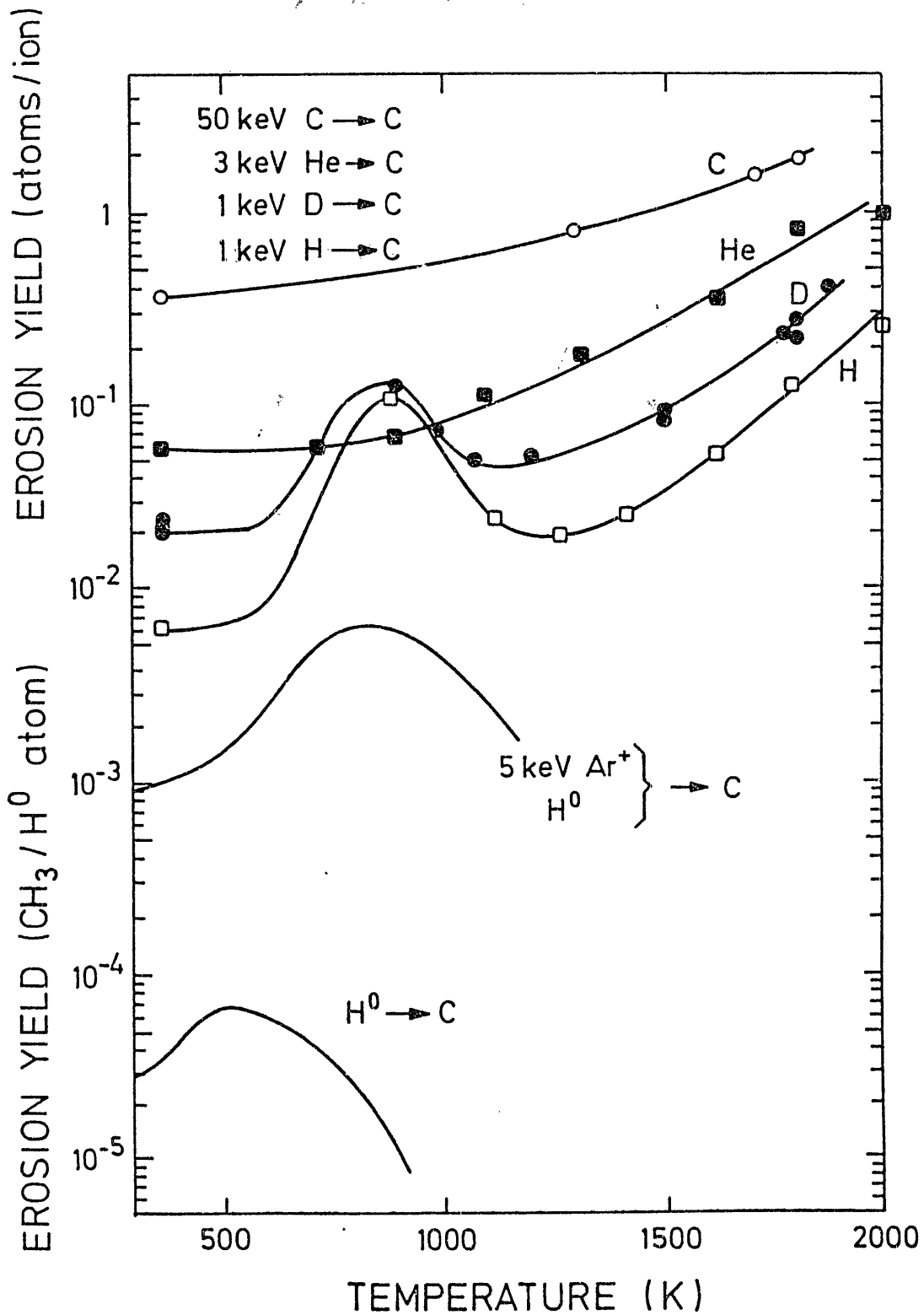


Fig. 3

PLASMA SURFACE INTERACTION PROCESSES AND POSSIBLE SYNERGISMS

Rainer Behrisch
Max Planck Institut für Plasmaphysik
EURATOM-Association
D-8046 Garching/München,
Federal Republic of Germany

and

J. B. Roberto
Solid State Division
Oak Ridge National Laboratory*
Oak Ridge, TN 37831 USA

The processes determining the plasma surface interaction in today's high temperature plasma experiments are investigated following several lines. First, in plasma devices, the particle and energy fluxes to the different first wall areas and the fluxes from the walls back into the plasma are measured and the boundary plasma parameters are determined. The surface composition and structure of the walls, limiters and divertor plates are analysed following exposure to many discharges. Secondly, the different surface processes which are expected to contribute to the plasma surface interaction (particularly to hydrogen particle balance and impurity introduction) are studied in simulation experiments using well defined particle beams.

The results of these different approaches can be combined to give a qualitative picture of plasma wall interaction processes in relatively few areas. In most cases, a consistent description of the plasma wall interaction and its influence on the plasma has not yet been achieved. A two dimensional theory which is necessary for describing the boundary plasma is in an early stage of development. There is only a limited effort toward a quantitative description of recycling and of the total particle balance. It is not clear whether there

*Operated by Martin Marietta Energy Systems, Inc. under contract DE-AC05-84OR21400 with the U.S. Department of Energy.

will be major sources for impurities other than sputtering. The criteria for the selection of wall materials are not yet established. For example, carbon appears to work best in plasma experiments, but shows relatively high erosion in ion bombardment simulation studies.

A major concern in using surface data measured from well defined ion beam experiments to explain wall phenomena in fusion devices is related to the quality of the simulation. In plasma experiments, the walls are bombarded by a large variety of particles having a broad distribution in energy and in angle of incidence. The effects of these different bombarding species do not always add linearly.

Problems of nonlinear additivity of different actions have been discussed for ages in theology, philosophy, and medicine. They are given the name synergism from the greek word syn - ergos which means cooperation.¹ This word has also been adopted in fusion research to describe wall phenomena where the combined effect of independent processes is significantly different from the individual effects considered separately.^{2,3}

Synergistic effects are expected to influence surface processes in several areas,³ however, their contribution to surface effects in plasma experiments has not yet been explored in any detail. Generally all effects connected with the thermal motion of the atoms of a solid such as diffusion in the bulk or at the surface, evaporation and sublimation, and chemical reactions may be increased or decreased due to simultaneous bombardment with energetic particles. During bombardment at high temperature, free interstitials and vacancies are produced generally increasing the diffusion. Implanted gas atoms (H, D, T, He) and impurities (O, C metals) change the surface layer composition. There are further synergisms due to bombardment with ions of different energies and/or

different atoms, and due to the simultaneous additional application of stresses and magnetic fields.

Synergisms have been identified in a variety of plasma surface interaction phenomena including hydrogen particle balance, impurity release, and mechanical and electromagnetic stresses. In particle balance, synergistic effects occur during simultaneous hydrogen bombardment and bombardment with other damage producing ions such as He or impurity ions. Here additional trapping centers are created which influence trapping, saturation concentrations, diffusion and surface recombination.

In impurity release, chemical or reactive sputtering has been found due to the formation of volatile hydrocarbons during implantation of carbon with hydrogen atoms at high temperatures. Similar effects are found for oxygen bombardment of carbon or some metals where the oxide sublimates at temperatures lower than the bulk material. Large chemical erosion has also been observed due to simultaneous exposure of a graphite surface to atomic hydrogen and a damaging ion flux. In addition, graphite shows an enhanced sublimation at temperatures $>1000^{\circ}\text{C}$ if it is simultaneously bombarded by energetic particles. On the other hand, chemical erosion of carbon with hydrogen atoms is considerably reduced by simultaneous deposition of metal atoms.

Finally mechanical stresses influence the surface topography and surface cracking due to ion bombardment. Melted surface layers can be destabilized by magnetic fields. Synergistic processes in plasma surface interactions have been reviewed in Ref. 3 and will be discussed in more detail in the contributions to this workshop.

REFERENCES

1. Webster's 3rd New International Dictionary, (G. C. Merriam Co., Springfield, Massachusetts, 1976).
2. Fusion Reactor Materials Program Plan, Section III - Plasma Material Interaction, DOE/ET-0032/3 (July 1978).
3. J. Roberto, R. Behrisch, Proc. VI Int. Conf. on Plasma Surface Interactions in Controlled Fusion Devices (Nagoya, Japan, May 14-18, 1984) to be published in J. Nucl. Mat. In this review detailed references are given.

Synergisms in Hydrogen Recycling - Session Summary

S.Imoto

Department of Nuclear Engineering, Osaka University
Suita 565, Japan

Under the session title "Synergisms on Hydrogen Recycling", we had two review talks and five comments.

In the first review talk, Doyle and Brice proposed an analytical formalism for evaluating the steady state plasma-driven hydrogen transport. The formalism included hydrogen trapping, recombination barriers to release at inner and outer surfaces, diffusion and the effect of thermal gradient. The starting equations used in this recycle model was essentially the same as that used in the DIFFUSE code, but the exponent of the concentration appearing in the recombination term was generalized to be a variant, r , instead of 2 in the earlier formalism. With some approximations, they deduced analytical simple equations which express the permeation flux, inventory and recycle time, and the results of calculation were found to agree quite well with the results of DIFFUSE code.

They classified the steady state hydrogen transport into nine regimes. The transport parameter, W , defines the mode of rate-determination into three regimes: diffusion controlled both sides, recombination controlled plasma side diffusion controlled back side, and recombination controlled both sides. The

trapping behavior is mainly controlled by the trap activation energy, and three regimes, that is, no trapping, trapping, and saturation are defined. Thus, by a combination of transport parameter and trapping behavior, nine regimes are obtained. For some of the regimes, the characteristic behavior was also mentioned: for example, the DD-saturation regime is well described by the Local Mixing Model.

The next application of the formalism is the calculation of tritium inventory and permeation for the machine of INTOR class, and the 16 metals including 304 stainless steels, Inconel and carbon were surveyed for permeation flux, tritium inventory and recycle time. The application to the nonisothermal permeation was also made by taking the effect of thermal gradient in bulk into account. They showed that, if the heat of transport, Q^* , has a negative value, such as seen in iron, the Soret effect helps in reducing tritium permeation through a wall. This finding was again raised in the last comment by Sugisaki.

In Fig.1 which was prepared by Doyle are beautifully displayed the synergistic effects of radiation enhanced diffusion, radiation damage, wall heating and surface changes on plasma-driven-permeation. Permeation flux (J), concentration of mobile hydrogen (C), concentration of trapped hydrogen (C_T), recycle time (T) and the time required to reach steady state (T_S) are given in very simple equations and the trend of increase or decrease in these parameters by a synergistic cause is shown by the arrow upward and downward, respectively. The estimation of whether the effect is favorite to machine operation or not is

also indicated in the figure.

I think the analytical formalism will largely contribute to the future progress in hydrogen recycling, because it not only provides physical insight into the recycling processes as shown in Fig.1, but also gives easier means to incorporate the plasma-surface interaction into a total hydrogen recycling model which treats both wall and plasma.

The second review talk was made by Waelbroeck. The talk started with the definition of synergism by Roberto and Behrish: "Synergisms refer to phenomena where the combined effect of different processes is significantly different from the individual effects taken separately".

I would like to trace the logic by Waelbroeck. First he compares the simplified recycle model with laboratory or machine experiments; if the model describes well the recycle behavior of wall materials, the synergisms play a minor role, and the behavior is called "normal". The normal behavior is seen in the case where the surfaces have carefully been conditioned and when the energy of the impinging hydrogen is low. But when there is a deviation from the normal behavior, it is attributed to the synergism. He proposes that, in cases where synergisms operate, the recycle equations should be completed by including new additional terms, not basically modified.

Then he throws a question: what will be the possible synergisms in tokamaks? There are many causes for the synergisms: adsorbed hydrogens, photons, electrons, energetic ions, neutrons, impurity fluxes, power flux to the wall and so

on. On these sources of synergistic effects Waelbroeck has made a comprehensive review, where each of sources was considered to much or less have a synergistic effect upon the hydrogen recycling. The synergistic effect is sometimes very complex; for example, the recombination coefficient k_p may be increased or decreased according to the kind of contaminant. Energetic ions have synergistic effects in several ways: by formation of H-induced traps, by hydrogen-induced desorption, by enhancement of diffusivity, by surface change that increases k_p . As seen in Figure 1 by Doyle, these processes totally induce an intricate effect on the recycling behavior of a wall material. Isotopic composition of plasma is also expected to be a cause of synergistic effect, and this problem was raised to an important discussion point by Behrish.

The conclusion of Waelbroeck is that synergisms probably exist in hydrogen recycling on the metal walls and they will modify the recycle factor and affect the density evolution of confined plasmas, and he put an emphasis on "the need of careful measurements of synergisms on well characterized, dirty surfaces of which conditioning should simulate that of tokamak walls". Thus his talk is very much suggestive in what an experiment we should perform and how we should develop a recycle model in order to realize the synergisms in hydrogen recycling.

In the first comment Yamawaki and Namba have proposed a new analytical model for hydrogen permeation which takes effects of surface oxide into account. Principal difference from previous models is that they have introduced explicit expressions for the

migration of atoms from the first layer to the second layer, the surface coverage of contaminant and the roughness factor into their model. They showed that the steady-state permeation was not affected by roughness factor and coverage at the front surface but by those at the back surface. On the otherhand, the transient response was controlled by the factors at the front surface. From the experimental results on transient response of vanadium metal, they showed that the gas driven hydrogen permeation through vanadium was dominantly rate-determined by surface adsorption-desorption process. This model appears to be particularly useful to treat the case where a rather thick film or coating covers the substitute, and the permeation data with a V/VO_2 couple obtained by their own study has been analyzed by this model.

In their model, and also in that by Doyle, the synergistic effects are not explicitly introduced in a manner suggested by Waelbroeck, but can be treated by making some parameters as variable. For example, in Yamawaki's model the "effective adsorbability", $\sigma(1-\theta)$, is treated as an important parameter to describe the surface character which should be modified by sputter cleaning. If the trap density which was assumed constant and uniform through the bulk during the plasma driven permeation is taken to be a variable, as suggested in Fig.1, the recycle equation would give solutions to more relevantly explain some synergistic effect due to radiation damage. These models are considered to possess such a flexibility as to adapt most of synergisms.

Tanabe, the second commentator, considers that the diffusion constant of hydrogen in bulk and that at near-surface should be treated as independent variables in the plasma-driven permeation. Previously he proposed an enhanced-diffusion model for the explanation of permeation spike appearing in the plasma-driven permeation, and in the present comment he concentrates his talk on experimental facts, in which the hydrogen diffusivity is changed by neutron irradiation, cold work and ion implantation. Some defects introduced by these treatments would decrease the diffusivity by acting as traps, but the tangled loops may overwhelmingly enhance the diffusivity, and Tanabe emphasizes the possibility of enhanced diffusion at near surface from his observations of microstructure of hydrogen implanted specimens.

The comment by Haasz is concerned with synergistic effects on near-surface hydrogen retention. He measured the trapping fluence of hydrogen or deuterium on pyrolytic graphite as well as single crystal graphite, each having different roughness. For the single crystal graphite the impurity coverage was also changed. The retention was found to be largely affected by the roughness and impurity coverage.

His most recent result on hydrogen retention at mixed particle immersing of carbon presented that there is no significant difference in hydrogen retention between the case of H^+ alone and the case of mixed particles of H^+ and neutral atoms. This makes a marked contrast to the methane formation: there is a very strong synergism in the methane formation when neutral atoms and ions together bombard the carbon. The detailed

comparison will be a key to solve the synergism.

Vernickel has made a comment on the influence of plasma-induced heating on hydrogen re-emission from graphite target. He evaluated the excess-reemission to be the order of 10^{-2} or less in the case of ASDEX upgrade. In this evaluation the fundamental data on hydrogen trapping in graphite obtained by Brice, Doyle, Wampler and others were most effectively utilized to solve a machine engineering problem. This is an excellent example for the application of fundamental data to engineering, and such a work should be encouraged to be continued. Based on his own data Vernickel also discussed the problem whether hot hydrogens push the trapped atoms into depth, induce thermal desorption or are reflected.

The last comment in the Monday afternoon was made by Sugisaki. He measured the thermomigration of tritium and in some cases other hydrogen isotopes in Nb, Ta, and Ti metals. He has found that hydrogen is driven down the thermal gradient in these metals and he determined the heat of transport from the experimental data. The conclusion is the same as deduced from the calculation by Doyle, but Sugisaki calls a special attention to the isotopic effect on thermomigration. In the case of Nb, the heat of transport for tritium is about twice that for protium above 500°C , and as a result the tritium permeation is much enhanced: the permeation with thermal gradient is about twice that without thermal gradient. Thus the thermomigration seems to have a large synergistic effect on hydrogen permeation, but the mathematical treatment of thermomigration in the frame of

diffusion equation is quite clear as realized from the complete agreement between the theory by Doyle and the experiment by Sugisaki. The problem still left to be solved is to elucidate the nature of the heat of transport for hydrogen isotopes in metals and alloys. From this point of view, the thermal gradient would be no more a synergism. The behavior of thermomigration is "normal" in the sense of Waelbroeck, because it is well described by the model.

As a conclusion I would like to cite an opinion presented at the summary discussion by Baskes, which, I wish, would keep stimulating the discussion, "What is a synergism in hydrogen recycling?", until the next workshop at the 7th Int. Conf. PSI. "If two supposedly independent processes produce the same effect, the simultaneous action of these processes should produce an effect equal to the sum of the individual processes acting alone. If the effect is not such a linear superposition, it is called a synergistic effect. In reality the synergistic effect occurs because the processes are not independent. Once we understand the dependence of the processes the synergism goes away, hence there are really no synergistic effects, only a lack of understanding of the underlying physics".

References

Entries 1 to 7 give speakers and titles of the contributions presented at the session. Most of the non-invited presentations 3 to 7 will be published in the Proceedings of the 6th Int. Conf. on Plasma Surface Interactions, to appear in the Journal of Nuclear Materials, North Holland, Amsterdam 1984.

1. B. L. Doyle/ Theory of Steady State Hydrogen Transport in Solids (invited)
2. F. Waelbroeck/ Synergisms Involving Hydrogen Recycling (invited)
3. M. Yamawaki/ Surface Effects on Hydrogen Permeation
4. T. Tanabe/ Hydrogen-Ion driven Permeation at High Temperatures.
5. A. A. Haasz/ Ion-Induced Synergistic Effects for CH₄ Production from Carbon under H⁺, H⁰ and e⁻ Impact
6. H. Vernickel/ On the Influence of Plasma-Induced Heating on the Re-Emission of Hydrogen from Graphite Targets
7. M. Sugisaki/ Thermomigration of Tritium in Nb, Ta and Ti Metals.

- ⊙ PERMEATION
- ⊙ INVENTORY MOBILE TRAPPED
- ⊙ TIMES RECYCLE
- STEADY STATE

$$J = \alpha\phi(1+1/W)$$

$$C = (\phi/K)^{1/2} (1+W)$$

$$C_T \propto N_T C$$

$$T = (R^2/D) (1+1/W^2)$$

$$T_{SS} = x_0^2 / (6D_{EFF})$$

$$W = R (\phi/K)^{1/2} / D$$

SYN: EFFECT	PLASMA-DRIVEN PERM. (PDP) + RAD. ENH. DIFF. D↑		PDP + RAD. DAMAGE N _T ↑		PDP + WALL HEATING T↑ (dT/dx↑)		PDP + SURFACE CHANGES K↑ K↓	
	W<1	W>1	W<1	W>1	W<1	W>1	W<1	
J	↑ B	→ N	→ N	→ N	B↑(↓)G	N→(↓)G	↓ G	↑ B
C	→ N	↓ G	→ N	→ N	G↓(↓)G	↓ G	↓ G	↑ B
C _T	→ N	↓ G	↑ B	↑ B	G↓(→)N	↓ G	↓ G	↑ B
T	↑ N	↓ N	→ N	→ N	↑↓ N	↓ N	↓ N	↑ N
T _{SS}	↓ B	↓ B	↑ G	↑ G	↓ B	↓ B	→ N	→ N

G : GOOD N : NEUTRAL B : BAD

Fig.1 Synergisms in plasma-driven-permeation (presented by Doyle)

STEADY STATE HYDROGEN TRANSPORT IN SOLIDS*

B. L. Doyle and D. K. Brice
Sandia National Laboratories, Albuquerque, NM 87185

The analytical formalism for evaluating the steady state hydrogen (tritium) inventory, recycle and permeation rate and recycle time for surfaces exposed to the plasma of an operating magnetic confinement fusion reactor is reviewed and new material relevant to the application of this theory is presented. The formalism includes hydrogen trapping, diffusion, and effects of thermal gradients (e.g., Ludwig-Soret effect), and is applicable for all orders of release kinetics at the inner and outer surfaces. The problem is formulated in terms of a unitless transport parameter, $W = (R\phi/D)(k_1/\phi)^{1/r}$ where r is the order of the release kinetics, R is the range of the implant, ϕ is the penetrating part of the incident flux, k_1 is the recombination coefficient and D is the diffusion coefficient. The steady state analytical theory is applied to several materials of interest to controlled fusion.

*This work performed at Sandia National Laboratories supported by the U.S. Department of Energy under contract #DE-AC04-76DP00789.

I. INTRODUCTION

Hydrogen isotope concerns in magnetic confinement fusion devices are becoming increasingly important as the era of D-T plasma device approaches. For the current generation of such fusion reactors (e.g., TFTR and JET) most of the H-(i.e., tritium) related worries are centered around low to moderate level inventories which build up in all in-vessel components, and H permeation is not expected to be significant. In the next, and certainly in the following, generation of reactors very high levels of tritium could be present either in a trapped or mobile form in walls and other internal parts. Thus tritium permeation through even thick wall materials may present problems.

Recycling of H at the walls of reactors has been and will continue to be a controlling factor in areas such as the time dependence of plasma density and the maintenance of a proper fuel balance. This latter aspect is critical in a two-component tokamak such as TFTR because the isotope exchange process which occurs during the H recycling step can upset the purity of the initially pure tritium discharge. For an ignition device, isotope exchange may cause problems at first, but not after equilibrium is reached.

Other new H-related concerns stimulated by the advent of D-T reactors result from fusion neutrons. These concerns include effects of n-damage on H transport and buildup in addition to synergisms which could exist between the n-flux (or neutron effects on materials and other H-related concerns such as permeation.

Computer simulations of the plasma wall interaction have been extremely valuable in assessing many of the key problem areas listed above. These codes include DIFFUSE^{1,2}, PERI³, TCODE⁴, and PIDAT.⁵ Codes such as these are the only way that exact time dependent solutions can be determined for the case of plasma-driven injection into a non-isothermal material which contains H traps.

For certain cases, however, much progress has been made in the derivation of analytical theories which can describe in general the H transport in materials at steady state⁶⁻¹³ and, under special conditions, various quantities such as recycle flux as a function of time.¹⁴⁻¹⁶ These analytical approaches, although approximations, have a few clear advantages over the rigorous numerical theories. First, they are easy and quick to use and can therefore provide guidance in selecting parameters for the exact calculations. Secondly, and perhaps most importantly, the analytical nature of these theories allows an analysis of the functional dependences and interrelationships which exist between the various plasma and material parameters. This second benefit leads to new physical insight into the complex plasma-surface interaction.

In this paper we review our analytic steady state hydrogen transport theory and its applications.¹¹⁻¹³ This transport formalism is here generalized to be applicable for any order of kinetics of the release reaction. The earlier three-part series of papers was applicable only for the case of second order release. In addition, expressions are developed which describe the plasma-side sub-surface concentration as a function of time and can be

used to calculate the time dependence of in-vessel pressure variations.

Before proceeding with the theory it is useful to examine how H transport in the wall fits into the general picture of the plasma surface interaction (PSI). In Fig. 1 a flow diagram is shown which illustrates the PSI aspect of a comprehensive plasma transport code by Howe¹⁷. This code models kinetic reflection, thermal diffusion and beam-induced detrapping at the wall surfaces. A step-by-step description of this model follows where the step numbers (given below in []) correspond to those shown in Fig. 1.

In Howe's model, hot H ions [1] diffusing across magnetic field lines eventually strike a limiter [2] and are all neutralized and reinjected into the plasma with approximately 5 eV energy. Upon reentering the plasma some of the H atoms are ionized [3] while others undergo Franck-Condon (FC) collisions or charge exchange (CX) [4] with hot H ions in the plasma, giving rise to fluxes of both hot (for CX 100's of eVs) and cool (for FC 10's of eVs) H atoms [5] which strike the wall. It should be noted at this point that this flux will be highly asymmetric (both poloidally and toroidally) with the maximum being near the limiters. Some of the incident H atoms are reflected [6] from the surface back into the plasma while the remainder penetrate [7] into the material of the wall. Of those H atoms which enter the first wall, some may become trapped at their end of range [8] in damage either resident in the material or produced by the particle irradiation. This trapping process may also result in the detrapping [9] of H isotopes

already present in the wall. This detrapped H, along with any H which was not trapped, diffuses and [10] eventually permeates either to the back surface [11], or the front surface [12], or becomes trapped in the bulk [13]. Upon reaching either surface the H can recombine with another H atom and be released as an H₂ molecule to re-enter the plasma [14] or the environment exterior to the first wall [15].

Figure 1 can be used qualitatively to provide insight on how material variables related to H affect important tokamak parameters. Consider H recycling for the case where the wall traps, or otherwise retards, only .1% of the CX or FC neutral flux. In typical large tokamaks the confinement time is around 100 ms, whereas the pulses endure approximately a second. As a result, each H atom in the plasma strikes the wall on the order of 10 times during each discharge. The probability that a H gets trapped in the wall during the discharge is $1 - .99^{10} = 10\%$, whereas for a .2% trapping coefficient this figure becomes 18%. This example illustrates how sensitive the "wall confinement" is on H trapping or holdup. Howe¹⁷ has shown that neutral beam-induced density clamping^{17,18} is the result of a small decrease in the wall recycle coefficient caused by the increased edge plasma energy during neutral beam injection.

Another effect illustrated in Fig. 1 is isotope exchange. If implantation trapping [8] is appreciable, and the tokamak has been operated for a long period of time with just one H isotope, say protium, then the near-surface of the wall saturates with H. Upon changing the working gas to deuterium (D), during the first stages of the D discharge the detrapping [9] which occurs in the wall

will be for H, which, as can be seen from the figure, can diffuse [10] to the surface and enter [14] the plasma. Thus the wall initially recycles H, not D, thereby upsetting the isotopic purity of the plasma.

The three primary H-material concerns in the PSI are also graphically displayed in Fig. 1, namely: 1) plasma wall recycle effects on the plasma itself; 2) H buildup in the wall leading to potential embrittlement and/or high H isotope inventories, and 3) the possibility that H isotopes can permeate the wall and enter the region outside the wall which, for future machines, will probably be a cooling system. Because of its importance, the PSI has been the subject of several recent reviews¹⁹ to which the reader is referred for further details.

II. THEORY

In what follows we have expanded the transport parameter formalism given in Ref. 11 to apply for all orders of the surface recombination process. The extended formalism still includes a general definition for the transport parameter, W , the "effective" ratio of implant depth to wall thickness, α , and the "effective" ratio of inner and outer surface recombination coefficients, γ . The general formalism also includes the effects of thermal gradients in the first wall material. Specifically thermomigration (Ludwig-Soret effect)²⁰ as well as the temperature dependence of the diffusivities and recombination coefficients are considered. This new formalism also allows for H trapping and the diffusion of H in the presence of traps.

The general equations governing the evolution of the system in time, t , and depth, x , are

$$\frac{\partial C(x, t)}{\partial t} = - \frac{\partial J(x, t)}{\partial x} + G(x, t) - \frac{\partial C_T(x, t)}{\partial t}, \quad (1a)$$

and

$$\frac{\partial C_T}{\partial t} = 4\pi R_T D \left\{ C(N_T - C_T) - \mu N_S C_T e^{-E_B/k_B T} \right\}. \quad (1b)$$

Figure 2 shows a schematic of the wall membrane and associated H-related quantities. In Eq. (1a) C is the atomic density of freely diffusing hydrogen, J is the local diffusive flux of this component of the hydrogen, $G(x, t)$ is the local rate of hydrogen implantation from the plasma, and C_T is the atomic density of trapped hydrogen. In Eq. (1b) R_T is the hydrogen trap radius, N_T is the trap density, N_S is the density of hydrogen solution sites, and D is the hydrogen diffusivity. The trap strength, E_B

is assumed constant in Eq. (1b) and the temperature, T , will in general be a function of both x and t . Note that E_B , as used here, is the energy difference between trap and solution sites. The Boltzmann constant is given by k_B . The parameter μ is a constant of order 1 which is required in order that local thermodynamic equilibrium between trapped and mobile hydrogen be reached in the steady state condition. Additional dependence on the temperature, beyond that explicitly indicated in Eq. (1b), is contained in the quantities D and J . The diffusivity, D , is given by an Arrhenius function

$$D = D_0 e^{-E_D/k_B T} , \quad (2)$$

where D_0 is a constant, and E_D is the activation energy for hydrogen diffusion.

Similarly,

$$J = -D \left\{ \frac{\partial C}{\partial x} + \frac{C Q^*}{k_B T^2} \frac{\partial T}{\partial x} \right\} \quad (3)$$

where the second term on the right is due to the Ludwig-Soret effect (diffusion driven by a thermal gradient),²⁰ with Q^* being the heat of transport associated with the effect. Experimental measurement of Q^* indicates that this quantity has a weak linear dependence on temperature, but this dependence will not be considered here.

A. Steady State Solutions

1. General

The steady state solutions to the above set of equations, i.e., solutions at large t when all the functions and parameters have become independent of t , are found by solving

$$\frac{dJ}{dx} = G(x) \quad , \quad (4a)$$

and

$$C(N_T - C_T) - \mu N_S C_T e^{-E_B/k_B T} = 0 \quad . \quad (4b) \quad (5b)$$

The solution of Eq. (4a) yields the steady state concentration of freely diffusing hydrogen, $C(x)$, and the (algebraic) solution of Eq. (4b) yields the steady state trapped hydrogen concentration, C_T , as a function of C . In order to solve Eq. (4a) we take $x = 0$ at the first wall-plasma interface, and assume that the first wall has a thickness of x_0 . The boundary conditions for the solution are

$$J_1 = -k_1 C_1^r \quad , \quad (5a)$$

and

$$J_2 = k_2 C_2^r \quad , \quad (5b)$$

where J_1 and J_2 are the diffusive hydrogen fluxes through the inner first wall surface and outer first wall surface, respectively. Likewise, k_1 is the hydrogen recombination coefficient at the inner first wall surface, C_1 is the freely diffusing hydrogen concentration just below the inner first wall surface, while k_2 and C_2 are similarly defined for the outer first wall surface. The power r is the kinetic order of the release reaction (i.e., $r = 2$ is for the quadratic kinetics usually assumed for H).

The implantation source function, $G(x)$ is given by

$$G(x) = \phi P(x) \quad , \quad (6)$$

where $P(x)$ is the normalized hydrogen implantation profile and ϕ is the penetrating hydrogen flux from the plasma. We note that if ϕ' is the incident hydrogen flux on the inner first wall surface,

then $\phi = \phi' (1 - R_e)$, where R_e is the reflection coefficient for hydrogen incident from the plasma.

Finally, conservation of hydrogen within the first wall requires that

$$\phi = |J_1| + |J_2| = k_1 C_1^r + k_2 C_2^r . \quad (7)$$

A first integration of Eq (4a) now yields

$$J(x) - J_1 = \int_0^x G(x') dx' , \quad (8)$$

or, using Eq. (3), and rearranging terms

$$\frac{dC}{dx} + C(x) \frac{Q^*}{k_B} \frac{1}{T^2} \frac{dT}{dx} = - \frac{J_1}{D} - \frac{1}{D} \int_0^x G(x') dx' . \quad (9)$$

A formal integration of Eq. (9) is easily carried out by defining the function $g(x)$ as

$$g(x) = (Q^*/k_B) \int_0^x \frac{dx}{T^2} \frac{dT}{dx} = (Q^*/k_B) (1/T_1 - 1/T(x)) , \quad (10)$$

where T_1 is the temperature at the inner first wall surface, resulting in the following expression for $C(x)$

$$C(x) = e^{-g(x)} \left\{ C_1 - J_1 \int_0^x \frac{e^{g(x')}}{D(x')} dx' - \int_0^x \frac{e^{g(x')}}{D(x')} \int_0^{x'} G(x'') dx'' \right\} . \quad (11)$$

Once the mobile H concentration, $C(x)$, is determined from Eq. (11), the trapped H concentration profile can be calculated through Eq. (4b).

2. Approximations

One of the most important results in Ref. 11 was that the recycling, permeation, and both trapped and mobile total inventories may be evaluated using an H implantation source term which is a delta function positioned at the first moment of the actual distribution (i.e., at the range R)

$$G(x) = \phi \delta(x-R) \quad . \quad (12)$$

After inserting this expression into Eq. (9) and performing the integral, we find for $x < R$

$$C(x) = C_1 + k_1 C_1^R x/D_1 \quad (13)$$

where $D_1 = D(x=0) = D(T_1)$. Due to the smallness of R , the diffusion coefficient D is assumed to be constant in depth for this part of the integral. For $x > R$ we find

$$C(x) = e^{-g(x)} \left\{ C_1 + k_1 C_1^R R/D_1 - k_2 C_2^R \int_R^x e^{g(x')} dx' / D(x') \right\} \quad . \quad (14) \quad (41b)$$

These equations are obviously valid only when $R \ll x_0$ or for the special case where $g(x')$ and $D(x')$ are constants.

To apply these equations to a specific case, one needs to know (as functions of temperature) all the material-dependent parameters which enter the various expressions. In addition, one needs to know the temperature profile $T(x)$, which depends not only on the thermal properties of the wall material but also on the manner in which energy is deposited into the wall and the manner in which the wall is cooled. In general, $T(x)$ will be a complex function of the operating characteristics and design of a particular machine. Often, however, solutions of some limited accuracy are quite useful if these less accurate solutions mimic the exact solutions in their dependence on the various parameter involved, since insight can be gained into the effects of parameter changes on the solutions.

Our procedure for obtaining the approximate expressions will be to replace exponential functions of the inverse temperature by exponentials of linear functions of x . Thus, for example we write

$$\frac{E_D}{k_B T(x)} = \frac{E_D}{k_B T_1} + \frac{x}{x_D} \quad (15)$$

and we choose x_D such that

$$\frac{E_D}{k_B T_2} = \frac{E_D}{k_B T_1} + \frac{x_0}{x_D} \quad (16)$$

which yields

$$x_D = x_0 \frac{k_B}{E_D} \frac{T_1 T_2}{(T_1 - T_2)} = x_0 \frac{k_B T_0}{E_D} \quad (17)$$

where

$$T_0 = T_1 T_2 / (T_1 - T_2) \quad (18)$$

Similarly,

$$\frac{E_B}{k_B T(x)} = \frac{E_B}{k_B T_1} + \frac{x}{x_B} \quad (19)$$

where,

$$x_B = x_0 \frac{k_B T_0}{E_B} \quad (20)$$

and

$$g(x) = x/x_S \quad (21)$$

with

$$x_S = -x_0 \frac{k_B T_0}{Q} \quad (22)$$

Note that for $T_2 \rightarrow T_1$ we have $|x_D| \rightarrow |x_B| \rightarrow |x_S| \rightarrow \infty$, i.e., the x -dependence disappears from the quantities listed above. We also point out that Eqs. (15), (16), and (21) all imply a particular temperature profile. In Ref. 11 it was shown that for values of $T_2/T_1 > 0.5$ this profile is closely approximated by a straight line, which would be the case for steady state heat loading at the plasma side surface only.

We also define δ by

$$1/\delta = 1/x_D + 1/x_S \quad . \quad (23)$$

These characteristic lengths and the approximations of Eqs. (15) - (22) then yield a diffusion coefficient

$$D(x) = D_1 e^{-x/x_D} \quad , \quad (24)$$

and a trapping coefficient

$$B(x) \equiv e^{-E_B/k_B T} = B_1 e^{-x/x_B} \quad , \quad (25)$$

where $B_1 = e^{-E_B/k_B T_1}$.

The recombination coefficients k_1 and k_2 are also temperature dependent and according to Baskes' theory²² are given by

$$k_i(T_i) = k_0 (500/T_i)^{1/2} e^{-E_k/k_B T_i} \quad (26)$$

where k_0 is a materials dependent constant, and E_k is an activation energy for recombination which depends on the heat of solution for hydrogen in the wall material and on the activation energy for diffusion. E_k may be either positive or negative. The k_i do not depend on the temperature profile; rather they depend only on T_i , the temperatures at the respective surfaces.

Utilizing Eqs. (21), (23) and (24), the integral in Eq. (14) can be easily evaluated to yield for $x > R$

$$C(x) = e^{-x/x_S} \left\{ C_R - k_2 C_2^r \frac{\delta}{D_1} (e^{x/\delta} - 1) \right\} \quad , \quad (27)$$

where C_R is the concentration at $x = R$ given by Eq. (13), and the approximation $e^{R/\delta} = 1$ has been used.

Let us now define dimensionless variables v and u by

$$v^r = k_2 C_2^r / \phi \quad , \quad (28a)$$

and

$$u^r = k_1 C_1^r / \phi \quad , \quad (28b)$$

and note that v^r is the fraction of hydrogen that permeates through the wall while u^r is the fraction of hydrogen recycled to the plasma. Furthermore, if we define the additional dimensionless parameters

$$W = (\phi R / D_1) (k_1 / \phi)^{1/r} \quad (29a)$$

$$\alpha = \frac{R}{x_0} \left(\frac{x_0 / \delta}{e^{x_0 / \delta} - 1} \right) \quad (29b)$$

and

$$\gamma = e^{x_0 / x_s} (k_1 / k_2)^{1/r} \quad (29c)$$

Here W is the transport parameter. Eqs. (7) and (27) (evaluated at $x = x_0$) can be combined utilizing the dimensionless quantities above to yield

$$\frac{W}{\alpha} v^r + \gamma v = (1 - v^r)^{1/r} + W \quad (30)$$

A general analytical solution to v is not possible but a very good approximation is

$$v^r = \alpha \left(\frac{1 + W}{W + \alpha(\gamma + 1)} \right) \quad (31)$$

which is exact for $r = 1$. Exact solutions for v^r as a function of the transport parameter W are given in Figs. 3 and 4 for $r = 1$ and 3. The values for v^r for $r = 2$ lie between those for $r = 1$ and 3. The approximation given in Eq. 31 (which also corresponds to the curves labeled $r = 1$ in Figs. 3 and 4) agree very well with the exact solution to Eq. 30, and it can be shown that this approximation is valid for $.1 < \gamma^r < \alpha^{-1}$.

Values for C_1 , C_R and C_2 can now be obtained by using the result in Eq. (31) with Eqs. (7), (13) (evaluated at $x = R$) and (28). These concentrations are plotted for $r = 2$ as a function of W for $\alpha = 10^{-6}$ and $\gamma = 1$ in Fig. 5. Sketches of the H profiles at steady state are also included as inserts in this figure.

Three distinct types of H distributions result, depending on the value of W .²³ For $W > 1 > \alpha(1 + \gamma^r)$ (Region I), the profile is highly peaked at $x = R$ and the two surface concentrations can be assumed to be negligible. This behavior is characteristic of diffusion-limited H transport for both surfaces; hence the profile is labeled DD in the inset. For $\alpha(1 + \gamma^r) < W < 1$ (Region II), $C_R \approx C_1$ and $C_2 \approx 0$ indicating H recombination-determined behavior at the plasma-side surface and diffusion-limited behavior on the back side (RD). For $W < \alpha(1 + \gamma^r)$ (Region III) the H profile becomes uniform, which is characteristic of recombination limited kinetics at both surfaces (RR). The parameter W can therefore be used to describe the transition from diffusion limited ($W > 1$) to one-surface recombination limited ($\alpha(1 + \gamma^r) < W < 1$) to two-surface recombination limited ($W < \alpha(1 + \gamma^r)$) H transport in materials. We note that for the unlikely case $\alpha(1 + \gamma^r) > 1$ the region boundaries must be redefined.

3. Application Equations

a. No Traps

It is clear that the potential for deleterious H -related material effects are at a maximum when the system is in steady state because the H concentrations are highest. Even though a considerable amount of time may be required to reach steady state, it is perhaps

instructive to calculate "worst case" values for these H-material concerns.

Using the equations developed thus far, it is easy to rewrite the H concentration profile given in Eq. (27) in terms of dimensionless quantities

$$C(x) \approx C_R e^{-x/x_S} \left[1 - \left\{ \frac{W}{W + \alpha(1 + \gamma^r)} \right\} \left(\frac{e^{x/\delta} - 1}{e^{x_0/\delta} - 1} \right) \right] \quad (32)$$

where

$$C_R = \left(\frac{\phi}{k} \right)^{1/r} (1 - v^r)^{1/r} (1 + W) \quad (33)$$

The quantity in braces in Eq. (32) equals 1 unless the H transport is recombination limited at both surfaces, in which case it equals 0. For the latter case (i.e., transport Region III) the H profile is linear for isothermal conditions or decreases exponentially with temperature gradients because of the Soret term. For the former case (i.e., diffusion-controlled transport at the back surface) several profiles are displayed in Fig. 6 for various values of x_D/x_0 and x_S/x_0 . When these quantities are both large (i.e., small temperature gradients) the profile drops linearly from C_R to nearly 0. When x_D/x_0 becomes small, the profile approaches a constant and illustrates that the change in the diffusion coefficient with depth dominates the H profile. When the term x_S/x_0 becomes small, the profile decays exponentially with the Soret term, thereby demonstrating the importance of the Soret effect on the H profile.

A quantity commonly cited to specify the suitability of a material with respect to potential H (i.e., tritium) buildup is the average H concentration which can be expressed as

$$\bar{c} = c_R \left\{ \frac{1}{x_0} \left[x_s \left(1 - e^{-x_0/x_s} \right) - \frac{x_D \left(e^{x_0/x_D} - 1 \right) - x_s \left(1 - e^{-x_0/x_s} \right)}{e^{x_0/\delta} - 1} \right] \right\} \quad (34)$$

It is straightforward to show that, when there is no temperature gradient (i.e., x_s and $x_D \rightarrow \infty$), the term in braces in Eq. (34) goes to 1/2. When an appreciable negative temperature gradient exists and when $x_D < x_s$ (the case most often found), then the term in braces approaches 1. In other words, the presence of a temperature gradient in the wall will, at the very most, only double the amount of H in the wall. (This result is true only for the case that $x_s > 0$ which will be shown in the discussion section to be the situation for most materials used for first wall applications.)

The rate at which H isotopes permeate a wall material is also very important in the design of future fusion reactors because this permeation will lead to tritium contamination of regions exterior to the vacuum vessel. The steady state H permeation rate is expressed by

$$J_2 = \phi v^r = \phi \alpha \left(\frac{1 + W}{W + \alpha(\gamma^r + 1)} \right) \quad (35)$$

The permeation is therefore directly proportional to the parameter α defined in Eq. (29b). For isothermal conditions (i.e. $x_0/\delta = 0$) the term in braces in Eq. (29b) goes to 1 and α becomes simply the ratio of the implant depth to the wall thickness. For negative temperature gradients, the term in braces can become

extremely small and thereby significantly reduce the amount of permeation which occurs. We therefore assign the name "permeation reduction factor" to the quantity in braces in Eq. (29b) and note that an identical reduction of the permeation would occur for isothermal conditions by simply increasing the thickness of the wall by the inverse of this factor.

The results expressed in Eqs. (34) and (35) therefore demonstrate the main benefit of a negative temperature gradient in the wall; an order of magnitude reduction of the permeation at the expense of increasing the average H concentration by at most a factor of 2.

b. With Traps

Equation (4b) can be solved for the trapped H concentration in terms of the mobile H concentration to give

$$C_T(x) = \frac{N_T C(x)}{C(x) + \mu N_S e^{-E_B/k_B T_1} e^{-x/x_B}} \quad (36)$$

where the exponential form of the trapping coefficient in Eq. (25) has been used. In general, the average trapped H concentration must be solved by integrating Eq. (36) numerically over the range $0 < x < x_0$. In Ref. 12 we showed that under certain approximations this integration could be done analytically. The main conclusion of those results, which will not be repeated here, was that the trapped fraction depends primarily on T_2 (the temperature on the "cool" side) and is only weakly dependent on T_0 and hence T_1 (the temperature on the "hot" side). For a wall at constant temperature, the average trapped H concentration is

$$\bar{C}_T = N_T \left[1 - \frac{\mu N_S e^{-E_B/kT_1} \ln Q}{C_R - C_2} \right] \quad (37)$$

where

$$Q = \frac{C_R + \mu N_S e^{-E_B/kT_1}}{C_2 + \mu N_S e^{-E_B/kT_1}} \quad (38)$$

When the traps are populated dilutely, it is easily shown that

$$\bar{C}_T = N_T (\bar{C}/N_S) e^{E_B/k_B T} \quad (39)$$

Using this relationship, the temperature T_{trap} at which the average concentration of trapped H equals the average concentration of mobile H is

$$T_{\text{trap}} = E_B / [k_B \ln(N_S/N_T)] \quad (40)$$

Another useful temperature to define is T_{sat} , the temperature at which the mobile H concentration just equals the atomic density of the material.

$$T_{\text{sat}} = E_D / [k_B \ln(D_0 N_S / R)] \quad (41)$$

Most materials will become saturated with implanted H at low temperatures at concentrations which range from 0.1 to 5 times N_S .^{45, 47}

Therefore T_{sat} represents the approximate temperature where saturation effects begin to be important.

The two temperatures above can be used to specify when the effects related to trapping and saturation must be considered.

For $T < T_{\text{sat}}$ the saturation effect is important; for

$T_{\text{sat}} < T < T_{\text{trap}}$ trapping must be considered, while for $T > T_{\text{trap}}$ neither trapping nor saturation need be included in calculating H inventories so that only the mobile H concentration is important.

The permeation through a wall membrane depends only on the mobile H (as indicated by Eq. (5b)); however, trapping can affect the diffusion coefficient D before steady state is reached. Using the McNabbFoster²⁴ formula for an "effective" diffusion coefficient

$$D_{\text{eff}} = \frac{D_0}{1 + \frac{N_T e^{E_B/kT}}{\mu N_S}} \quad (42)$$

The time required to reach steady state is

$$t_{\text{ss}} = x_0^2 / (6D_{\text{eff}}) \quad (43)$$

Because D_{eff} can be decreased by several orders of magnitude according to Eq. (42) the presence of traps can significantly increase the "time-to-breakthrough" of the H permeation.

Traps can also influence permeation by modifying D through radiation-enhanced diffusion.²⁵⁻²⁹ In this case, however, the diffusion coefficient is increased; hence this effect could hasten break-through as well as affecting W and its associated parameters.

B. Temporal Solutions

For diffusion-limited H transport (i.e., $W > 1$) Erents and McCracken¹⁴ have shown that

$$J_1 = \phi \operatorname{Erfc} [R / (2\sqrt{Dt})] \quad (44)$$

This equation can be shown to result from a solution of Eq. (1) with no traps for the delta function implant distribution given in Eq. (12). The boundary condition for the solution is $C_1 = 0$. By defining a normalized time

$$\phi_1 = Dt/R^2, \quad (45)$$

and rewriting in terms of our other normalized parameters, Eq. (44) can be expressed as

$$u^r(\phi_1) = \text{Erfc} [1/2\phi_1^{1/2}] \quad (46)$$

where u^r represents the H fraction recycled to the plasma. This recycling fraction is plotted (dashed line) versus ϕ_1 in the lower panel of Fig. 7.

For $W < 1$, or recombination-controlled release, the result obtained in Ref. 10 can be generalized for any order of release kinetics to yield

$$u(\theta_2) = \frac{1}{\pi} \int_0^{\theta_2} \frac{1 - u^r(\theta_2')}{\sqrt{\theta_2 - \theta_2'}} d\theta_2' \quad (47)$$

where

$$\theta_2 = W^2Dt/R^2 \quad (48)$$

with W , the transport parameter, given by Eq. (33a). This result is similar to that obtained by Hotston and McCracken.¹⁵ A plot of u^r (i.e., J_1/ϕ) vs θ_2 for $r = 1, 2$ and 3 is also plotted in the lower panel of Fig. 7. These solutions to Eq. (47) were found numerically.

It can be seen from the lower panel of Fig. 7 that for all of the cases above including both diffusion and recombination controlled H release, the recycle fraction J_1/ϕ is approximately 0.5 when either θ_1 or θ_2 equals 1. Thus, the recycle time (the time when the fractional recycling is 0.5) can be approximated by the expression

$$\tau = (R^2/D)(1 + 1/W^2) \quad (49)$$

which is identical to the result found for quadratic kinetics in Ref. 10.

After a discharge is terminated (i.e., $\phi = 0$) the normalized plasma side surface concentration u can be expressed as

$$u(\theta) = 1 - \int_0^\theta \frac{u^r(\theta') d\theta'}{\sqrt{\theta - \theta'}} \quad (50)$$

if the discharge was of sufficient duration so that the concentration of H in the wall is nearly constant near the plasma side. This condition requires that the situation be recombination controlled during the discharge; we therefore drop the suffix 2 on θ . J_1/ϕ (i.e., u^r) is plotted for this case in the upper panel of Fig. 7.

The quantity commonly measured in a H recycling experiment is the pressure change in the vacuum vessel.³⁰⁻³³ Such an experiment can be performed during and after a glow discharge or immediately following a tokamak discharge. Using the result of Howe and Langley³³ for the pressure change during a constant flux discharge for the case of an unpumped vessel:

$$P(t) = P_0 - N_W(t)K_B T_1 / (2V) \quad (51a)$$

where P_0 is the initial pressure, A is the surface area and V is the volume of the vessel and N_W is the areal density of H in the wall. Using the derivation above, the fractional pressure change can be expressed as

$$\Delta P/P_0 = \frac{-A\phi k_B T_1 \gamma I(\theta)}{2V} \quad (51b)$$

where ΔP is the pressure change, and $I(\theta)$ is the integral

$$I(\theta) = \int_0^\theta [1 - u^r(\theta')] d\theta' \quad (52)$$

where Eq. (47) is used to determine u .

Equation (51) also describes the fractional pressure change which occurs at the termination of a discharge. In this case the

change is positive and the integral I is given by

$$I(\theta) = \int_0^{\theta} u^r(\theta') d\theta' \quad (53)$$

and $u(\theta)$ comes from Eq. (50).

For either case, when $t \ll \tau$ the integral I can be shown to be

$$I = \theta \quad (t \ll \tau) \quad (54)$$

and when $t \gg \tau$

$$I = (4\theta/\pi)^{1/2} \quad (t \gg \tau) \quad (55)$$

To demonstrate these limits, the power of θ determined as $d(\log I)/(d \log \theta)$ was determined as a function of θ for $r = 1, 2$ and 3 by numerically integrating both Eqs. (52) and (53) using numerical solutions of the appropriate u 's. The results of these calculations are plotted in Fig. 8. It can be seen from this figure that the power of θ starts at 1 for $\theta \ll 1$ and goes to $1/2$ for $\theta \gg 1$ as indicated above. The region in between exhibits a dependence on r , the order of the release reaction; however, this dependence is weak, which indicates that the shape of pressure change curves are not very sensitive to the kinetic order of the recombination process.

The equations above can be fit to experiments to yield, 1) for $t \ll \tau$, the flux ϕ when the fractional pressure change is linear in time, and 2) for $t \gg \tau$, the quantity $\sqrt{D}(\phi/k)^{1/r}$ for $W < 1$ and $\theta R/D$ for $W > 1$ when the fractional pressure change is changing as $t^{1/2}$. These results indicate that pressure change measurements can be used to determine r for the case $W < 1$ and $t \gg \tau$ by measuring the coefficient of $t^{1/2}$ as a function of ϕ .

The curves for $r = 2$ in Fig. 8 were least square fit with the function

$$n(\theta) = \frac{1 + .5(\theta/a)^b}{1 + (\theta/a)^b} \quad (56)$$

for both the during discharge and after discharge cases with the resulting parameters: $a = 1.3$, $b = .84$ for during; $a = 1.0$, $b = .42$ for after. This parameterization can be used to fit pressure change data for the case of quadratic kinetics.

III. DISCUSSION

A. $r \neq 2$

The theory developed above is applicable for any kinetic order, r , of the hydrogen recombination or surface release reaction; however it is anticipated that most of its usage will be for $r = 2$ (quadratic) kinetics. Pressure change measurements are by far the most common method of determining k ; however, this technique is relatively insensitive to r unless the flux dependence is studied systematically. Waelbroeck et al⁷ have made such measurements for SS 1.4301 and their results indicate $r = 2$. Recent experiments by Myers and Wampler³⁴ have clearly shown that the H release from 304 stainless steel also obeys second order kinetics. Never-the-less it is possible that $r \neq 2$ for some materials under special plasma exposure conditions. The formalism can still be used for these cases.

B. $r = 2$

In this section we address the application of the transport theory for quadratic release kinetics to a wide variety of materials either in use or proposed for use in first walls of fusion reactions. For $r = 2$ the transport parameter W , becomes

$$W = R(\phi k_1)^{1/2}/D_1 \quad (57)$$

This transport parameter is quite similar to the permeation number defined by Waelbroek, et al.⁸. The only difference is that we use the characteristic length R, the range of the implant, whereas they use x_0 , the total wall thickness. With appropriate redefinitions, their permeation number could be used in lieu of our transport parameter.

1. Data

To use the above formulas for the H interaction with the wall, materials parameters such as the H diffusion and recombination coefficients, Soret energy, trap concentration and binding energy, and bulk atomic density must be known. Table 1 lists the material parameters used in the calculations which follow. The reader is referred to the articles cited in the reference column for measurements of the various parameters. In addition, the parameters ϕ and R were assumed to be $10^{16}/\text{cm}^2\text{s}$ and 10^{-6} cm, respectively. The k_0 values, when not measured, were calculated from Baskes' theory²² assuming a sticking coefficient of 1. In cases for which a range of Q^* values existed, the maximum was selected. Values for N_T/N_S are only estimates for most of the metals, and the E_B values, when available, were averaged.

Using the values given in Table 1, the diffusion and recombination coefficients and transport parameter W are plotted in Figs. 9, 10, and 11 respectively for all of the materials listed in Table 1. The three types of H transport delineated by W are indicated on the right side of Fig. 11. It is interesting to note that for $T > 300$ C almost all of the materials are in the middle region where the H transport rate is determined by recombination at the plasma side surface.

Two curves are plotted for stainless steel. SS_1 uses the recombination coefficient measured by Myers and Wampler³⁴ while SS_2

uses the same except with k_0 decreased by a factor of 1000 to simulate a reduced sticking factor²². It is well-known that the measured values of k_1 for SS are widely scattered presumably because of variations in surface conditions^{19c}.

The temperatures T_{sat} and T_{trap} in Table 1 come from the definitions in Eqs. (40) and (41). Values entered as * are above the melting temperature of the materials or so high that no practical upper limit to the maximum temperature for trapping can be defined. For these cases trapping must always be considered. By considering these temperatures together with the transport parameters plotted in Fig. 11, a H transport problem can completely specified in terms of which processes, diffusion or surface release, rate limits the mobile H motion and whether trapping effects must be considered to accurately predict the H buildup.

2. Isothermal Calculations

In Figure 12 the normalized steady-state permeation flux (J_2/ϕ) and inventory of H (C/N_s) together with the recycle time τ are plotted for isothermal conditions without traps. The right hand scales are for a 1 cm thick wall of area 10^6 cm^2 , comparable to that for an INTOR class machine.

As an example of how these curves can be used, examine SS_1 . For reference, we assume the maximum acceptable tritium inventory is 1 kg and the permeation is 1 g/day. Using these rather arbitrary limits, the H (i.e., tritium) inventory and permeation are tolerable for $T > 100 \text{ C}$ and $T < 500 \text{ C}$, respectively, which represents a fairly reasonable "safe" operating range. On the other hand for SS_2 (which represents oxidized steel) these calculations indicate that no

temperature exists where the steady-state inventory and permeation are simultaneously tolerable. Of course, as Baskes⁴⁶ has pointed out, it would take nearly a decade for the permeation and inventory to approach these limits.

The normalized permeation flux J_2/ϕ ranges from α to $1/2$ when $\gamma = 1$. It can be seen from Fig. 2 that the lower limit is reached for a large number of materials at low temperatures ($T < 100$ C). In contrast, the higher limit is approached by the hydride formers Zr, V, and Ta.

It is interesting to note from Fig. 12 that both the average H concentrations and recycle times have minima over this temperature range for some of the materials (e.g., Mo, Al, B, W, Cu, Ni, and SS₁) at the temperature where $W = -E_D/2E_K$. For these materials, the release of H is retarded at low T by diffusion and at high T by the recombination process.

3. Nonisothermal Calculations

Unfortunately, the calculations for nonisothermal conditions with H trapping cannot be presented nearly as compactly as can those presented in the previous section. For space reasons we therefore examine only 304 SS, Fe, INCONEL and Al in this section. The calculations for these materials under conditions identical to those above except with the outer wall (side 2) held at $T_2 = 100$ C and allowing the inner wall temperature to vary are plotted in Fig. 13. The calculations assume a linear temperature profile. The solid and dashed curves correspond to sticking coefficients of 1 and 0.001 respectively. C_{TOT} denotes the total H inventory, both mobile and trapped; however, the trapped inventory dominates for

for all of these materials. The permeating H flux is denoted by J_2 and \dot{C}_{TOT} represents the approximate rate of H buildup in the wall.²⁴ The number of days to "break-through" can be estimated by dividing \dot{C}_{TOT} by C_{TOT} .

The results plotted in Fig. 13 demonstrate the benefits, at least for these materials, of the temperature gradient mentioned above. The existence of a temperature gradient tends to significantly decrease permeation at high inner wall temperatures while resulting in only a modest increase in the inventory. The net result is an extension of the "safe" operating range of the inner wall temperature, T_1 . For example, while the "oxidized" SS₂ case mentioned in the isothermal section had no "safe" T_1 range, Fig. 13 indicates that for $T_2 = 100$ C and $T_1 > 400$ C the inventory is < 1 kg and the permeation is < 1 g/day. This fact indicates that, on the basis of T permeation control, temperature gradients may be highly desirable in walls and other internal components of future fusion reactors.

In order to better conceptualize the effects of nonisothermal conditions on permeation, it is useful to examine the permeation reduction factor (the term in braces in Eq. (29b)). A contour plot of the permeation reduction factor vs. $Q^*/k_B T_0$ (i.e., $-x_O/x_S$) and $E_D/k_B T_0$ (i.e., x_O/x_D) is given in Fig. 14. A curve for the metals is shown in this figure where Q^* is given in Table 1. For Al, Q^* was set = 0. All curves in such a diagram begin in the origin indicating the case $T_1 = T_2$ and are straight lines when T_1 is increased. Although these curves are valid for all combinations of T_1 and T_2 (where $T_1 > T_2$) the special cases $T_2 = 100$ C

and $T_1 = 200$ C, 300 C, etc., are indicated by the solid dots in the figure, as indicated for Al. The final dot in each row, which only occurs for V on this plot, corresponds to $T_0 = T_2$ ($T_1 \rightarrow \infty$). It can be surmised from Fig. 4 that: 1) for Fe the Soret effect drastically reduces permeation, 2) for SS, Ni and INCONEL the Soret effect results in a very small reduction in permeation, while 3) for the reactive metals, the Soret effect increases permeation.

IV. SUMMARY

A simple theory of H transport in fusion first wall materials was developed. The theory is based upon a delta function profile, centered about the implanted H range with arbitrary order release kinetics at both surfaces. The model includes the effects of trapping and thermal gradients. The problem is formulated in terms of a unitless parameter, $W = (R\phi/D)(k_1/\phi)^{1/r}$ where r is the order of the release kinetics, R is the range of the implant, ϕ is the penetrating part of the incident flux, k_1 is the recombination coefficient and D is the diffusion coefficient.

Equations pertinent to important H-materials concerns, such as recycle times, tritium inventories and permeation fluxes, were derived and applied to several materials representative of those proposed for use in fusion reactors. Some conclusions which can be drawn from these calculations are: 1) for $Q^*/E_B > 0$ (Ta, Zr, Ti, V), where Q^* is the thermomigration energy and E_B is the diffusion activation energy, the Soret effect tends to cancel the benefits of a temperature gradient on reducing permeation; 2) for $Q^*/E_B \sim 0$ (SS, Ni, Inconel) the Soret effect is negligible; and 3) for $Q^*/E_B < 0$ (Fe) the Soret effect dramatically helps in

reducing T permeation through a wall. Another important conclusion is that the H trapping under nonisothermal conditions depends strongly on the coolant-side temperature but is only weakly dependent on the plasma-side temperature.

We have also derived equations which describe the build-up to quasi-steady state. Through these equations the pressure change experienced in the vacuum vessel during and after discharges is calculated and a simple approximation is derived which can be used to fit pressure change data and thereby determine the recycle constant.

The transport parameter concept results in a natural classification of the transport behavior of hydrogen in all materials at temperatures for which the solutionized hydrogen is mobile. The analytical results provide physical insight into the process governing hydrogen permeation and inventory and are especially useful to understand the inter-relationships which exist between the various plasma and materials parameters. This last benefit should be particularly helpful in conceptualizing the impact of synergisms on the plasma surface interaction.

References

1. M. I. Baskes, Sandia National Laboratories Report, SAND83-8231 and SAND80-8201.
2. M. I. Baskes, Sandia National Laboratories Report, SAND80-8201.
3. P. Wienhold, I. Ali-Kahn, K. J. Dietz, M. Profant and F. Waelbroeck, J. Nucl. Mater. 85/86 (1979) 1001 and P. Wienhold, M. Profant, F. Waelbroeck, J. Winter, Rep. Jul-1825 (1983).
4. D. F. Holland and B. J. Merrill, IEEE, Pub. No. 81CH1715-2 NPS.
5. W. Möller, IPP Report, IPP 9/44 Nov. 1983.
6. I. Ali-Kahn, K. J. Dietz, F. A. Waelbroeck, P. Wienhold, J. Nucl. Mater. 76&77 (1978) 337.
7. F. Waelbroeck, J. Winter and P. Wienhold, J. Nucl. Mater., 103/104, (1981) 471.
8. F. Waelbroeck, P. Wienhold and J. Winter, J. Nucl. Mater., 111/112 (1982) 185.
9. B. L. Doyle, Surface Data for Fusion Devices, eds., N. Itoh and E. W. Thomas, IPPJ-AM-21 (1981) 37.
10. B.L. Doyle, J. Nucl. Mater. 111/112 (1982) 628.
11. D. K. Brice and B. L. Doyle, Part I, to be published in J. Nucl. Mater.
12. B. L. Doyle and D. K. Brice, Part II, 3rd FRM meeting, Albuquerque, 1983, to be published in J. Nucl. Mater.
13. D. K. Brice, Part III, Loc. cit. 12.
14. S. K. Erents and G. M. McCracken, J. Phys. D2 (1969) 1397.
15. E. S. Hotston and G. M. McCracken, J. Nucl. Mater. 68 (1977) 277.

16. H. C. Howe and R. Langley, *J. Vac. Sci. Technol* A1, (1983), 1435.
17. H. C. Howe, *J. Nucl. Mater.* 93/94 (1980) 17.
18. Y. Shimomura, JAERI Report, JAERI-M 9065 (1980).
19. a. A. G. M. McCracken and P. E. Stott, *Nuclear Fusion* 19 (1979) 889.
 b. F. Waelbroeck, I. Ali Kahn, K. J. Dietz, and P. Wienhold, *J. de Phys.* C7 (1979) 313; and Ref. 8.
 c. K. L. Wilson, *J. Nucl. Mater.*, 103/104 (1981) 493.
 d. R. A. Kerst, *Loc. cit.* 12.
20. S. R. DeGroot, *Thermodynamics of Irreversible Processes*, (North-Holland, Amsterdam, 1966) p. 111.
21. O. D. Gonzales and R. A. Oriani, *Trans. AIME*, 233 (1965) 1878.
22. M. I. Baskes, *J. Nucl. Mater.* 92 (1980) 318.
23. D. K. Brice, B. L. Doyle and A. A. Haasz, in preparation.
24. A. McNabb and P. K. Foster, *Trans. AIME* 227 (1963) 619.
25. V. M. Sharapov, A. E. Gorodetsky, A. P. Zakharov, and A. I. Pavlov, USSR Input to INTOR Workshop Session IV, Phase 2A (March 1982).
26. T. Tanabe, N. Saito, Y. Etoh, and S. Imoto, *J. Nucl. Mater.* 103&104 483 (1981).
27. T. Tanabe, Y. Furuyama and S. Imoto, *Loc. cit.* 12.
28. R. Dobrozemsky, *Proc. Symposium on Atomic and Surface Physics*, Maria Alm/Salzburg, Austria, W. Lindinger, ed. (1980).
29. R. Dobrozemsky, *Vacuum Technology and Vacuum Metallurgy*, Vol. 2, Proceedings of the Eighth International Vacuum Congress (1980) 15.

30. J. Winter, F. G. Waelbroeck, P. Wienhold, E. Rota, and T. Banno, to be published JVST-A, 1984
31. H. F. Dylla, J. L. Cecchi and R. J. Knize, PPPL Report PPPL-2046 (1984).
32. K. J. Dietz, J. Winter, P. Wienhold, F. Waelbroeck, to be published.
33. R. A. Langley and H. C. Howe, to be published J. Nucl. Mater., 1984.
34. S. M. Myers and W. R. Wampler, J. Nucl. Mater. 111/112 (1982) 579.
35. K. L. Wilson, Nuclear Fusion, in press.
36. K. L. Wilson, FED-INTOR Report, Phase-2A (1982) 272.
37. H. Wipf and G. Alefeld, Phys. Stat. Sol. 23 (1974) 175.
38. S. M. Myers, IEEE Trans. Nuc. Sci. NS-30 (1983) 1175.
39. E. Rota, F. Waelbroeck, P. Wienhold and J. Winter, J. Nucl. Mater., 111/112 (1982) 233.
40. F. Besenbacher, J. Bøttiger and S. M. Myers, J. Appl. Phys. 53 (1982) 3536.
41. D. T. Peterson and M. F. Smith, Met. Trans. 13A (1982) 821.
42. S. Morozumi, M. Kitada, K. Abe, and S. Koba, J. Nucl. Mater., 33 (1969) 261.
43. W. R. Wampler, Loc. cit. 12.
44. D. K. Brice, B. L. Doyle and W. R. Wampler, J. Nucl. Mater., 111/112 (1982) 598.
45. B. L. Doyle, D.K. Brice, W. R. Wampler and S. T. Picraux, J. Nucl. Mater., 93/94 (1980) 551.

46. M. I. Baskes, K. L. Wilson and W. Bauer, FED-INTOR Report, Phase 2A (1982) 5.
47. W. Möller, Nucl. Instrum. Meth. 209/210 (1983) 773.

Table 1. Parameters used in Calculations

	N_s (#/cm ³)	D_o (cm ² /s)	E_D (eV)	k_o (cm ⁴ /s)	E_k (eV)	Q^* (eV)	N_T/N_s	E_B (eV)	T_{sat} (°K)	T_{traps} (°K)	References
SS	8.5(22)	3.8(-3)	.56	9.6(-20)	.34	-.065	.01	.22	268	554	34, 35, 37, 38
Fe- α	8.4(22)	7.8(-4)	.08	5.9(-17)	-.20	-.35	.01	.62	41	*	22, 37, 39
INCONEL	8.6(22)	1.7(-2)	.54	2.8(-19)	.37	-.075	.01	.34	243	856	39, 37, 40
Al	6.0(22)	2.1(-1)	.47	2.4(-19)	-.37	(0)	.04	.8	195	*	35
Mo	6.4(22)	4.8(-3)	.39	3.1(-17)	-.15	-	.05	.8	187	*	35
Cu	8.5(22)	1.1(-2)	.40	1.3(-16)	.03	-	.01	.6	183	*	35
Ni	9.1(22)	6.9(-3)	.41	2.4(-17)	.25	-.075	.01	.34	191	856	35, 37, 40
W	6.3(22)	4.1(-3)	.39	5.2(-18)	-.56	-	.01	.8	188	*	35
Ti	5.6(22)	1.8(-2)	.54	1.0(-16)	.98	.26	-	-	247	-	35, 37
V	7.2(22)	5.2(-4)	.08	1.2(-15)	.68	.06	-	-	42	-	36, 41
Ta	5.5(22)	5.0(-4)	.16	1.0(-15)	.72	.33	-	-	85	-	36, 41
Zr	4.3(22)	4.2(-3)	.41	5.6(-16)	1.26	.26	-	-	201	-	22, 42
Be	12.3(22)	3.0(-7)	.19	4.2(-12)	.19	-	.25	1.5	145	*	36, 43
Si	5.0(22)	9.4(-3)	.48	4.4(-19)	-1.39	-	.5	1.5	231	*	10, 45
C	11.3(22)	7.0(-3)	.50	3.8(-18)	.45	-	.4	2.35	423	*	36, 44
B	13.0(22)	1.0(-3)	.85	1.5(-21)	.75	-	.45	1.15	226	*	36

Values in brackets give the order of magnitude, e.g., 8.5(22) = 8.5×10^{22} .

Average trap energy listed for INCONEL is that for Ni.

Soret energy Q^* for Al is set to zero.

T_{traps} entries of * indicate no upper limit.

Entries of - not available.

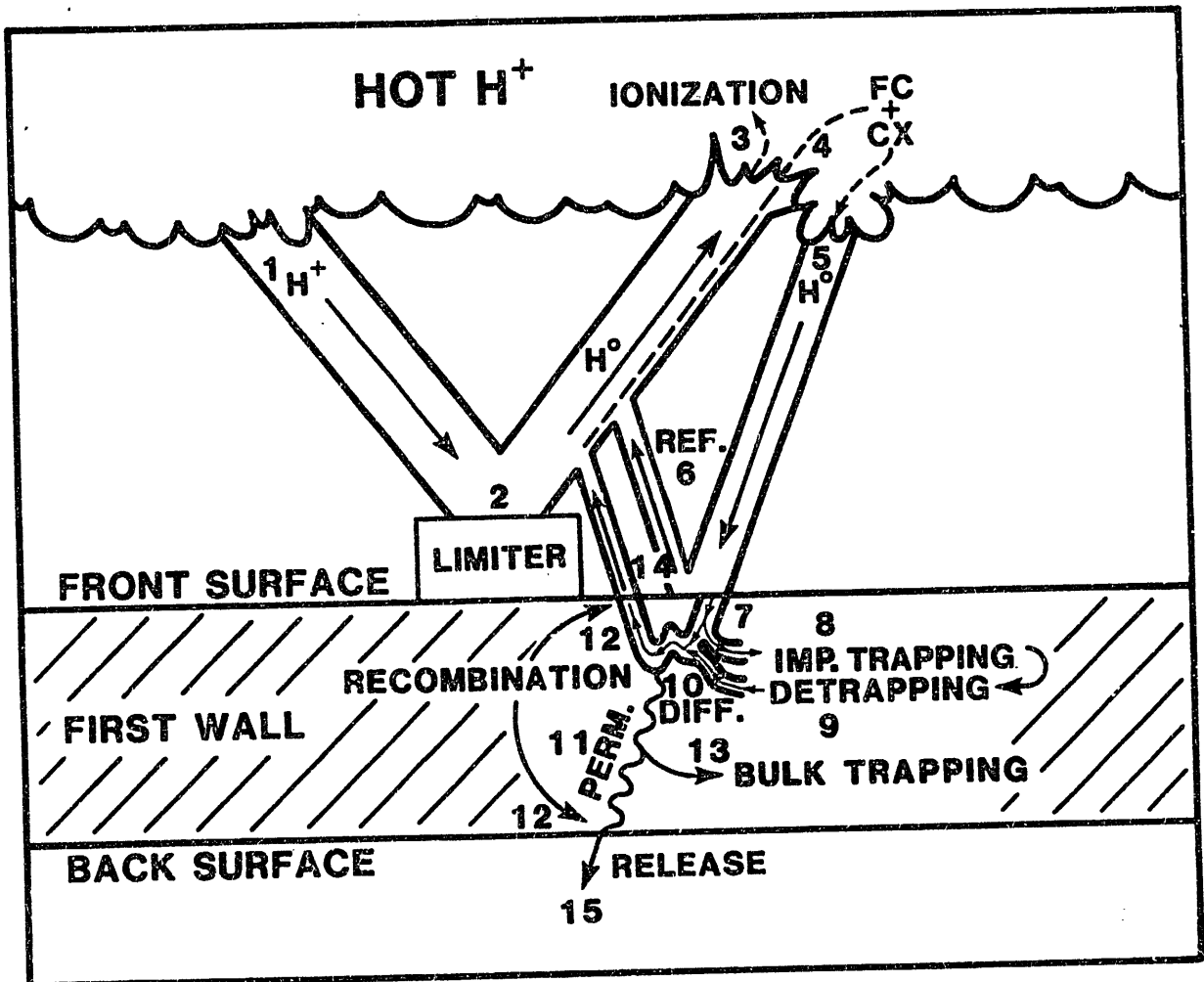


Fig. 1. Flow diagram of plasma-surface interaction based on Howe's theory. See text for step-by-step explanation.

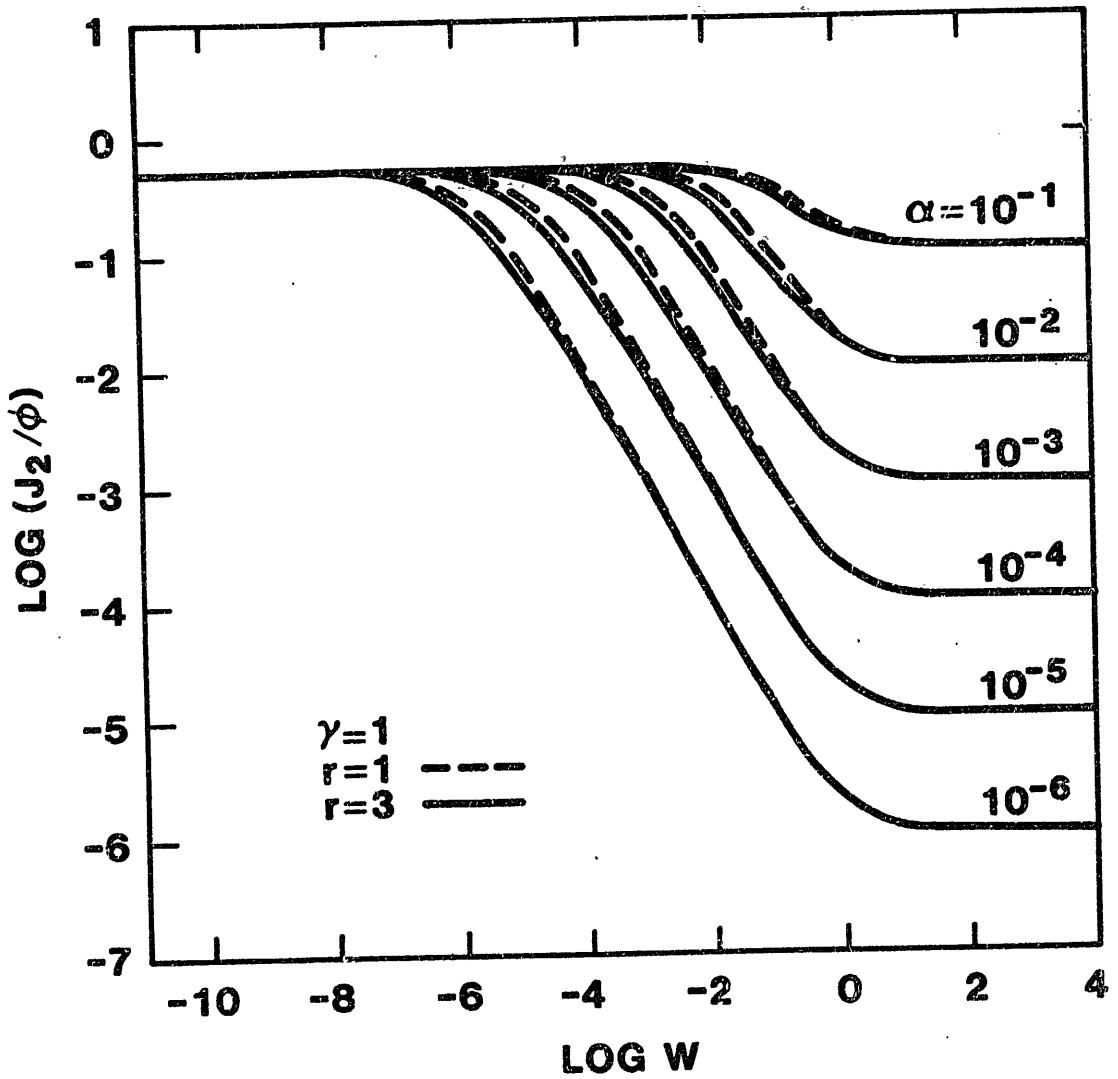


Fig. 3. Log-log plot of v^r , for $r=1$ and 3, versus the transport parameter for several values of α and for $\gamma = 1$. Each of these curves represents exact solutions to Eq. 30 and the dashed curve is for $r=1$.

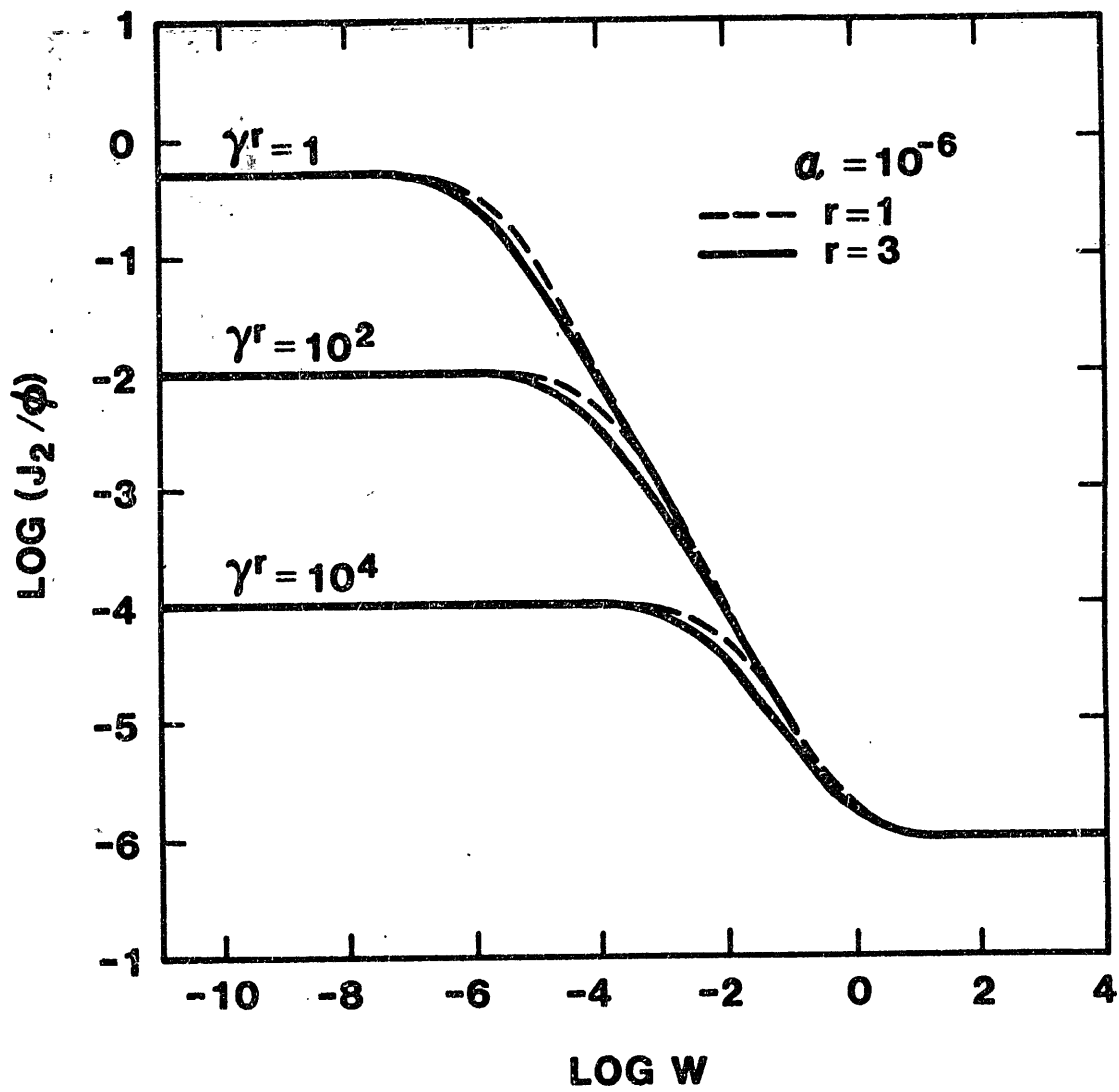


Fig. 4. Same plot as for Fig. 3 except for different values of γ .

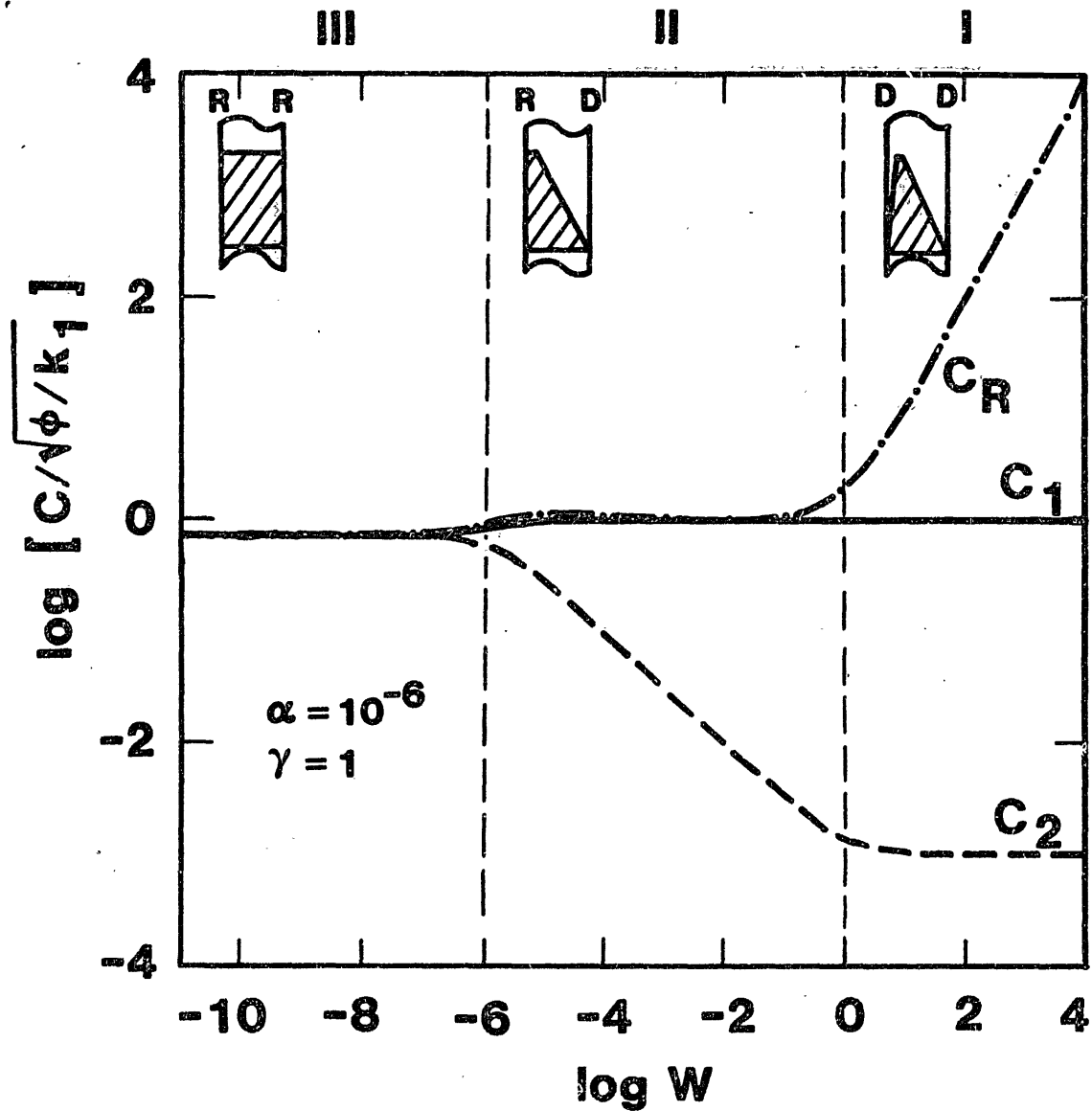


Fig. 5. Three normalized H concentrations as a function of W for $r = 2$. C_1 (solid curve) is the plasma-side surface concentration, C_2 (dashed curve) is the back-side surface concentration while C_R (dot-dashed curve) is the H concentration at depth R . The inserts show sketches of the steady-state H profiles for the three regions of W (I, II, and III).

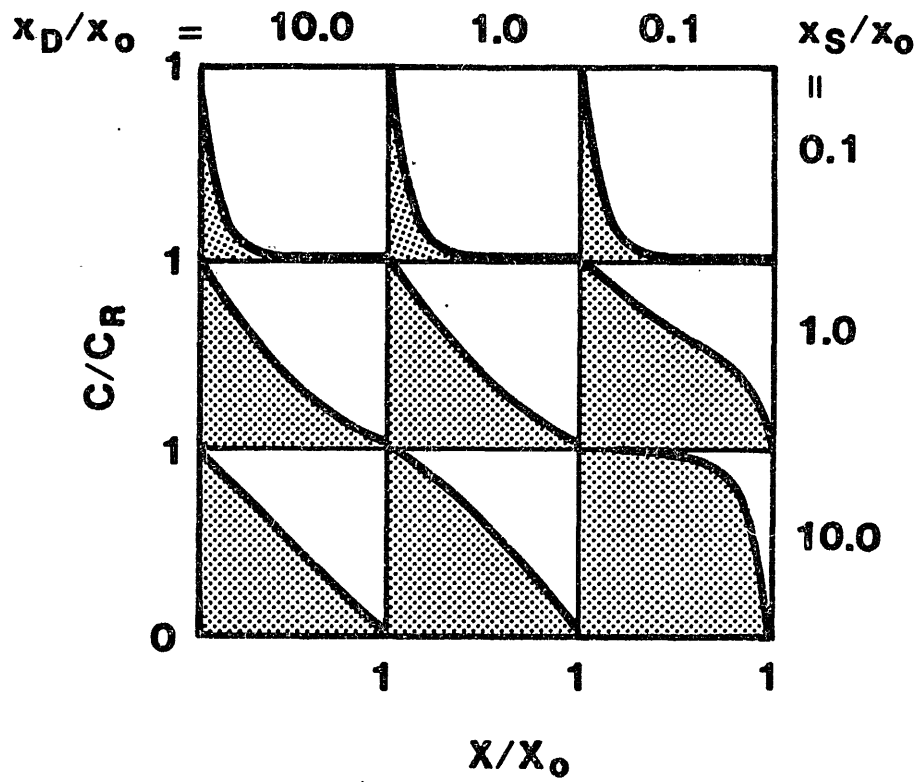


Fig. 6. H profiles for $x_D/x_0 = 10, 1.0, 0.1$ and $x_S/x_D = 10, 1.0, 0.1$.

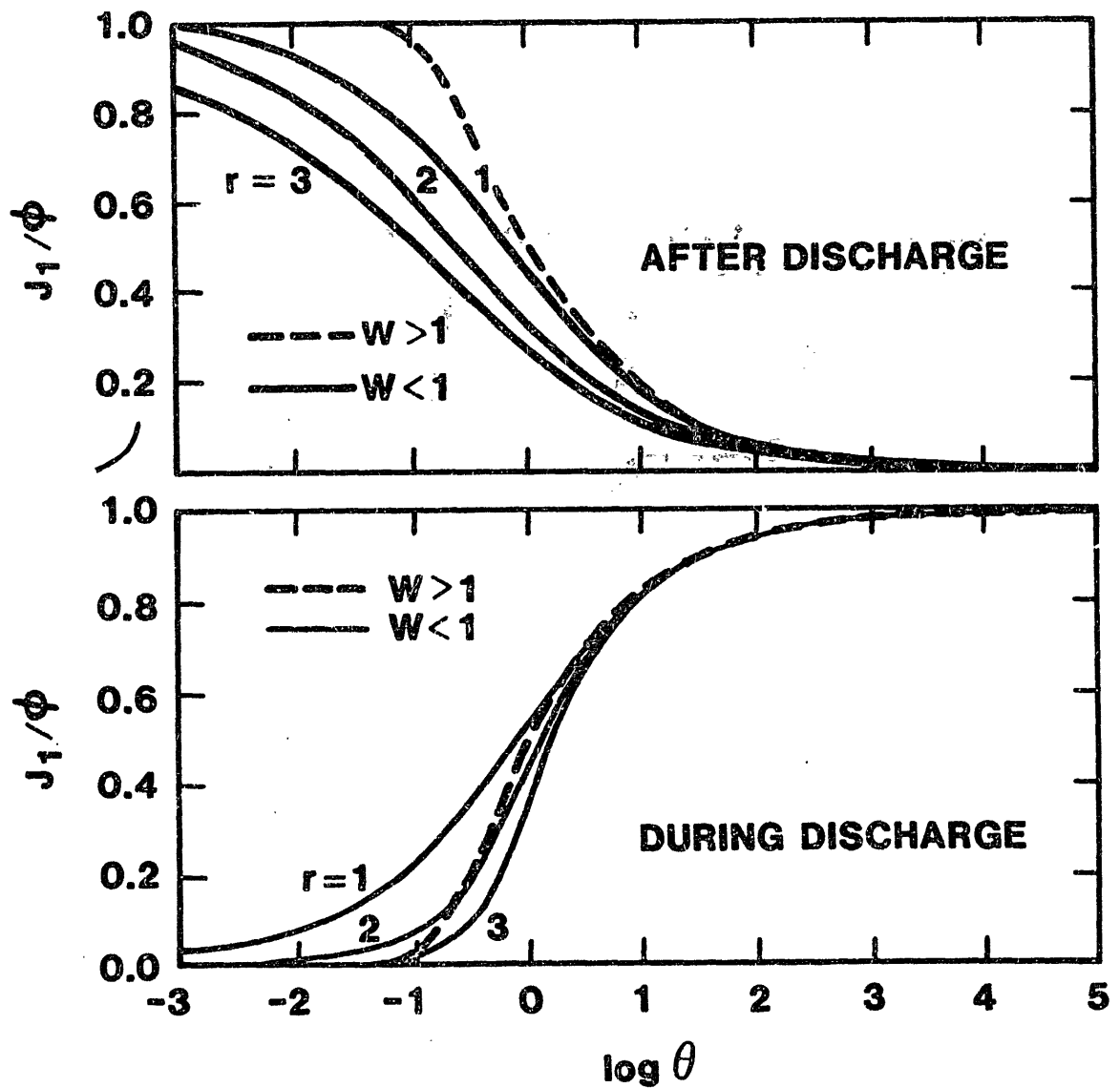


Fig. 7. Recycle flux, J_0 , normalized to ϕ versus θ . For the dashed curve ($W > 1$), which represents diffusion limited-H transport and $\theta = Dt/R^2$; whereas, for the solid curves ($W < 1$), in which case H transport is recombination-limited, $\theta = w^2Dt/R^2$ and curves are plotted for $r = 1, 2$ and 3 for both during (lower) and after (upper) exposure.

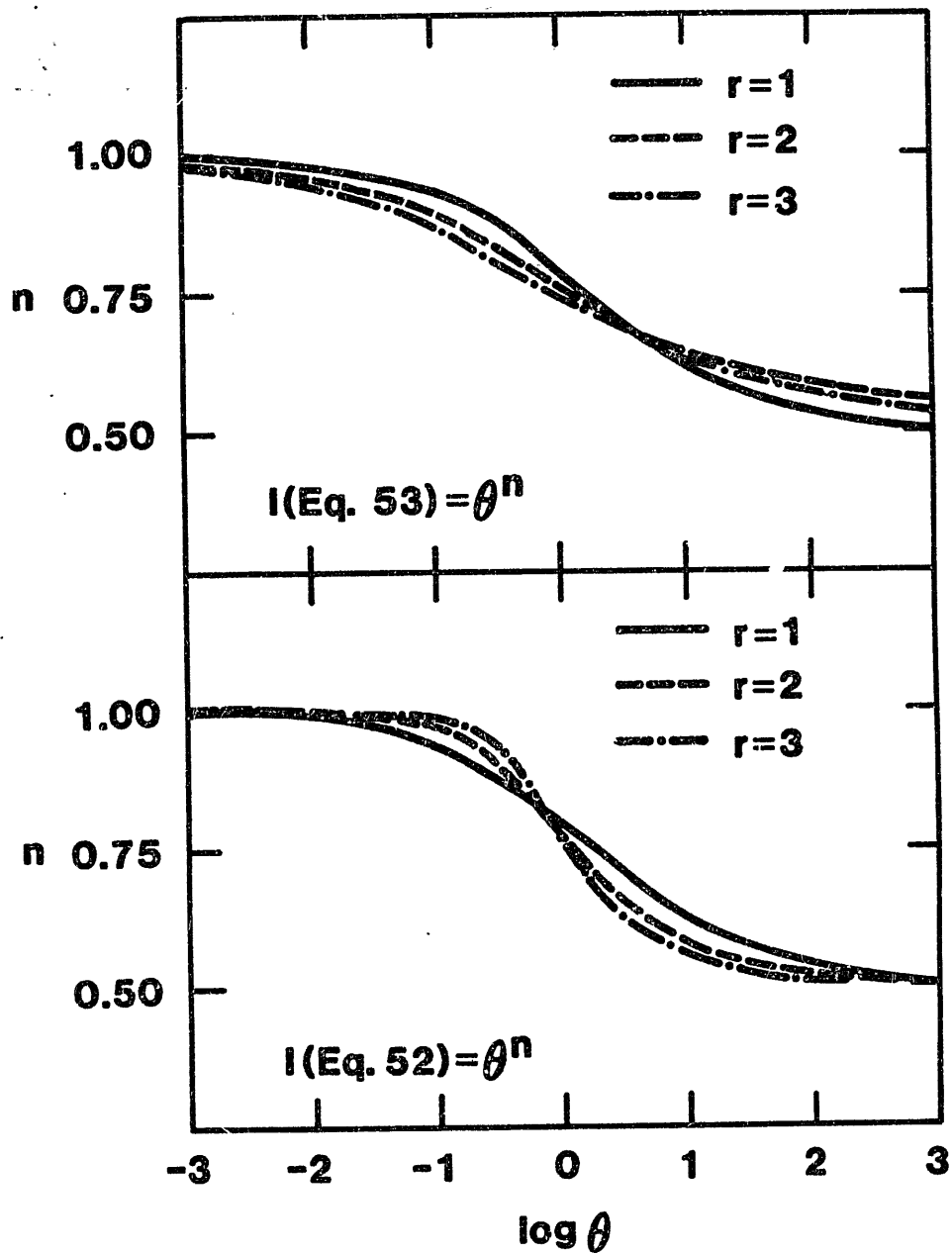


Fig. 8. n , (in the equation $\Delta P/P \propto \theta^n$) vs. θ for $r = 1, 2,$ and 3 and for both during and after a constant flux plasma exposure.

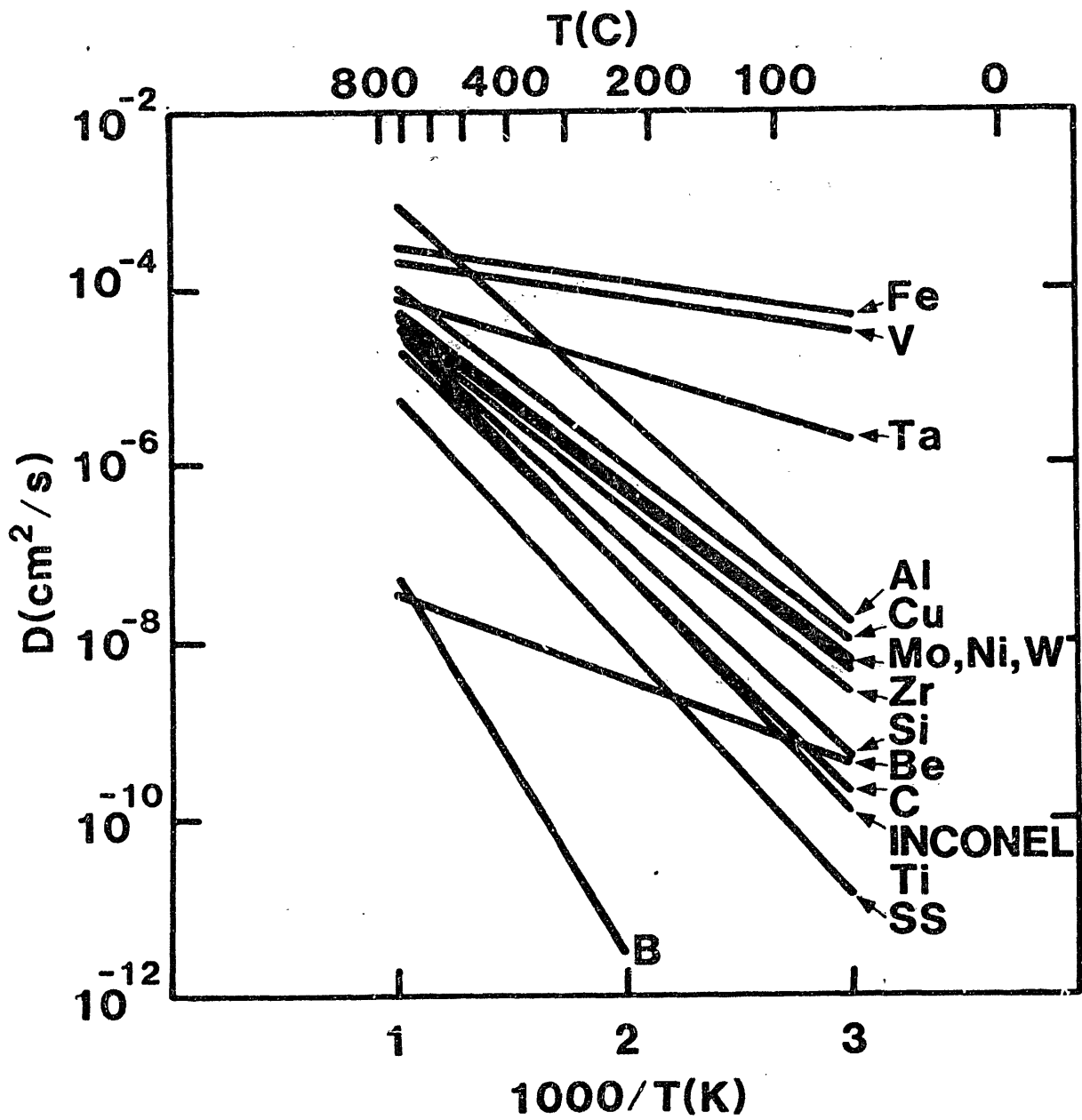


Fig.9. Arrhenius plots of the diffusion coefficient D of the materials listed in Table 1.

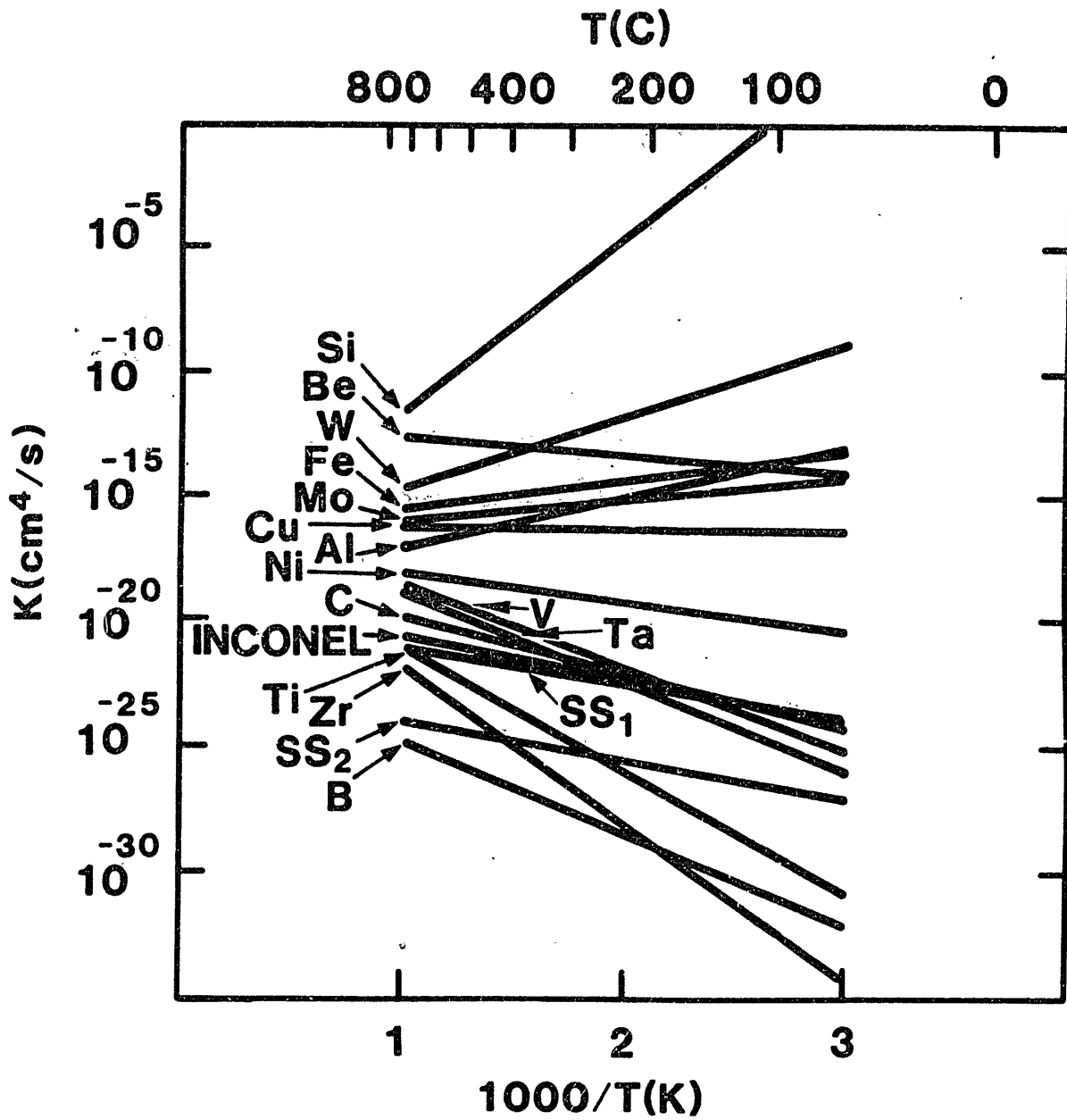


Fig. 10. Same as Fig. 9 except for the recombination coefficient k .

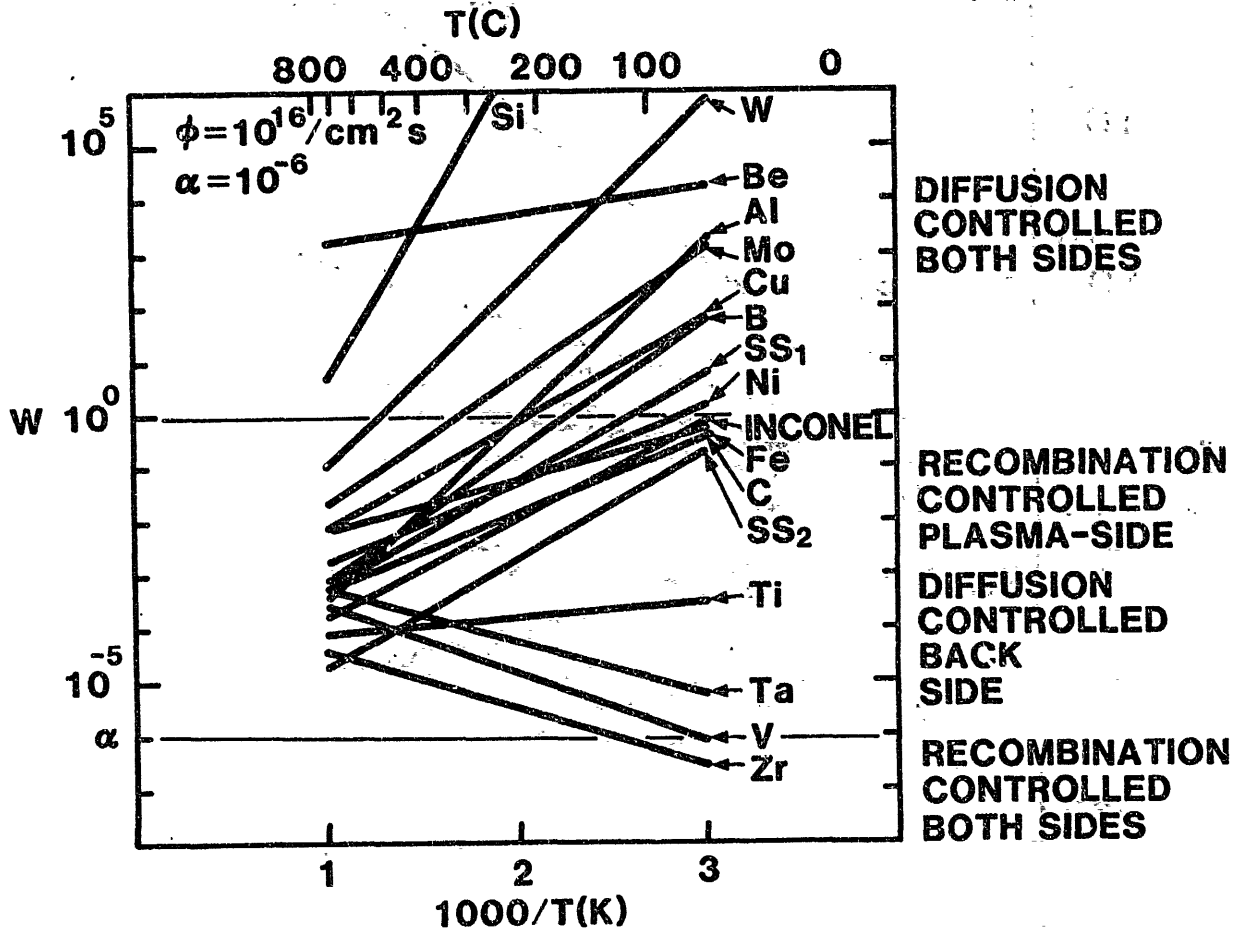


Fig. 11. Transport parameter W versus $1000/T$ for the materials listed in Table 1 for a penetrating particle flux of $\phi = 10^{16} \text{ cm}^{-2} \text{ s}^{-1}$ and an effective penetration ratio $\alpha = 10^{-6}$.

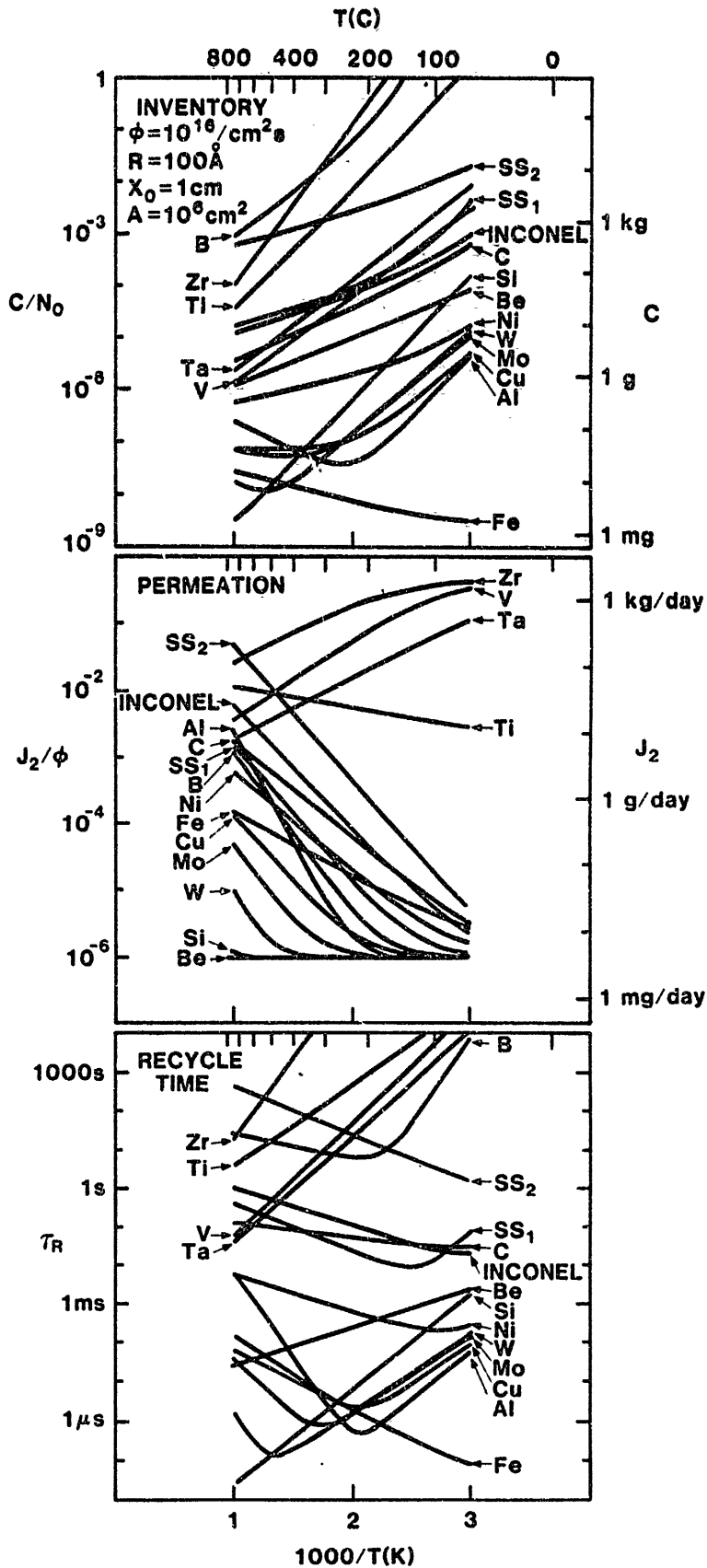


Fig.12. Recycle time, normalized permeation flux, and inventory for various materials in steady state for a 1 cm thick wall ($\phi = 10^{16} cm^{-2}s^{-1}$, $\alpha = 10^{-6}$) with $10^6 cm^2$ area.

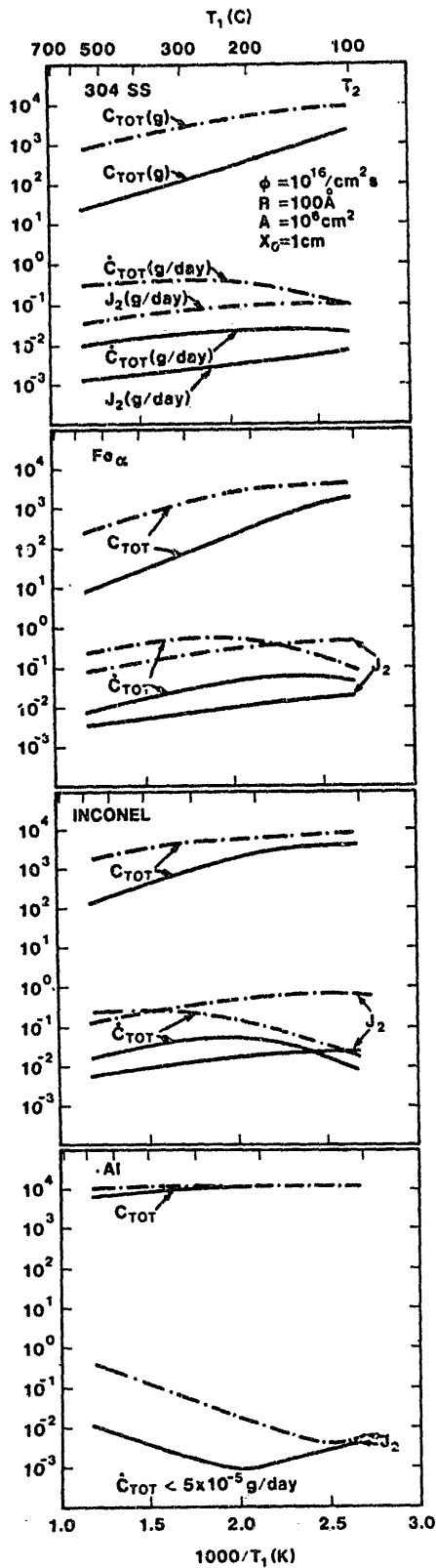


Fig.13. Inventory (C_{TOT}) permeation (J_2), and buildup rate (C) for $T_2 = 100$ C and varying T_1 for 304 SS, Fe, INCONEL and Al. These calculations are for a linear T profile. The solid and dashed curves correspond to sticking coefficients of 1 and 10^{-3} respectively.

PERMEATION REDUCTION FACTOR

$$J_2(T_1=T \neq T_2) / J_2(T_1=T_2=T)$$

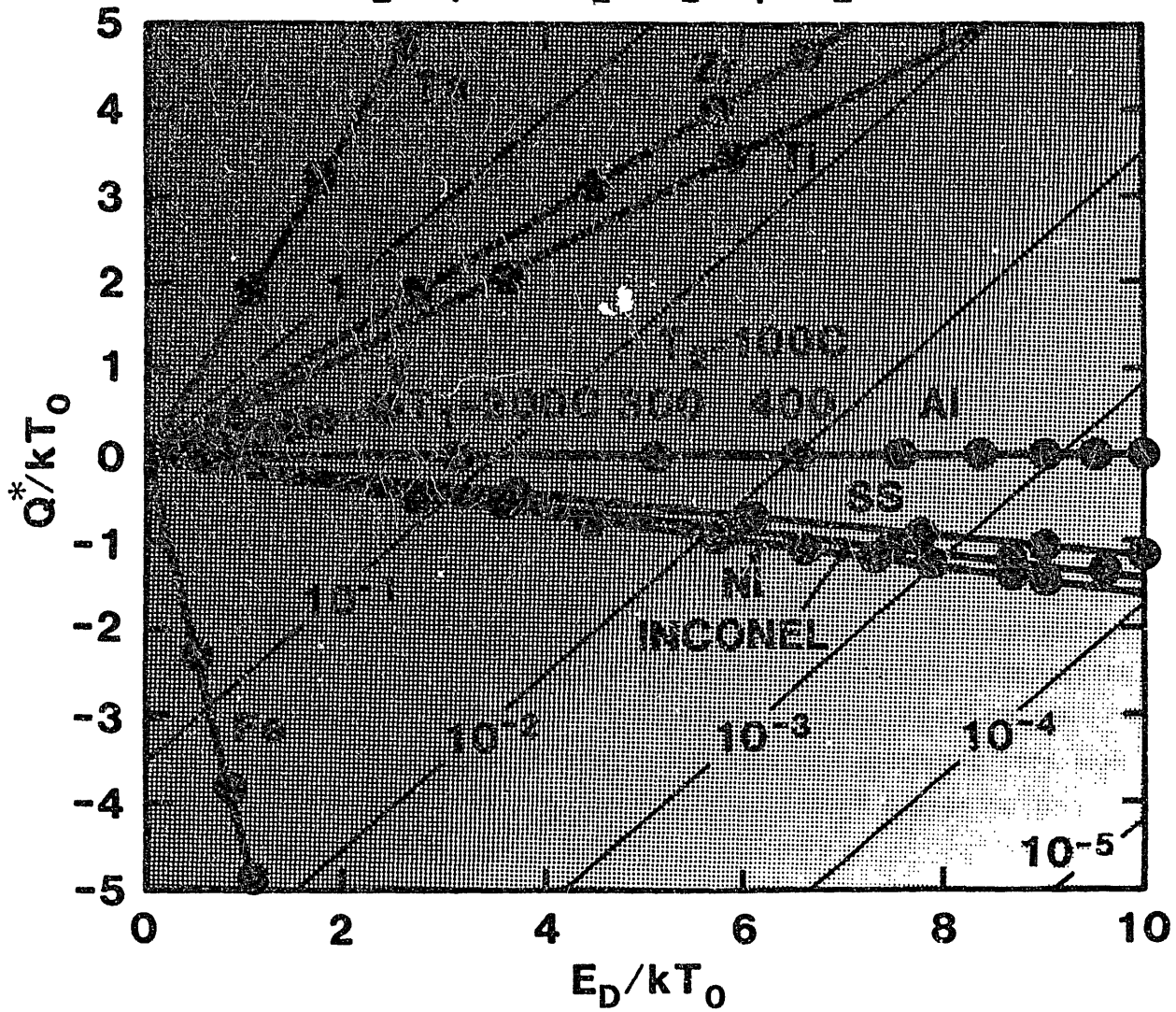


Fig.14. Contour plot of the permeation reduction factor vs Q^*/kT_0 and E_D/kT_0 . These calculations use the exponential approximation.

Synergisms in Surface Erosion - Session Summary

J. Bohdansky, J. Roth

Max-Planck-Institut für Plasmaphysik, EURATOM Association
D-8046 Garching/München, Federal Republic of Germany

Abstract

Chemical erosion of graphite under hydrogen ion bombardment and the sputtering of Mo and W by oxygen ions was discussed in the session on "synergisms on surface erosion". The invited contributions are reviewed and the current understanding of the different effects are summarized. The relevance of these effects to the impurity production in fusion devices is discussed.

INTRODUCTION

The session was devoted to synergisms in ion bombardment-induced erosion with the main emphasis on graphite material. An invited summary on chemical sputtering by Auciello /1/ was followed by invited contributions by Vietzke /2/ on the simultaneous interaction of atomic hydrogen and energetic ions and by Roth /3/ on the state of knowledge on radiation-enhanced sublimation of graphite. Subsequently, an invited contribution by Saidoh /4/ treated chemical effects in erosion of Mo and W due to bombardment by oxygen. These presentations were discussed at length. The papers and the discussions are reviewed below and an attempt is made to formulate current models on the chemical erosion mechanisms which evolved from new results presented both at the PSI conference and at the Workshop. The relevance of the results to fusion is also discussed.

A) CHEMICAL SPUTTERING

Chemical sputtering of graphite, i.e. the formation of volatile hydrocarbons in the interaction of graphite with hydrogen isotopes, has been reviewed recently /5/. At the 6th PSI conference and the subsequent workshop on synergistic effects, new experimental results were presented which lead to a better understanding of the basic processes. This summary is based primarily on results by Auciello et al. /1,6,7/ on the interaction of thermal atomic hydrogen with graphite, by Vietzke et al. /2,8/ on the simultaneous interaction of thermal atomic hydrogen and energetic ions and by Vietzke et al. /2,8/ and Auciello /7/ on the action of energetic ions only as well as on data from ref. /5/.

1. THERMAL ATOMIC HYDROGEN

This section will be mainly concerned with the action of atomic hydrogen, because measurable erosion of graphite by thermal molecular hydrogen is seldom reported. This section will be mainly concerned with the action of atomic hydrogen. However, depending on the origin source of atomic hydrogen, e.g. extraction from a plasma discharge /9/ dissociation at a hot filament /1,6,7,10/ or emission from a hot oven /2,8,11/, the graphite surface is also subject to some molecular hydrogen flux.

The data are presented mostly as reaction yields vs. temperature or reaction yields vs. atom fluence at a given temperature. The reported

erosion yields show large scatter in absolute magnitude, which is attributed /5/ to the different methods of hydrogen production, to the difficulties involved in determining the absolute flux of hydrogen atoms at the surface and to differences in the surface conditions of different graphites. More recent data by Auciello /1/, acquired under clean UHV conditions shows better agreement.

The yield data vs. temperature clearly fall into two groups: one group of data with a maximum yield value near 500 K and another group with a maximum around 800 K. It has been argued, that a shift in the position of the maximum may be explained by different hydrogen atom fluxes and hydrogen surface saturation effects /5/. However, in the data shown, the two groups of data correspond to two different fluences of hydrogen (see ref. /1/).

In the initial phase of hydrogen exposure the yield shows a maximum which decreases subsequently to a steady state value. Both the maximum and the steady state depend on the temperature. The initial peak (activated surface) increases up to a temperature of 800 K, whereas the steady state data show a maximum at 500 K (deactivated surface). Gould /10/ reported that after reaching the steady state value the surface can be re-activated by annealing above 1200 K. Though the precise nature of the activated surface state is unknown, the observation that at 1200 K all absorbed hydrogen is re-emitted has lead Gould to the conclusion that at large hydrogen coverage precursor states of the methane formation process may give rise to stable surface species, CH_n which if occurring in adjacent surface sites, could block further reaction with hydrogen.

On the basis of residual gas analysis it was previously concluded that CH_4 molecules are desorbed. It was shown by Vietzke et al. /8/ that predominantly CH_3 radicals are released. For the measurement it was required that the released molecules were detected before they could undergo any further reaction at an inner surface of the vacuum vessel. Although the CH_3 molecules must be assumed to be bound to the graphite surface by an energy of several eV, Vietzke et al. /8/ argue that the recombination energy in the transition from CH_2 to CH_3 may be high enough to desorb the CH_3 radicals. Earlier investigations by Balooch and Olander

/11/ using a modulated H^0 beam were explained by assuming the formation of methane to be proportional to the 3rd power of the surface concentration of hydrogen. This finding does not exclude the formation of CH_3 instead of CH_4 .

II. SYNERGISM BETWEEN THERMAL ATOMS AND ENERGETIC IONS

At the workshop, Vietzke /8/ presented further results on the synergistic effects between thermal hydrogen atoms and energetic ions. Also here, he reported ^{that} the release of the yield was found to increase with deposited energy into the surface layer. This increase was found for H, He, Ne and Ar ions. For Ar ions a factor of 50 increase in CH_3 yield was observed from that for H^0 alone (fig. 1). The yield from these activated state showed the same temperature dependence as the yield from the activated surface state for thermal hydrogen atoms alone (ct. ref. /1/).

The activation was retained immediately after the simultaneous Ar^+ irradiation was stopped, but decreased with further H^0 exposure. However, in contrast to the activated surface for thermal hydrogen atoms alone, degassing of the surface above 1200 K resulted in annealing of the active surface state. It is therefore concluded /8/, that Ar^+ ion bombardment facilitates the formation of precursors for the CH_3 formation. Vietzke et. al. /8/ propose that CH_2 complexes are formed during simultaneous ion bombardment and that the surface coverage may be of the order of 2 monolayers, independent of temperature.

Alternatively, the similar temperature dependence of the activated state in Auciello's data /6/ and the state of activation created during ion bombardment can be explained by the assumption that ion bombardment causes the site-blocking complexes to be removed thereby leading to a drastic increase of yield. Addition of thermal hydrogen after stopping the ion bombardment would lead to renewed formation of site-blocking complexes and consequently to a decrease of the erosion yield. Degassing of hydrogen above 1200 K would cause all precursors to anneal.

III. ENERGETIC HYDROGEN IONS

The yield of volatile hydrocarbons under energetic hydrogen bombardment is also shown in fig. 1. It is more than an order of magnitude higher than the synergistic action of thermal hydrogen atoms and Ar ions. The fact that the yield shows the same temperature dependence as that from activated surface sites would suggest a similar kinetics. But, Vietzke et al. /8/ found that CH₄ molecules are released here. They explain this observation by the assumption that the hydrocarbon is formed on inner surfaces of the graphite as explained below.

IV. SYNERGISM BETWEEN HYDROGEN IONS AND ATOMIC AND MOLECULAR HYDROGEN

Using different hydrogen isotopes Vietzke et al. /8/ showed that the synergistic action of atomic hydrogen and hydrogen ions leads to a drastic increase in reaction yield similar to the case of atomic hydrogen and argon ions. For atomic hydrogen and 5 keV D⁺ ions a much larger CH₃ yield is reported than for atomic hydrogen alone. Auciello et al. /7/ deduced a similar yield increase from a comparison of the yields with energetic hydrogen ions alone and with simultaneous atomic hydrogen.

Surprisingly the observed mass spectra showed little isotopically mixed molecules. Fig. 2a shows the mass spectrum obtained by simultaneous interaction of a flux of 2×10^{16} H⁰/cm²s and 4×10^{14} D⁺/cm² s with pyrolytic graphite. It is compared with the spectrum expected from a surface with equal concentrations of H and D (Fig. 2b). From such a surface the emission of CH₃ and CH₄ is much less probable than the emission of mixed molecules CH_nD_m. If, however, CH₃ and CD₄ are formed on different surfaces, a spectrum as shown in fig. 2c results. The peaks at mass 16 and 18 are due to recombination of CH₃ and dissociation of CD₄ in the quadrupole. This spectrum is very similar to the experimental one with the exception of a small mixed peak at mass 17.

Concerning the influence of molecular hydrogen, which inevitably is present in most experiments with atomic hydrogen, there were first reports by Auciello et al. /7/ , that simultaneous irradiation of graphite with hydrogen ions and exposure to molecular hydrogen leads to a considerable yield enhancement.

From these new experimental data the following picture emerges (Fig.3). Thermal atomic hydrogen reacts with graphite atoms at the surface to form CH_3 by sequential addition of hydrogen atoms to surface atoms /11/. Eventually CH_3 is released /8/. For high surface concentrations of hydrogen stable surface complexes are expected to be found by adjacent precursor radicals (like CH_2), thus decreasing the CH_3 yield to a steady state value /6,10/

Energetic hydrogen ion bombardment and synergistic action of atomic hydrogen and energetic ions is thought to accelerate the formation of the precursor either due to the deposited energy or by the elimination of the site-blocking effect, when the surface may be covered by one to two monolayers of CH_2 complexes /2/. The rate limiting step is then the addition of the third hydrogen atom in the formation of CH_3 . This formation should be linearly dependent on the surface concentration of hydrogen, in agreement with the successful empirical model by Erents et al. /12/. Energetic hydrogen or deuterium ions penetrate the surface and agglomerate at the end of range until a critical lattice concentration is reached. Hydrogen is then released through pores or microchannels and CH_3 or CD_3 is produced at the inner surface of these pores. On its way to the surface CD_3 combines with H or D in wall collision and eventually CD_4 or CD_3H is observed as reaction products.

B) RADIATION-ENHANCED SUBLIMATION

At temperatures above 1200 K a further increase of the erosion yield of graphite was observed /13,14 /. This effect has been termed radiation-enhanced sublimation. Thermal carbon atoms /14,15 / are released isotropically /13/. The yield was found to increase with increasing temperature (see fig. 3) and to be proportional to the energy deposited into the surface layer at a given temperature /16/. These data were reviewed on the Workshop on Synergistic Effects and a detailed model was presented by Roth and Möller /3,17 /.

I. ATOMIC MODEL AND COMPUTER SIMULATION

The model employed is taken from the radiation damage theory in graphite which was developed to explain the anisotropic dimensional swelling of

graphite under neutron irradiation /18/. The swelling is parallel and the contraction is perpendicular to the c-axis and shows roughly the same temperature dependence as the radiation enhanced sublimation yield /17/. The model assumes Frenkel-pairs are created in the material by the radiation and that^{that} the interstitials are very mobile between graphite planes already at room temperature, whereas vacancies become mobile only above 1200 K. Interstitials recombine with vacancies, diffuse to grain boundaries, or cluster into additional lattice planes at fixed nuclei. Vacancies may also cluster to form vacancy lines which collapse leaving no recombination centers for interstitials. The observed dimensional changes can be explained /18/ by assuming threshold displacement energy of 25-30 for the creation of a Frenkel-pair, 3.5 eV activation energy for vacancy diffusion and 10^{16} to 10^{17} fixed nuclei/cm³. For the case of ion bombardment, this model was slightly modified :

The surface represents a sink for both interstitials and vacancies. As a boundary condition the surface concentration of interstitials and vacancies has been set to zero. All interstitials arriving at the surface are assumed to evaporate. Thus the enhanced sublimation yield is given by the gradient of the interstitial concentration profile at the surface. The model calculations are compared with experimental data, in Fig. 4 as a function of temperature for bombardment with different ions and in Fig. 5 as a function of energy for bombardment with hydrogen and deuterium at 1800 K. The data used for the calculation are taken from literature and are given in table 1. The agreement between experiment and model calculation is good and lies within a factor of 2.

Table 1

Incident ion flux	$10^{16}/\text{cm}^2\text{sec}$
damage profile	TRIM code
displacement energy	25 eV
interstitial migration energy	0.3 eV
vacancy migration energy	3.5 eV
pre-exponential factor of interstitial and vacancy migration	7.1×10^{-4}
vacancy-interstitial and vacancy-vacancy recombination radius	0.21 nm

C. CHEMICAL EFFECTS IN SPUTTERING DUE TO OXYGEN

Saidhoh discussed sputtering experiments of oxide layers on metals (Mo, W) / 4/. The oxide layer was formed either by the implanted oxygen ions or by partial pressure of oxygen in the target chamber. The effects of the oxygen partial pressure on Mo targets was investigated. Both the target temperature and the oxygen pressure were changed in this experiment. Three different conditions could be identified: (1) If an oxide film was formed the Mo sputtering was reduced mainly due to a depletion of Mo in the oxide layer. (2) At very high temperatures ($\sim 1400^\circ\text{C}$) the oxide was observed to evaporate and the erosion yield was given by the sputtering yield of pure Mo superimposed on the erosion yield caused by oxidation and the evaporation of the oxide. (3) At intermediate temperatures a mixture of oxide and metal sputtering occurs together with oxide evaporation. The superposition is not linear (synergistic effects) and the interaction is not well understood.

Basically the same behaviour was found when the target was bombarded by CO^+ or O^+ ions. In fig. 6 the Mo sputtering yield is shown as a function of target temperature for different ion energies. The data are taken from different references /4,19/.

At low temperature the sputtering yields are lower than expected for physical sputtering from a pure Mo surface. The expected values are indicated by the dotted lines at the right hand side of the graph and are calculated from a semi-empirical expression /20/. At very high temperature the data seem to approximate the superposition of the physical sputtering of pure metal surfaces and the evaporation of MoO_3 as indicated by the dashed line. In the intermediate range the superposition of mixed processes may cause temperature dependence as observed. It should be noted that the sputtering of a solid oxide shows a similar temperature dependence. Kelly and Lam explained this behaviour by a combined action of physical sputtering and thermal spikes /21/.

D) RELEVANCE FOR FUSION

I. CHEMICAL SPUTTERING

Due to the extensive use of graphite as limiter materials, investigations of the erosion of graphite by energetic hydrogen and the related synergistic effects are of great importance for current fusion experiments. The experiments discussed above emphasize this importance. The enhanced erosion by chemical effects in particular can result in an intolerable high release of impurities.

One should be cautious, though, because an uncritical use of the presented results for estimating the erosion of graphite limiters can be misleading. The irradiation conditions in a fusion device are different from the conditions of the experiments presented at the workshop. The hydrogen flux to a limiter surface is orders of magnitude higher ($10^{17} - 10^{19}$ particles $\text{cm}^{-2} \text{ s}^{-1}$) and the particle energy is considerably lower (about 10 eV to 100 eV) compared to the present experiments. Experimental results show the methane yield to be flux-dependent (Fig.7), in agreement with a model for the chemical erosion based on methane formation. The model was given by Erents et al./12/ and shows reasonable agreement with the measured flux dependence of the methane yield in the range of $10^{-15} - 10^{-17} \text{ H}^+/\text{cm}^2 \text{ s}$ (Fig. 7). The erosion yield for graphite measured by the weight loss method (also shown in Fig. 7) does not agree with the model so well, the experimental data do not reflect a flux dependence of the erosion yield.

A discrepancy between the methane yield and the erosion yield of graphite is also seen in the energy dependence of the yield. In fig. 8 the chemical erosion yield at peak temperature, the corresponding methane yield; and the yield for physical sputtering (300^oK) are compared at a particle flux of 10^{15} D⁺/cm² sec. Chemical and physical erosion yield differ by a factor of 10. According to the Erents model /12/ this difference should disappear at a flux of 10^{18} D⁺/cm²sec (dashed line in fig. 8) as the chemical sputtering yield is reduced (see fig. 7) because the physical sputtering yield does not depend on the particle flux.

As reported at the workshop, the erosion yield is also enhanced by the combined action of thermal and energetic hydrogen. Such an effect may not be of importance for the chemical erosion of graphite limiters. The flux of neutral particles to the limiter is small compared to the flux of hydrogen ions. The situation would be different for the first-wall where the energetic and thermal particles are mainly neutral and the low energy component can be high.

II. RADIATION-ENHANCED SUBLIMATION

Chemical erosion occurs at temperatures around 600^oC. At temperatures above 1000^oC an increase in the erosion yield was observed which can be explained by an enhanced sublimation /13/. Roth presented a model for this enhanced sublimation at the workshop. The model is based on the generation and diffusion of vacancies and interstitials. Computer calculations based on this model show good agreement with experimental results /17/ (figs. 4 and 5). Such calculations also show a flux dependence of this effect /22/. In Fig. 9 calculated yield values for 1800^oC and a flux of 10^{16} , 10^{17} , 10^{18} D⁺/cm²sec are compared to the physical sputtering at room temperature. The effect is reduced at higher fluxes also in the case of radiation-enhanced sublimation. Due to the higher threshold of this effect the yield for a particle flux of 10^{18} cm⁻² sec⁻¹ is comparable with the physical sputtering for ion energies \sim 50 eV.

The calculations for chemical sputtering and radiation enhanced sublimation together with estimations as discussed previously indicate only a moderate importance of chemical effects for the erosion of graphite limiters in

fusion devices. However, all these estimates are based on extrapolations which contain a certain degree of uncertainty. Experiments at high particle flux are needed in order to give a decisive answer about the importance of the effects here discussed.

III. OXYGEN SPUTTERING

In nearly all fusion plasma experiments oxygen is one of the main plasma impurities. Therefore oxygen sputtering is important in most fusion devices. Due to the rare events of charge exchange neutralization for multiple charged oxygen ions, oxygen sputtering may be mainly important on limiters and divertor plates.

As suggested above, the physical sputtering by oxygen ions is modified mainly by the formation of oxide films and/or by the evaporation of the oxide. The latter depends on the target temperature.

In the case of graphite the oxide is volatile at room temperature and the erosion is caused by the combination of physical sputtering and the evaporation of the oxide /19/. At higher temperature (750°C) no change in the erosion yield was found as both processes are independent of temperature in the investigated temperature range.

For metals, e.g. for Mo, the sputtering process is rather more complex. However, if the plasma is sufficiently clean, the erosion of the limiter or divertor plates may be dominated by hydrogen sputtering in which case the formation of an oxide film may be prevented. Physical sputtering of a clean surface by oxygen may be the only erosion mechanism for the oxygen bombardment. The sputtering yield of this process can be estimated from the measured yield data for Ne, by using semi-empirical expressions for the sputtering yield or by computer calculations /23/. At high oxygen impurity levels the situation is different. In this case a better understanding of the effects is necessary in order to make estimates for the impurity production at the limiter/divertor subjected to oxygen ion bombardment.

References

1. O. Auciello, "Synergism in Materials Erosion due to Multispecies Impact" (invited)
2. E. Vietzke, "Simultaneous Interaction of Atomic Hydrogen and Energetic Ions on Graphite"
3. J. Roth, "Radiation-Enhanced Sublimation of Graphite"
4. M. Saidoh, "Chemical Effects in Erosion of Mo and W Induced by Energetic Oxygen.
5. J. Roth, in: Sputtering by Particle Bombardment II" ed. R. Behrisch, TAP 52, Springer-Verlag (Berlin 1983)
6. C. S. Pitcher, O. Auciello, A. A. Haasz, P. C. Stangeby, presented at the 6th PSI Conference, Nagoya, Japan (1984) to be published in J. Nucl. Mat.
7. A. A. Haasz, O. Auciello, P. C. Stangeby, I. S. Youle, presented at the 6th PSI Conference, Nagoya, Japan (1984) to be published in J. Nucl. Mat.
8. E. Vietzke, K. Flashkamp, V. Philipps, presented at the 6th PSI Conference, Nagoya, Japan (1984) to be published in J. Nucl. Mat.
9. D. E. Rosner, H. Allendorf, Proc. Int. Conf. Heter. Kinetics at Elevated Temp. (Univ. Pensilvania 1969) p. 231
10. R. K. Gould, J. Chem, Phys. 63, 1825 (1975)
11. M. Balooch, D. R. Olander, J. Chem, Phys. 63, 4772 (1975)

12. S. K. Erents, C. M. Braganza, G. M. McCracken, J. Nucl. Mat. 63, 799 (76)
13. J. Roth, J. Bohdansky, K. L. Wilson, J. Nucl. Mat. 111 & 112, 775 (1982)
14. V. Philipps, K. Flaskamp, E. Vietzke, J. Nucl. Mat. 111 & 112, 781 (1982)
15. E. Vietzke, K. Flaskamp, M. Hennes, V. Philipps, Nucl. Instr. Meth. B2, 617 (1984)
16. J. Roth, J. B. Roberto, K. L. Wilson, J. Nucl. Mat. 122 & 123, 1447 (1984)
17. J. Roth, W. Moller, presented at the IBMM 84, Cornell University, Ithaca, NY (1984) to be published in Nucl. Instr. Methods B.
18. B. T. Kelly, Carbon 15, 117 (1977)
19. E. Hechtl, J. Bohdansky, J. Nucl. Mat. 122 & 123, (1984) 1431
20. J. Bohdansky, Nucl. Instr. Methods in Phys. Res. B2 (1984) 587
21. R. Kelly, N. Q. Lam, Radiat. Eff. 18, (1973) 37 and ibid 32 (1977) 91
22. W. Moller, priv. communication
23. J. P. Biersack, W. Eckstein, Appl. Phys. A 34 (1984) 73
24. J. N. Smith, C. H. Meyer, J. Nucl. Mat. 76 & 77, (1978) 193

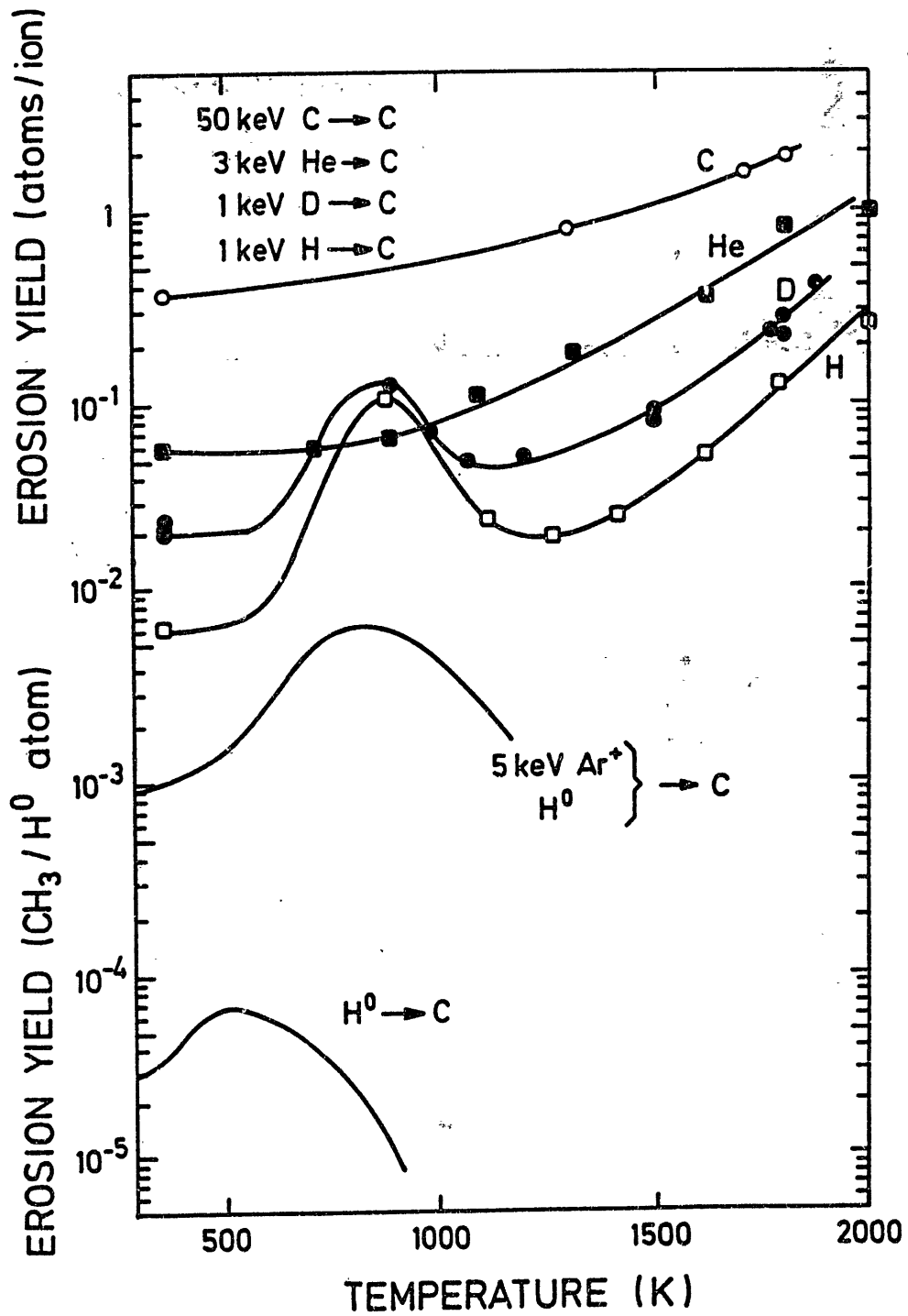


Fig. 1 The chemical erosion yield versus graphite temperature for different irradiation conditions. The data are taken from ref. / 8,13,16 /.

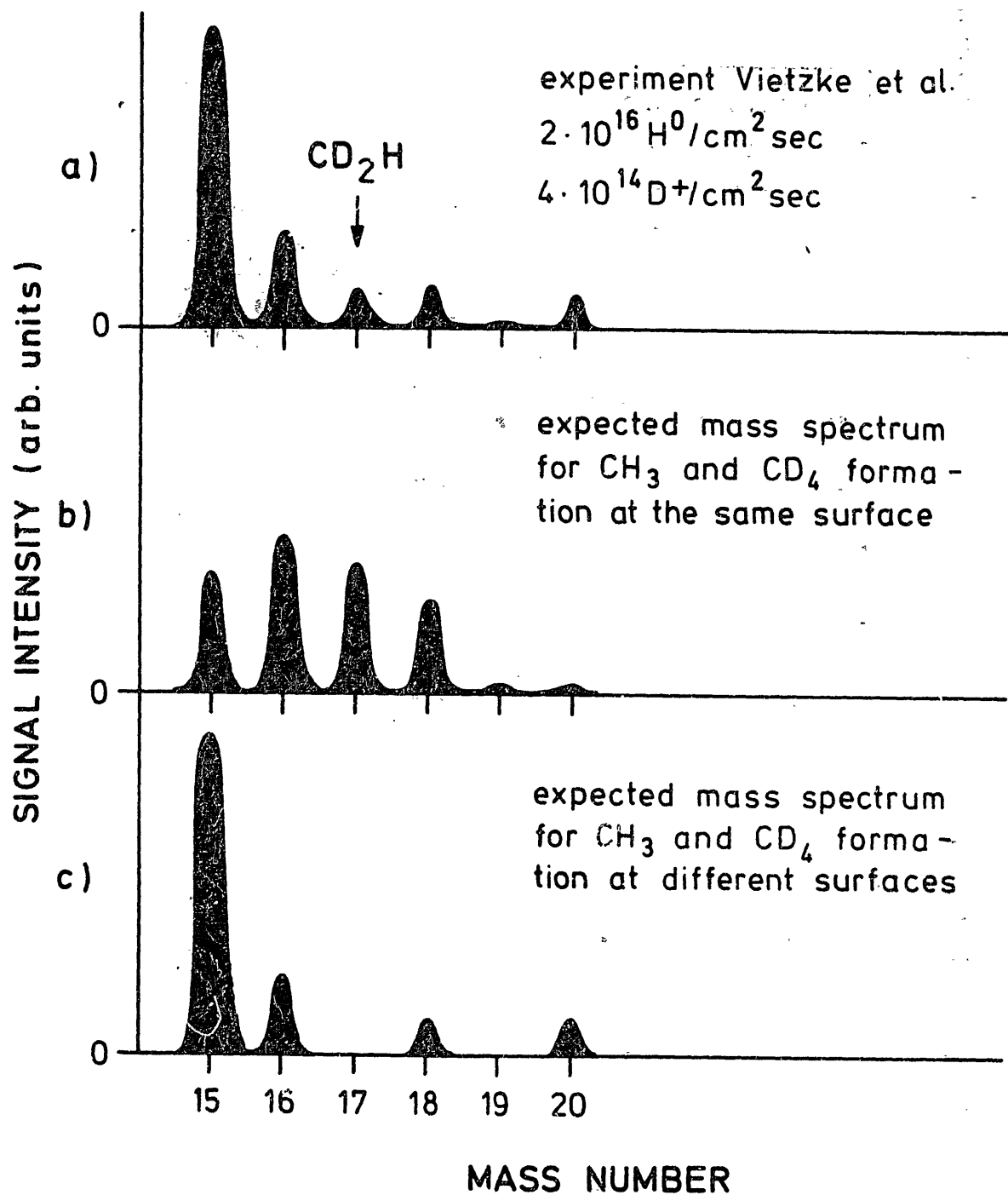


Fig.2 Measured (a) / 6/ and constructed (b+c) mass spectra for simultaneous H^0 and D^+ bombardment of graphite. The assumption of CH_3 and CD_4 formation at the same (b) or different (c) surfaces is made for the constructed spectra.

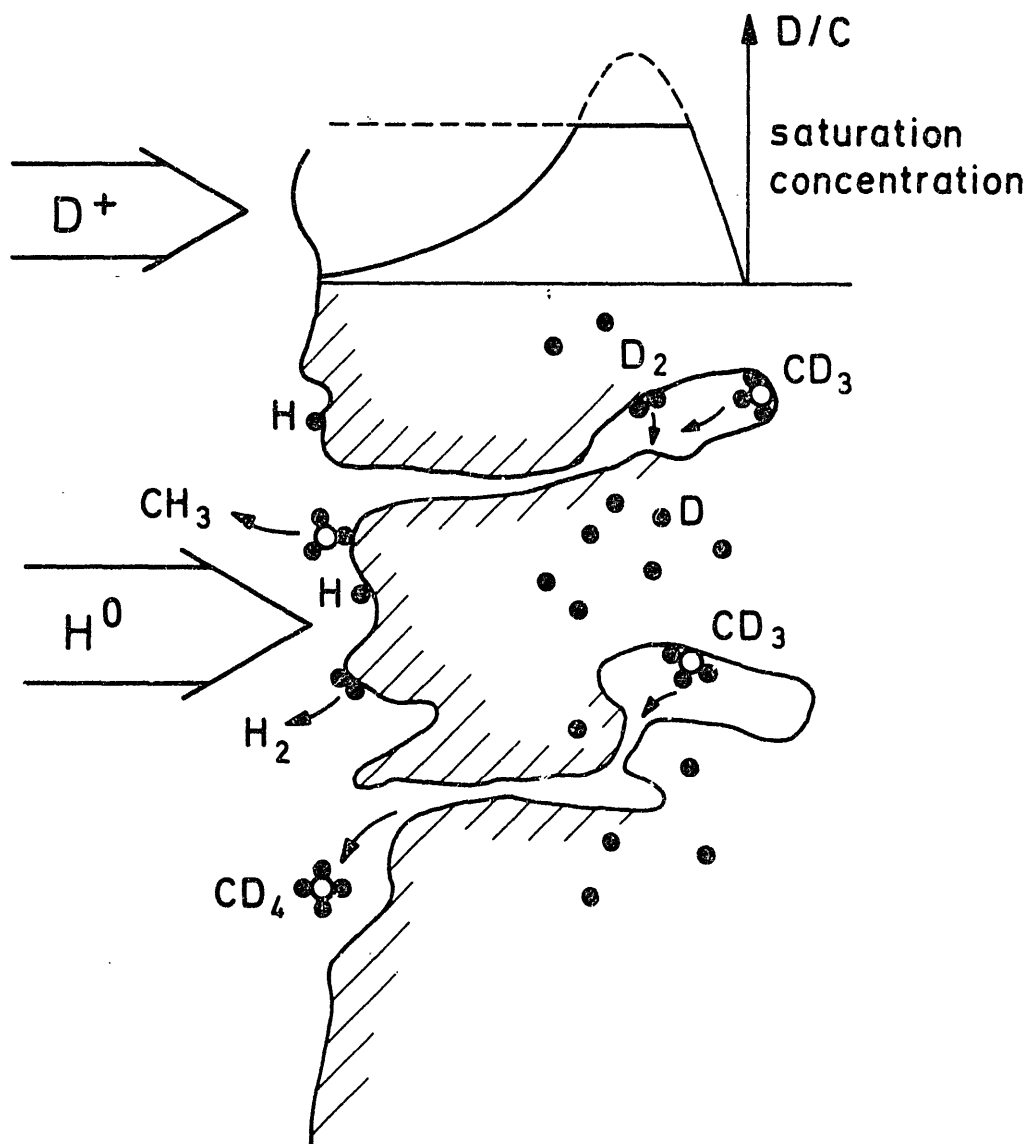


Fig.3 Schematic model for simultaneous bombardment of carbon with hydrogen atoms and deuterium ions. Implanted deuterium is released through channels and pores where it can form CD_3 and recombine to CD_4 on its way to the surface. Atomic hydrogen, however, forms CH_3 at the front surface only. Thus, only little mixed molecules are formed.

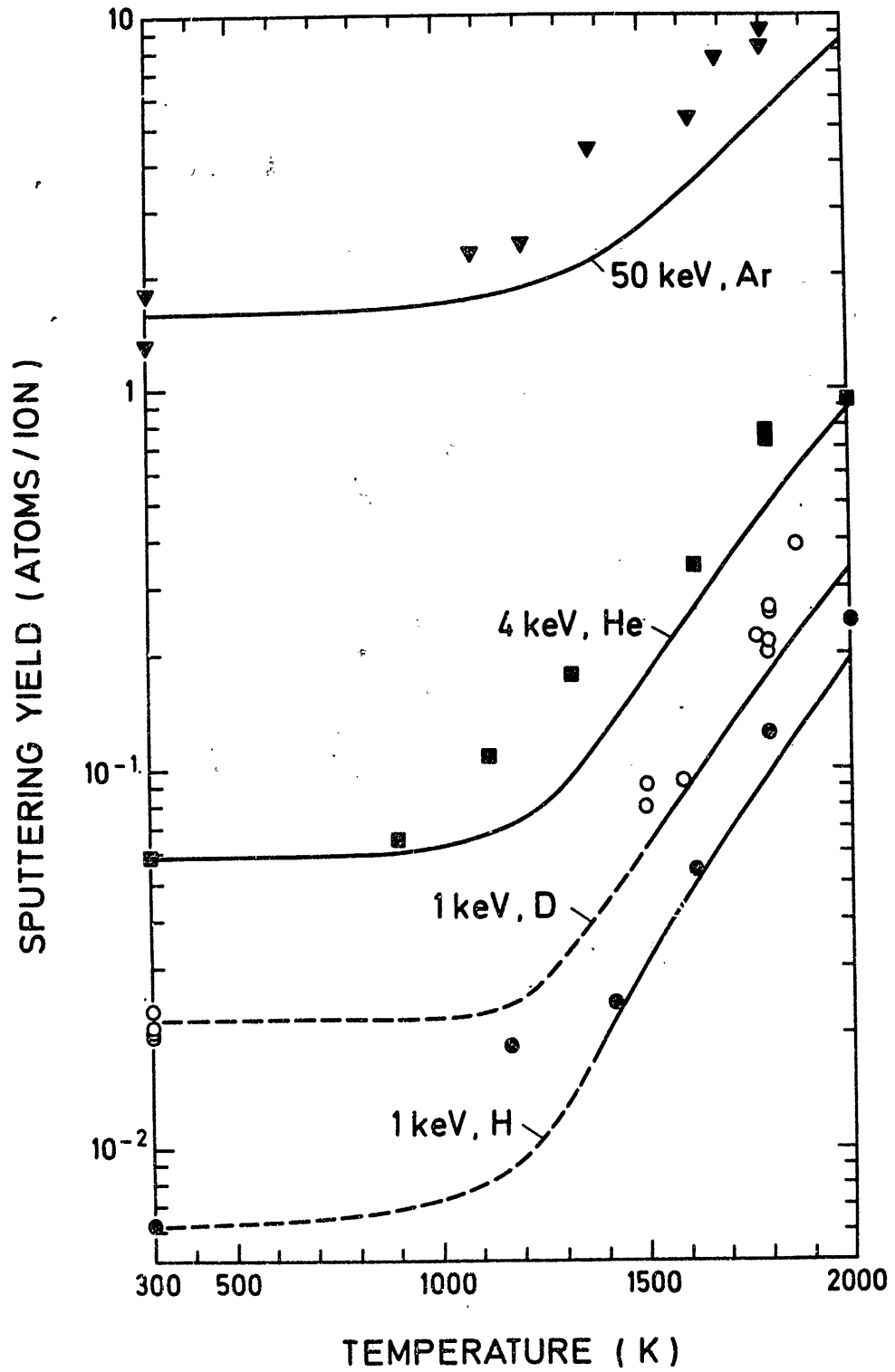


Fig.4 Comparison of model calculations /17/ and measured data /11, 14/ for the radiation enhanced sublimation of graphite by different ions. The yield is given in dependence of the temperature.

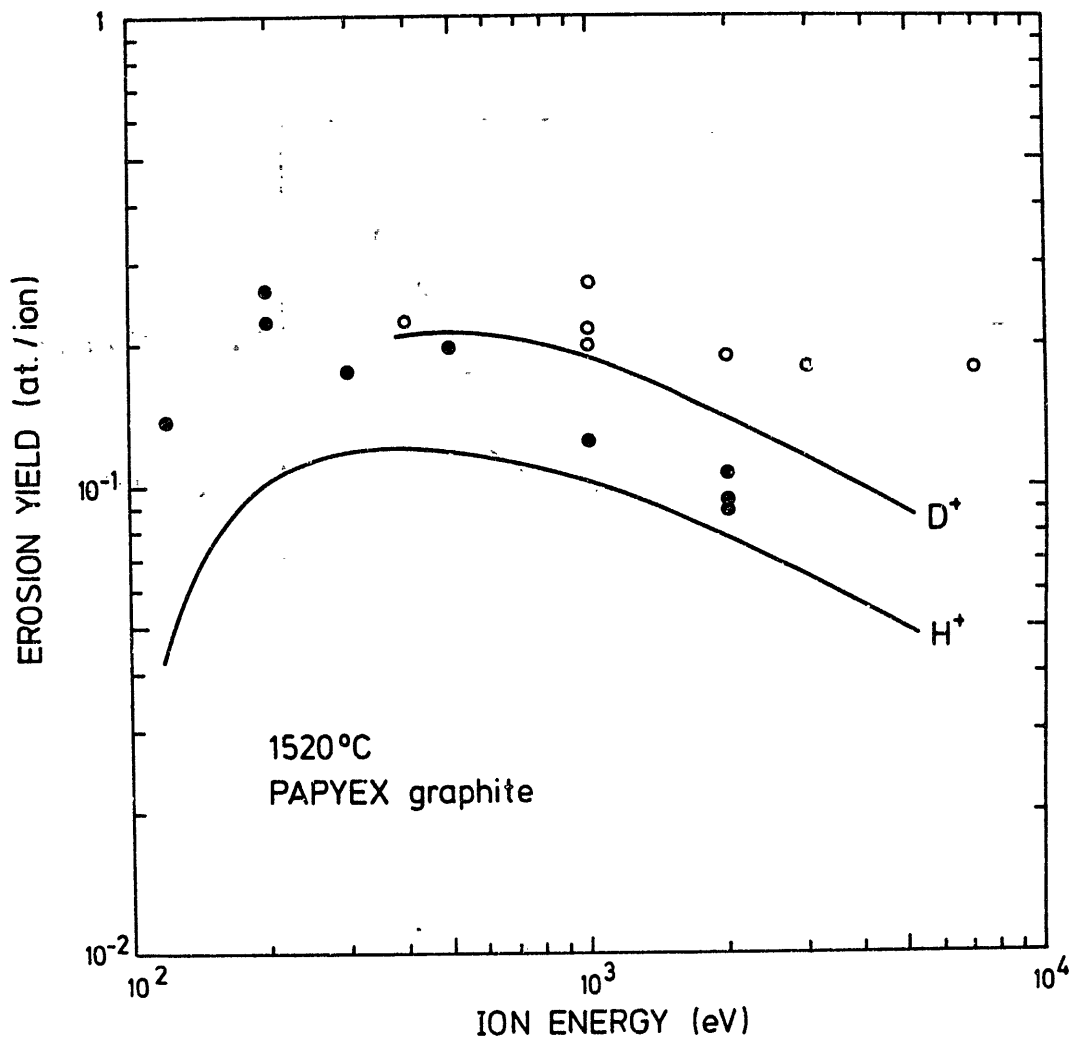


Fig.5 Comparison of model calculations /17/ and measured data /13,16/ for the radiation enhanced sublimation of graphite at 1520°C. The yield is given for H⁺ (full points) and D⁺(open points) in dependence on ion energy.

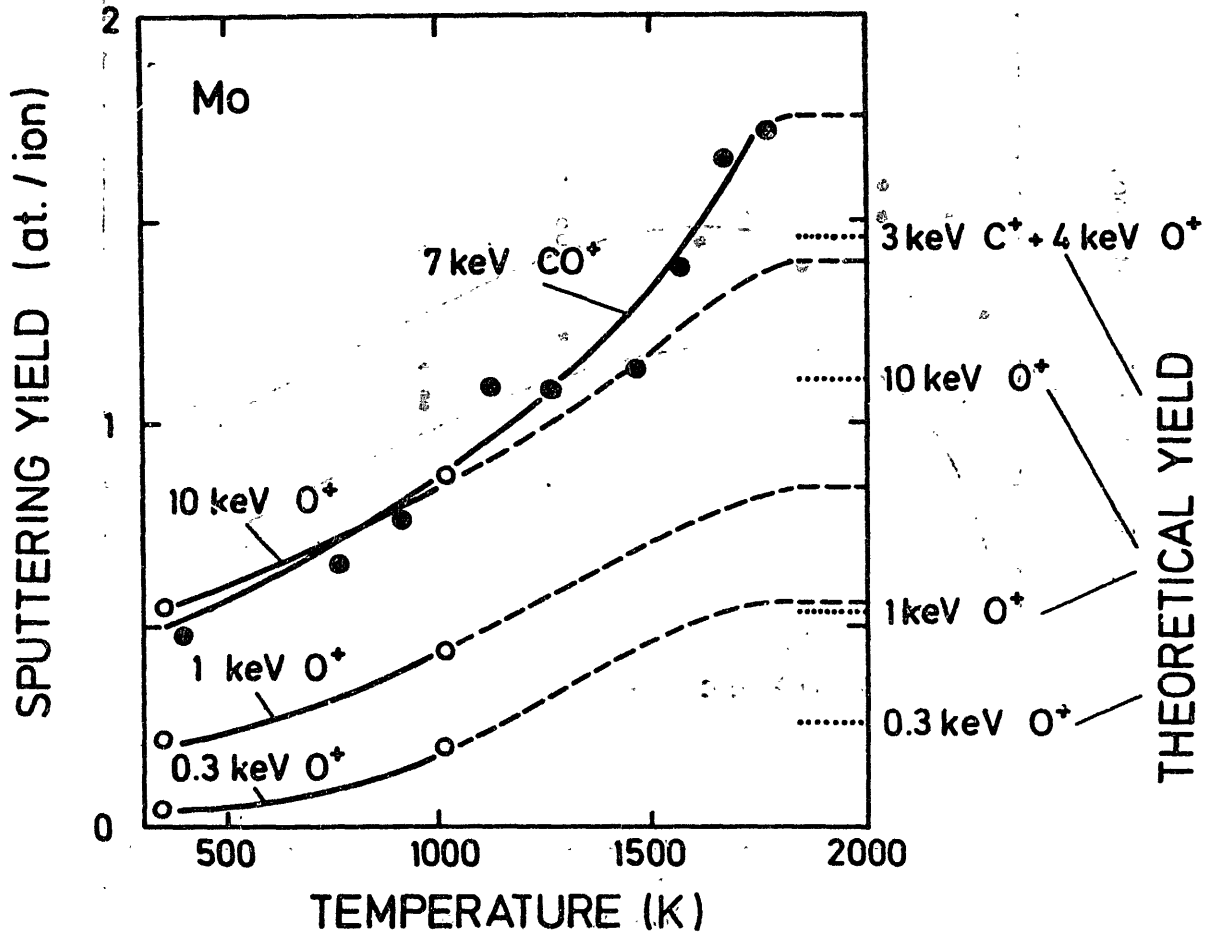


Fig.6 The O⁺ and CO⁺ sputtering yield of graphite in dependence of temperature. The data are taken from ref. /4/ (full points) and 119 (open points). Extrapolations are taken according to /20/.

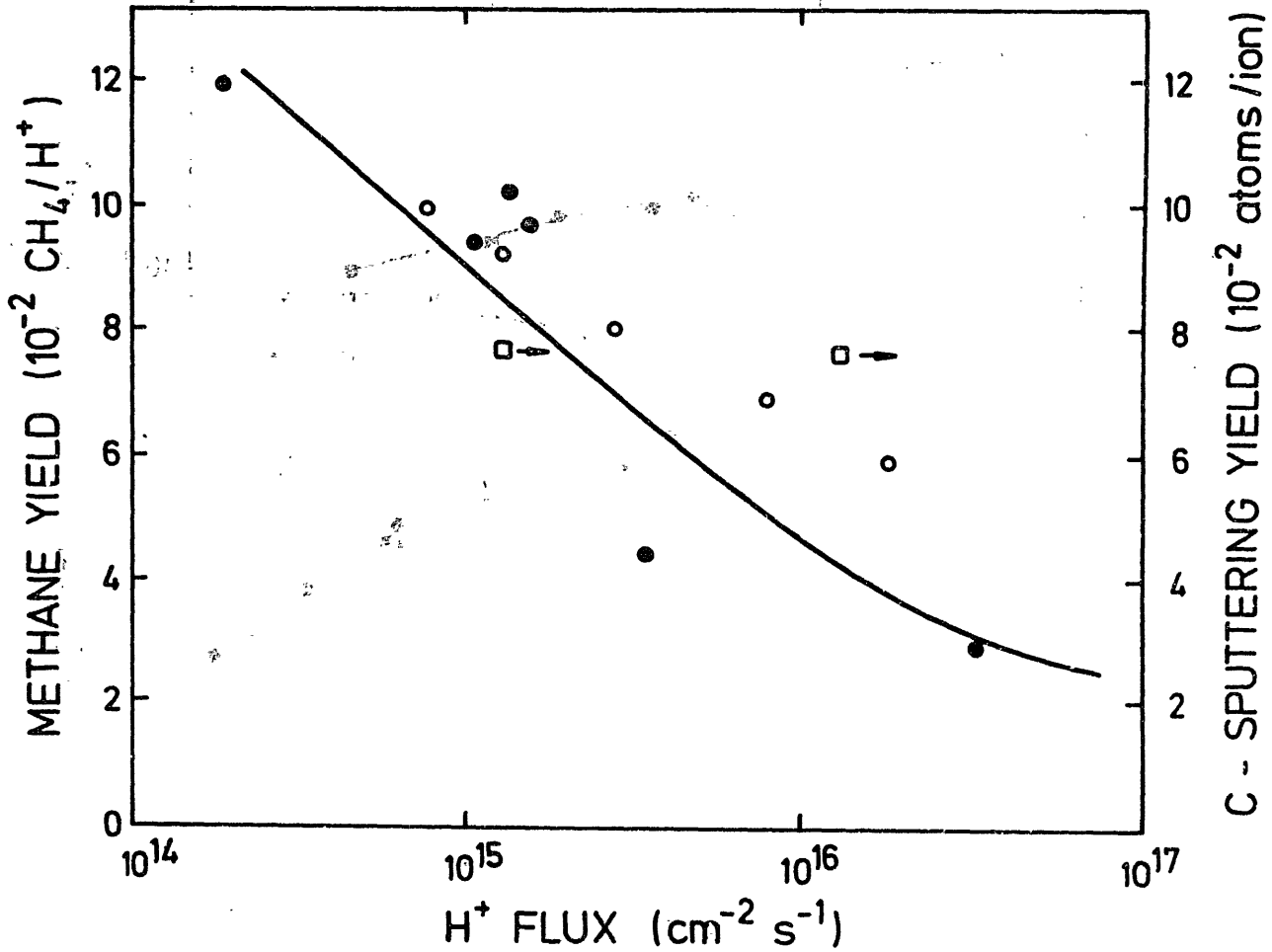


Fig.7 Collection of different methane yield data by Smith and Mayer (full points) /24/ for different hydrogen fluxes as compared to the flux dependence of the yield in the model by Erents et al. (solid line). Recent values for methane formation of 2 keV H^+ ions are also given (open points). Data for the carbon yield gained by weight loss measurements are also shown (open square).

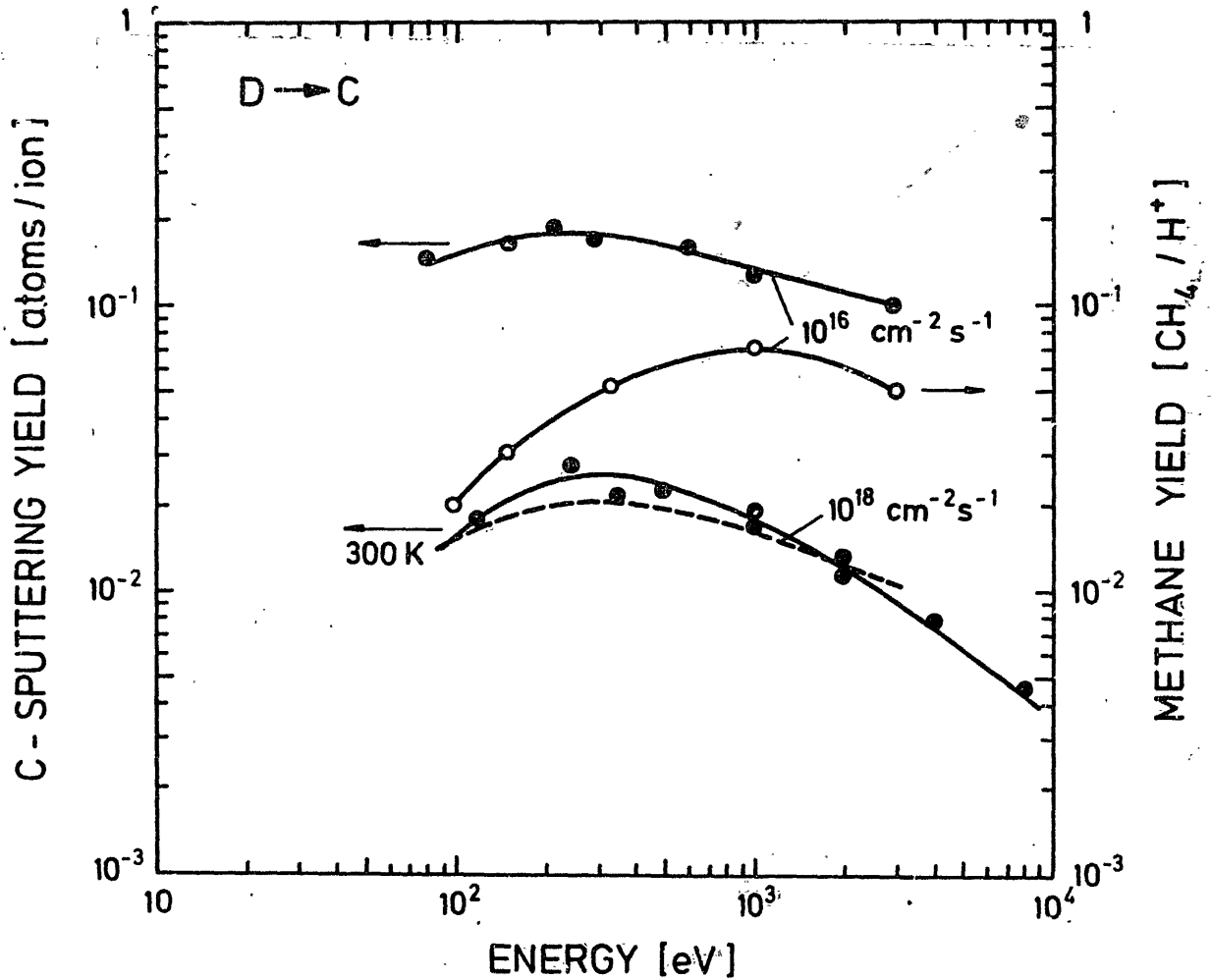


Fig. 8 The chemical erosion yield at peak temperature, (full points) the methane yield (open points) and the yield for physical sputtering (300^oK) are compared. The data are given in dependence of ion energy. All data are given at a particle flux of 10¹⁵ particles per cm² and sec. The dashed line gives the estimated chemical sputtering yield for a flux of 10¹⁸ particles per cm²sec. according to the model of Erents /12/.

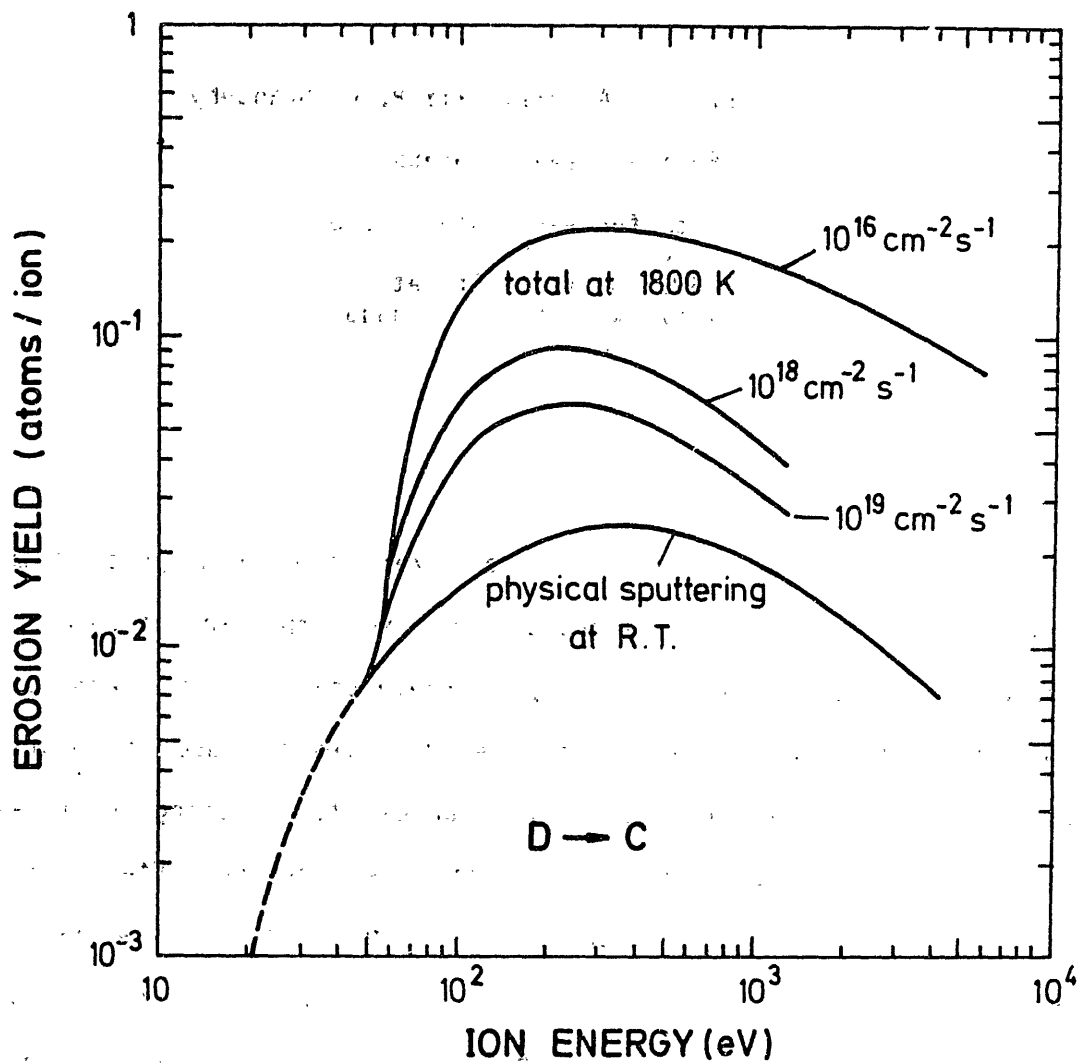


Fig.9 Comparison of physical sputtering and radiation enhanced sublimation at 1800°K for graphite bombarded by D^+ ions. The yield is given versus ion energy for three different ion fluxes /22/.

SYNERGISM IN MATERIALS EROSION
DUE TO MULTISPECIES IMPACT

O. Auciello, A. A. Haasz and P. C. Stangeby

Fusion Research Group

Institute for Aerospace Studies
University of Toronto
4925 Dufferin Street
Downsview, Ontario, Canada
M3H 5T6

Abstract

Plasma-surface interaction phenomena have become a subject of major interest because of their relevance in two important technological developments of recent decades, viz, microelectronics and thermonuclear fusion. Microelectronic fabrication often involves the use of relatively low-pressure/low-temperature plasma discharges for etching micron-size features in integrated circuits; here erosion is a desired effect. Fusion plasmas, by contrast, cause erosion of the fusion device inner walls, which is generally not desirable. In both cases surfaces are bombarded simultaneously by plasma species which include ions, neutral atoms, electrons and photons, which might lead to enhanced erosion due to synergistic effects.

Work performed to date suggests that similar chemistry may be involved in the erosion process associated with some semiconductor and fusion related materials: SiF_4 , SiCl_4 and CH_4 are, for example, some of the principal species evolving from Si and C surfaces, causing the observed erosion. Considerable effort has been expended on studies involving synergistic

effects for semiconductor fabrication. Research on synergism related to the erosion of fusion materials (C and carbon compounds) commenced comparatively recently; however, its importance has been increasingly recognized, and evidence of possible synergistic erosion of graphite has recently been obtained in the PLT fusion device.

In light of the interdisciplinary nature of the subject, experimental and theoretical work on synergistic effects in erosion of both semiconductors and fusion materials will be critically reviewed here in an attempt to unify concepts related to results and mechanisms proposed to explain the observed phenomena, and to explore possible new avenues of research.

1.0 INTRODUCTION

2.0 CHEMICAL EROSION

2.1 Chemical Erosion of Materials by Low-Energy Species

- (a) General Mechanisms for Sub-eV Atoms - Surface Reactivity
- (b) Temperature Dependence of Erosion Yield

2.2 Chemical Erosion of Materials by Energetic Reactive Ions

- (a) Semiconductor Materials
- (b) Fusion Materials (Carbon)

3.0 ION-INDUCED SYNERGISMS

3.1 Experimental Evidence

- (a) Semiconductor Materials
- (b) Fusion Materials (Carbon)

3.2 Models for Ion-Induced Synergisms

- (a) Semiconductors
- (b) Fusion Materials (Carbon)

4.0 ELECTRON-INDUCED SYNERGISMS

- (a) Semiconductor Materials
- (b) Fusion Materials (Carbon)

5.0 PHOTON-INDUCED SYNERGISTIC EFFECTS

- (a) Semiconductor Materials
- (b) Fusion Materials (Carbon)

6.0 CONCLUSIONS

1.0 INTRODUCTION

The erosion of surfaces due to the interaction of particles and electromagnetic radiation with materials has become a subject of major interest, and therefore the object of extensive studies, as a consequence of the relevance of erosion processes in two important technological developments of recent decades, viz, microelectronics and thermonuclear fusion. The scope of this review is limited to chemical reactions between reactive gaseous species and solid surfaces leading to the formation of volatile molecules and consequently surface erosion. This erosion process is distinct from physical sputtering, which results in surface erosion by ejection of atoms due to momentum transfer only. Chemical reactions which lead to volatile products involve surface processes which occur in complicated plasma environments for both semiconductor and thermonuclear fusion technologies. Surfaces exposed to these plasmas are generally bombarded, simultaneously, by a combination of particles [ions (inert and reactive), neutrals (reactive), electrons] and photons. In the case of fusion, neutrons will have to be added to the list of particles in future reactors. Device fabrication in microelectronics often involves the use of relatively low temperature plasma discharges, which are used to etch micron-size features in integrated circuits;¹ here erosion is a desirable effect. Fusion plasmas, by contrast, produce erosion of the fusion device inner walls, which is generally not desirable.²⁻⁵

In both cases, surfaces are bombarded simultaneously by plasma species producing, generally, an enhanced chemical erosion due to synergistic effects.^{1,6,7} These will be defined here in accordance with the general consensus reached at a recent Workshop on Synergistic Effects,⁸ i.e., synergism relates to phenomena where the combined effect of independent

processes is greater than the linear superposition of the same effects when occurring separately.

Ion- and electron-assisted etching, as employed in microelectronics, benefit from the directional nature of these energetic particles which impact on a surface immersed in a plasma. This effect is used to advantage in many applications where microcircuit fabrication requires the etching of patterns with vertical sidewalls and little or no undercutting of masked features.^{1,9} It is generally accepted among researchers in microelectronics technology that ion and electron bombardment accelerates etching in many gasification reactions occurring on surfaces impacted by sub-eV reactive species (F, Cl, etc.), which are generally produced in plasmas fed with appropriate gases (F₂, XF₂, CF₄/O₂, Cl₂, CCl₄, CF₃Cl, etc.). However, it is not totally clear at present, in most cases, what the underlying mechanisms responsible for this erosion enhancement might be. In principle, ion bombardment may accelerate any one or all of the steps involved in etching,¹⁰ these steps being: (1) non-dissociative adsorption of sub-eV gas-phase species on the surface of the material etched, (2) dissociation of the adsorbed species, i.e., dissociative chemisorption, (3) reaction between adsorbed atoms and the surface to form an adsorbed product molecule, (4) desorption of the product molecule into the gas phase, and (5) the removal of non-reactive residues that may be left on the surface. Any one of the steps mentioned above may be the rate limiting one to the overall erosion process, and the sensitivity of the rate limiting step to ion, electron, and/or photon irradiation will determine whether or not an enhancement of the overall etching reaction occurs.

Not only particle-assisted, but also photon-enhanced etching of semiconductors (using visible or UV lasers) was observed in early

studies,^{11,12} although it was only recently that its potential application in microcircuit fabrication was demonstrated.¹³⁻¹⁵ An important attribute of this technique is that high-spatial resolution etching can be accomplished by "direct writing", i.e., without the use of photolithography.¹³ However, laser-enhanced chemical etching is still rather slow in many cases, when compared to particle-assisted erosion.¹⁵

In contrast to the microelectronics technology case, erosion of inner walls in fusion devices is generally an undesirable effect. The surface erosion is produced, in this case, by simultaneous bombardment of reactive hydrogenic ions and neutrals (H^+/H^0 and isotopes), helium and impurity ions, neutrons (on future devices), electrons, and photons. This multispecies impact may produce, as shown in recent laboratory simulations,^{6,16-18} significant synergistic effects which lead to an enhanced erosion of carbonaceous materials currently being used in several major fusion devices, and projected for future machines. In fact, evidence for synergistically-induced enhanced erosion of carbon, has recently been noted in the PLT fusion device. An abnormally high erosion was observed on the leading edge of a carbon probe cap exposed to RF-heated plasmas in PLT; model calculations indicate that synergism between the thermalized reactive plasma and fast ions might be responsible for this effect. Clearly, better understanding of this phenomenon will be necessary if carbonaceous materials are to find continuing use in fusion.

Work performed to date^{1,7,8-22} suggests that similar chemistry may be involved in erosion processes associated with some semiconductor and fusion related materials; for example, SiF_4 , $SiCl_4$, and CH_4 have been identified as some of the main species evolving from semiconductor and carbonaceous surfaces, causing the observed erosion. For the latter case, recent

results^{6,16,18} suggest that CH₃ may be the main desorbing species. However, the basic mechanism for the formation of CH₃ is still expected to be similar to that proposed for semiconductor related species. Considerable effort has been expended on studies involving synergistic effects in relation to semiconductor fabrication. By comparison, work on synergism related to the erosion of fusion materials has not been as extensive; however, its importance has been recognized recently and efforts are presently increasing in this area of research.

In light of the interdisciplinary nature of the subject, experimental and theoretical work on synergistic effects in erosion of both semi-conductors and fusion materials will be reviewed here, in an attempt to unify concepts related to results and mechanisms proposed to explain this phenomenon and to explore possible new avenues of research. Additionally, chemical erosion due to single species impact by sub-eV reactive atoms and energetic reactive ions will be briefly reviewed as these exposures involve processes germane to synergism.

2.0 CHEMICAL EROSION

Enhanced erosion of many solid materials may result from the simultaneous interaction of ions, neutrals, electrons, and/or photons with surfaces. Ions considered here (whether chemically reactive or not) have generally high enough energies (10's or 100's eV) to enable them to displace lattice atoms in the material. Electrons and photons, on the other hand, may be more efficient in activating electronic excitations, while neutrals (usually reactive species) are characterized by energies from sub-eV to keV range, and presumably behave as ions. Although the concept of synergism has been mainly associated with processes involving the simultaneous bombardment of surfaces by combinations of energetic (reactive or not) and low energy

reactive species from the gas phase, electrons and photons, in principle, synergism may also occur when incoming particles interact with "reactive" species previously implanted in the material and subsequently diffusing to the surface. In fact, chemical erosion of carbon, for example, under energetic ion (H^+ , D^+ or eventually T^+) bombardment alone,²³⁻³⁸ may be partially due to a continuously occurring synergistic effect between the incoming ions and those previously implanted.

An accurate understanding of erosion mechanisms due to single species impact by low energy (0 to 10's eV) and energetic particles ($\gtrsim 100$ eV) may be useful in order to reach a better comprehension of synergistic effects. Therefore, a brief review on etching/erosion by the individual species mentioned above will be presented here as an introduction to the main subject of the paper, in such a way as to establish a common framework for the understanding of erosion of semiconductors and fusion materials. For the latter case, only carbon and carbonaceous compounds, and hydrogenic species impact will be considered here.

2.1 Chemical Erosion of Materials by Low-Energy Species

Historically, chemical reactions between gaseous species and solid surfaces were described even before sputtering was identified as the removal of surface atoms from a cathode due to the impact of energetic ions from a gas discharge. Chemical reactions on the electrodes of a gas discharge tube such as oxidation in an oxygen atmosphere and reduction in a hydrogen discharge were first recognized as early as 1852.³⁹ Perhaps, it is thus not surprising that low- and high-pressure plasma discharges have grown to find widespread use in the microelectronics industry for etching integrated circuits. Etching of semiconductor materials immersed in plasmas generally involves synergistic effects;^{1,7,9,40} however, in order to better understand

synergism, research has been performed using low energy (~ 1 eV) species. Similarly, a better comprehension of chemical processes in the erosion of carbonaceous materials exposed to ~ 1 eV atomic hydrogen is necessary to acquire a better insight into the possible synergistic effects of interest to fusion applications. The chemical erosion produced by the interactions described above is defined as the process whereby atoms of a material leave the surface as part of thermalized molecules after reacting with ~ 1 eV gaseous species.

According to this definition, the appearance of chemical erosion may be inferred from different experimental observations, namely:

- (i) The erosion yield should show strong variations with surface temperature. This, however, may not be a sufficient condition; for example, carbon erosion due to bombardment by energetic ions (H^+ , D^+) at temperatures of ~ 1200 to $2000K$, shows a strong temperature dependence, although no hydrocarbon formation, characteristic of chemical erosion, is evident.^{36,41}
- (ii) Molecules involving atoms of eroded materials and gaseous species should be observable.
- (iii) Compared to physical sputtering, which is due to momentum transfer by energetic ions,⁴² no sharp threshold as a function of gaseous species energy should be observed in the case of chemical erosion.
- (iv) The energy distribution of molecules leaving the surface should be close to or equivalent to the target surface temperature, although perhaps the chemical energy of reaction will influence molecular energies.
- (v) Chemical erosion should be strongly selective for different combinations of target atoms and reactive species.

(vi) The activation and inhibition of the erosion process, by the state of the reactive species and surface atoms, should be pronounced.

A detailed description of experimental and theoretical work related to each one of the points described above can be found in a comprehensive review published recently.²¹ Therefore, only details of information germane to synergistic effects will be discussed here.

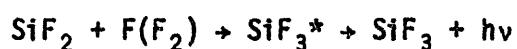
(a) General Mechanisms for Sub-eV Atoms - Surface Reactivity

Similarities between C and Si reactivity under exposure to sub-eV atoms will be analyzed in an attempt to unify concepts useful for the understanding of synergism.

Chemical erosion of Si by F, perhaps one of the best known systems in semiconductor etching, is the example that may most closely resemble the H-C system in fusion technology. Therefore, Si-F will be discussed mainly for comparison purposes. Sub-eV F atoms react spontaneously with Si and Si-compounds (e.g., SiO₂, Si₃N₄ and SiC) to form volatile molecules responsible for the erosion process.^{7,43} One of the main volatile molecules initially observed in F-Si reaction was SiF₄^{7,9,10,44,45} while CH₄ was the main species detected for the H-C system.^{16,22,46-52} More recently, however, SiF₂ has also been observed to desorb from Si⁴⁵ and CH₃ has been detected as the main species evolving from carbon, with CH₄ being a minor component.¹⁸ In any case, the initial steps in the mechanism leading to SiF₂, SiF₄ and CH₃ and/or CH₄ may still be similar as indicated in Figs. 1 and 2 (see discussion below). The resemblance between C and Si reactivity extends still further, since CF₄ (observed as CF₃ mainly due to CF₄ dissociation) can be produced on graphite,⁵³ and SiH₄ has been detected during the interaction of H⁺ ions with Si at different temperatures.^{21, 54, 55}

Considering all of the above, it is not surprising that at least one of

the postulated mechanisms for the Si-F⁴⁰ and C-H^{49,50} reactions are similar. This similitude might further be used to gain some insight into the C-H system from the existing knowledge and understanding of the Si-F system. The extensive surface analysis techniques that have been successfully used in obtaining relevant information for the Si-F chemistry have not as of yet been fully applied to the C-H system. Figures 1 and 2 show schematically the mechanisms postulated for the formation of SiF₄ (Flamm-Donnelly⁴⁰) and CH₄, respectively. Both mechanisms involve successive steps in which F and H atoms impinging on the surface react with Si and C atoms, respectively, to form SiF_x (x = 1, 2, 3) and CH_x (x = 1, 2, 3) precursors with a final fast step leading to SiF₄ and CH₄ formation. The final step leading to CH₄ formation may have to be revised in view of recent results.¹⁸ The presence of SiF₂ molecules has been detected on Si surfaces by electron spectroscopy for chemical analysis (ESCA),⁵⁶ which has shown that F binds to Si with bonds that exhibit the chemical shift characteristic of SiF₂ molecules. More recently, Vasile and Stevie⁴⁵ detected SiF₂ molecules evolving from Si surfaces by using an experimental technique capable of detecting radicals desorbing from surfaces. They reported a lower limit for the ratio of SiF₂/SiF₄ emitted from the surface in the range 0.1 - 0.3. Additionally, SiF₂ desorption was identified in the broadband visible chemiluminescence observed during Si etching in F-containing plasmas^{44,57} and undissociated fluorine;⁵⁸ the emitting species was identified⁵⁹ as an excited trifluorosilyl radical arising from the gas phase reaction



Although some experimental evidence seems to support the Flamm-Donnelly mechanism for Si etching by F,⁴⁰ an alternative model, recently proposed by Winters et al,⁷ must also be considered. Processes included in this model

are briefly discussed below (see Ref. 7 for more details and references therein).

- (1) The adsorption step in the etching reaction probably proceeds through the formation of precursor states (this is similar to the case in Ref. 40) which could strongly influence the reaction kinetics.
- (2) Phenomena known in oxidation reactions are likely to have a strong influence on or dominate etching reactions. (a) Etching, according to this model, analogous to oxidation, is likely to occur from a "reconstructed" surface. (b) Field-assisted mechanisms of the Mott-Cabrera type⁶⁰⁻⁶² involving place exchange and motion of cations and/or anions are likely to influence or dominate etching reactions.
- (3) Spontaneous etching will probably not be observed for halogenated surfaces which contain only a chemisorbed layer.
- (4) Spontaneous etching is generally a consequence of processes which lead mainly to the formation of saturated (as opposed to unsaturated) molecules.
- (5) The activation energy for the etching reaction may change depending upon the flux and types of incident particles.

According to Winters et al,⁷ it appears that the presently available experimental evidence does not clearly allow for unambiguous differentiation between the Flamm-Donnelly⁴⁰ and Winters et al⁷ models.

Attempts to detect CH_x ($x = 1, 2, 3$) precursors on graphite surfaces by using Raman spectroscopy were less successful. The evidence is mainly related to ion bombardment instead of sub-eV atoms. Wright et al⁶³ could not observe possible local-mode bands which would have characterized C-H or

C-D vibrations on surfaces implanted with H^+ and D^+ ions. By contrast, Patrick and Choyke^{64, 65} have previously found a strong luminescence of H^+ and D^+ implanted 6H and 4H SiC, which they believe to be associated with the presence of C-H and C-D vibrational modes at 370 and 274 meV (2980 and 2210 cm^{-1}), respectively. They further concluded that the implanted H or D atom diffuses to a bombardment-induced Si vacancy to form a C-H or C-D bond with one of four neighbouring C atoms; Si-H or Si-D modes were not observed. Indirect evidence of the existence of CH_3 precursors on graphite surfaces has been obtained recently by Vietzke et al^{6, 16, 18} during studies related to ion-enhanced erosion of graphite under simultaneous bombardment by Ar^+ ions (5 keV) and sub-eV H^0 atoms. By locating a quadrupole mass analyser close to, and looking at a graphite surface, they were able to detect CH_3 molecules desorbing from the sample in greater amounts than CH_4 , as indicated by the CH_3^+ and CH_4^+ signals in the quadrupole. Considering that CH_3^+ is 83% of CH_4^+ in the usual break-up pattern of CH_4 , the most probable explanation for a greater CH_3^+ signal is that CH_3 molecules are evolving from the surface.

(b) Temperature Dependence of Erosion Yield

The temperature dependence of the erosion yield for both Si-F and C-H systems shows, perhaps among all observations which characterize chemical erosion, the most relevant difference in relation to the Si-F and C-H reactivities. Figure 3, which shows the temperature dependence for the Si-F system indicates that XeF_2 etches Si faster than F atoms. This is surprising since etching by F_2 molecules is negligible⁵⁸ (this being similar for H_2 in the C-H case⁵⁰), even though the F-F bond dissociation energy (155 kJ/mole) is smaller than the first Xe-F bond dissociation energy (226-242 kJ/mole). The difference was recently attributed⁶⁶ to distinct adsorption

of F_2 and XeF_2 due to higher polarizability of XeF_2 with respect to F and F_2 . Flamm et al⁶⁶ indicated that previous assumptions^{9,10,53,67} about similar behaviour of F and XeF_2 in Si etching, based on data taken under drastically different conditions,^{10,44,67} may not have been solidly supported.

The temperature dependence of the erosion yield for sub-eV H^0/C interaction shows also discrepancies, although of somewhat different nature than those for the Si-F system. Methane yields due to bombardment of carbon by <1 eV H^0 are extremely inconsistent according to published results²⁰⁻²² (see Fig. 4). Two principal features of the anomalies are noted: (i) the yields span almost four orders of magnitude, and (ii) some studies show the existence of a maximum in the CH_4 yields vs carbon temperature curve, while others indicate no maximum (see Fig. 4). In addition, the observed temperature maxima appear to be located at one of the following two temperature ranges: 500-600K and 750-850K. The reported discrepancies in the spread of CH_4 yields have been attributed to the use of different types of carbon as well as surface conditioning, different vacuum environments, and/or different methods of producing sub-eV H^0 .^{22,70} The difference in curve shapes (see Fig. 4), as experimentally observed, might be explained by considering two states of reactivity for carbon:^{22,70} "activated" and "deactivated" states. The "activated" state is characterized by a relatively high CH_4/H^0 yield (see inset in Fig. 4) and can be regained by heating the carbon to temperatures $> 1200K$.^{22,50,69,70} The "deactivated" state, associated with lower methane yields, is produced by exposing the activated surface to a certain H^0 fluence. Curves A, C, E, K, L, M and N represent "activated" yields, while B, D, D', F, I, J and O correspond to "deactivated" yields. Abe et al⁵² reported results which

indicate that they have also observed the temperature-induced activation effect. They did not explicitly recognize that the target temperature treatment, previous to surface exposure to sub-eV H^0 , may have been responsible for an initially high CH_4 production rate (the target was heated up to $\sim 1300K$ for 60 min). However, they indicated that graphite surfaces can be made less reactive after exposure to sufficiently high sub-eV H^0 fluences.

Groups which obtained curves D,¹⁶ I,⁴⁹ and J⁴⁹ may have overlooked this phenomenon, due to the fact that their H^0 beam related experiments involved rather long exposures of the target to the H^0 beam before data points were taken (phase sensitive detection methods were necessary). This would imply that the transient peak corresponding to the "activated" state may have been lost, since the decay occurs in approximately less than about thirty seconds for the H^0 fluences used.^{22,70} Curves K,⁴⁷ L⁶⁸ and M⁴⁸ were obtained in plasma environments and high pressure and high H^0 fluxes. It is not certain whether the surfaces were also exposed to ions; additionally, erosion rates were generally extremely high, $\sim 10^{16}C/cm^2s$. Therefore, it cannot be concluded which one of these effects might have caused activation. However, Curve C, obtained by exposing pyrolytic graphite to sub-eV H^0 over the first 28 seconds after stopping a simultaneous H^0/Ar^+ (5 keV) irradiation of the sample,¹⁶ indicates that ion bombardment may be even more effective than preheating in activating carbon surfaces. In fact, other recent studies with sub-eV H^0 and H^+ ions also indicate that carbon surfaces can be activated by ion bombardment.¹⁷ In view of this analysis, the plasma related experiments may have involved ion-induced activation.

The temperature-induced activation effect has been confirmed recently, by new experiments with the H_2 backfill method of H^0 production⁷¹ and also

by using a UHV (RF) H^0 beam source to bombard carbon targets.⁶⁹ For the former case, the tungsten filament used to create H^0 atoms was reduced in size to diminish sample heating by radiation, allowing CH_4 yields to be measured at target temperatures down to $\sim 500K$. These results confirmed the existence of a peak for the deactivated yield at about 500-600K, a feature previously not observed in some backfilling experiments^{22,70} due to experimental limitations, but observed in H^0 beam work.^{16,18,69} Moreover, the state of activation of the surface ("deactivated" curves: D, D', F, O; "partially activated": curve C; "fully activated": curves A, E, K, L, M, N, all in Fig. 4; and Mass 15 curve in Fig. 12 of ion-induced synergism section) may be an alternative explanation, in addition to those proposed above (different surface structure, preparation, etc.), for the observed shifts in the maxima of the CH_4 vs carbon temperature curves. Further studies will be necessary to elucidate this point.

It is not clear yet what the temperature and ion-induced activation mechanisms might be, and further experiments will be necessary to understand the phenomenon. However, a tentative hypothesis⁷² indicates that temperature may promote the formation of CH_3 precursors by reaction of loosely bound C atoms with H^0 present on the carbon surface after being retained during H^0 exposures. In fact, CH_3 (from the break-up of CH_4 in a quadrupole) and H_2 have been observed to desorb from graphite during temperature-induced activation,⁷¹ indicating that hydrogen atoms trapped during previous exposures react at the target surface. Once the active precursors are exhausted the carbon is in the deactivated state and the formation of CH_4 will require a sequence of steps as indicated in Fig. 2. Alternatively, the reaction between H/C surface complexes may lead to the formation of a stable H/C surface complex, which would destroy available

sites for CH_4 formation contributing to the surface deactivation.⁵⁰ Two quantitative models have been developed to explain the sub-eV H^0/C reaction data presented in Fig. 4. The first, due to Balooch and Olander⁴⁹ assumes an H^0 gas in thermal and chemical equilibrium with the solid surface producing a number of adsorbed H^0 atoms equal to the product of the incident atomic hydrogen intensity, I_0 , and a sticking coefficient for H^0 .^{49,73-75} This and other assumptions, including the CH_4 formation mechanism illustrated in Fig. 2, were the bases for developing a set of kinetic equations for fitting the experimental curves I and J of Fig. 4. The second model was developed by Gould,⁵⁰ and it differs from the previous one mainly by the fact that Gould's kinematic equations account for the activation and deactivation effect for fitting the experimental curves E and F in Fig. 4. Recently, Roth has shown²¹ that a theoretical curve with a peak at about 550-650K can be obtained for the methane yield as a function of target temperature, by using Balooch and Olander's equations,⁴⁹ but changing I_0 (a parameter kept constant in Balooch and Olander's original calculations⁴⁹) and including an H^0 saturation surface coverage (c_0). A curve with a peak was obtained for a theoretically assumed²¹ $I_0 = 10^{19} \text{ H}^0/\text{cm}^2\text{s}$ and $c_0 = 10^{13} \text{ H}^0/\text{cm}^2$ (c_0 as measured by Gould⁵⁰). However, Balooch and Olander's model⁴⁹ appears to be unable to explain the activated and deactivated peaks as Gould's approach⁵⁰ does.

2.2 Chemical Erosion of Materials by Energetic Reactive Ions

(a) Semiconductor Materials

Most of the research and production applications involving bombardment of semiconductor surfaces by reactive ions alone has been done by using broad-beam ion sources of the type described in a recent review.⁷⁶ These sources generally include a discharge chamber where ions are produced by

either direct-current electron bombardment or r.f. discharges, and the efficiency of ion production is enhanced by different magnetic field configurations. Beams of several centimeters in diameter, tens of eV to keV in energy, and wide current ranges have been obtained. One of the main advantages of using these beams, rather than plasma related experiments, is the possibility of changing bombardment parameters (energy, ion current, angle of bombardment with respect to the sample, background pressure, etc) independently, permitting controlled experiments to be performed to elucidate the importance of each parameter in the overall etching process. The same type of sources used in microelectronics are now scaled up to appropriate dimensions, finding applications in fusion technology for neutral beam injection.

The scope of research performed to date and currently being performed on chemical erosion of materials, mainly semiconductors, by reactive ion beams is so wide that it cannot be encompassed in the space available for this review. Therefore, let it suffice to say that research in this area, as well as in the fusion materials case, has shown that the sputtering yield of materials due to reactive ion bombardment can be higher than the physical sputtering produced by inert ions. Figure 5 shows, as an example, the different erosion yields of SiO_2 when bombarded by CF_4^+ and Ar^+ ions. Reports on reactive ion-beam etching of Si, SiO_2 , and photoresists with CF_4 , CCl_4 , CHF_3 , Cl_2 , etc, have proliferated in the last years (see Ref. 76 and references therein). The emphasis has been on the etching of Si and SiO_2 where erosion rates at 500-1000 \AA /min have been achieved. Due to the fact that neutral particles cannot be totally eliminated in the beams described above, synergistic effects may be present under certain conditions leading to enhanced erosion.

By contrast to erosion, a variety of physical and chemical properties of materials - over large areas - can be modified by reactive ion implantation using broad-beam sources. Examples are hardness, friction, mechanical resistance, corrosion resistance, bonding, fatigue, adhesion, electrochemical and catalytic behaviour. These properties depend greatly on the structure and composition of the surface layer within about 1 μm from the surface. Such ion beam sources could also be used, in principle, to modify the properties of materials over the large areas needed for some fusion applications. In this way surface properties could be changed to improve erosion resistance, retention, permeation characteristics, etc, in the quest for developing the most appropriate materials for the fusion environment.

(b) Fusion Materials (Carbon)

Detailed descriptions of results related to observations characterizing chemical erosion phenomena for energetic ion (H^+ , D^+ , He^+ , etc) bombardment have been published in two recent reviews.^{21,78} The present review includes new relevant data,^{37,38} particularly in relation to the chemical sputtering/erosion yield dependence on the energy of hydrogenic ions, which is of direct interest to fusion technology (Fig. 6). The term "chemical sputtering" has been widely used in the literature. However, it might be more appropriate to refer to erosion by formation of volatile products as "chemical erosion", since sputtering involves the idea of momentum transfer⁴² while volatiles generally leave the surface with energies equivalent to the target temperature, therefore having, in general, a Maxwellian velocity distribution.

Methane yields resulting from the bombardment of carbon by energetic hydrogenic ions ($\sim 0.1 - 100$ keV) have been extensively studied, and the

yield dependence on beam flux density and carbon temperature is consistent, among results obtained by different groups, generally to within a factor of five^{20,21,78,79} (see Figs. 6 and 7). This agreement is reasonably good, considering that yields have been measured by different methods (weight loss or volume loss, and calibrated measurements of the CH₄ partial pressures), and various types of graphites have been used in different experiments.²¹ Radiation-induced amorphization⁶³ may lead, at high fluences, to similar surface structure diminishing or eliminating structural differences for distinct types of graphite. In nearly all cases the chemical sputtering yield exhibits a maximum at temperatures between 720K and 920K (Fig. 7) as was also observed for the sub-eV H⁰ impact case (Fig. 4). However, there is a marked difference between the sputtering yields for hydrogenic ions and sub-eV H⁰ atoms. The maximum of the chemical sputtering yield due to ions reaches values spreading from $\sim 10^{-2}$ to 10^{-1} atoms per ion for target temperatures of 720-920K (Fig. 7) while the yield due to sub-eV H⁰ atoms is of the order of 10^{-4} - 10^{-3} CH₄/H⁰.

The interpretation of data may be complicated by the appearance of hysteresis effects in the CH₄ yield vs target temperature curves (Fig. 8). It has been observed that reaction probabilities are higher when increasing the target temperature than when decreasing from initially high temperatures.²¹ This effect has been observed not only for hydrogen ion bombardment but also for sub-eV atoms for the hydrogen and oxygen-carbon interactions.^{49,80} It has been explained as a result of the existence of different surface concentrations of reactive atoms in the material at the start of the measurements, which may lead to a drastic reduction of the chemical erosion after high-temperature annealing of the sample. However, in view of new phenomena recently observed, i.e., ion-induced activation and

synergism in graphite^{6,17,18,81} and their dependence on target temperature, these effects should be considered at least in the case of ion bombardment, when trying to explain the observed hysteresis. Additionally, the different methane yields observed for different doses (see Fig. 8) were related to the hydrogen surface concentration, which leads to the methane production.²¹ However, an alternative or concurrent mechanism should also be considered, viz, the development of ion-induced topography features on bombarded surfaces (Refs. 82-86 and references therein). It has been shown in a recent review⁸⁴ that dense arrays of cones, ridges, etc, generally developed on bombarded surfaces, may induce retrapping of sputtered atoms, thereby decreasing the observed sputtering yield by a factor of 30 to 100, depending on bombardment parameters and materials. Surface textures such as those mentioned above have already been observed on graphite.^{49,87} Textured surfaces may be advantageous, as has been recently suggested,^{78,82-86} in fusion device applications.

Finally, the data on sputtering yield vs beam energy dependence for $H^+/D^+/He^+$ -carbon interaction, found in the literature (Fig. 6) show two sets of curves with peaks (albeit some of the peaks are quite shallow) at about 200-300 eV and 1-3 keV. As with the spread in the measured yields (Figs. 6 and 7), the difference in the occurrence of the peaks might also be attributed to differences in the types of carbon, target preparation procedures, bombardment parameters, or measurement methods. In an attempt to explain the energy and temperature dependence of the CH_4 yield, Yamada and Sone³⁷ have made improvements on a model previously developed by Erents et al⁸⁸ for H^+/D^+ -C interactions. The improved model includes surface deposited energy and reflection of ions as new parameters, which depend on

the energy of the bombarding ions. Essentially, the model involves the adjustment of four parameters to experimental data. Yamada and Sone's calculations appear to fit their experimental data with curves having peaks at about 1-3 keV. However, it is not clear whether slight changes in the fitting parameters may lead to shifts in the calculated curves such that experimental curves with peaks at about 200-300 eV may be fitted as well. Alternatively, computer calculations²¹ of surface energy deposition of hydrogenic ions penetrating carbon indicate that there is a maximum (for energy transfers >8 eV) in energy deposited in the lattice at about 200-300 eV (Fig. 3.30 of Ref. 21), which correlates well with the observed maximum at 200-300 eV in the sputtering yield curves²¹ (Fig. 6). Little can be concluded at the moment regarding the use of the Yamada-Sone model³⁷ in deciding which set of data is more accurate. In any case, from the application point of view in fusion devices, it may not be relevant whether the maximum yield is at 200-300 eV or 1-3 keV since the yields are very similar (Fig. 6).

3.0 ION-INDUCED SYNERGISMS

Ion-assisted etching has become one of the most useful techniques to fabricate micron-sized features on semiconductor surfaces. Its potential has not been fully exploited yet, mainly because of the lack of a more definite understanding of the underlying mechanisms. Much has already been done in basic research related to this field,^{1,7} but still more work is necessary to elucidate many unknowns. Work done until now^{1,7} has allowed us to identify the influence of several parameters in ion-assisted etching in semiconductors, i.e., substrate characteristics (crystallinity, reactivity, etc) and temperature, ion energy, ion and reactive neutral fluxes, substrate

temperature, and the gas phase and gas-surface chemistry. Ion-induced synergistic effects in the erosion of fusion materials, mainly carbonaceous compounds and pure carbon, is, on the other hand, a matter of concern because the possible occurrence of an undesirable enhanced rate of impurity introduction into the plasma. Ideally, this effect should be diminished to very low levels in fusion devices, although the production of a wall-protecting impurity-dominated, radiating plasma edge may be desirable. Considering the generalities mentioned above, the main focus of this section will be on the state of the present understanding of synergistic effects independent of their desirability.

It has been widely observed, and is generally accepted now that ion bombardment accelerates erosion in many gasification reactions on surfaces, but in several cases it is not clear yet how this enhancement occurs. Moreover, possible mechanisms have already been identified to explain the experimental observations. The general consensus at present is that ion bombardment may accelerate any one or all of the steps involved in erosion,⁹ as described in detail in the introduction to this review. The sensitivity of the rate limiting step to ion bombardment will determine whether or not ion enhancement of the overall erosion reaction occurs.

3.1 Experimental Evidence

(a) Semiconductor Materials

Ion energies and fluxes appropriate for anisotropic etching of semiconductors can be achieved by using several different combinations of operating conditions and reactors (when plasma etching is used) or ion/reactive sub-eV species beam combinations.^{1,7} In plasma etching, intense ion bombardment of surfaces can be achieved under particular conditions, which lead into the regime known as "reactive ion etching"

(RIE).¹ The terminology RIE is somewhat misleading because the chemical nature of the ions are of secondary importance, the relevant effect being the interplay between energy transferred by ion impact and reactions occurring between substrate and uncharged reactive radicals and atoms. At relatively high pressure and high frequency, ion energies are low, surface damage is minimal, and anisotropy, when observed, is caused by the presence of recombinants (see Sec. 3.2 on models). Anisotropic etching of Si in plasmas of Cl_2 - C_2F_6 mixtures at 13.6 MHz and 5-30 Pa pressure is an example of a case of low energy ions.¹ At relatively low pressure ($\lesssim 5$ Pa) or high pressure and low frequency, ion energies are high (a few hundred eV) and surface damage-induced anisotropy may be produced. Etching of Si in Cl_2 plasmas at 100 KHz-13 MHz and 3 Pa is an example of the high energy ions case.¹ Relatively low energy ion bombardment ($\lesssim 50$ eV) can also lead to anisotropic etching in certain plasmas due to the formation of a protective film on vertical surfaces of patterns that receive little ion bombardment (inhibitor mechanism⁸⁹). Intermediate pressures and high applied frequencies provide conditions that favour this mechanism.

Several diagnostic techniques have been developed to detect and characterize short-lived ions, neutrals and free radicals, as well as stable reaction products in the plasma, in order to relate them to ion-assisted etching mechanisms.¹ These techniques include mass spectrometry, optical diagnostic methods for monitoring species in excited states, and laser-induced fluorescence.

Figure 9 shows, as an example, results related to one of the early observations of ion-assisted etching of semiconductors.⁹ Si samples were irradiated with Ar^+ (450 eV) ions and exposed to a XeF_2 flux of $\sim 2 \times 10^{15}$

molecules/s, in such a way that both species impacted the surface both independently and simultaneously. The etch rate was determined by measuring the frequency change of a quartz crystal microbalance (on which Si was deposited); this is a very sensitive technique for measuring sputtering yield.⁸⁹⁻⁹¹ Ar⁺ ions were used in order to eliminate any chemical contribution from the ions, and also to utilize the high sputtering yield characteristics of Ar⁺ for keeping the surface dynamically clean during the experiments.⁹ The erosion enhancement due to combined bombardment by Ar⁺ ions and XeF₂ is clearly demonstrated by the fact that the etch rate is about eight times the sum of the etch rates due to each species measured separately (Fig. 9). The transient peak response of the etch rate immediately following the initiation of Ar⁺ bombardment (200s < t < 300s) was attributed in part to some ion-induced strains and/or temperature excursions in the quartz crystal which may affect the resonance frequency, and in part to a decrease in the steady state surface coverage of fluorine caused by the Ar⁺ bombardment. However, new results,^{6,16,17} related to the H-C system, indicate that transient effects, similar to those in Fig. 9, may be due to ion-induced activation of surfaces. Therefore, an alternative interpretation of the transient in Fig. 9 may warrant some consideration. The transient fall-off observed after shutting-off the XeF₂ gas (640s < t < 750s) was attributed to the fact that it was not possible to decrease the XeF₂ gas flow instantaneously to zero, and consequently, the transient resulted from the spontaneous reaction of XeF₂ with Si⁹ while the flux was decaying.

Similar ion-enhanced chemistry has been observed for F₂ on Si, F₂ on C, Cl₂ on Si, and O₂ on C.⁹ These systems are interesting because it appears that there is no spontaneous reaction between molecular species

(without the presence of ions) and materials as indicated above. Etching rates have consistently been below detectable limits ($< 0.1 \text{ \AA}/\text{min}$).⁹ Therefore the etching is mainly due to ion-enhanced chemistry. Figure 10 shows, as an example, the etching rate vs time behavior (similar for all systems mentioned above) for $\text{Cl}_2 + \text{Ar}^+$ on Si. The initial drop in etching when Cl_2 is added to Ar^+ bombardment, was attributed to an excess of Cl_2 adsorption which exceeded the etching process for a short period of time causing the Si sample to gain mass. The etch rate increased later by a factor of four over that due to Ar^+ bombardment alone. The etch rate dropped to zero almost instantaneously, although not shown in Fig. 9, when the Ar^+ beam was turned off; this was due to the fact that Cl_2 does not etch Si.

In other work,⁹² the effect of the collision cascade on ion-enhanced gas-surface chemistry was studied by changing the mass of the incident ions (He^+ , Ne^+ , and Ar^+) at a fixed energy (1 keV). Two systems were analyzed, namely, Si-F and Si- Cl_2 , which differ in that Si is spontaneously etched at room temperature by XeF_2 , whereas there is no observable etching of Si in Cl_2 at room temperature. The experimental procedure used to study both systems involved the simultaneous and individual bombardment of samples by 1 keV ions and a flow of active gas through a stainless steel tube, directed onto the surface. Figure 11 shows, as an example, the erosion enhancement in Si simultaneously bombarded by Ne^+ (1 keV) and XeF_2 . Similar curves were obtained for Si bombarded by $\text{Ne}^+ + \text{Cl}_2$, except that, because Cl_2 does not spontaneously etch Si at room temperature, curve (b) in Fig. 11 was zero for the Cl_2 -Si case. Figures 12a and b show the ion mass effect in ion-enhanced erosion of Si for both the Si- XeF_2 and the Si- Cl_2 systems, respectively.

The implication of these results will be analyzed in the models section to follow.

The simultaneous interaction of ions and reactive species with surfaces does not always lead to an enhanced erosion. It has been observed that reactive gases that form involatile compounds actually decrease the ion-induced sputtering yield of materials with which they react. These effects have been observed in semiconductors bombarded by ions in the presence of gases such as O_2 for instance. The Si- Ar^+ - O_2 system is an example of ion/reactive gas-induced reduction in sputtering yield.⁹ Work is currently in progress in order to better understand this phenomenon.

(b) Fusion Materials (Carbon)

Ion-induced synergistic effects of interest in erosion of fusion materials are related mainly to simultaneous bombardment of carbonaceous materials by energetic hydrogenic (H^+ , D^+ , T^+) and impurity ions and low energy hydrogenic atoms (H^0 , D^0 , T^0). Clear evidence for the existence of ion-induced enhancement, in the erosion of carbon, was first obtained by Vietzke et al.,¹⁶ in experiments involving the simultaneous bombardment of pyrolytic graphite by Ar^+ (5 keV) ions and sub-eV H^0 atoms, produced by dissociation of H_2 in a hot W tube and delivered as a narrow beam onto the target surface. Figure 13 shows the temperature dependence of the reaction probability for the H^0/Ar^+ irradiation with an intensity ratio of $H^0/Ar^+ \approx 1500$ (1.6×10^{16} H^0/cm^2s and 1.1×10^{13} Ar^+/cm^2s).⁶ At this relatively low ion intensity the reaction probability was observed to increase by a factor of 50 over that corresponding to sub-eV H^0 bombardment alone. A noteworthy feature of this result is that CH_3 species evolving from the surface were observed to be more abundant than CH_4 ones. This difference was detectable due to the particular experimental arrangement used, in which a quadrupole

mass spectrometer was positioned near and looking at the target surface. Other results obtained by Yamada and Sone⁹³ have shown a lower limit of $3 \times 10^{-2} \text{ CH}_4/\text{H}^0$ for the erosion rate of graphite due to simultaneous impact by H^0 atoms and H^+ ions.

More recently, the Toronto group performed systematic experiments¹⁷ related to H^+/H^0 -induced synergistic effects on graphite. These involved the bombardment of pyrolytic graphite¹⁷ by H^+ ions (60-5000 eV) and sub-eV H^0 atoms, the latter produced by H_2 dissociation on a hot W filament facing the sample. This particular technique, well described elsewhere,²² entails the presence of H_2 ($\sim 4 \times 10^{-4}$ torr) in the target chamber, and hence the simultaneous presence of H_2 and H^0 in contact with the surface during H^+ ion bombardment. A typical sequence of events and the corresponding temporal behavior of the methane (monitored through mass 15) signal is shown in Fig. 14. The quadrupole used to monitor mass 15 was not in line of sight to the target but acted as an RGA. The shape and level of the CH_4 signal due to H^0 exposure alone is consistent with previous findings (see Ref. 22 and Section 2.1-b of this review for detailed explanation). The gradual temporal increase of the CH_4 signal, from the initiation of the H^+/H^0 bombardment, towards a higher steady state level may be interpreted as an indication of a damage-related mechanism for the synergistic effect, consistent with a build-up of ion-induced surface damage towards a steady state level (see discussions in Sec. 3.2 on models). The decay of the CH_4 signal towards a residual level, by exposure to H^0 alone, after turning off the H^+ ions, is a clear indication of the existence of an ion-induced activation effect, as previously discussed in Section 2.1.b of this review. This effect has also been observed by Veprek et al (see Fig. 3 of Ref. 81). Further evidence of this effect can be found elsewhere (see Fig. 7 of Ref. 6, and Ref.

38) where the effect of sample deactivation by exposure to H^0 alone, after an ion (H^+ or Ar^+) + H^0 bombardment, was shown to result in a reduction of CH_4 signals.

The significance of the Toronto Group's H^+/H^0 synergism findings¹⁷ for fusion applications is manifested in Fig. 15. This figure illustrates the CH_4 yield enhancement, as a function of H^+ flux (with the H^0 flux density being kept constant at $\sim 6 \times 10^{14} H^0/cm^2s$ and H_2 pressure kept at 4×10^{-4} Torr) for 300 eV protons, at graphite temperatures of 750-800K, this being the temperature for which maximum production of methane is generally observed. Yields due to bombardment by H^+ ions alone in vacuum, H^0 alone, H^+H_2 , and $H^+H^0H_2$ are shown. The ratio of the ($H^+H^0H_2$) yield to the (H^+H_2) yield is about 2 when the H^+ and H^0 flux densities are about the same ($6 \times 10^{14}/cm^2s$ or $\sim 20 \mu AH^+$). This implies that for equal numbers of H^0 and H^+ , in the presence of H_2 , the H^0 atoms are "upgraded" to H^+ ion efficiency for the production of CH_4 . If the relative H^+ flux density is increased, a slight decrease and subsequent levelling-off in the yield ratio is observed for the flux levels studied.¹⁷ On the other hand, a monotonic increase in the yield ratio is observed as the relative H^+ flux density decreases. This implies that small quantities of H^+ ions are sufficient to increase the carbon reactivity, probably by some damage-related mechanism, leading to enhanced CH_4 formation via carbon reaction with sub-eV H^0 atoms. For example, an ion flux of only 10% of the H^0 flux appears to be sufficient to increase the CH_4 production by all H^0 atoms to ion efficiency levels. Yields of the order of 0.2-0.4 CH_4/H^+ (in the presence of H_2 at $\sim 4 \times 10^{-4}$ Torr and a fixed H^0 flux of $\sim 6 \times 10^{14} H^0/cm^2s$) have been measured for carbon at 750-800K over an H^+ flux range of 3×10^{13} to $10^{15} H^+/cm^2s$.¹⁷ These yields are close to yields (~ 0.3) calculated from erosion measurements on heavily etched carbon probes exposed to r.f. discharges in the PLT device, which appear to be explainable only if

synergistic effects are considered.¹⁹ Other measurements⁹⁴ of carbon erosion due to $H^+ + H^0$ bombardment resulted in much lower erosion yields than those mentioned above. This discrepancy may be due to the fact that different experimental parameters were used. Further work is therefore necessary to explain this inconsistency.

A further series of experiments, aimed at checking the "ion-induced damage" hypothesis,^{6,22,81} were also performed.¹⁷ The experimental process involved an initial bombardment of the sample with ions for a certain period of time at a particular H^+ flux, which was then followed by exposing the sample to H^0 atoms. The CH_4 signal temporal evolution was characterized by an initial transient peak, similar to the one observed in the case of the temperature-induced activation phenomenon (see inset of Fig. 4). This effect correlates with the hypothesis that ion-induced damage sites^{6,22,81} may enhance the graphite reactivity which is subsequently reduced by reactions with H^0 atoms. The initial value of CH_4 production due to H^0 atoms (the transient peak), but normalized by the "damage-inducing" H^+ flux, is plotted as a function of the H^+ flux in Fig. 15. It can be seen that the synergistic CH_4 yields due to $H^0 + H^+ + H_2$ bombardment are approximately equal to the sum of the CH_4 yields for $H^+ + H_2$ irradiation and that corresponding to H^0 exposure after H^+ -induced "activation". This indicates that the ion-induced damage may produce similar increases in carbon reactivity for both sequential and simultaneous H^+ and H^0 exposure processes. In fact, Veprek et al.'s⁸¹ results constitute good evidence in support of the damage related mechanism. They used He^+ ions for damaging the samples, therefore precluding the occurrence of chemical effects, as may be the case when bombarding with H^+ ions (creation of active sites by precursor formation). However, Vietzke et al.⁹⁵ do not observe ion-induced activation when

bombarding sequentially with Ar^+ ions and H^0 atoms. Further work is therefore necessary to clarify this discrepancy.

Additional effects observed in $\text{H}^+ + \text{H}^0 + \text{H}_2$ interactions with carbon relate to synergistic CH_4 yields vs target temperature dependence.¹⁷ Figure 16 shows, for example that the temperature for which CH_4 production is maximum seems to depend weakly on proton energy. Figure 17 shows a more extensive study of the energy dependence of synergistic CH_4 production, for which the H^0 flux was kept constant at $\sim 6 \times 10^{14} \text{ H}^0/\text{cm}^2\text{s}$. It can be seen that for the highest H^+ flux used ($\sim 10^{15} \text{ H}^+/\text{cm}^2\text{s}$), the CH_4 production falls monotonically as the energy increases from 300 eV to 5000 eV. This flux level was not achieved for $< 300 \text{ eV H}^+$ energy. For the lower fluxes, however, the energy range was extended to 70 eV (little difference was observed in yields at 70 eV and 100 eV), and a definite fall-off at both the low and high energies was observed. Although shallow, a maximum appears to exist between 300 and 2000 eV. If the ion-induced damage hypothesis proposed to explain the observed synergism is indeed correct, then an energy dependence similar to that observed in Fig. 17 may in principle be explicable. Other experimental results seem to confirm the damage related hypothesis.⁶ In fact, measurements of carbon reactivity under $\text{X}^+ + \text{H}^0$ bombardment ($\text{X}^+ \equiv \text{Ar}^+, \text{Ne}^+, \text{He}^+$) as a function of energy of the X^+ ions indicate that the reactivity follows qualitatively a behaviour similar to the nuclear stopping power.⁶

Recent experiments performed by Vietzke et al.,^{6,18} produced information relevant to the understanding of the synergistic effects in the erosion of carbon. One of the main results relates to experiments in which a change-over of hydrogenic species was performed. Carbon surfaces were bombarded simultaneously by Ar^+ and H^0 species, followed by a 100s period

without irradiation. The reactivity of the sample when exposed to D^0 atoms was subsequently determined. It was observed that CH_2D and CHD_2 are formed instead of CH_3 which would appear if the prepared surface was exposed to H^0 instead of D^0 . Similar change-over experiments, although performed for retention studies by Ashida et al.⁹⁶ support the results mentioned above, which favour the precursor formation mechanism proposed to explain synergism,^{6,18} as will be discussed below.

Again, in fusion materials (other than carbonaceous), as in the case of semiconductor materials, ion bombardment of materials in the presence of reactive species may lead to a reduced erosion. It has been observed that metals bombarded by ions, in the presence of reactive gases which form non-volatile compounds, exhibit reduced sputtering yields. This effect has been observed for several systems (Ref. 97 and references therein) including N_2 , O_2 , H_2 on Ti with simultaneous Ar^+ bombardment and He^+ , D^+ , H^+ on Fe (see Fig. 18 and Refs. 98-100), which may be of direct interest to fusion applications.

Mechanisms proposed to explain many of the experimental observations described previously will be discussed in the next section.

3.1 Models for Ion-Induced Synergism

(a) Semiconductors

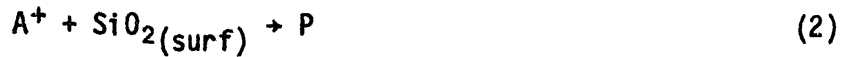
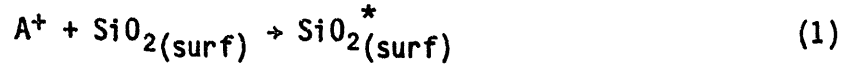
Three mechanisms have been proposed to account for the ion-enhanced chemical reactions that lead to enhanced etching:

- (i) The first one, called chemically enhanced physical sputtering, was proposed by Mauer et al.¹⁰¹ Their main hypothesis was that SiF_x radicals, for example, on the fluorinated Si surface have a larger sputtering yield than elemental Si, presumably due to a

lower binding energy. Therefore, enhanced etching is a consequence of an increased physical sputtering yield.

- (ii) A second mechanism, originally suggested by Coburn et al.⁹ and later expanded by Flamm and Donnelly⁴⁰ suggests that enhanced chemical reactions can be produced by ion-induced damage, such that highly active sites are created in the lattice, presumably due to displacement of atoms and breaking of bonds.
- (iii) The third mechanism has been proposed more recently by Winters et al.⁷ who suggest that the most likely mechanism to dominate in many situations is analogous to those operating in oxidation. Briefly, oxidation may involve electrons passing through an oxide film (e.g., by tunnelling) to the outer chemisorbed layer to form oxygen anions with metal cations being produced at the metal-oxide interface. The strong electric field generated by this process is able to pull ions through the film. Fehner and Mott⁶² have proposed that this can best be explained by a place exchange mechanism, i.e., metal and oxygen ions exchange positions in the lattice. The analogue mechanism proposed by Winters et al.⁷ to account for ion-induced enhanced etching in some semiconductors, implies that place exchange and more extended field-enhanced motion of cations and/or anions leads to compound formation. If these compounds consist of molecules (e.g., saturated halocarbons) which are weakly bound to the surface, then they will subsequently desorb into the gas phase. The activation energy for the motion of cations and/or anions can in principle be also supplied by the ion-induced collision cascade.

The mechanisms described above have been proposed mainly on phenomenological bases. Perhaps, the only mechanism for which some attempt at quantification has been made is the ion-induced damage one. Donnelly et al.¹⁰² have recently developed a formalism which allows calculation of some ion-enhanced etching rates for SiO₂ films. The etching mechanism in this case can be described by the following reactions:



where A⁺ is a positive ion, SiO₂(surf) represents a stable fluorinated surface at steady state, SiO₂^{*}(surf) describes the ion-damaged surface, and P accounts for product molecules which desorb rapidly. Reaction (4) corresponds to physical sputtering, while (3) represents chemical (e.g., isotropic) etching by fluorine atoms at a rate given by⁴⁴

$$R(\text{\AA}/\text{min}) = 6.14 \times 10^{-13} n_F T^{1/2} \exp(-E_a/kT) \quad (5)$$

with

$$E_a = 0.163 \text{ eV}, \quad n_F \lesssim 2 \times 10^{15} \text{ F/cm}^3 \quad \text{and } T = 40^\circ\text{C}.$$

Reaction probabilities $\epsilon_F(SiO_2^*)$ and $\epsilon_F(SiO_2)$ are defined as the number of SiO₂ molecules leaving the surface per incident F atom for damaged and undamaged material, respectively. Considering that only a fraction θ of the surface, which has been damaged, exhibits enhanced reactivity, the total etch rate (molecules/cm²s) can be written as¹⁰²

$$\frac{dP}{dt} = J_+ \phi_s + \frac{n_F V_F}{4} [\epsilon_F(SiO_2^*)^\theta + \epsilon_F(SiO_2)^{(1-\theta)}] \quad (6)$$

where J₊ is the ion flux, ϕ_s is the number of SiO₂ molecules removed per

incident ion, and $n_F \bar{V}_F / 4$ is the F atom impingement rate. At steady state the fraction of damaged surface is constant, yielding¹⁰²

$$\frac{d[\text{SiO}_2^*(\text{surf})]}{dt} = J_{+\phi_d}(1-\theta) - \frac{n_F \bar{V}_F}{4} \epsilon_F(\text{SiO}_2^*)^\theta = 0 \quad (7)$$

where $J_{+\phi_d}$ is an efficiency factor for reaction (1). Solving for θ and substituting into Eq. (6), gives the erosion yield:

$$\frac{dP}{dt} = J_{+\phi_s} + \frac{n_F \bar{V}_F}{4} \epsilon_F(\text{SiO}_2^*) \left[\frac{1 + \epsilon_F(\text{SiO}_2^*)^{n_F \bar{V}_F / (4 J_{+\phi_d})}}{1 + \epsilon_F(\text{SiO}_2^*)^{n_F \bar{V}_F / (4 J_{+\phi_d})}} \right] \quad (8)$$

where $J_{+\phi_d}$ is assumed constant. For the limit where $n_F \lesssim 1 \times 10^{14} \text{F/cm}^3$, Eq. (8) reduces to

$$\frac{dP}{dt} = J_{+\phi_s} + \frac{n_F \bar{V}_F \epsilon_F(\text{SiO}_2^*)}{4} \quad (9)$$

Equation (9) was used to calculate the ion-enhanced etch rate of SiO_2 in a CF_4/O_2 plasma. The calculated sputtering rate was $190 \pm 120 \text{ \AA/min}$, which should be compared with the experimental value of 100 \AA/min .¹⁰² The higher value of 190 \AA/min could be due, according to Donnelly et al.,¹⁰² to sputtered material redeposition suppression which may normally occur in plasmas of higher densities than the one used for the experiment described above. Further details on this mechanism can be found in a communication by Donnelly et al.¹⁰² Figure 19 illustrates the mechanism of surface-damage enhanced erosion which may lead to anisotropic etching, a feature desirable in many applications in microelectronics.

Still another mechanism involving rearrangement of bonds has been proposed recently,¹⁰³ mainly in relation to the (XeF₂-Si) and (Cl₂-Si) systems. The model is based on two main hypotheses for the enhancement mechanism:

- (1) ions excite SiF₂ (SiCl₂) molecules formed on the surface,⁵⁶ and
- (2) the excited state of the surface is assumed to have an average lifetime τ .

While in the excited state, the molecules may react with the physisorbed gas on the surface with higher reaction probability than the non-excited molecules, leading to an ion-enhanced etch rate. A formalism was developed in an attempt to quantify the model. However, some of the hypotheses are debatable, and some mathematical inaccuracies have been detected. Therefore, no further discussion of this model will be presented here.

In other work,⁷ evidence has been presented which suggests that the lattice damage mechanism is unimportant at least for the F-Si system. The authors recognized, however, that the damage mechanism may very well be relevant for other cases, one of which may be SiO₂, as described previously. The evidence obtained by Winters et al.⁷ relates to measurements of the erosion yield of a Si film damaged by 2000 eV Ar⁺ ions. The 20-40 Å damaged layer was exposed to XeF₂ which resulted in an etch rate characteristic of the spontaneous etch rate normally observed on undamaged Si. However, recent experiments by Winters et al.^{103a} indicate that damage-enhanced erosion may occur in some Si samples. It is not clear at present the reason for this random behavior.

Winters et al.⁷ pointed out that many experimental results suggest that both physical sputtering and chemical erosion mechanisms are present in various etching environments; physical sputtering having the well known meaning established by Sigmund,¹⁰⁴ and chemical erosion being interpreted as the process whereby ion bombardment induces chemical reactions producing weakly bound molecules which are subsequently desorbed.⁵³ The "recombinant"

or "clearing" mechanism for anisotropic etching (see Fig. 20) proposed⁵³ to explain reactivity of XeF_2 with Si subjected to simultaneous Ar^+ bombardment may involve sputtering of recombinant radicals adsorbed on the surface. The incident ions are believed to sputter or "clear" fluoride product species from the surface and leave "bare" areas with which XeF_2 is more reactive. Although it is doubtful according to Donnelly et al.,¹⁰² that this could lead to anisotropic etching of Si in a plasma when F atoms are the predominant etchant,⁶⁶ such a "clearing" mechanism could conceivably explain anisotropic etching of SiO_2 in F atom-generating plasmas. Donnelly et al recently developed¹⁰² a formalism to calculate etch rates based on this mechanism. However, for large ion-induced enhancements they obtained an equation similar to Eq. (8) where ϕ_d and $\epsilon_{\text{F}(\text{SiO}_2^*)}$ are replaced by ϕ_c (number of product molecules removed per incident ion) and ϵ_{sc} (sticking coefficient for F atoms on a "clear" SiO_2 surface), respectively. Although neither of the "damage" or "clearing" mechanisms can be rejected, there is some evidence in support of the damage hypothesis.¹⁰²

Obviously, if both physical sputtering and chemical erosion are involved in ion-induced synergistic effects, parameters fundamental to these processes will be important. Some of the more relevant processes investigated in detail include:

- (1) Sputter yields in the presence and absence of an active gas: Winters et al.⁷ concluded, after a detailed analysis of various systems, that the rate of physical sputtering always drops in the presence of chemically active gases, and whenever the latter causes an ion-induced etch rate to be strongly enhanced, then mechanisms in addition to physical sputtering are probably operative.

- (2) Mass dependence of yield: Yields (atoms/ion) measured in physical sputtering related experiments depend quite strongly on the mass of the incident ion, whereas ion-induced etching reactions appear to have a much smaller mass dependence.
- (3) Yields vs. ion angle of incidence dependence: Physical sputtering is characterized by yields with a maximum at angles of 60-70° with respect to the surface normal, a distinctive characteristic of energy deposition in a narrow region near the surface, while chemical sputtering is distinguished by yields which are largest at normal incidence, and decreases monotonically as the angle increases (see Fig. 8 of Ref. 7). This result suggests that the etching yield is more sensitive to total deposited energy rather than to the energy deposited in a narrow region near the surface.
- (4) Velocity of ejected species: Velocity distributions of ejected species from semiconductor surfaces have been measured for the XeF₂/Si^{102a} and Cl₂/Si^{102b} systems. A roughly 1/E² dependence was observed at high energies for SiF₃ (indicative of SiF₄), SiF₂ and SiF (see Fig. 9 of Ref. 7), indicating that physical sputtering is a contributing mechanism. However, two maxima appear in the spectrum which correlate with binding energies of 0.1 and 0.5 eV. These are indicative of weakly bound species which would desorb⁷, therefore indicating the existence of other mechanisms additional to physical sputtering.

In relation to the Cl₂/Si system, recent results by Sanders et al.^{102b}, involving measurements of kinetic energy distributions of molecular products, from the reaction Si/Cl₂ + Ar⁺, indicate that more than 90% of them have energies above thermal values. These results were interpreted^{102b} as an indication that the mechanism of the ion-bombardment-induced reaction is far from stimulating the thermal reaction path. Instead, it appears that the main fraction of the products may result from sputtering^{102b}.

(b) Fusion Materials (Carbon)

The consensus regarding the mechanism for ion-induced synergistic effects in fusion materials(carbonaceous) erosion appears to be more uniform. All the evidence ^{6, 16 - 18} strongly suggest that ion-induced damage

is the operative mechanism, at least insofar as the best known material (graphite) is concerned. Similar to the semiconductor case, the models proposed to date to explain synergism in graphite are mainly phenomenological.

Evidence for ion-induced damage in graphite using Raman spectroscopy, was obtained by Wright et al.⁶³ The spectra they observed for ion bombarded (fluence of $\sim 2 \times 10^{19}$ D⁺/cm²) graphite was characteristic of broad structureless bands. After sample annealing at 1300K the Raman structure characteristic of a microcrystalline structure was partially recovered. This observation, together with observed decreases in CH₄ production levels after annealing damaged graphite,^{6,16-18} is indicative of a possible C-H bond breaking process which may help to promote movement of vacancies and interstitials leading to annealing.⁶ Considering that no significant enhancement in the erosion of graphite is observed when the sample is bombarded simultaneously by H⁰ atoms and electrons (see next section), while ions produce a large enhancement, it can be concluded that collisional energy transfer to the carbon lattice is mainly responsible for the enhanced strong reactivity rather than any electronic excitation. Recent results obtained by Vietzke et al.⁶ seem to confirm the previous assumption. They measured the reactivity in the H⁰/X⁺-C reaction as a function of energy of the energetic ions, and found that the reaction probability from 1 keV to 5 keV rises for Ar⁺, slightly rises for Ne⁺ and falls for He⁺ bombardment.⁶ Based on these results Vietzke et al.⁶ proposed that the reaction proceeds stepwise, such that a fast reaction between H⁺ ions and H⁰ on the surface produces precursors (CH, CH₂) which are stable up to ~ 1200 K. This fast

reaction is the real synergistic effect.¹⁸ In a second step these precursors can react with additional H⁰ atoms forming CH₃ which leaves the surface.¹⁸

Additional evidence in favour of the precursor formation model is that related to the H⁰/D⁰ change-over experiments^{6,18,96} described in Section 3.1(b). This precursor formation mechanism is similar to the one suggested by the Toronto group as a possible explanation of temperature-induced activation of graphite⁷² (see Section 2.1(b) of this review). Other results related to CH₄ production as a function of H⁺ ion energy, obtained recently,¹⁷ support the ion-induced mechanism.

Data obtained to date strongly support the ion-induced damage mechanism as the most logical to explain ion-induced synergistic effects in graphite erosion. However, further work is necessary, particularly measurements of CH₄ yields as a function of angle of incidence of bombarding species, and velocity distributions of volatile products. Such experiments would greatly assist in achieving a better understanding of the details of synergistic effects.

4.0 ELECTRON-INDUCED SYNERGISTIC EFFECTS

Combined bombardment of materials by ions (reactives or inert) and reactive sub-eV atoms has produced "substantial" synergistic effects, as discussed in the previous section, for both semiconductor and fusion materials. Electron-induced synergistic effects, by contrast, appear to influence erosion of semiconductor and fusion materials in different ways. Unfortunately, the state of understanding of electron-induced synergisms is not as well developed as is its counterpart for ions. Only phenomenological interpretations of the experimental results have been attempted so far.

(a) Semiconductor Materials

The most interesting system, both technologically and from a "mechanism" viewpoint, is the electron-stimulated etching of SiO_2 , Si_3N_4 , and SiC in the presence of XeF_2 gas. It has been shown⁹ that XeF_2 does not spontaneously attack SiO_2 , Si_3N_4 or SiC in the absence of radiation nor does electron radiation by itself produce etching. The last statement may not be generally applicable to all carbides, nor to all such compounds produced by different techniques. In fact, evidence has been presented recently¹⁰⁵ which suggests that plasma sprayed TiC on Inconel (600) may dissociate under electron impact. X-ray analyses of irradiated samples have shown the presence of TiC , Ti and C on surfaces previously characterized as being TiC only.¹⁰⁵ By contrast, TiC chemically-vapour-deposited on POCO graphite has shown no signs of electron-induced dissociation.¹⁰⁵

Other work demonstrated that electron bombardment of SiO_2 , Si_3N_4 and SiC in the presence of XeF_2 produced etching at appreciable rates, in such a way that erosion occurred only on the area of the sample which was subjected to electron bombardment (Ref. 7 and references therein). The behaviour of the compounds mentioned above was similar (see Fig. 21 for illustrative purposes). Two different experimental procedures were used to demonstrate the effect, differing in the sequence by which the surfaces were exposed to electrons and XeF_2 . Although substantial, the etch rate observed in Fig. 21 is smaller than those produced by plasma etching of the same materials (etch rates above 1600 Å/min have been readily achieved), where the enhanced erosion is attributed mainly to ions.⁴⁰

Auger spectra of SiO_2 , Si_3N_4 and SiC surfaces taken during exposure to XeF_2 indicated that fluorine was present on the surface,⁹ while no Xe was detected on it. This result suggested that the rate limiting step in these

systems was the formation of SiF_4 volatile molecules. Therefore, it seemed reasonable to assume that electron-stimulated etching was a result of electrons helping F atoms to react with these compounds to form SiF_4 . Since F does not react with them spontaneously, it has been suggested that a possible mechanism for the observed electron-enhanced erosion relates to the ability of electrons to dissociate these compounds, producing elemental Si on the surface which can be readily removed by XeF_2 with which Si reacts spontaneously. It is known, for example, that SiO_2 films can be dissociated by electron bombardment to produce elemental Si on the surface of such films.^{106,107} The electron impact may break the Si-O bond,¹⁰⁷ allowing oxygen to evaporate as O_2 .

Electron bombardment, on the other hand, may enhance surface chemical reactivity for film deposition, opposite to etching. It has been shown for example that carbon deposition may be produced on metallic films under electron irradiation in the presence of hydrocarbon vapours.¹⁰⁸ This effect may be due to radiation-enhanced gas-surface chemistry leading to non-volatile products, and may be used advantageously to solve a large number of device fabrication problems in microelectronics. Additionally, it has been shown that electron bombardment can enhance oxidation of semiconductors, in particular Si,^{109,110} a process widely applied in microelectronics technology, although the basic mechanisms are not well understood yet.

(b) Fusion Materials (Carbon)

Electron-induced synergistic effects relevant to fusion applications relate, mainly, to the erosion of carbonaceous materials (graphite, and compounds such as SiC, TiC, etc) when bombarded simultaneously by electrons and low-energy hydrogenic atoms. The existence of a "substantial"

electron-induced synergistic effect in the production of methane has been a matter of some controversy. One set of studies¹¹¹⁻¹¹³ (A) has shown what appeared to be a strong enhancement of CH₄ yields (~20-fold over the yields due to H⁰ bombardment alone), as a result of electron impact on carbon of various types. Yields as high as 0.1 CH₄/e have been reported.¹¹¹⁻¹¹³ A "second"^{70,114,115} (B) and "third set"^{6,16} (C) of studies have shown, by contrast, relatively small enhancements with an upper limit of ~50%-100%.

In the A studies, data related to the apparently strong effect¹¹¹⁻¹¹³ were obtained by using the backfilling technique, i.e., H⁰ atoms were generated by H₂ dissociation on a hot W filament¹¹⁶ located together with the carbon sample in a high vacuum chamber filled with H₂ at pressures ranging from 1.3×10⁻⁶ to 6.5×10⁻⁴ Pa. Methane evolving from the target was detected by using a quadrupole mass spectrometer in the RGA mode. Preparation procedures for samples (bake-out history, cleaning, etc) were generally not reported, and H⁰ fluxes were estimated from Hickmott's results¹¹⁶ (not measured for the particular experiments) to be ~10¹⁵ H⁰/cm²s. Electrons of 40 to 600 eV energy with fluxes of ~10¹³ e/cm²s were used for irradiation.¹¹¹⁻¹¹³

In the B, studies data related to the observation of a relatively small electron-induced enhancement in CH₄ production were obtained by also using the backfilling technique.^{70,114,115} However, systematic experimental procedures for sample preparation and characterization, as well as for conditioning of the UHV system used in the experiments, were followed.^{70,114,115} These precautions were taken because of the identification of spurious methane signals that could be confused with those due to a true synergistic effect. It was observed, for example, that relatively large amounts of CH₄ can be desorbed from different carbons

(papyex, pyrolytic graphite, etc), as received from suppliers, by electron bombardment alone in vacuum (no H^0 impact). Methane yields up to $0.01 CH_4/e$ were measured under these conditions.^{70,114,115} Such spurious methane signals might originate from the desorption of H/D complexes and/or hydrocarbons formed at the surface during desorption of large amounts of hydrogen already in the samples. The manufacturing processes of many types of graphite involving prolonged high-temperature heating of carbon in air, may lead to substantial uptake of H_2O and reactions leading to the inclusion of hydrogen, hydrocarbons, and other impurities.¹¹⁷ In the B studies, the samples and system were baked at temperatures of 1200-1900K for 1-24 hours, and 500K for 24 hours, respectively; this reduced CH_4 spurious signals, due to electron impact alone, to 10^{-4} - $10^{-5} CH_4/e$.

In the B studies, a second source of spurious signals was identified as the desorption of CH_4 from the target chamber and quadrupole walls due to H_2 and H^0 impact on them when backfilling the system. A similar effect has been observed also by other groups.^{118,119} Bombardment of the walls with H^0 while keeping the sample hot ($\sim 1000K$) reduced the CH_4 background signals from $\sim 5 \times 10^{-3}$ to less than $10^{-4} CH_4/H_2$ when backfilling, and consequently during experiments. After such stringent conditioning of the vacuum system, methane production was approximately doubled during $H^0 + e^-$ bombardment over the case of H^0 exposure alone. Measured yields varied in the range 10^{-4} - $10^{-3} CH_4$ per electron or per H^0 for bombarding fluxes of $\sim 10^{15} H^0/cm^2s$ (as measured in-situ) and $\sim 10^{16}$ electrons/s (electron energy: 100-500 eV).^{70,114,115} H_2 backfill pressures of about 5×10^{-2} Pa were necessary to produce the H^0 fluxes mentioned above.^{22,70} According to these experiments^{70,114,115} the backfilling technique can only be used reliably in erosion studies, if spurious effects are minimized by following stringent conditioning procedures for the experimental system.

In the C studies,^{6,16} where a small electron-induced synergistic effect was also observed, the H^0 was produced by a beam source. In this way, sub-eV H^0 atoms impacted on the carbon surface after being focussed in a beam, restricting the simultaneous interaction of H^0 and electrons (from a gun) to a confined area, in such a way that the spurious effects mentioned above were diminished to very small values.

Some experiments performed recently^{120,121} suggest a possible mechanism whereby electrons may produce synergistic effects when impacting on graphite simultaneously with H^0 . Electrons may excite low energy transitions between the π -valence and π -conduction bands producing a highly reactive excited state that may enhance the H^0/C reaction. However, the lack of information^{120,121} on relevant parameters of the experimental method and some inconsistencies with previous results¹¹¹⁻¹¹³ makes difficult the analysis of the new data.^{120,121} In any case, the principal conclusion, regarding the use of graphite in fusion device environments, is that electron-induced synergistic effects for methane production appear to be small and will generally be negligible compared with ion-induced synergism, at least when considered separately.

There are two questions, however, that may warrant consideration. Firstly, what would be the level of CH_4 production for electron-induced enhancement on graphite loaded with high doses of hydrogenic species as may occur in a fusion device? Secondly, what would be the effect of electrons when added to the $H^+ + H^0$ bombarding species?

5.0 PHOTON-INDUCED SYNERGISTIC EFFECTS

(a) Semiconductor Materials

The increasing interest in developing new techniques for processing electronic materials was responsible for the discovery of ion and electron

assisted chemical processing of semiconductors. It was only a matter of time then until one of the new powerful sources of radiation, i.e., lasers, was tested with the same purpose. Early studies^{11,12,122} demonstrated the feasibility of photon-enhanced chemical reactions; however, it was only recently that several groups started research in this field, encouraged by its potential applications in microelectronics. It has been observed that laser photons with wavelengths in the range from UV to the infrared could be readily focussed onto solid surfaces and therefore were well suited for promoting surface reactions with high spatial resolution. Also, the monochromaticity, the coherence and the high photon flux of the laser light are highly advantageous. Indeed, dry chemical etching,^{13(a,d),14,123-125} doping of semiconductors¹²⁴ and chemical-enhanced vapour deposition^{124,126} have been demonstrated. Laser-enhanced electrochemical plating and etching for the liquid-solid systems have also been reported.¹²⁷

More recently, work has been directed at acquiring a better understanding of the various reaction mechanisms involved in photon-enhanced chemical etching; this is the most interesting aspect, in relation to fusion applications, owing to its relevance in the understanding of possible similar processes in a fusion device environment. Photons can influence, as ions and electrons do, any one or all of the steps involved in etching, as described in the introduction. Therefore, several mechanisms can account for photon-enhanced chemical reaction effects.¹⁴

(1) Chemical Etching Activated by Molecular Vibrational Excitation

It has been shown that irradiation was able to excite reactive molecules into highly vibrationally excited states and thereby enhance the process of

dissociative chemisorption and subsequent surface reactions to form volatile products.^{14,128} This mechanism was demonstrated for the Si-SF₆ system, where reaction occurred only when SF₆ molecules were vibrationally excited. It was shown that the surface reaction yield as a function of laser intensity used in the experiment follows the relation $EY = I^{3.5}$, indicating that three or more photons were likely to be involved in promoting SF₆ molecules into high vibrational levels to overcome the activation barrier for reaction. Furthermore, it was observed that collisional deactivation of excited molecules with the gas reduced the lifetime of the excited state, therefore localizing the excited molecules to a small region just above the Si surface.

(2) Chemical Etching by Photon-Generated Radicals

Photons can dissociate molecules also to produce reactive radicals either by multiple photon excitation of the ground electronic state or single photon photolysis involving excited electronic states. This effect was also observed with the Si-SF₆ system. The main difference between this and the vibrational excitation mechanism is that even fluorine atoms generated several mm away from the surface can still survive collisions with other gas phase molecules and diffuse to the surface for reaction.

(3) Chemical Etching by Photon Excitation of Solids

Surface reactions can also be induced by the solid excitation alone. This effect has been observed in the interactions of XeF₂ gas with Si, SiO₂, Ta and Te films. The gas molecules do not absorb the infrared photons in this case, and the only effect of the radiation is to cause lattice excitation and heating so that the F atoms landing on the surface can rearrange to form SiF₄ molecules which subsequently desorb into the gas phase.

It is not known at the moment whether some or all of these phenomena occur in a fusion device environment in such a way as to stimulate chemistry between hydrogen and impurity molecules and/or atoms and carbonaceous surfaces. However, the possibility exists and may warrant some investigation.

(b) Fusion Materials (Carbon)

Recent work^{120,121} has shown that CH₄ evolves from carbon samples (papyex) when these are bombarded simultaneously by UV photons, from a high pressure Hg arc lamp, and supposedly, sub-eV H⁰ atoms. There is some uncertainty, however, as to the actual H⁰ fluxes used in the experiments since they are not indicated in the written reports^{120,121} and information on relevant experimental parameters is not presented. A mechanism similar to that described for electron-induced synergism in carbon (see Sec. 4b) has been proposed^{120,121} to explain the photon-induced enhancement of carbon erosion. Again, the lack of vital information makes the analysis of the data difficult.

6.0 CONCLUSIONS

Research performed to date, directed at obtaining a better understanding of plasma-surface interaction phenomena, has shown again the importance of interdisciplinary activity in science. Phenomena occurring in two different fields of science, such as microelectronics fabrication and fusion technology, may relate to common physical mechanisms, suggesting that an improved interdisciplinary focus may be beneficial. It has been indicated in this review that similar chemistry may operate in reactions involving different gaseous environments and materials. Chemical erosion phenomena, the subject of major interest in this review, may be highly

beneficial in semiconductor technology or detrimental in fusion technology, depending on the particular circumstances.

General mechanisms for erosion processes of semiconductors (Si for example) and fusion materials (graphite for example) may be very similar, as shown in studies related to the formation of SiF_4 and CH_4 , respectively. These studies indicated that precursor formation [SiF_x ($x = 1, 2, 3$) or CH_x ($x = 1, 2, 3$)] may be considered as a similar mechanism for both Si and C erosion in different gaseous environments. However, some differences may exist regarding, for instance, the temperature dependence of chemical reactions, and the final species evolving from surfaces, which are responsible for erosion. Both materials may be eroded by energetic ion (whether reactive or not) bombardment alone, although some differences may exist in the mechanisms ultimately responsible for ion-induced erosion, as indicated by different evolutions of sputtering yields (the main parameter in erosion processes) with respect to ion angle of incidence and energy.

Ion-induced synergistic effects have been observed in erosion processes of both semiconductors and carbon. However, results obtained in research related to microelectronics suggest that various mechanisms may be operative depending on physical parameters; chemically enhanced physical sputtering, ion damage-induced chemical reaction and chemical sputtering (ion-induced chemical reaction) have been identified as three of the most likely mechanisms to occur in etching of semiconductors. By contrast, work in fusion technology (related to carbon) has shown that ion-induced damage may explain most of the effects observed in ion-induced synergism.

The implications of the existence of these effects in both microelectronics fabrication and fusion technology applications are rather different. Synergism is highly beneficial in the first case permitting

creation, via etching of semiconductor surfaces, of sophisticated microelectronic circuits. In fusion, synergistic erosion may have both desirable and undesirable implications. The creation of a wall-protecting, impurity-dominated, radiating edge plasma may be required in fusion devices and controlled erosion processes could play a useful role. On the other hand, radiative cooling of the plasma core by impurities is highly undesirable, as is deterioration of wall structural components by erosion; in addition, contamination of the DT fuel recycle loop by molecules such as CF_4 is undesirable. Further work is necessary to answer several open questions.

ACKNOWLEDGMENTS

This research was supported by the Canadian Fusion Fuels Technology Program, The Natural Sciences and Engineering Research Council of Canada and the Ontario Ministry of Energy. We thank C. Perez for his contribution related to the commissioning of the experimental facilities used in our work, and the members of the Fusion Research Group at the Aerospace Institute (Univ. of Toronto) for help with some experiments. We thank all authors cited in the figure captions for kindly allowing us to include them in the review. Finally, We thank J. Bohdansky, J. Roth, E. Vietzke, and H.F. Winters for useful discussions.

REFERENCES

1. V.M. Donnelly, D.E. Ibbotson, and D.L. Flamm: in "Ion Bombardment Modification of Surfaces: Fundamentals and Applications"; Eds. O. Auciello and R. Kelly (Elsevier Science Publ., Holland, 1984) p. 323.
2. M.A. Abdou, in Proc. of the 12th Symposium on Fusion Technology - EURATOM, Julich, 1982 (Pergamon Press, 1983) p.39.
3. H. Vernickel, R. Behrisch, B. Scherzer, and F. Wagner, Eds., "Plasma Surface Interaction in Fusion Devices", J. Nucl. Mater. 93/94 (1980).
4. D.M. Gruen, S. Veprek, and R.B. Wright, in Plasma Chemistry I, Eds. S. Veprek and M. Venugopalan (Springer-Verlag, 1980) p.45.
5. R.W. Conn: in "Fusion Materials Development in the U.S., Effects of Radiation on Materials"; 11th Conference, ASTM - STP 782, Eds. H.R. Brager and J.S. Perrin, American Society of Testing and Materials, 1982, p.1159.
6. E. Vietzke, M. Erdweg, F. Flaskamp and V. Philipps, Proc. of the 9th Inter. Vacuum Congress and 5th Inter. Conference on Solid Surfaces: Invited Speaker Volume, Ed. J.L. de Segovia (ASEVA, Spain, 1983) p.627.
7. H.F. Winters, J.W. Coburn, and T.J. Chuang, J. Vac. Sci. Technol. B1, 469 (1983).
8. Workshop on Synergistic Effects in Surface Phenomena Related to Plasma-Wall Interactions, Nagoya, Japan, May 21-23, 1984.
9. J.W. Coburn and H.F. Winters, J. Appl. Phys. 50, 3189 (1979).
10. H.F. Winters and J.W. Coburn, Appl. Phys. Lett. 34, 70 (1979).

11. M.K. Sullivan and G.A. Kolb, *Electrochem. Techn.* 6, 430 (1968).
12. L.L. Sveshnikova, V.I. Donin, and S.M. Repinskii, *Sov. Tech. Phys. Lett.* 3, 223 (1977).
13. D.J. Ehrlich, R.M. Osgood Jr., and T.F. Deutsch, *Appl. Phys. Lett.* (a)36, 698 (1980); (b)36, 916 (1980); (c)38, 399 (1981); (d) 38, 1018 (1981).
14. T.J. Chuang, *J. Chem. Phys.* 72, 6303 (1980).
15. T.J. Chuang, *IBM J. Res. and Develop.* 26(#2), 145 (1982).
16. E. Vietzke, K. Flaskamp, and V. Phillips, *J. Nucl. Mater.* 111/112, 763 (1982).
17. A.A. Haasz, O. Auciello, P.C. Stangeby, and I.S. Youle, *Proc. 6th Inter. Conf. on Plasma-Surface Interactions in Controlled Fusion Devices, Nagoya, Japan, 1984*, *J. Nucl. Mater.* (in press).
18. E. Vietzke, K. Flaskamp and V. Philipps, *6th Inter. Conference on Plasma-Surface Interactions in Controlled Fusion Devices, Nagoya-Japan, 1984*, *J. Nucl. Mater.* (in press).
19. D. Manos, T. Bennett, R. Budny, S. A. Cohen, S. Kilpatrick, and J. Timberlake, *30th Natl. AVS Symposium, Boston (USA), 1983*, *J. Vac. Sci. and Technol. A* (in press).
20. G.M. McCracken and P.E. Stott, *Nuclear Fusion* 19, 889 (1979).
21. J. Roth: in "Chemical Sputtering", *Sputtering by Particle Bombardment II*, Ed. R. Behrisch (Springer-Verlag, 1983) p.91.
22. P.C. Stangeby, O. Auciello, and A.A. Haasz, *J. Vac. Sci. and Technol.* A1, 1425 (1983).
23. D. Rosenberg and G.K. Wehner, *J. Appl. Phys.* 33, 1842 (1962).
24. (a) J. Roth, J. Bohdansky, W. Poschenrieder, M.K. Sinha, *J. Nucl. Mater* 63, 222 (1976).

- (b) J. Roth and J. Bohdansky: IEA Workshop on Graphite, Rigi-Kaltbad, Switzerland (Oct. 1982).
25. J. Bohdansky, J. Roth, and M.K. Sinha: in Proc. 9th Symposium on Fusion Technology (Pergamon, London 1976) p.541.
26. B. Feinberg and R.S. Post, J. Vac. Sci. Technol. 13, 443 (1976).
27. N.P. Busharov, E.A. Gorbатов, V.M. Gusev, M.I. Guseva, Yu.V. Martynenko, Sov. J. Plasma Phys. 2, 321 (1976).
28. S.K. Erents, C.M. Braganza, and G.M. McCracken, J. Nucl. Mater. 63, 399 (1976).
29. (a) J.N. Smith Jr., C.H. Meyer Jr., J.K. Layton, Nucl. Technol. 29, 318 (1976);
(b) J. Nucl. Mater. 67, 234 (1977).
30. K. Sone, H. Ohtsuka, T. Abe, R. Yamada, K. Obara, O. Tsukakoshi, T. Nausaway, T. Satake, M. Mizuno, and S. Komiya: In Proc. Inter. Symposium on Plasma-Wall Interaction, Julich 1976 (Pergamon Press, 1977) p.323.
31. J. Bohdansky, H.L. Bay, and W. Ottenberger, J. Nucl. Mater. 76, 163 (1978).
32. J.A. Borders, R.A. Langley, K.L. Wilson, J. Nucl. Mater. 76, 168 (1978).
33. C.M. Braganza, S.K. Erents, G.M. McCracken, J. Nucl. Mater. 75, 220 (1978).
34. R. Yamada, K. Nakamura, K. Sone, and M. Saidoh, J. Nucl. Mater. 95, 278 (1980).
35. R. Yamada, K. Nakamura, and M. Saidoh, J. Nucl. Mater. 98, 167 (1981.)
36. J. Roth, J. Bohdansky, and K.L. Wilson, J. Nucl. Mater. 111/112, 775 (1982).

37. R. Yamada and K. Sone, J. Nucl. Mater. 116, 200 (1983).
38. O. Auciello, A. A. Haasz, P. C. Stangeby, and I. S. Youle (to be published).
39. W.R. Grove, Philos. Trans. R. Soc. London 11, 87 (1852).
40. D.L. Flamm and V.M. Donnelly, Plasma Chem. and Plasma Processing 1, 317 (1981).
41. V. Philipps, K. Flaskamp and E. Vietzke, J. Nucl. Mater. 111/112, 781 (1982).
42. P. Sigmund, in "Sputtering by Ion Bombardment I", Ed. R. Behrisch (Springer-Verlag, 1981), p.9-71.
43. D.E. Ibbotson, D.L. Flamm, J.S. Mucha, and V.M. Donnelly, Appl. Phys. Lett. (in press).
44. D.L. Flamm, V.M. Donnelly, and J.A. Mucha, J. Appl. Phys. 52, 3633 (1981).
45. M.J. Vasile and F.A. Stevie, J. Appl. Phys. 53, 3799 (1982).
46. A.B. King and H. Wise, J. Phys. Chem. 67, 1163 (1963).
47. B.J. Wood and H. Wise, J. Phys. Chem. 73, 1348 (1969).
48. M. Coulon and L. Bonnetain, J. Chem. Phys. 71, 711 (1974).
49. M.B. Balooch, and D.R. Olander, J. Chem. Phys. 63, 4772 (1975).
50. R.K. Gould, J. Chem. Phys. 63, 1825 (1975).
51. R.R. Rye, Surf. Sci. 69, 653 (1977).
52. T. Abe, K. Obara, and Y. Murakami, J. Nucl. Mater. 91, 223 (1980).
53. Y.Y. Tu, T.J. Chuang, H.F. Winters, Phys. Rev. B23, 8231 (1981).
54. A.P. Webb and S. Veprék, Chem. Phys. Lett. 62, 173 (1979).
55. S. Veprék and V. Mareček, Solid State Electron. 11, 683 (1968).
56. T.J. Chuang, J. Appl. Phys. 51, 5273 (1980).

57. V.M. Donnelly and D.L. Flamm, J. Appl. Phys. 51, 5273 (1980).
58. J.A. Mucha, V.M. Donnelly, D.L. Flamm, and L.M. Webb, J. Phys. Chem. 85, 3529 (1981).
59. J.A. Mucha, D.L. Flamm, and V.M. Donnelly, J. Appl. Phys. 53, 4553 (1982).
60. N.F. Mott, Trans. Faraday Soc. 43, 429 (1940).
61. N. Cabrera and N.F. Mott, Rep. Prog. Phys. 12, 163 (1949).
62. F.P. Fehner and N.F. Mott, J. Oxidation Met. 2, 59 (1970).
63. R.B. Wright, R. Varma, and D.M. Gruen, J. Nucl. Mater. 63, 415 (1976).
64. W.J. Choyke and L. Patrick, Phys. Rev. Lett. 20, 355 (1972); Phys. Rev. B9, 3214 (1974).
65. W. J. Choyke and L. Patrick, Phys Rev. B8, 1660 (1973).
66. D.L. Flamm, D.E. Ibbotson, J.A. Mucha, and V.M. Donnelly, Solid State Technology, 26, 117 (1983).
67. U. Gerlach-Meyer, J.W. Coburn, E. Kay, Surf. Sci. 103, 177 (1981).
68. D.E. Rosner and H.D. Allendorf, in Heterogeneous Kinetics at Elevated Temperatures, Proc. of the Inter. Conference of the University of Pennsylvania, 1969, Eds. G.R. Belton and W.L. Warrell (Plenum, New York, 1970) p.231.
69. C.S. Pitcher, O. Auciello, A.A. Haasz, and P.C. Stangeby, 6th Inter. Conference on Plasma Surface Interactions in Controlled Fusion Devices, Nagoya, Japan 1984, J. Nucl. Mater. (in press).
70. A.A. Haasz, P.C. Stangeby, and O. Auciello, J. Nucl. Mater. 111/112, 757 (1982).

71. A. A. Haasz, O. Auciello and P. C. Stangeby (in preparation).
72. O. Auciello, A.A. Haasz and P.C. Stangeby, 9th Inter. Vacuum Congress and 5th Inter. Conference on Solid Surfaces, Nucl. Technol./Fusion (in press).
73. J.C. Batty, R.E. Stickney, J. Chem. Phys. 51, 4475 (1969).
74. G.A. Bitel, J. Vac. Sci. Technol. 6, 224 (1969).
75. K. Flaskamp, H.R. Ihle, G. Stocklin, E. Vietzke, K. Vogelbruck, and C.H. Wu, Proc. Inter. Symposium on Plasma-Wall Interaction, Julich-1976 (Pergamon Press, 1977) p.285.
76. H.R. Kaufman, J.J. Cuomo, and J.M.E. Harper, J. Vac. Sci. Technol. 21, 725 (1982).
77. J.M.E. Harper, J.J. Cuomo, and H.R. Kaufman, J. Vac. Sci. Technol. 21, 737 (1982).
78. H.H. Andersen and H.L. Bay: in "Sputtering by Particle Bombardment I", Ed. R. Behrisch (Springer-Verlag, 1981), p. 145.
79. R. Behrisch, J. Nucl. Mater. 85/86, 1047 (1979).
80. D.R. Olander, W. Siekhaus, R. Jones, J.A. Schwarz, J. Chem. Phys. 57, 408 (1972).
81. S. Veprek, A.P. Web, H.R. Oswald, and H. Stuessi, J. Nucl. Mater. 68, 32 (1977).
82. O. Auciello, R. Kelly, and R. Iricibar, Rad. Eff. 46, 105 (1979)
83. R. Kelly and O. Auciello, Surf. Sci. 100, 135 (1980).
84. O. Auciello, Rad. Eff. 60, 1 (1982).
85. O. Auciello, J. Vac. Sci. Technol. 19, 841 (1981).
86. O. Auciello: in "Ion Bombardment Modification of Surfaces: Fundamentals and Applications"; Eds. O. Auciello and R. Kelly (Elsevier Science Publ., Holland, 1984) p.1 and 435.

87. B.A. Banks: in "Ion Bombardment Modification of Surfaces: Fundamentals and Applications", Eds. O. Auciello and R. Kelly (Elsevier Science Publ., Holland, 1984) p.339.
88. S.K. Erents, C.M. Braganza, and G.M. McCracken, J. Nucl. Mater. 63, 399 (1976).
89. C.J. Mogab and H.J. Levenstein, J. Vac. Sci. Technol. 17, 721 (1980).
90. E.P. EerNisse, J. Vac. Sci. Technol., 12, 564 (1975).
91. H.K. Pulker, Thin Solid Films, 32, 27 (1976).
92. U. Gerlach-Meyer, J.W. Coburn, and E. Kay, Surf. Sci. 103, 177 (1981).
93. R. Yamada and K. Sone, J. Nucl. Mater. (in press).
94. E. Vietzke, Workshop on Synergistic Effects in Surface Phenomena Related to Plasma-Wall Interaction (1984, unpublished).
95. E. Vietzke (private communication).
96. K. Ashida, K. Ichimura, M. Matsuyama, H. Miyake and K. Watanabe, J. Nucl. Mater. 111/112, 769 (1982).
97. O. Auciello, R.A. Baragiola, E.R. Salvatelli, and J. L. Spino, in "Ion Implantation in Semiconducors" 1976, Eds. F. Chernow, J.A. Borders, and D.K. Brice (Plenum, New York, 1977), p. 231.
98. W.O. Hofer and H. Liebl, in Ion Beam Surface Layer Analysis, Eds. O. Meyer, G. Linker, and F. Kappeler (Plenum Press, New York, 1976), p. 659.
99. W.O. Hofer, H.L. Bay, P. J. Martin, J. Nucl. Mater. 76/77, 156 (1978).
100. R. Behrisch, J. Roth, J. Bohdanský, A.P. Martinelli, B. Schweer, D. Rusbuldt, and E. Hintz, J. Nucl. Mater. 94/95, 645 (1980).
101. J. L. Mauer, J.S. Logan, L.B. Zielinski, and G.S. Schwartz, J. Vac. Sci. Technol. 15, 1734 (1978).

102. V.M. Donnelly, D.L. Flamm, W.C. Dantremont-Smith, and D.J. Werder, J. Appl. Phys. 55, 242 (1984).
- 102a. R.A. Haring, A. Haring, F.W. Saris, and A.E. de Vries, Appl. Phys. Lett. 41, 174 (1982).
- 102b. F.H.M. Sanders, A.W. Kolfshoten, J. Dieleman, R.A. Haring, A. Haring, A.E. de Vries, J. Vac. Sci. Technol. A2, 487 (1984).
103. U. Gerlach-Meyer, Surf. Sci. 103, 524 (1981).
- 103a. H.F. Winters (private communication, 1984).
104. P. Sigmund, Phys. Rev. 184, 383 (1969); 187, 768 (1969).
105. O. Auciello, A.A. Haasz, and P.C. Stangeby, J. Vac. Sci. Technol. A2, 630 (1984).
106. S. Thomas, J. Appl. Phys. 45, 161 (1974).
107. B. Carriere and B. Lang, Surf. Sci. 64, 209 (1977).
108. A.N. Broers, W.W. Molzen, J.J. Cuomo, and N.D. Wittels, Appl. Phys. Lett. 29, 596 (1976).
109. M.C. Munoz, and J.L. Sacedon, J. Chem. Phys. 74, 4693 (1981).
110. W. Reuter and K. Wittmaack, Appl. Surf. Sci. 5, 221 (1980).
111. C.I.H. Ashby and R.R. Rye, J. Nucl. Mater. 92, 141 (1980).
112. C.I.H. Ashby and R.R. Rye, J. Nucl. Mater. 103/104, 489 (1981).
113. C.I.H. Ashby, J. Nucl. Mater. 111/112, 750 (1982).
114. O. Auciello, A.A. Haasz, P.C. Stangeby, and P.R. Underhill, in proc. of the 9th Symposium on Engineering Problems of Fusion Research, Chicago, 1981, Ed. C.K. Choi (IEEE, New York, 1981) p.252.
115. O. Auciello, A.A. Haasz, and P.C. Stangeby, Phys. Rev. Lett. 50, 783 (1983).
116. T.W. Hickmott, J. Appl. Phys. 31, 128 (1960).
117. H.B. Palmer, in "Chemistry and Physics of Carbon", Ed. P.L. Walker Jr., vol. 1 (M. Dekker Inc., New York, 1965) p.265.
118. K.J. Dietz, F. Waelbroeck, and P. Wienhold, in "Cleaning of Large Metallic Vessels for Plasma Confinement Devices", Kernforschungsanlage Julick Report No. JUL-1448, 1977 (unpublished).

119. H.F. Dylla and W.R. Blanchard, J. Vac. Sci. Technol. A1, 1297 (1983).
120. C.I.H. Ashby, Appl. Phys. Lett. 43, 610 (1983).
121. C.I.H. Ashby, J. Vac. Sci. Technol. A1, 935 (1983).
122. I.M. Beterov, V.P. Chebotaev, N.I. Yurshina, and B. Ya. Yurshin, Sov. J. Quantum Electron 8, 1310 (1978).
123. J.I. Steinfeld, T.G. Anderson, C. Reiser, D.R. Denison, L.D. Hartsough and J.R. Hollahan, J. Electrochem. Soc. 127, 514 (1980).
124. D.J. Ehrlich, R.M. Osgood Jr., and T.F. Deutsch, IEEE J. Quant. Electr. QE-16, 1233 (1980), and references therein.
125. T.J. Chuang, J. Vac. Sci. Technol. 18, 638 (1981).
126. S.D. Allen and M. Bass, J. Vac. Sci. Technol. 16, 431 (1979); also S.D. Allen, SPIE 198, 49 (1979).
127. R.J. von Gutfeld, E.E. Tynan, R.L. Melcher, and S.E. Blum, Appl. Phys. Lett. 35, 651 (1979).
128. T.J. Chuang, J. Chem. Phys. 74, 1453 (1981).

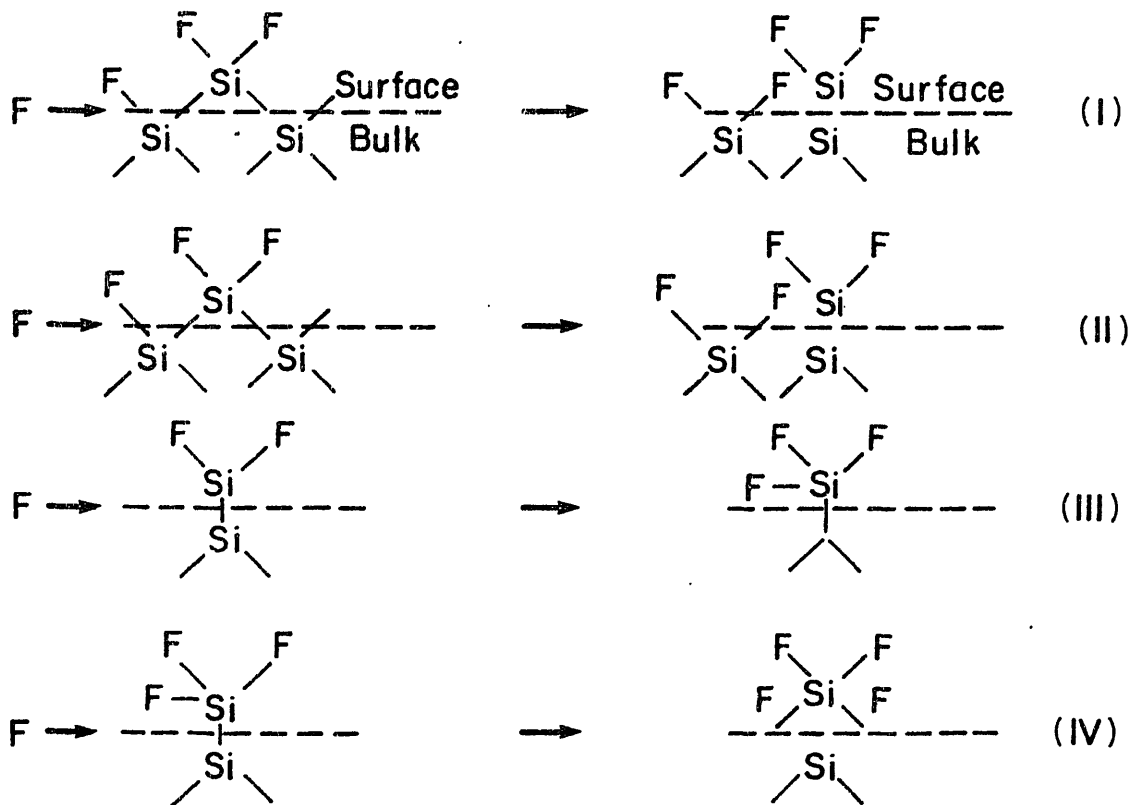


Fig. 1 Mechanism of Si etching by F atoms.

(I) Concerted reaction breaks bonds, resulting in $\text{SiF}_2(\text{s})$;
 (II) Concerted reaction results in bound fluorosilicon radicals;
 (II)-(IV) Further fluorination of bound radicals liberates gaseous SiF_4 . Experiments were interpreted by the authors of this mechanism as showing that (I) and (II) are channels of a single, rate-limiting branching reaction (Flamm and Donnelly⁴⁰).

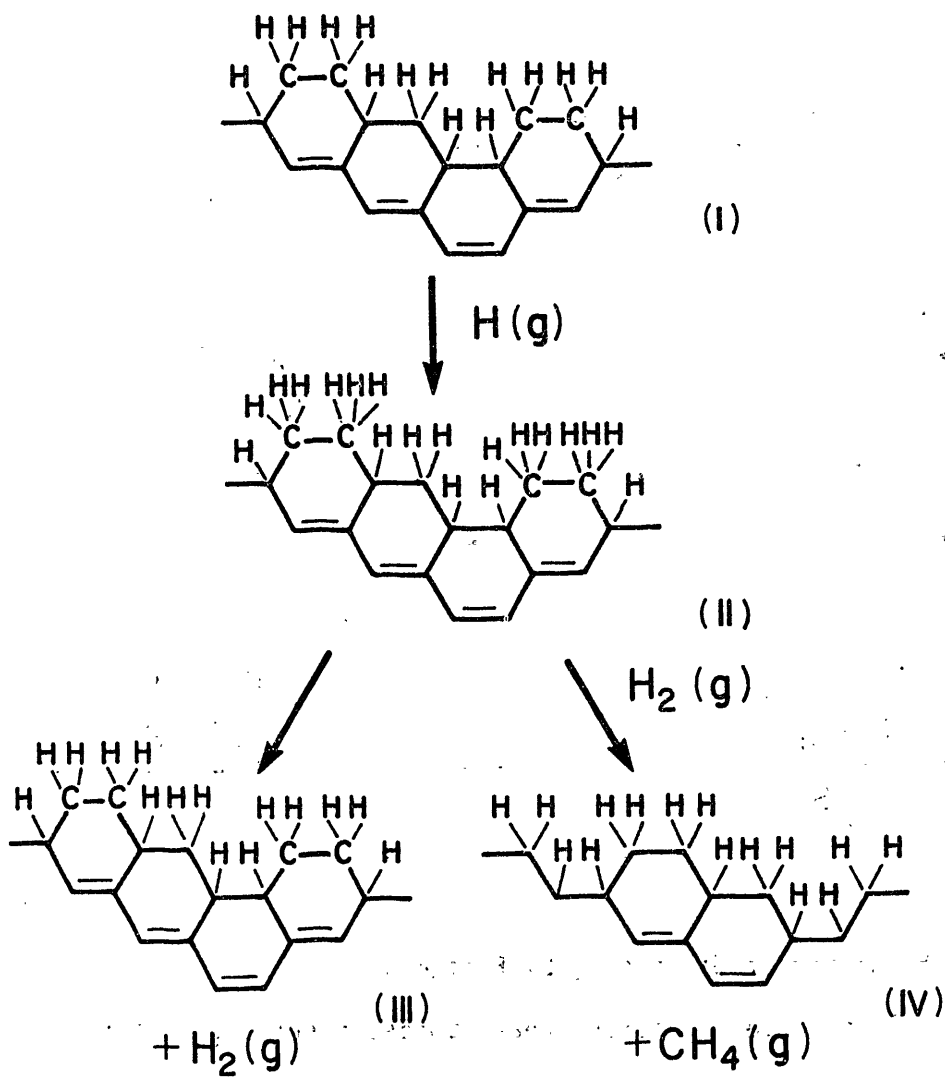


Fig. 2 Conceptual illustration of the mechanism for CH₄ formation in sub-eV H⁰-C interaction. Notice the competitive reaction channel leading to H⁰ recombination on the surface, which results in H₂ desorption (Wood and Wise⁴⁷).

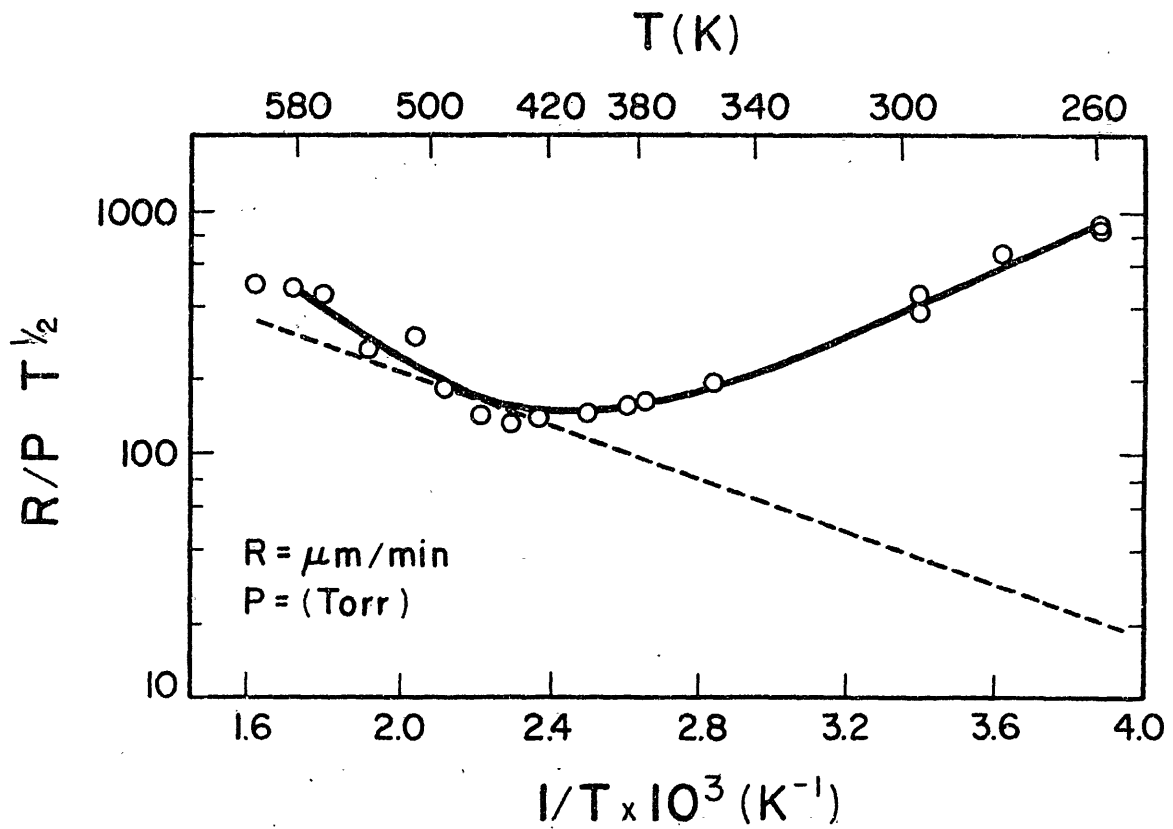


Fig. 3 Etch rate of (100) Si by XeF_2 (points and connecting solid curve), and Si etch rate by F-atoms (dotted line) vs temperature. (Flamm et al.⁶⁶).

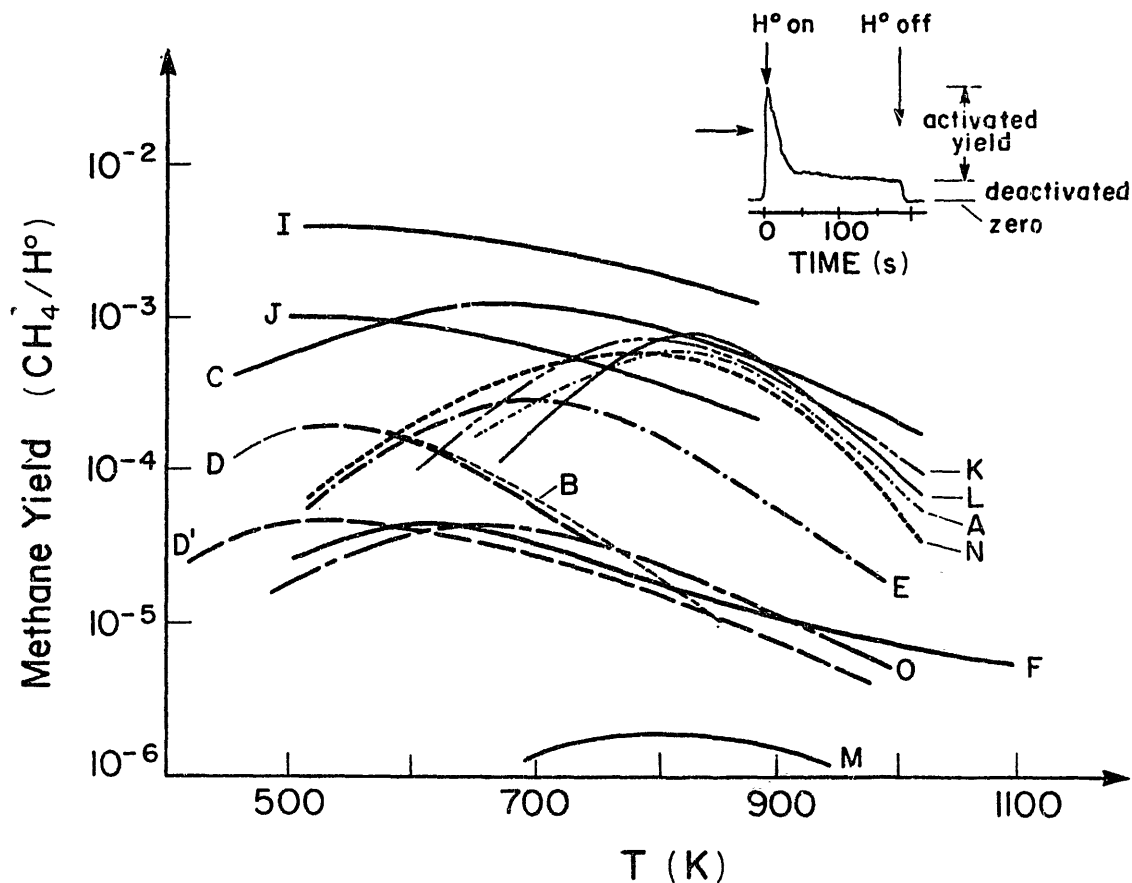


Fig. 4 Methane yields for $\lesssim 1$ eV atomic hydrogen-carbon interaction from various studies. (A) Stangeby, Auciello, Haasz,²² thermally reactivated papyex (H_2 backfilling method). (B) As A, but deactivated. (C) Vietzke, Flaskamp, Phillipps¹⁶ supposedly ion bombardment reactivated pyrolytic graphite (basal plane). (D) As C, but deactivated. (D') New results by Vietzke et al.¹⁸ with supposedly deactivated graphite. (E) Gould,⁵⁰ results on thermally reactivated spectroscopic grade graphite (H_2 backfilling method). (F) As E, but deactivated. (I) Balooch and Olander's data⁴⁹ on supposedly deactivated pyrolytic graphite (prism plane). (J) Same as I on basal plane. (K) Wood and Wise,⁴⁷ high pressure-plasma study (probably activated carbon). (L) Rossner and Allendorf,⁶⁸ high pressure study on electrographite. (M) Coulon and Bonnetain,⁴⁸ high pressure study on amorphous carbon. (N) Pitcher et al.⁶⁹ thermally reactivated pyrolytic graphite (sub-eV H^0 beam method). (O) As N, but deactivated. Insert shows the evolution in time of the CH_4 signal at a fixed target temperature, as measured by the Toronto Group (curves A, B, N, O). The transient peak almost disappears at about 500K and 1000K acquiring intermediate values and passing through a maximum at intermediate temperatures.

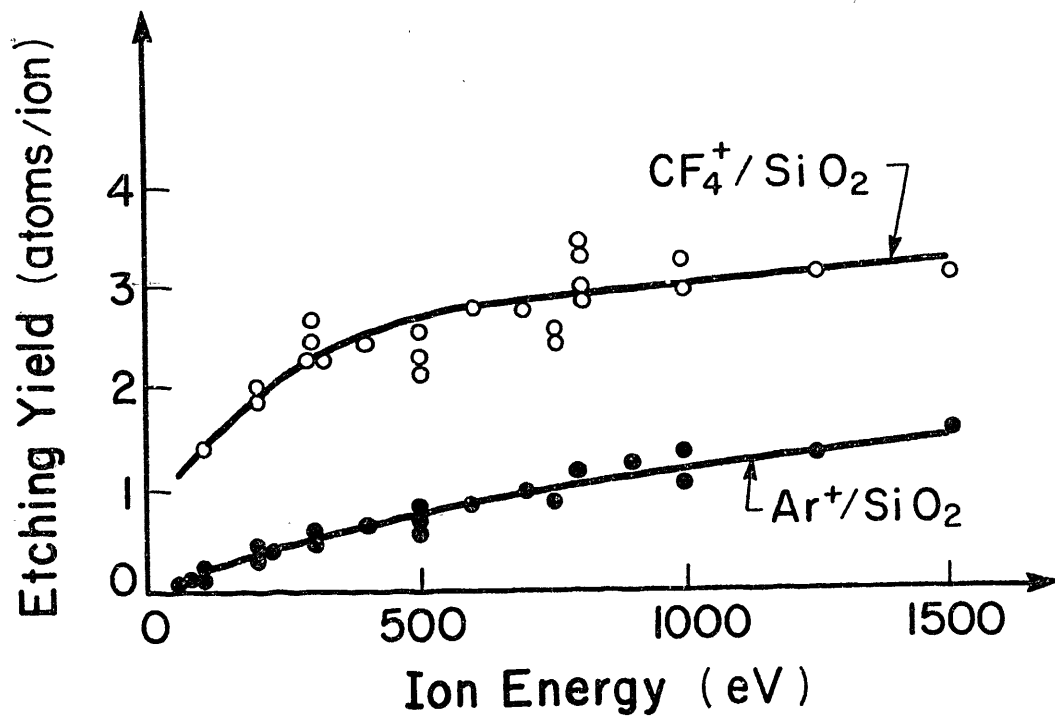


Fig. 5 Etching yields vs ion energy for SiO_2 using Ar^+ and CF_4^+ ions (Harper et al.⁷⁷).

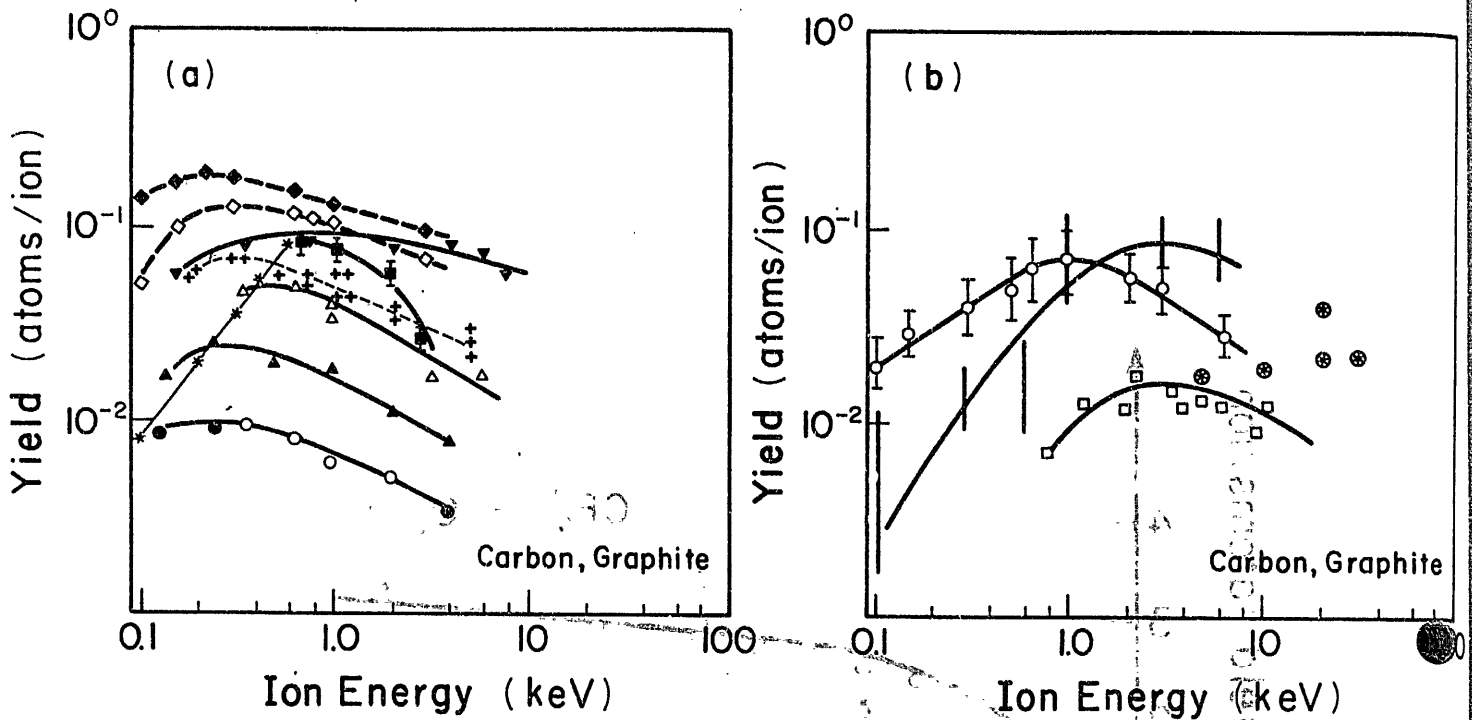


Fig. 6 Experimental sputtering yield data for carbon bombarded by hydrogenic and helium ions as obtained by different groups. Symbol \perp means perpendicular bombardment, PG means pyrolytic graphite, and QMS means quadrupole mass spectrometry.

(a) * ⁴He⁺, Rosenberg & Wehner,²³ unspecified carbon, weight loss (570-870 K) (1962).

■ H⁺ Roth et al.^{24(a)} PG, weight loss (\perp , 920K) (1976).

● & ○ H⁺, ▲ D⁺, ▼ ⁴He⁺, Boldansky et al.³¹ PG, weight loss (\perp , Target at Room Temp.) (1978).

△ D⁺, Borders et al.³² POCO AXF-Q1, RBS on sputter deposit (\perp , 300K) (1978)

◇ H⁺, ◆ D⁺, Roth et al.^{24(b)}, papyex, weight loss (\perp , 900K) (1982).

+ H⁺, Auciello et al.³⁸ PG, QMS-CH₄ (45°, 750-800K) (1984).

(b) | H⁺, Sone et al.³⁰ PG, weight increase/sputter deposit (\perp , 770K) (1976).

□ H⁺, Smith et al.²⁹ PG, weight loss (\perp , 300K) (1977).

⊙ H⁺, Braganza et al.³³ (1978).

○ H⁺, Yamada et al.³⁵ PG, QMS-CH₄ (\perp , 798K) (1981).

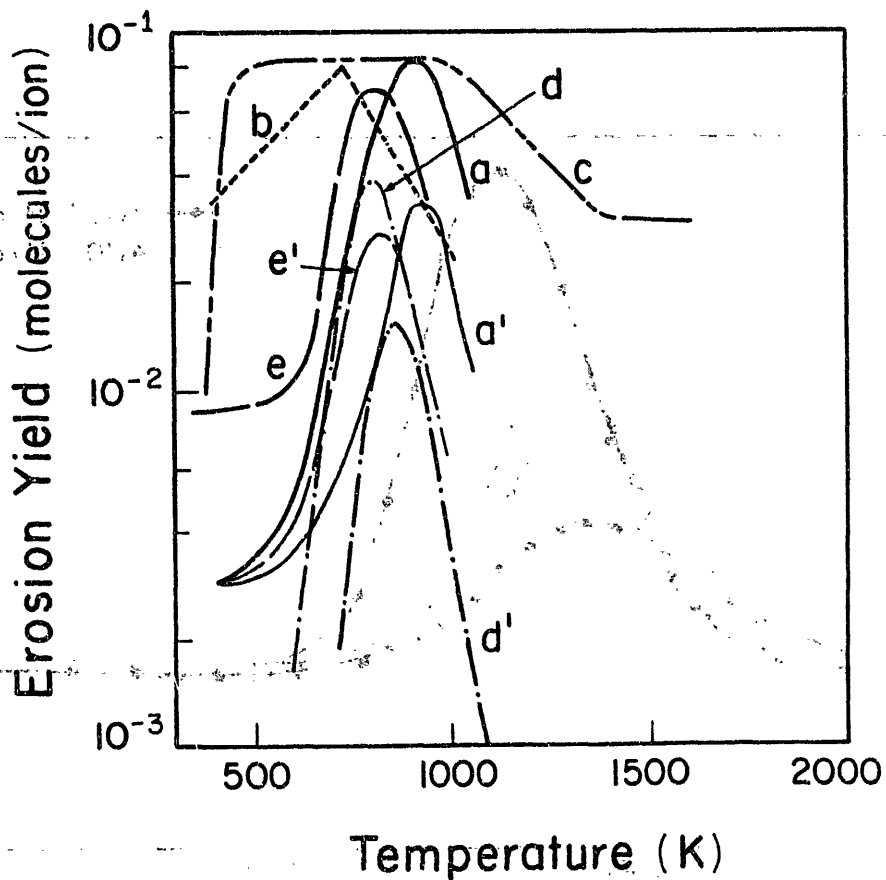


Fig. 7 Erosion yield of graphites due to interaction with hydrogen as a function of temperature; a,^{24a} b,²⁶ c²⁷ measured by change in weight or volume, and d,^{28,33} e³⁴ measured by emission of CH₄. The differences between a-a', d-d' and e-e' indicate the ranges of reaction yields for different incident ion energies (Roth²¹)

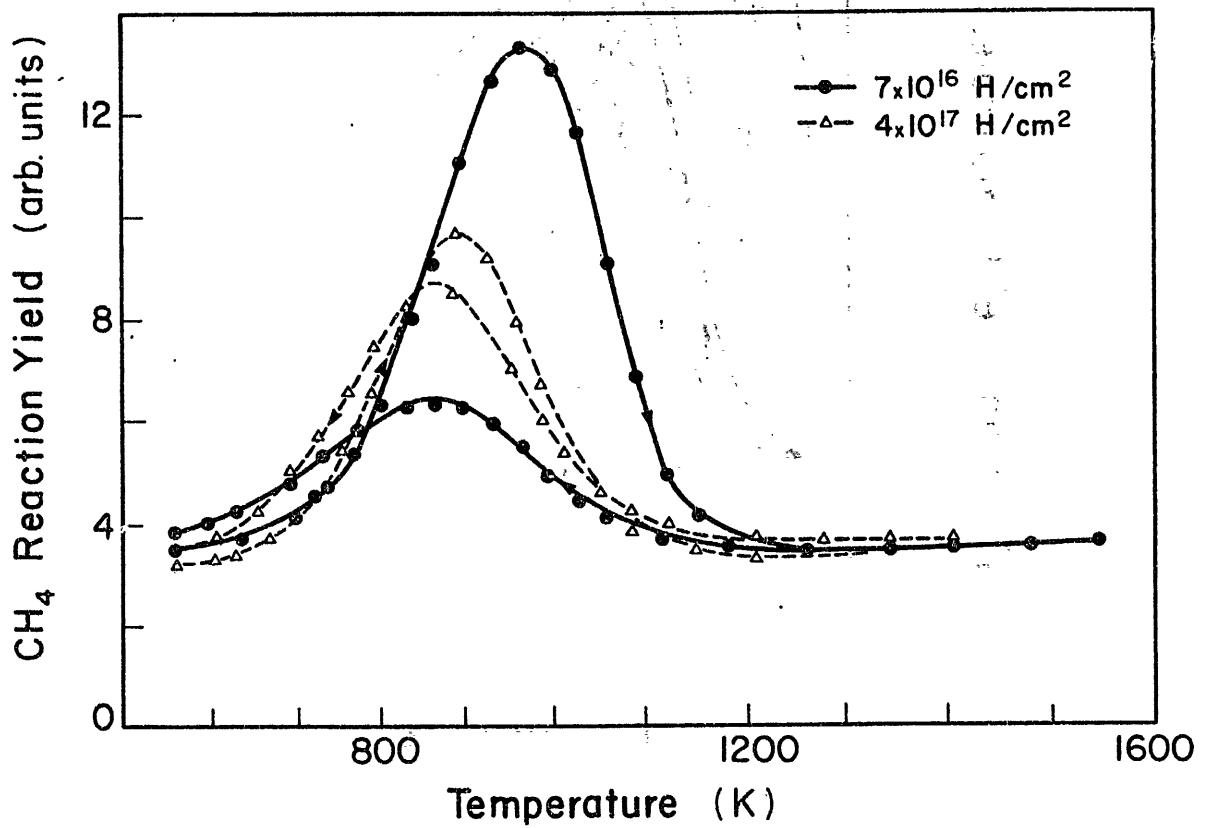


Fig. 8 Variation of the CH₄ reaction yield with target temperature for 2 keV H⁺ bombardment of graphite. Arrows on the curves through the data indicate the direction of temperature change while the data were obtained (Roth²¹).

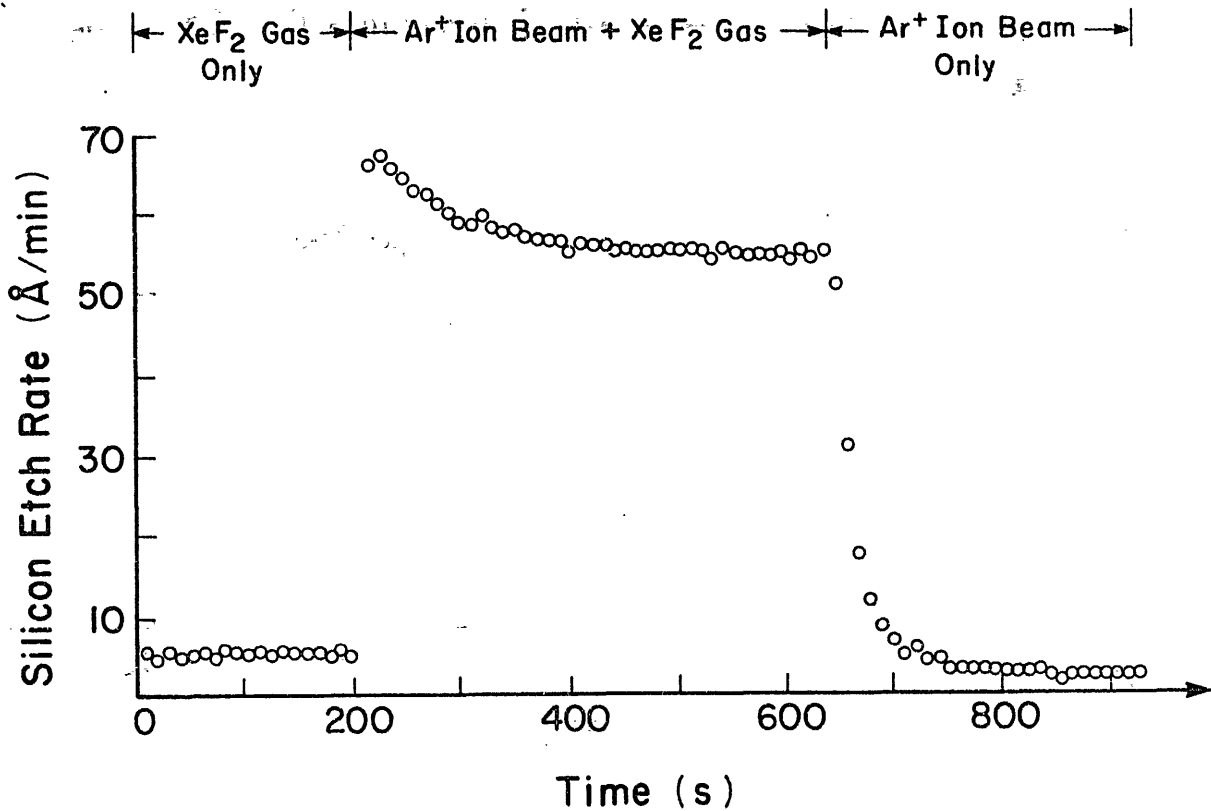


Fig. 9 Si etch rate for ion-assisted gas-surface chemistry using Ar⁺ and XeF₂ on silicon (volatile reaction product). Ar⁺ energy: 450 eV; Ar⁺ current: 0 μA for t < 200s, 2.5 μA for t > 200s; XeF₂ flow: 2×10¹⁵ molecules/s for t < 660s and flow is off for t > 660s. The Ar⁺ current density and the XeF₂ flux were not uniform over the Si surface. The effective area for the Ar⁺ current and the XeF₂ flux were estimated at 0.1 cm² and 0.3 cm², respectively (Coburn and Winters⁹).

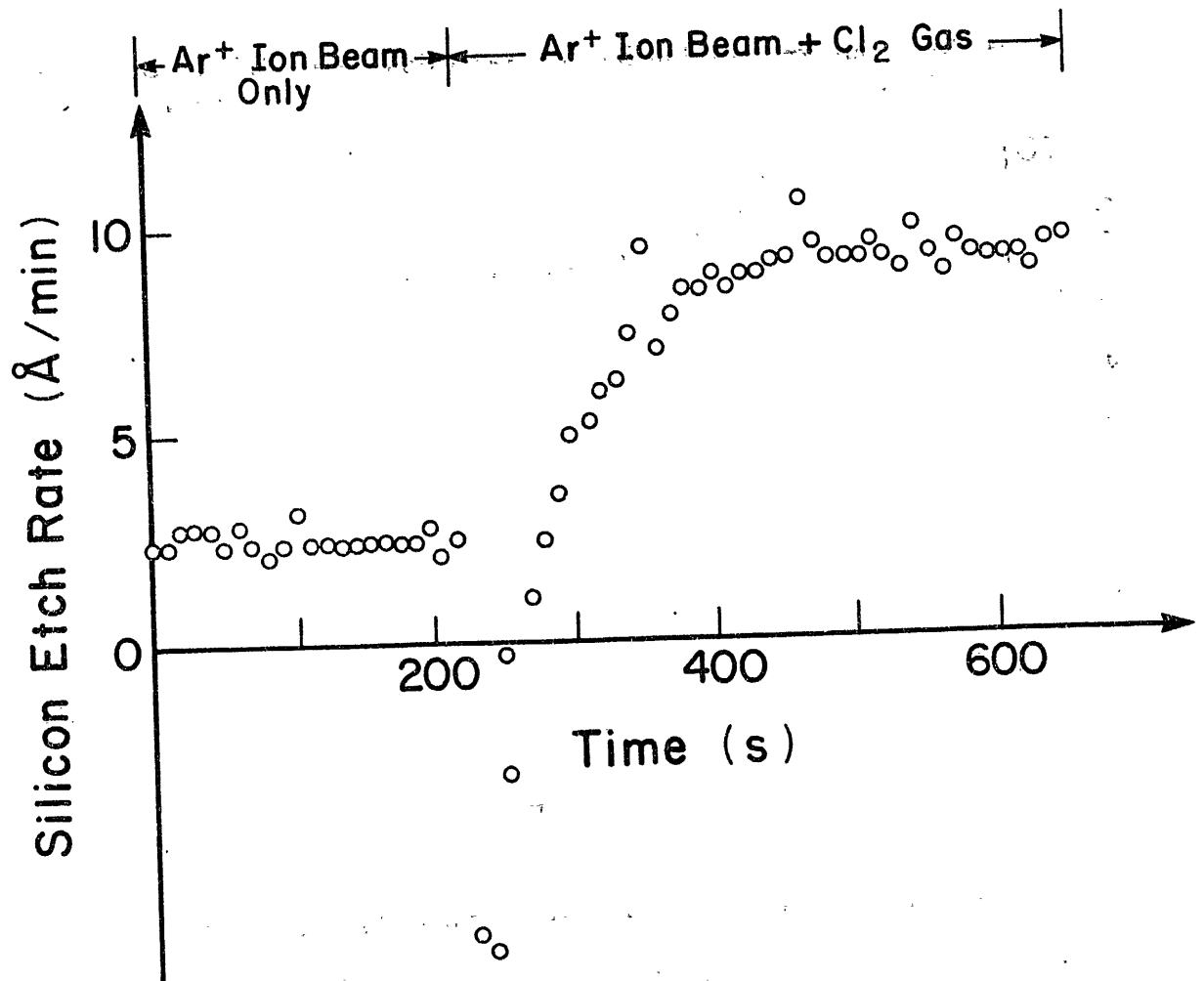


Fig. 10 Etch rate for ion-assisted gas-surface chemistry using Ar⁺ and Cl₂ on silicon (volatile reaction product). Ar⁺ energy: 450 eV; Ar⁺ current: 1.0 μA; Cl₂ flow off for t < 220s, Cl₂ flow = 7×10¹⁵ molecules/s for t > 220s (Coburn and Winters⁹).

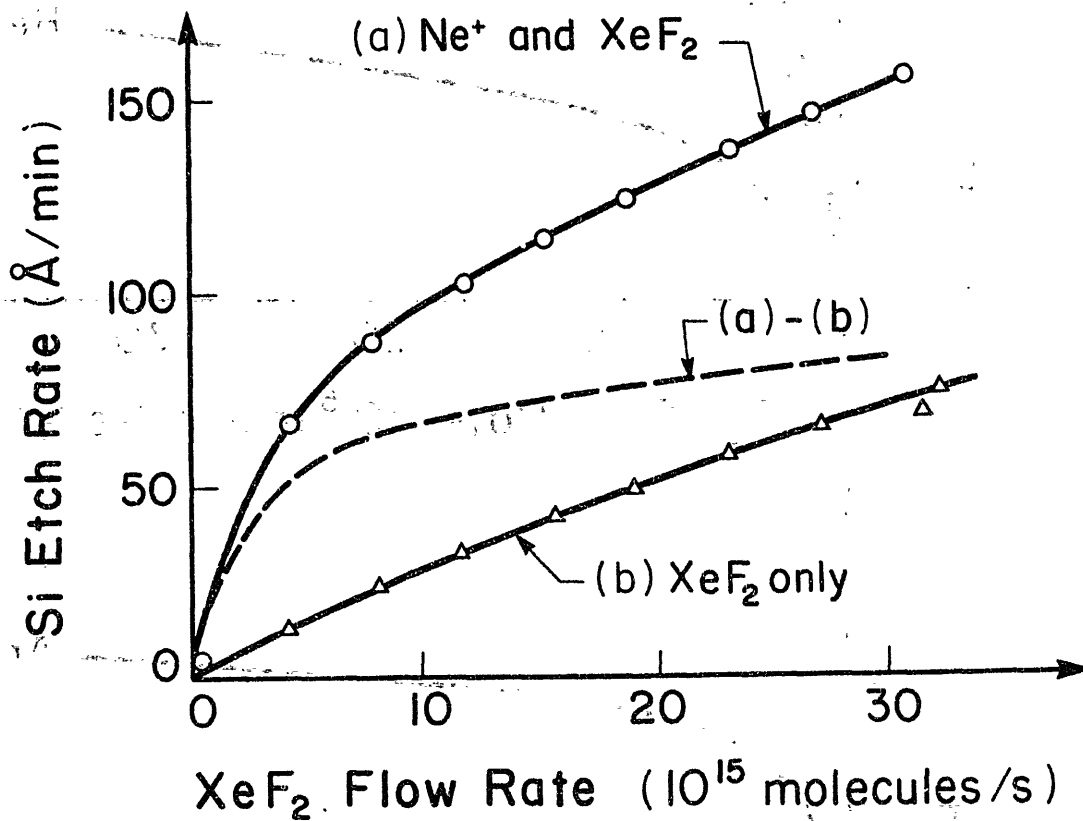


Fig. 11 Etch rate of Si as a function of the XeF₂ flow rate: (a) with XeF₂ and Ne⁺ simultaneously incident on the Si surface; (b) with XeF₂ only; (a)-(b) the ion-enhanced portion of the etch rate obtained by subtracting curve (b) from curve (a). Ion beam parameters: energy: 1 keV; current: 0.44 μA; area: 8 mm². To convert the XeF₂ flow rate to a gas flux, an estimate of the effective area of the gas jet is about 0.5 cm² (Gerlach-Meyer et al.⁹²).

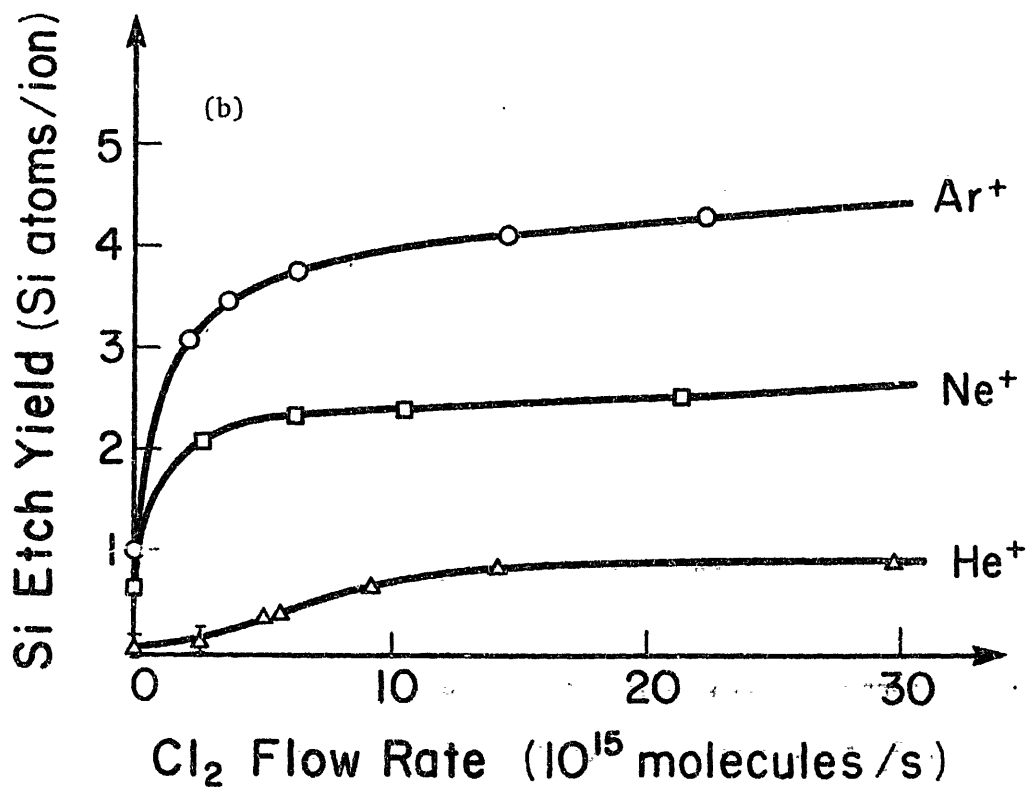
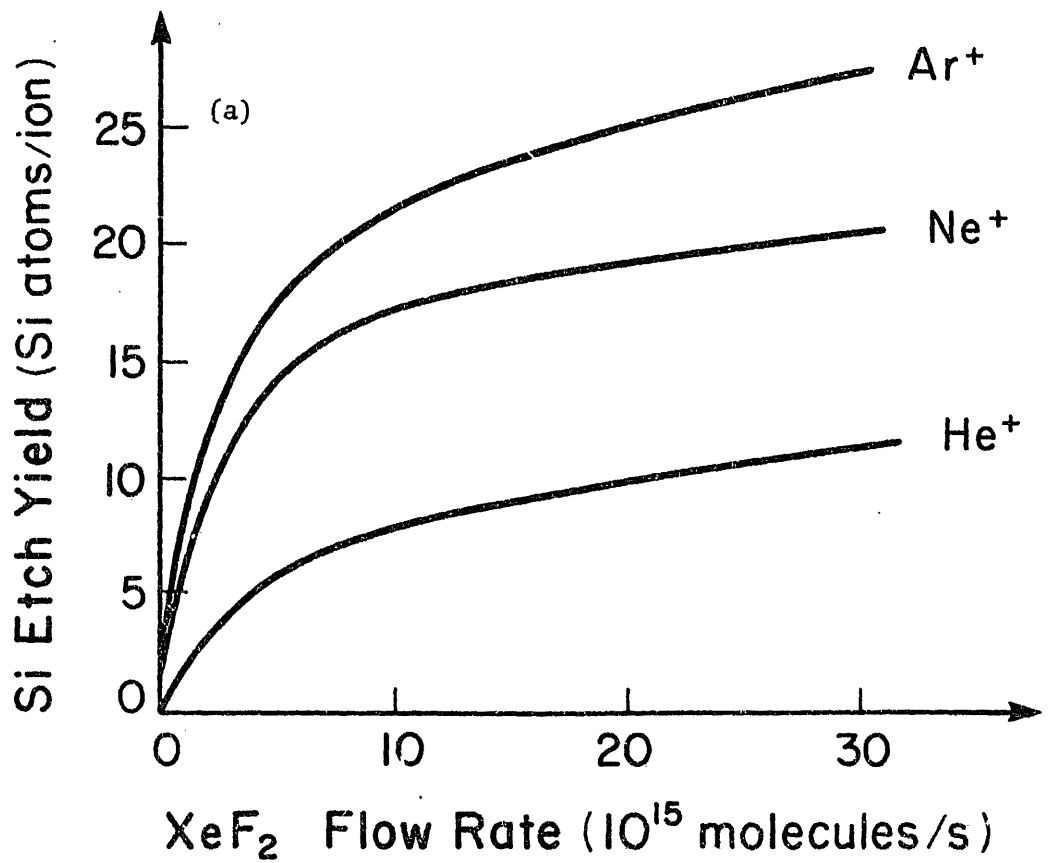


Fig. 12 (a) Etch yield of Si as a function of the XeF_2 flow for 1 keV He^+ , Ne^+ , and Ar^+ . All curves were obtained by subtraction of etch yields as indicated in Fig. 11. (b) Same as (a) for the Si- Cl_2 system. Notice the different yields for both systems (Gerlach-Meyer et al.⁹²).

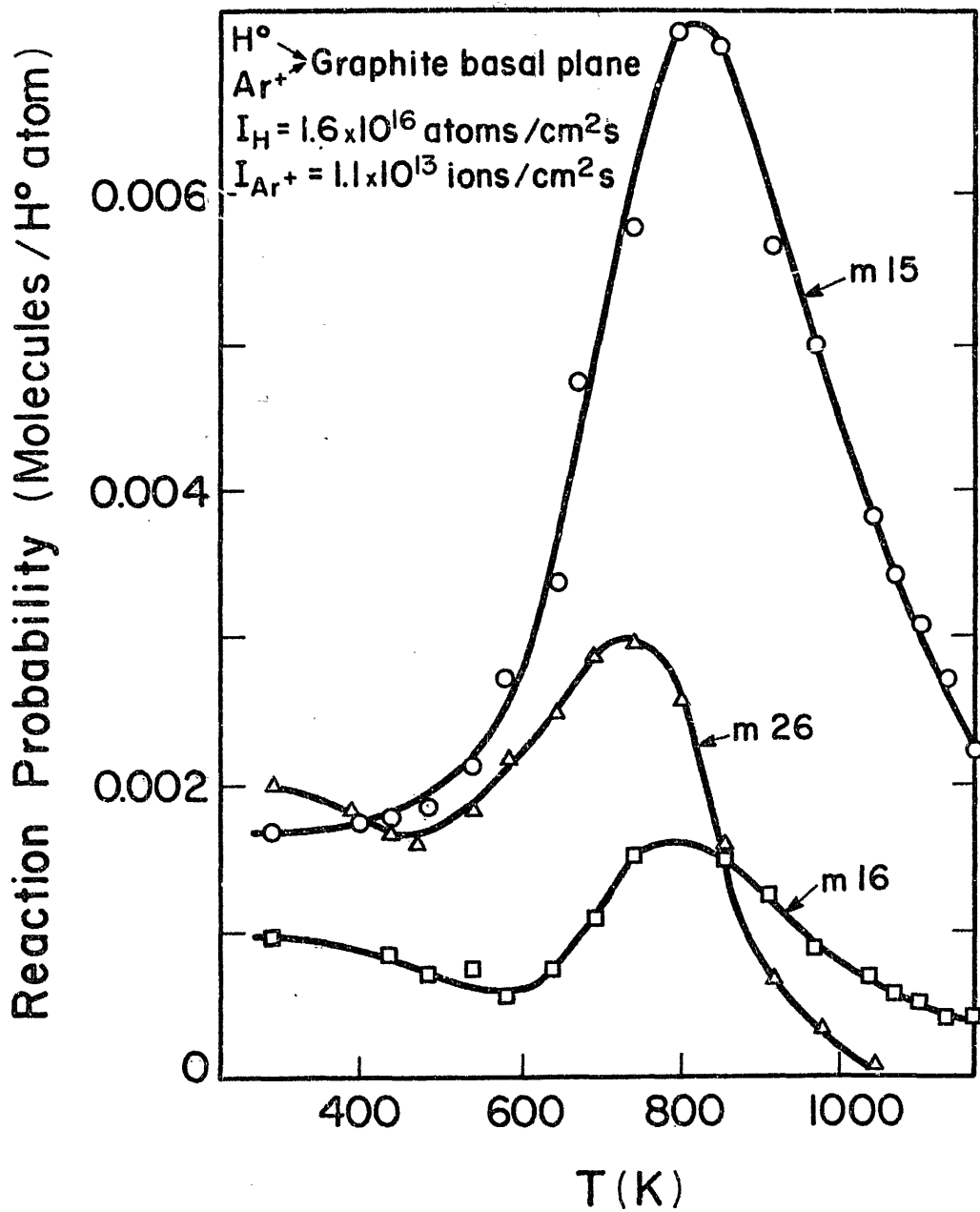


Fig. 13 Temperature dependence of reaction probability (molecules/incident H° -atom) for mass 15 (CH_3), mass 16 (CH_4) and C_2 compounds (mass 26) by simultaneous H° -atom/ Ar^+ -ion (5 keV) irradiation of graphite. The CH_4 peak at 800 K is uncertain due to possible recombination of the CH_3 radical with the walls and the limited pumping speed of the ionizer (Vietzke et al.⁶).

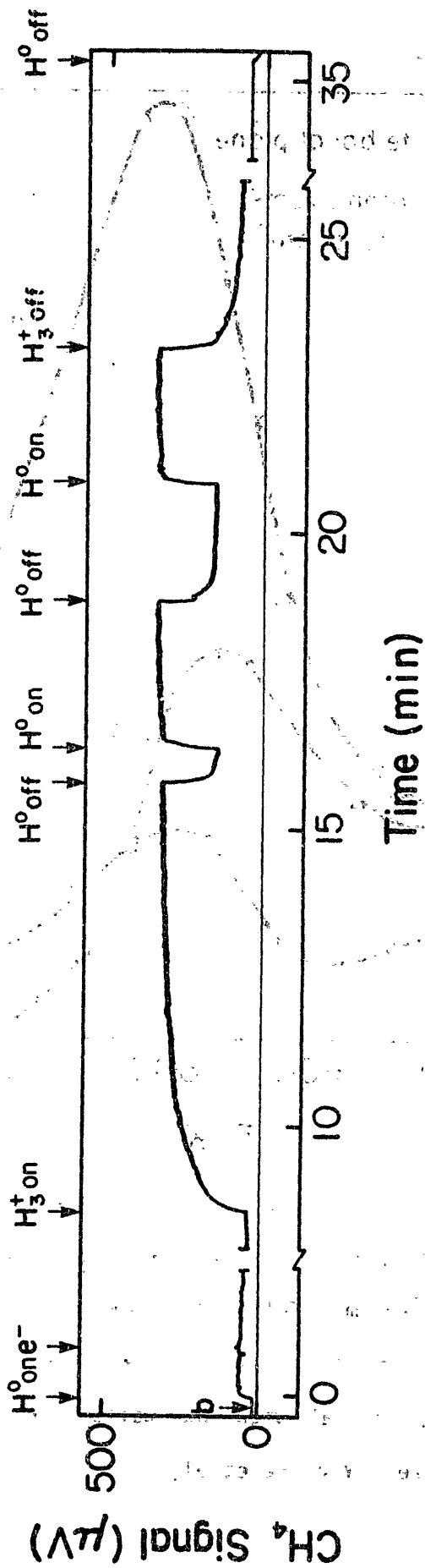


Fig. 14 Quadrupole signal (mass 15) showing the time evolution of methane production for 300 eV proton energy and 7×10^{14} H^+ /cm²s. The background methane signal in the absence of both H^+ and H^0 is indicated by 'b'. The H^0 flux density was $\sim 6 \times 10^{14}$ H^0 /cm²s (Haasz et al.¹⁷).

RESEARCH LABORATORY OF PLASMA PHYSICS

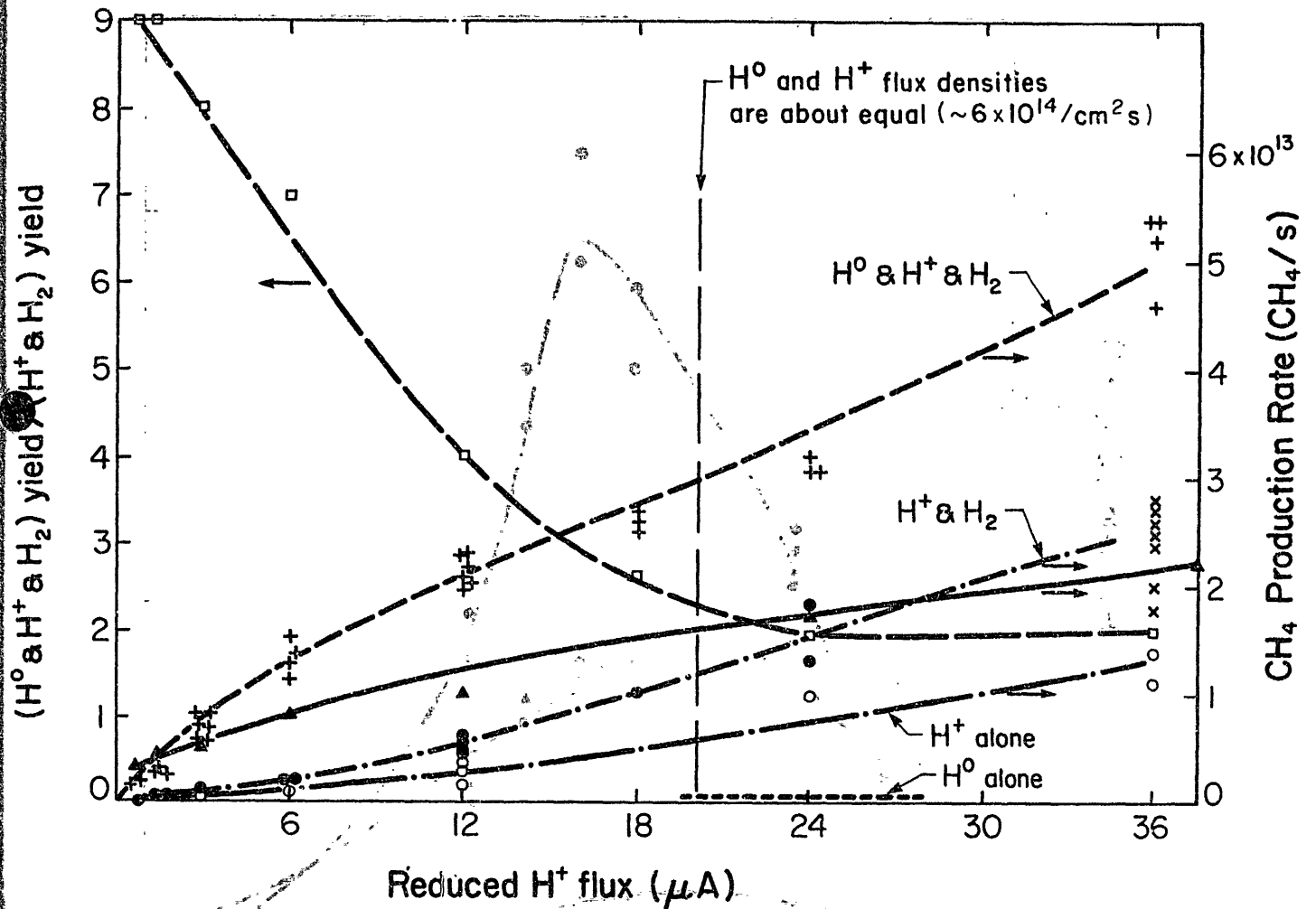


Fig. 15 Methane production rate from carbon (at 750-800K) as a function of H⁺ ion flux (at 300 eV) under various conditions: o H⁺ in vacuum, ● H⁺ + H₂ (~4 × 10⁻⁴ torr), + H⁺ + H⁰ + H₂ (H⁰ flux ~6 × 10¹⁴/cm²s and P_{H₂} ~4 × 10⁻⁴ torr). Also shown is the level of CH₄ due to H⁰ alone. The ratio of methane production (or yields) for the cases (H⁰+H⁺+H₂) and (H⁺ + H₂) is indicated by □. The symbol ▲ shows the methane production due to sequential exposure of carbon to H⁺ ions and H⁰ (Haasz et al.¹⁷).

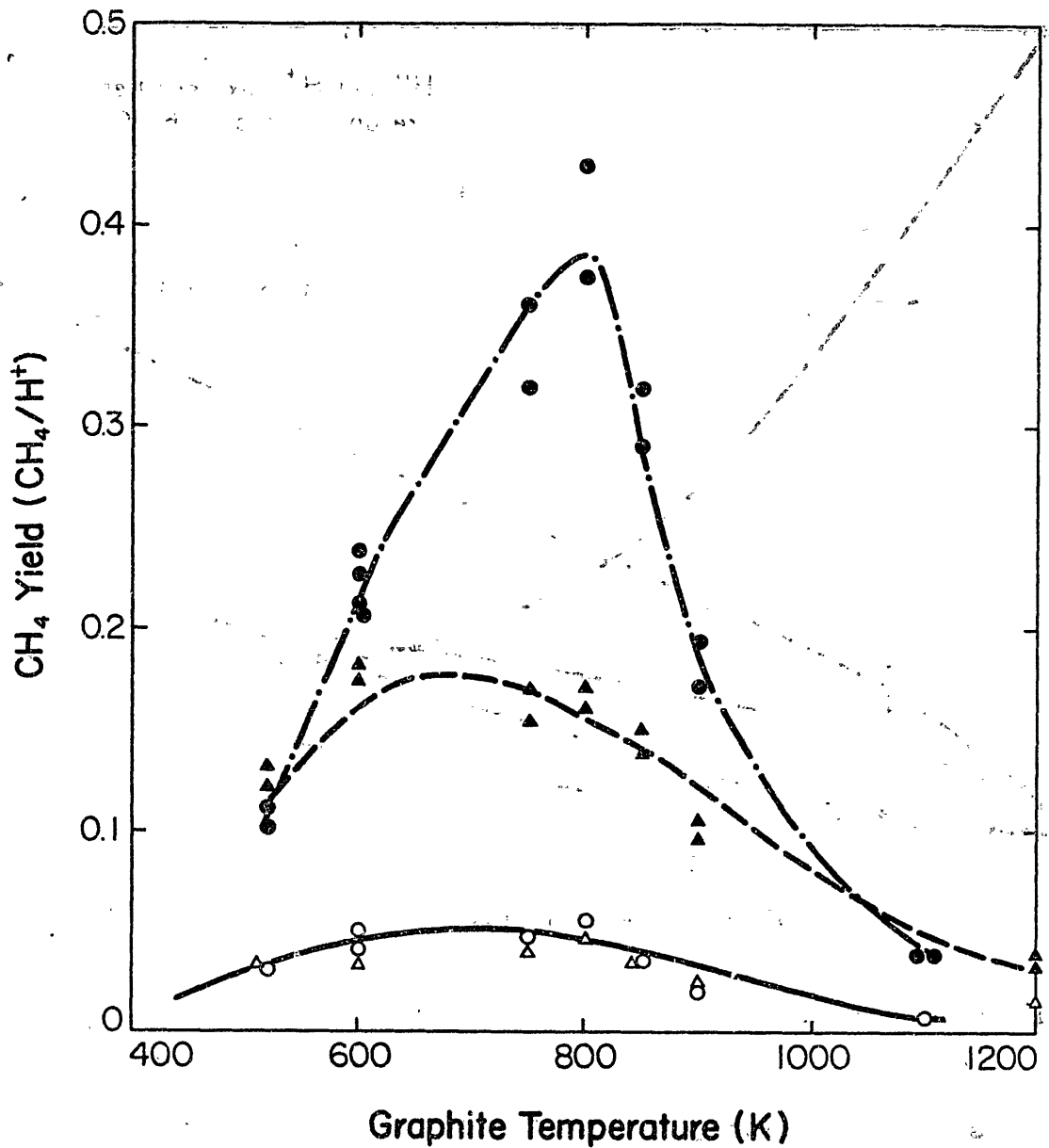


Fig. 16 Temperature dependence of "synergistic" methane yield due to sub-eV H⁰ ($\sim 6 \times 10^{14}$ H⁰/cm²s) and H⁺ ions ($\sim 2 \times 10^{14}$ H⁺/cm²s) in the presence of H₂ for two H⁺ energies: ● 300 eV and ▲ 100 eV. The corresponding yields for H⁺ and H₂ (i.e., no H⁰) are also shown: ○ 300 eV and △ 100 eV (Haasz et al.¹⁷).

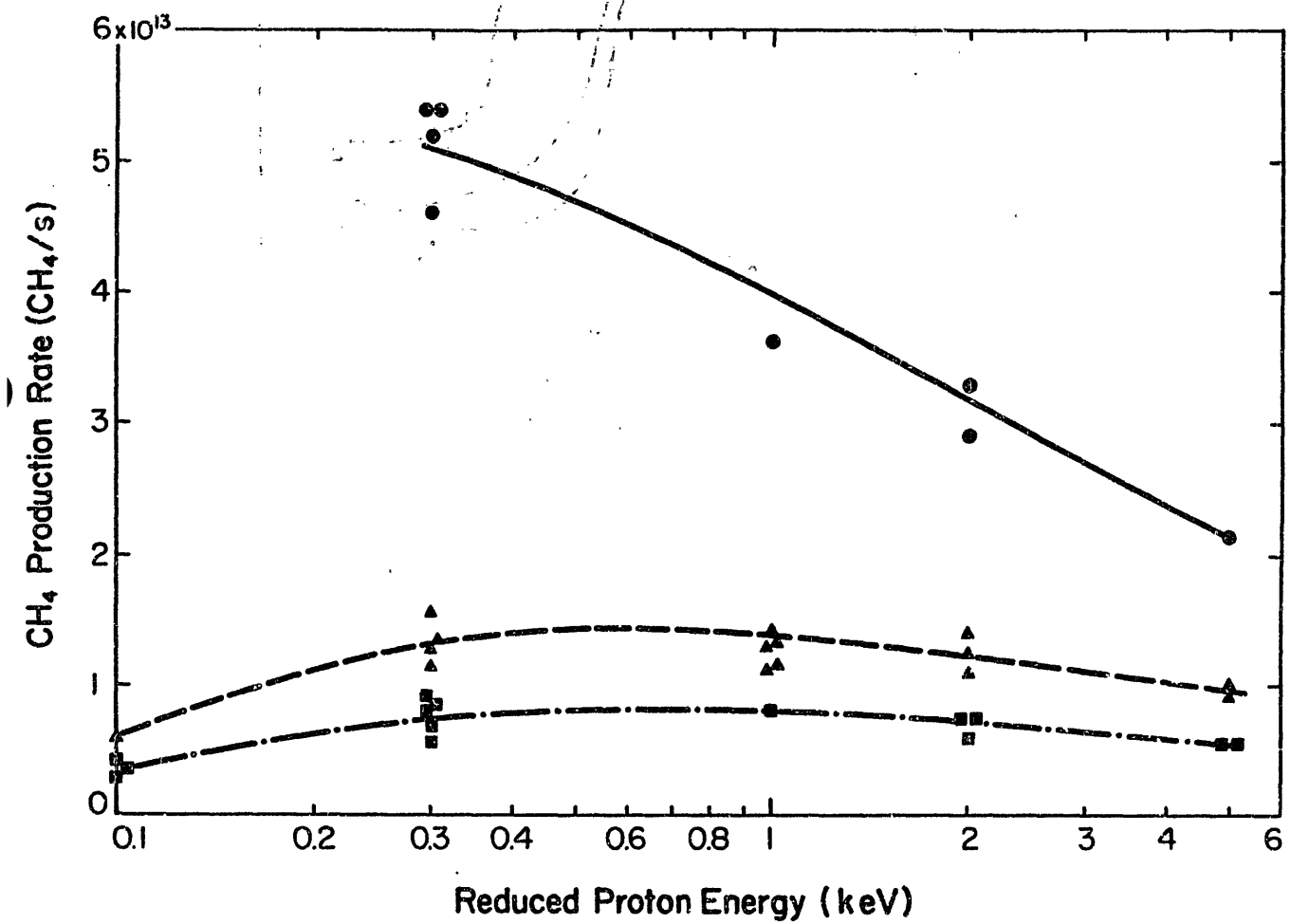


Fig. 17 Energy dependence of "synergistic" methane production from carbon (at 750-800K) for three H⁺ fluxes: ● 1.1 × 10¹⁵ H⁺/cm²s, ▲ 2 × 10¹⁴ H⁺/cm²s, ■ 10¹⁴ H⁺/cm²s. For all cases the H⁰ flux was ~6 × 10¹⁴ H⁰/cm²s and P_{H₂} ~4 × 10⁻⁴ Torr (Haasz et al.¹⁷).

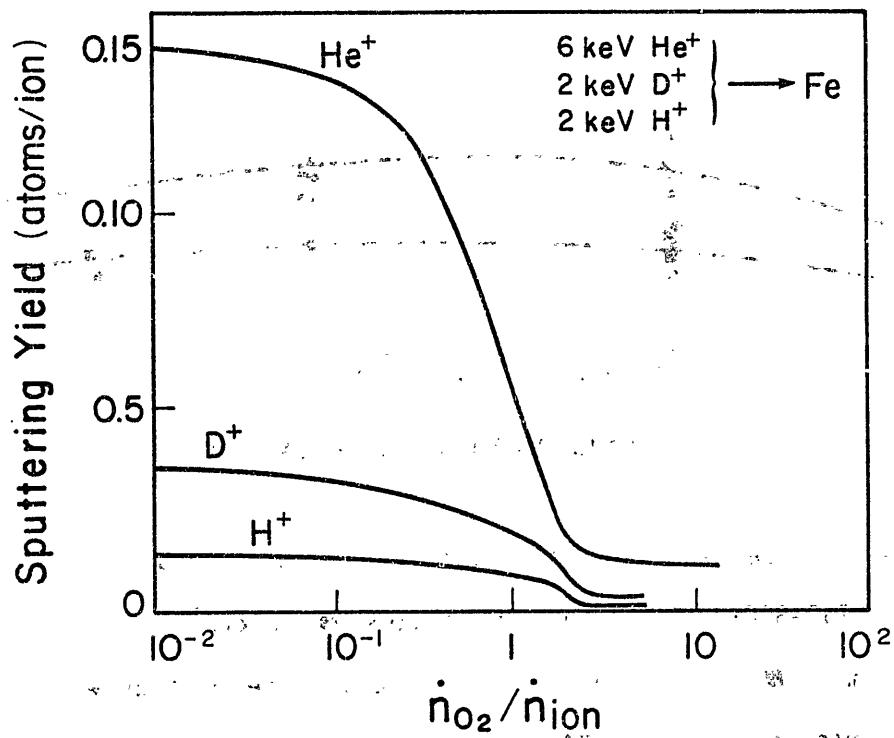
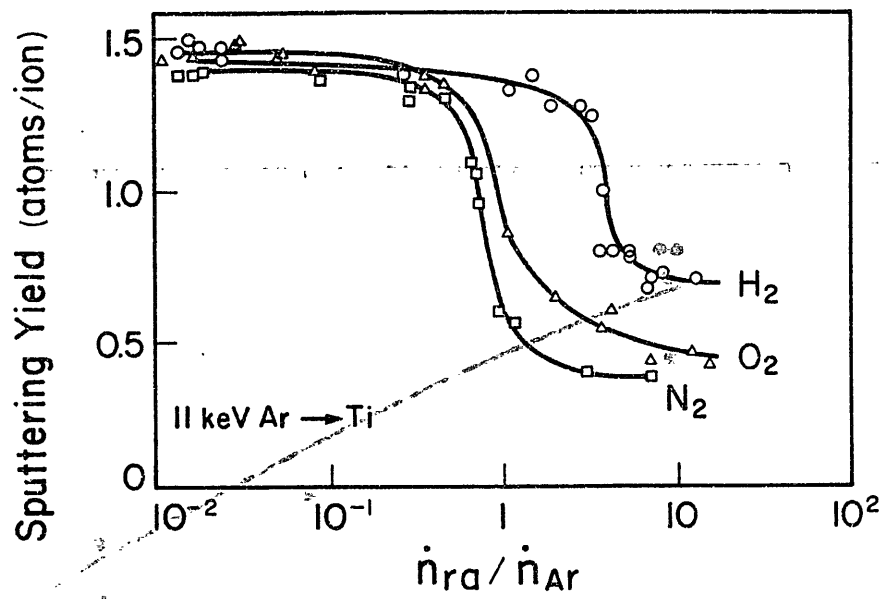
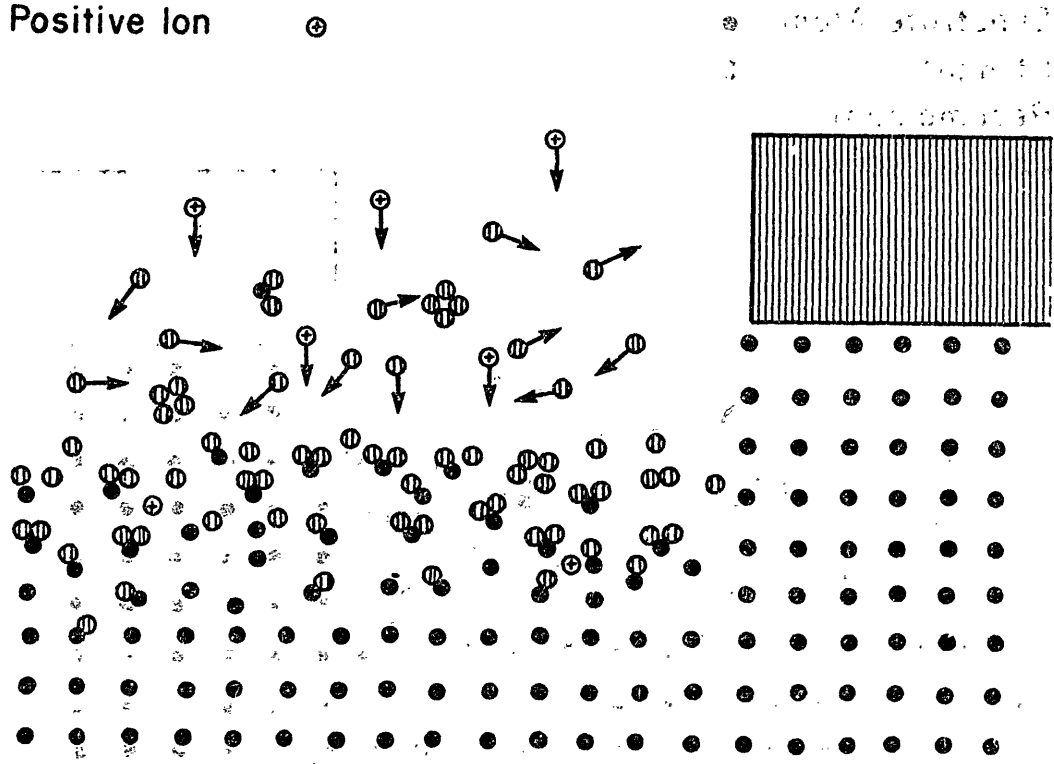


Fig. 18 Dependence of the sputtering of Ti and Fe by Ar, He, H and D on the partial pressure of reactive atoms (Refs. 97-99).

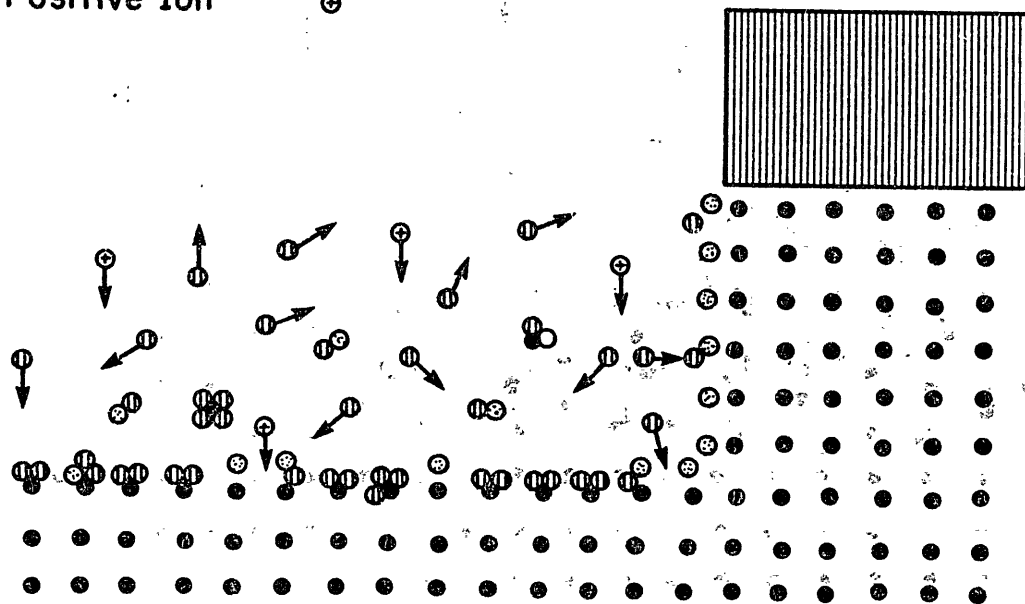
Substrate Atom ●
 Etchant ⊕
 Positive Ion ⊕



Surface Damage Induced Anisotropy

Fig. 19 Mechanism of surface-damage-induced anisotropy. Damage produced by incident ions allows accelerated attack by etchant radicals on horizontal surfaces (Flamm and Donnelly⁴⁰).

Substrate Atom ●
 Etchant ⊕
 Recombinant ⊖
 Positive Ion ⊕



Recombinant Mechanism of Anisotropy

Fig. 20 Recombinant mechanism of anisotropy. "Recombinant" species inhibit etching of feature sidewalls while ion-induced recombinant desorption or ion-enhanced substrate gasification proceeds on horizontal surface (Flamm and Donnelly⁴⁰).

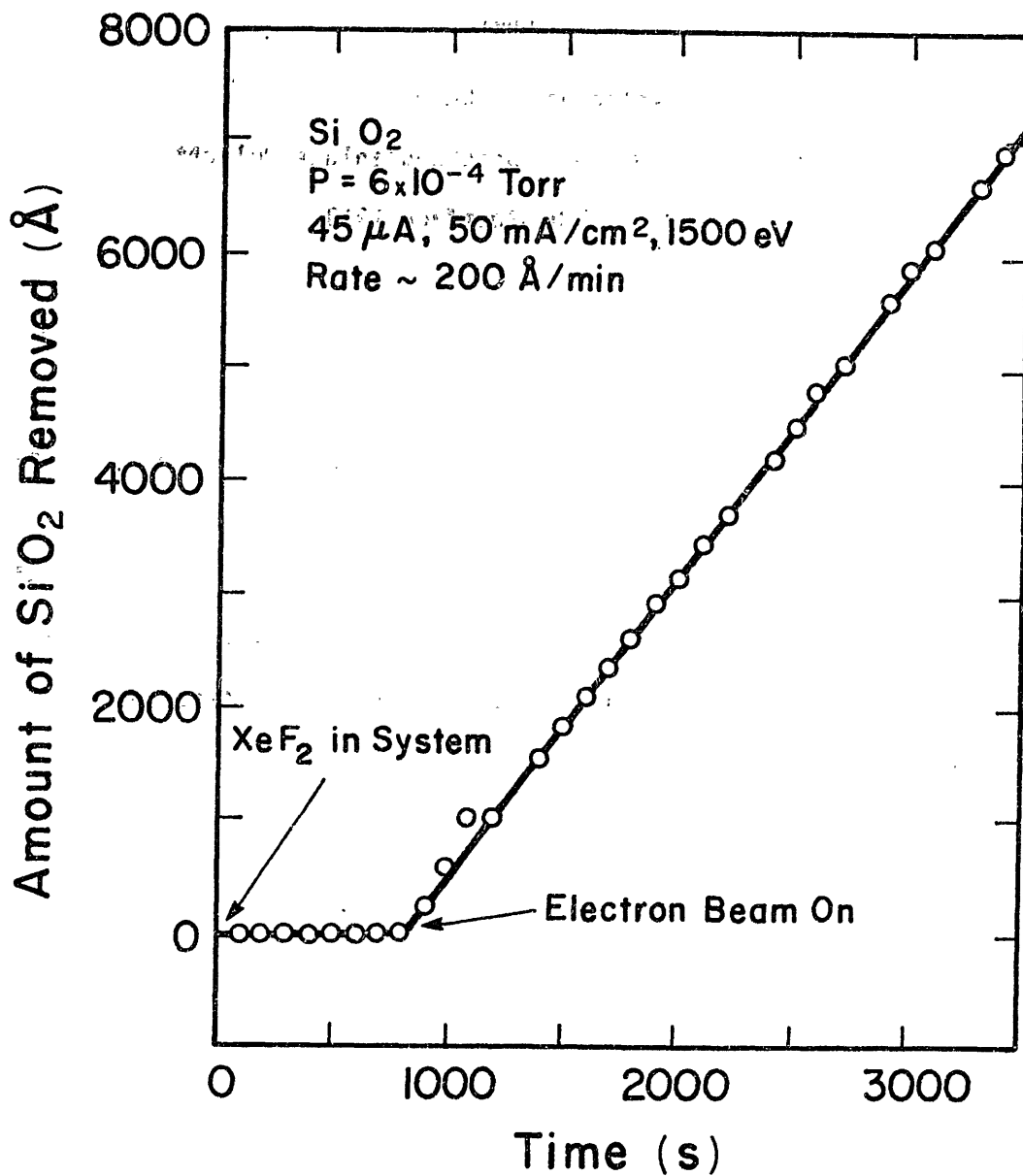


Fig. 21 Electron-assisted gas-surface chemistry using 1500 eV electrons and XeF₂ on SiO₂. $P(\text{total}) = 6 \times 10^{-4}$ Torr with most of the ambient gas being xenon. Neither exposure to XeF₂ nor an electron beam produces etching by itself. Simultaneous exposure produces an etch rate of $\sim 200 \text{ \AA/min}$ (Coburn and Winters⁹).

Synergistic Effects Related to Surface Composition

- Session Summary -

Wolfgang O. Hofer

Projekt Kernfusion, Kernforschungsanlage Jülich*

D-5170 Jülich, Postfach 1913

ABSTRACT

Preceded by an introduction to nomenclature, an overview is given of the session on "Surface Composition and Desorption" at the Workshop on "Synergistic Effects in Surface Phenomena Related To Plasma-Wall Interactions", Nagoya, 1984. This summary of conclusions and highlights is interspersed with personal remarks and supplemented with additional references to relevant work in this field.

*)EURATOM Association

INTRODUCTION

Surface composition and structure of first wall components in plasma machines will undergo substantial changes owing to a variety of phenomena initiated by energetic particle bombardment, quantum radiation, and phonon generation in the near-surface lattice. These phenomena are atomic relocation processes, thermally activated processes, and sorption/desorption.

Atomic relocation processes are caused by either or both the interaction of energetic primary particles with target atoms (i.e. primary recoils), and interactions of higher generation recoils, so-called cascade recoils. Relocation processes may occur into the vacuum in which case the process is referred to as (physical) sputtering, or into deeper regions of the solid, so-called recoil implantation /10/. In fusion-relevant plasmas the slowing down of hydrogen nuclei is the most frequent interaction and in this case primary recoils play the dominant role /11/. With heavier particles such as C-, N-, O impurities cascade recoils must also be taken into account. Owing to their substantially larger nuclear interaction cross section, relocations by impurities are more effective by two to four orders of magnitude, thus balancing their deficiency in flux density. It is still an open question whether and when plasma or impurity particles play the dominant role in present day magnetic confinement systems.

Thermally activated processes pertinent in this context are diffusion, segregation, and sublimation/evaporation. Since the fundamental process of these phenomena is point defect generation and migration, additional production of vacancies and interstitial atoms by energetic nuclear collisions generally has a strong influence on the reaction rates.

Sorption and desorption processes are governed by the vacuum environment, the surface reactivity and the aforementioned two processes. Desorption of surface atoms may be of thermal origin or particle induced. In the latter case this can be plain sputtering of surface layers or - as in the case of electron-induced desorption - the transition from a bonding to an anti-bonding state followed by repulsion.

In the same way as these processes change the composition of the near-surface region, this modified composition may have an influence on syn-acting processes. For instance, sorption of reactive gases on metal surfaces changes the sputtering yield approximately inversely to the sublimation energy. This in turn results in temperature-dependent sputtering yields when volatile compounds are formed; see, for instance contributions /3/, /6/, and Saidoh's contribution in Session 3. Such an interplay between different phenomena (A,B,C...) on a given effect ϵ is likely to give rise to a synergistic effect, that is when the combined effect $\epsilon(A+B)$ deviates from the sum of the partial effects, $\epsilon(A)$, $\epsilon(B)$

$$\epsilon(A+B) \neq \epsilon(A) + \epsilon(B).$$

In this definition synergism is synonymous with nonlinearity.

In the following the phenomena and effects discussed in the session on effects related to surface composition will be put together. The backbone of this session was a series of nine oral contributions, listed as entries /1/ to /9/ in the References. In the Summary Session, the present author discussed the highlights and gave some personal estimates of the magnitude and relevance of synergistic effects to be expected in plasma surface interaction (PSI).

EFFECTS RELATED TO DIFFUSION AND SEGREGATION

The profound influence of energetic particle bombardment on the transport of matter in solids by way of collisional relocation and radiation-enhanced diffusion was discussed by A.R. Krauss /2/ in the case of a dilute copper-lithium (approx. 3 at %) alloy. The idea behind this project, suggested several years ago /12/, is that lithium segregates at the surface and thereby protects the copper matrix from being sputtered; the driving force in this process is minimization of the free (surface) energy, also referred to as Gibbsian segregation. Recent results of computer simulations were shown which demonstrate the effectiveness of this process. The Cu self-sputtering yield exceeds unity, i.e. reaches a precarious run-away situation, at energies as high as 1.5 keV - as opposed to 340 eV without Li segregation (TRIM simulation). Moreover, lithium, when released from the surface, is not only much less harmful to plasma radiation losses and fuel consumption, it is also predominately ejected as positive ions - as opposed to almost all metal particles which are generally sputtered as neutral particles. The electrically charged flux of sputtered particles, however, can be directed back to the wall by electric (negative bias applied to the wall) or magnetic means. Fig. 1 shows experimental proof. In this respect, oxygen - in the form of an oxide /13/ or as sorbed oxygen /1/ - serves the same purpose: reduction of the partial metal yield and enhancement of the excited and ionized fraction.

An impressive and for present-day plasma machines highly relevant example of synacting segregation and sputtering was demonstrated by Morita /3/, Fig. 2: carbon atoms can diffuse from a carbon or carbide substrate through a several hundred nm thick nickel layer, segregate as graphite on the sur-

face and thereby protect Ni from being sputtered; care must be exercised, however, at higher flux densities of primary particles, where the rates of sputtering and segregation are about equal. In this intermediate regime a volatile Ni-carbide is formed which results in Ni-sputtering yields larger than the yield from clean nickel. At even higher flux densities the partial yield drops again, surprisingly to a level lower than that of a pure nickel, an effect which is not yet fully understood. In view of the widespread use of Inconel, a Ni-base alloy, in plasma machines this result has a high degree of relevance.

The influence of segregation on sputtering of nickel-base alloys was also shown by H. Shimizu /5/: Cu-Ni alloys, which have a tendency to Cu-segregation, clearly show deviations from stoichiometry in the sputtered flux, an effect which is, furthermore, emission-angle-dependent. On the other hand, Co-Ni alloys showed no segregation and thus give the same sputtered fluxes as the surface and bulk composition. High-resolution electron microscopy furthermore revealed an approximately 10 nm thick amorphous surface layer; pure metals, on the other hand, generally do not amorphize upon particle irradiation, as is evidenced, for instance, by anisotropic emission from single crystals.

EFFECTS RELATED TO SUBLIMATION/EVAPORATION

With pure metals there is generally no synergism for sputtering and sublimation /14,15/. The situation is different, however, for the erosion of oxides and carbides. As exemplified by the peak of the Ni-yield in Fig. 2, the sputtering yield rises with temperature in cases of volatile compounds such as Ni_3C , WO_3 , MoO_3 , CH_4 ; see /16/ and Saidoh, Session 3.

There is another effect of high lattice temperatures on sputtering which should not be overlooked, namely surface morphology. Sputtering at fluences exceeding 10^{17} ions/cm² is generally associated with the development of surface structures /4, 17-21/. These structures exert a strong influence on the angular distribution as well as on the total sputtering yield, an effect which it was suggested could be taken advantage of with first wall components; honey comb structures and needle-covered surfaces were considered to reduce erosion, see /22/ and references therein.

The size and shape of these structures depend, however, on the lattice temperature. Enhanced surface mobility tends to smoothen surface irregularities on clean targets while it is, according to Ref. 18, a precondition for cone formation on two- and multicomponent systems /20/. Thus, there is the possibility of a true synergistic effect in surface erosion by particle bombardment and thermal energy by way of surface morphology.

Hasuyama /4/ presented interesting angular distribution measurements on polycrystalline gold. At fluences less than 10^{16} cm⁻², this group found pronounced over-cosine distributions which changed into the expected cosine ejection characteristic at fluences exceeding 10^{17} cm⁻². At these fluences,

the surfaces are no longer as flat as at $< 10^{16}$ cm⁻²; they show marked roughening and the first developing cones. In keeping with the theory given in Ref. /19/, such surfaces transform ejection characteristics of whatever form into cosine distributions owing to multiple averaging processes. - Such experiments are not of pure academic interest, but are also of importance in applied plasma wall interaction as they furnish information on the angle with which neutral particles enter the plasma and thus on the projected ionization length.

EFFECTS RELATED TO SORPTION AND DESORPTION

Sorption of reactive gases on first wall components will always be of concern in plasma surface interaction since, first of all, hydrogen, the working gas itself, is chemically active; furthermore, the leak rates required to avoid monolayer recoverage of cleaned surfaces over several hours, have not been reached. In machines like ASDEX, PDX and TEXTOR the recoverage time is in the order of several seconds ($p \lesssim 10^{-7}$ mbar). Furthermore, when one visualizes that it takes only some 10^{20} atoms for a monolayer coverage of the entire inner structure, the importance of virtual leaks and surfaces not accessible to glow or discharge cleaning becomes clear. Accordingly, there is a great deal of interest in sorption/desorption phenomena especially under technical circumstances - which, in fact, means simultaneous influence of a multitude of parameters. Half of the presentations dealt directly with sorption or desorption phenomena and they all concerned oxygen and hydrogen (isotopes) on Al, Ni and stainless steel /6-9/.

Sorption of atomic and molecular deuterium on stainless steel as well as its subsequent desorption was studied by Matsunami et al. /8/. The nuclear reaction $D(^3\text{He}, \alpha) \text{H}$ was used in order to obtain absolute numbers for the deuterium density as well as depth distribution (100 nm scale). Sorption of D was more effective than D_2 by a factor of 10 and saturated at about a monolayer. The surface damage created by energetic particle bombardment particularly promotes sorption of D_2 . Desorption by 5 keV Ar^+ and H^+ bombardment showed that all of the sorbed D was situated within the top-most three atomic layers. From the size of the desorption cross section as well as its energy dependence it was concluded that desorption by Ar^+ ions is predominantly due to knock-on of cascade atoms, whereas desorption by H^+ impact is a primary knock-on event; see also Ref. /23-25/. There are thus great similarities to the mechanisms of sputtering.

The situation is different, however, when these athermal processes have to compete with thermal ones. Tanabe, /6/ and Fig. 3, studied desorption of O and C from polycrystalline Ni and Al by hydrogen bombardment and found only in the case of oxygen on Ni a marked influence of the lattice temperature. He gave an explanation based on thermodynamics but this was not possible for any of the other systems; these are clearly collision-dominated. He emphasized the importance of chemical reactions* in general and, in the present case, the role of water molecules in residual gas. With reference to the R-tokamak project at Nagoya /26/, the inefficient reduction of aluminium oxide will require a modified conditioning technique should aluminium oxide turn out to be unacceptable.

*It seems pertinent here to call attention also to the work of Staib et al. /30/ and v. Seggern and Tschersich /31/.

Collisional desorption by keV ions is always accompanied by implantation, namely direct implantation and recoil implantation. The former case is most important with neutral beam injection, the effect of charge exchange neutrals, and tritium inventory considerations. Sagara /7/ studied implantation and retention of 1 keV H_2^+ on aluminium. Again in connection with the R-tokamak project, and guided by the idea of aluminium's being passive with respect to chemisorption, this group looked for possible trapping mechanisms. They found radiation damage to be very effective indeed; also sorbed oxygen was identified as an efficient trap increasing hydrogen retention. Both of these trapping types are anticipated to cause true synergistic effects in plasma machines. - Recoil implantation, on the other hand, is in most cases in PSI of adverse nature as it leads to the incorporation of adsorbed impurity species. Being associated inherently with elastic (nuclear) collisions it can be avoided only by keeping collisional desorption in the inelastic (electronic) interaction regime; this restricts primary particles to electrons, (x-ray quanta), and hydrogen.

Segregation is also influenced by changes of the surface composition due to sorption or implantation. Mosser /9/ studied segregation in NiCr, FeNiCr, FeSi, and FeAl alloys under the influence of oxygen. Auger and photoelectron spectroscopy (AES, XPS) were applied to determine the chemical state and the amount of the oxide formed. Oxygen was either implanted (4 keV) or sorbed from the gas phase. As a rule of thumb he found preferential segregation of that constituent which formed the oxide of highest binding energy; the most important of these are, Cr_2O_3 , Al_2O_3 , and SiO_2 . Implantation had no particular effect except for the larger oxygen penetration depth.

CONCLUDING REMARKS

In the Summary Session of the Workshop the main results in this area were considered from the present author's point of view. With the help of Fig. 4, which is essentially taken from Ref. /13/, he tried to link several of the new findings. These are especially

- reduction of the erosion yield by overlayers /1-3,27/ or surface compounds /3,13/. Sacrificing overlayers may be more effective but their replenishment is as vital as it is difficult to achieve. Surface compounds, on the other hand, form on their own under the influence of particle radiation and reactive gases (synergism: radiation assisted oxidation, /13/ and references therein). Since their protective action is incomplete it might be necessary to have recourse to
- increasing the ionized fraction in the sputtered flux and preventing it from entering the main plasma. Key issues of the effectiveness of this method are: the charged fraction must be increased to nearly 100 %; can high ionization densities in the sheath plasma achieve the same effect? And if so,
- the momentum (angular) distribution of released wall particles is crucial for their penetration depth and motion in the edge plasma. It should be noted that electrical retention as demonstrated in Fig. 1 is no longer effective with postionized particles since they have traversed the plasma sheath before ionization. Momentum and magnetic field strength determine their further behaviour. The momentum distribution, on the other hand, is influenced by surface structures and these in turn change with particle fluence, wall temperature, and surface coverage.

It thus appears that any change of the state of the surface - in particular its chemical composition and morphology - gives rise to a series of interrelated effects at the first wall of magnetic confinement systems. The most pronounced ones - with this expectation the author concluded his summary - will be found with phenomena associated with electronic surface interaction. The more than two orders of magnitude increase in the charged fraction of the sputtered flux caused by a surface oxide (Fig. 4) is as strong an indication of the importance of inelastic effects, as is the example with which he finished the summary:

the sheath potential difference between a plasma and its contacting wall is determined by the plasma (electron) temperature and the flux of charged particles leaving the surface. This flux is composed of secondary electrons and, generally to a much smaller extent, ions. High electron yields reduce the sheath potential and thus the energy of positive ions impinging on the surface /28/ as well as the probability of unipolar arcing /29/. Since electron emission is extremely sensitive to surface composition there is thus another way of controlling wall erosion as well as plasma purity and temperature.

REFERENCES

Entries 1 to 9 give speaker and title of the contributions presented at the session. Most of the non-invited presentations /3/ to /9/ will be published in the Proceedings of the 6th Int. Conf. on Plasma Surface Interactions, to appear in volume 128 & 129 of the Journal of Nuclear Materials, North Holland, Amsterdam 1984.

- /1/ D.M. Gruen "Effect of Surface Coverage and Composition on Desorption and Related Phenomena" (invited)
- /2/ A.R. Krauss "Synergistic Sputtering Properties of Binary Alloys" (invited)
- /3/ K. Morita "Self-Sustained Carbon-Coating on Metal Surfaces"
- /4/ H. Hasuyama "Influence of Surface Structures on Angular Distributions in Sputtering"
- /5/ H. Shimizu "Effect of Surface Segregation on the Angular Distribution of Atoms Sputtered from Binary Alloys"
- /6/ T. Tanabe "Effect of Residual Gases on Hydrogen-Sputtering"
- /7/ A. Sagara "Hydrogen-Bombardment of Aluminium Surfaces"
- /8/ N. Matsunami "Ion-Induced Desorption Yields of Hydrogen"
- /9/ A. Mosser "Oxygen-Induced Segregation"
- /10/ U. Littmark and W.O. Hofer, Nucl. Instr. Meth. 170 (1980) 177, and "The Theory of Recoil Mixing in Solids" in "Thin Film and Depth Profile Analysis" Ed. H.E. Oechsner, p. 159-200, Vol. 37, 1984 Topics in Current Physics, Springer Verl. Heidelberg
These articles reference the key publications on collisional relocation phenomena.
- /11/ U. Littmark and S. Fedder, Nucl. Instr. Meth. 194 (1982) 607
- /12/ A.R. Krauss and D.M. Gruen, J. Nucl. Mater. 63 1976) 380
- /13/ W.O. Hofer, H.L. Bay and P.J. Martin, J. Nucl. Mater. 76 & 77 (1978) 156
- /14/ K. Besocke, S. Berger, W.O. Hofer and U. Littmark, Radiation Eff. 66 (1982) 35
W.O. Hofer, K. Besocke, B. Stritzker, Appl. Phys. A 30 (1983) 83
- /15/ P. Sigmund and M. Szymonski, Appl. Phys. A 33 (1984) 141
- /16/ R. Kelly and N.Q. Lam, Radiat. Eff. 18 (1973) 37
ibid. 32 (1977) 91 and 80 (1984) 273

- /17/ A. Güntherschulze and W. Tollmien, Z. Physik 119 (1942) 685
- /18/ G.K. Wehner and D.J. Hajicek, J. Appl. Phys. 42 (1971) 1145
- /19/ U. Littmark and W.O. Hofer, J. Mater. Sci. 13 (1978) 2577
- /20/ J. Roth, J. Bohdanski, W.O. Hofer and J. Kirschner in Proc. Int. Symp. on Plasma Wall Interact., Jülich 1976, Pergamon Press Oxford 1977, p. 309
- /21/ G. Carter, B. Navinsek, and J.L. Whitton in Sputtering by Particle Bombardment II, Ed. R. Behrisch Springer Series "Topics in Applied Physics" Springer-Verlag Berlin 1983 p. 231-266
- /22/ D.M. Mattox and D.J. Sharp, J. Nucl. Mater. 80 (1979) 115
J.K. Panitz and D.J. Sharp, J. Vac. Sci. Technol. 17 (1980) 282
- /23/ R. Bastasz and L.G. Haggmark, J. Nucl. Mater. 103 & 104 (1981) 499
and 111 & 112 (1982) 805
R. Bastasz, J. Vac. Sci. Technol. A 2 (1984) 638
- /24/ H.F. Winters and P. Sigmund, J. Appl. Phys. 45 (1974) 4760
- /25/ E. Taglauer, W. Heiland and J. Onsgaard, Nucl. Instr. Meth. 168 (1980) 571
- /26/ A. Miyahara, H. Momota, Y. Hamada, K. Kawamura and Y. Akimune, Report IPPJ-500 (1981)
A. Miyahara, J. Nucl. Mater. 111 & 112 (1982) 461
- /27/ R. Behrisch, J. Roth, J. Bohdanský, A.P. Martinelli, B. Schweer, D. Rusbüldt and E. Hintz, J. Nucl. Mater. 93 & 94 (1980) 645
- /28/ G. Fuchs and N. Nicolai, J. Nucl. Mater. 76 & 77 (1978) 573
- /29/ P.J. Harbour and M.F.A. Harrison, ibid. 513
- /30/ P. Staib, H.F. Dylla and S.M. Rossnagel, J. Vac. Sci. Technol. 17 (1980) 291
- /31/ J. v. Seggern and K.G. Tschersich, J. Nucl. Mater. 93 & 94 (1980) 806
and 111 & 112 (1982) 489

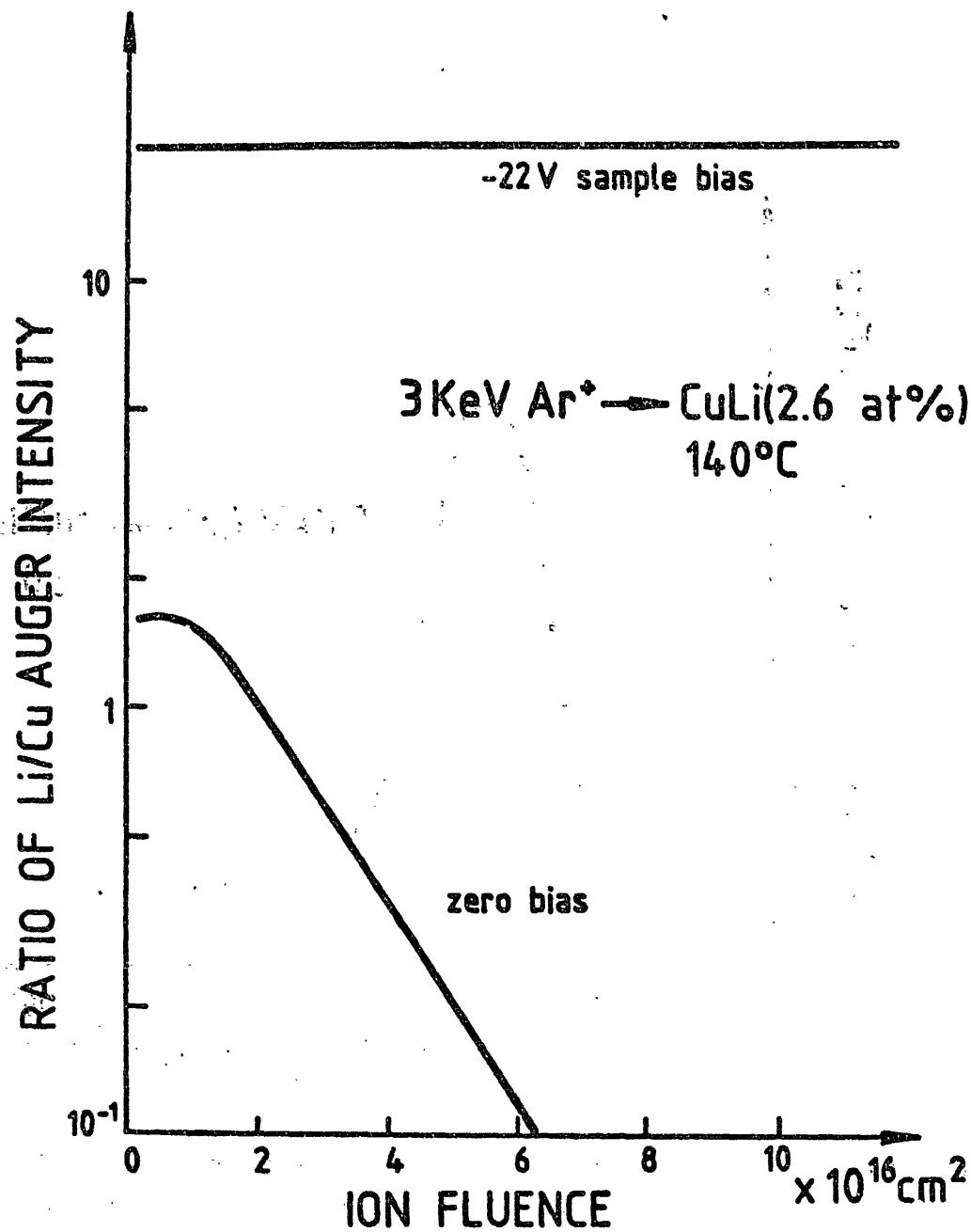


Fig. 1: Bombardment of a dilute Cu-Li alloy at elevated temperature with and without negative bias on the target. The Li surface concentration was measured by Auger electron spectroscopy. Since most of the sputtered Li particles are ejected as ions, the surface coverage hardly changes when a negative target potential prevents Li^+ from leaving the surface. Without bias the Li surface layer is eroded away at a speed determined by the sputtering and segregation rates. From Krauss et al. /2/.

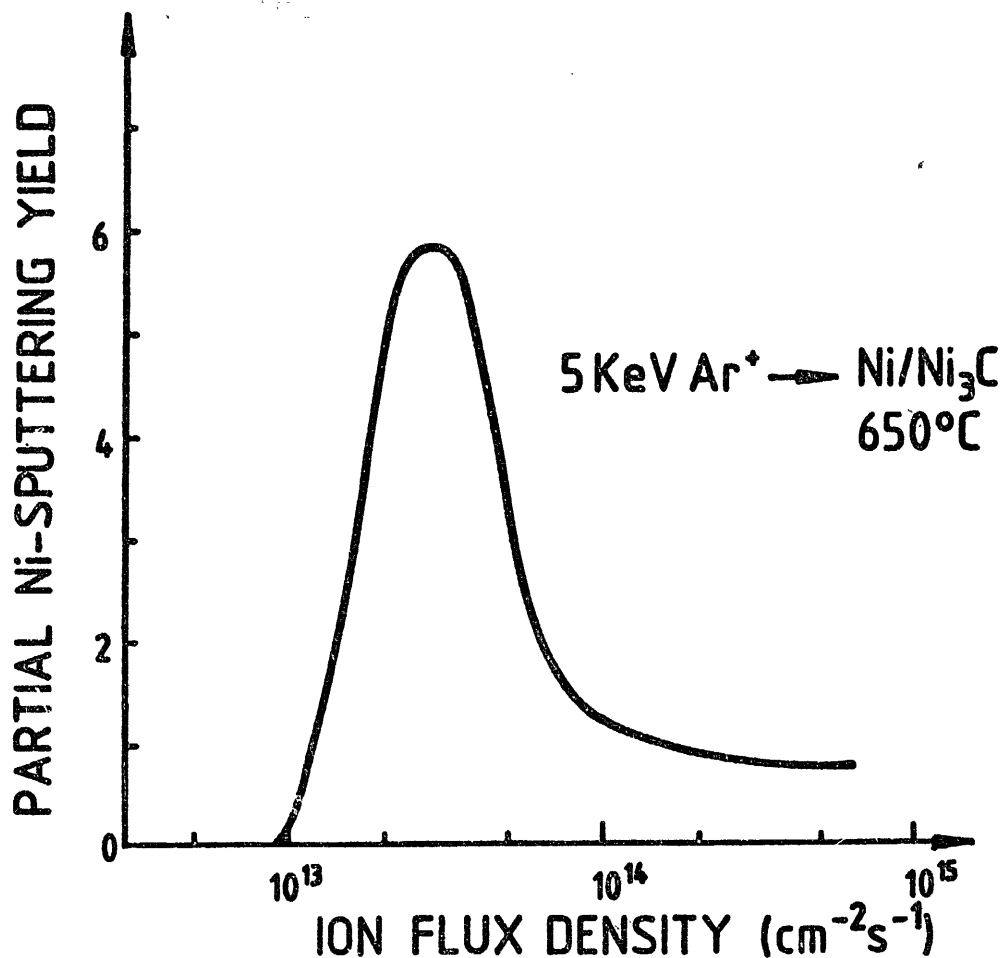


Fig. 2: Reduction of partial metal sputtering yield by self-sustaining carbon surface layers. Carbon, from a graphite or carbide substrate, diffuses at elevated temperatures through the Ni-layer, segregates at the front surface and protects Ni from sputtering. Below a critical flux density, the protection is complete, while above this level a C-Ni compound of low surface binding energy is formed, thus causing enhanced erosion. At still higher flux densities some low-density carbide seems to work as partial protection again. From Morita et al. /3/.

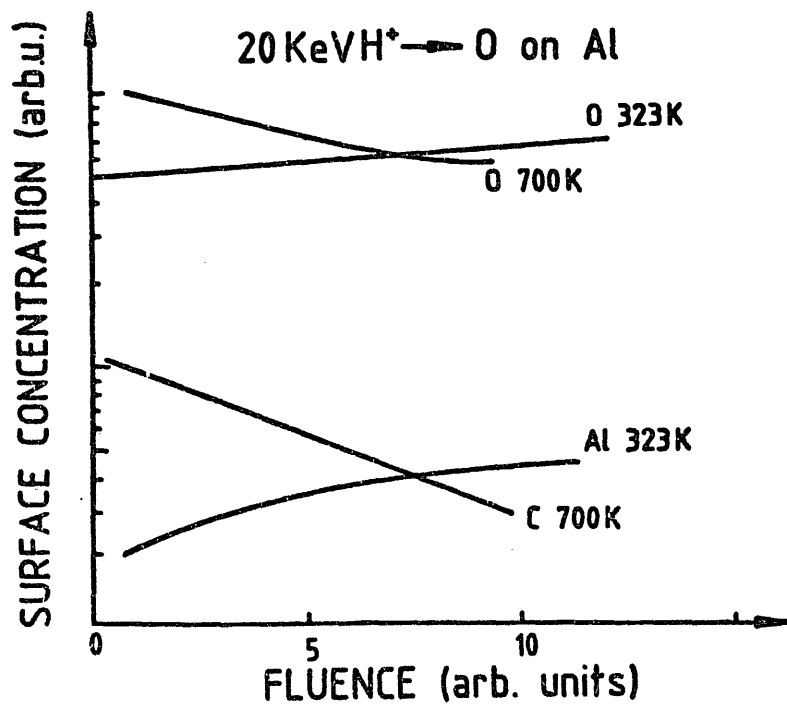
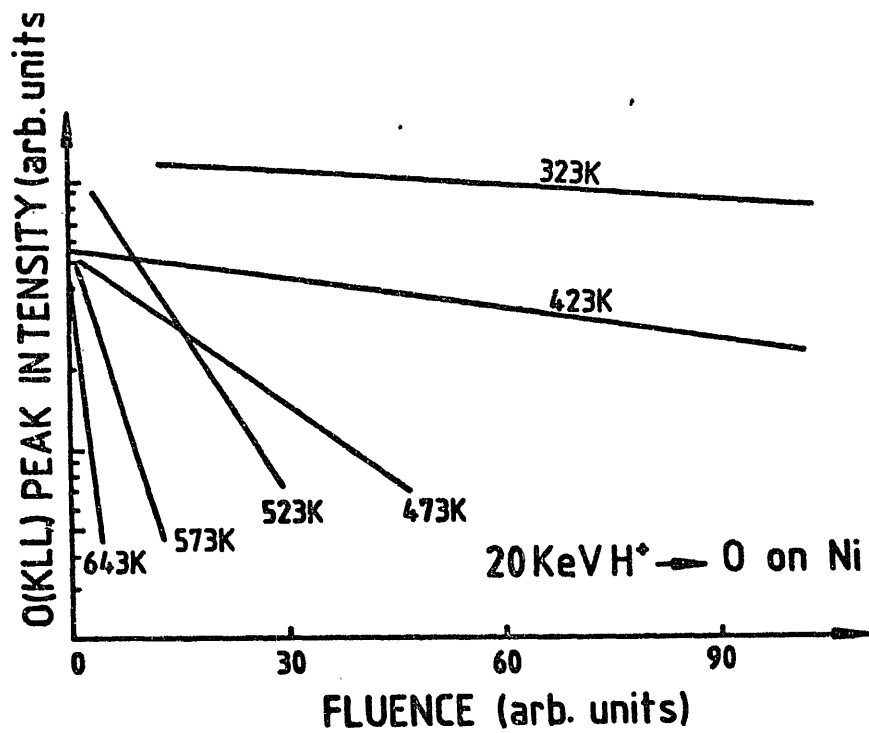


Fig. 3: Desorption of low-Z impurities from polycrystalline Al- and Ni surfaces by hydrogen bombardment.

- a) Fluence dependence of oxygen removal from nickel at various temperatures
- b) same as a) but with signal from the aluminium base and carbon contaminant.

From Tanabe /6/.

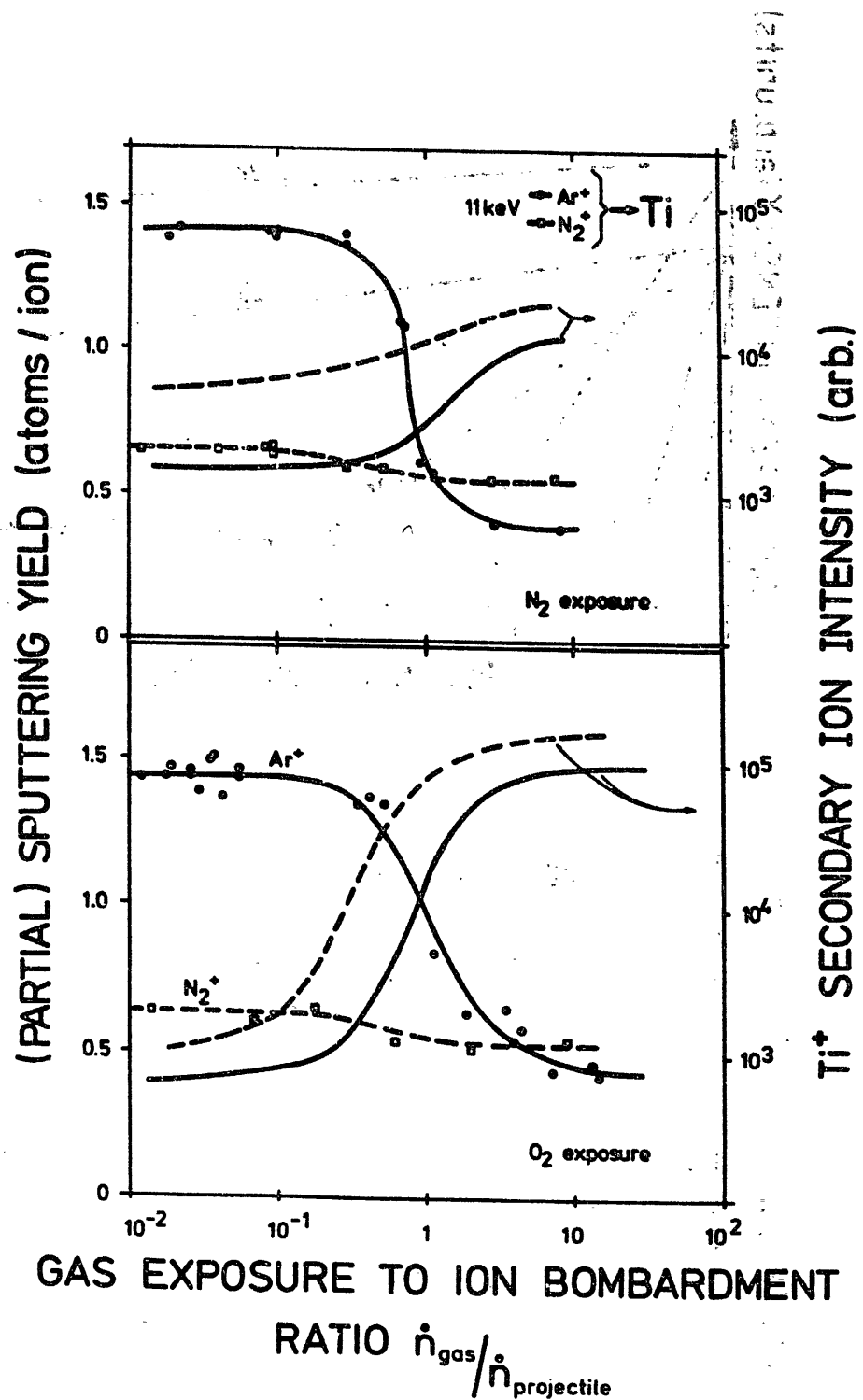


Fig. 4: Influence of surface oxides and nitrides on the partial metal sputtering yield and the ionized flux of sputtered particles. Nitrides are formed either by direct implantation (5.5 keV/atom) or by exposure to nitrogen simultaneous with 11 keV Ar^+ bombardment. From Hofer et al. /13/.

EFFECTS OF MONOLAYER COVERAGES ON SUBSTRATE SPUTTERING YIELDS*

D. M. Gruen, A. R. Krauss, and M. J. Pellin

Materials Science and Technology Program
Chemistry Division
Argonne National Laboratory
Argonne, IL 60439

Abstract

Materials currently being used or considered for plasma-side applications are not entirely satisfactory, particularly in the medium edge temperature (~100-300 eV) regime. A new approach to impurity control based on self-sustaining surface segregated low-Z layers with high secondary ion fractions has been suggested and tested in laboratory experiments.

A crucial requirement is that substrate sputtering yields be reduced about an order of magnitude by monolayer adsorbate coverages. Theoretical and experimental evidence is adduced to support the contention that overlayer coverages (a monolayer of Li on Cu) result in profound reductions of substrate (e.g., Cu) sputtering yields. The conclusion that a material such as a dilute alloy of Li in Cu could function as a limiter or a divertor plate material is, in part, based on the fact that more than 85% of the sputtered flux originates in the first atomic layer (e.g., Li) of the target.

*Work performed under the auspices of the U.S. Department of Energy.

I. Introduction

Impurity control is becoming increasingly important in magnetic confinement fusion machines as devices operate with pulse lengths on the order of seconds and make use, for example, of large area Faraday shields for ICRF antennas immersed in the plasma edge.

A large number of properties are important for materials selection involving impurity control systems such as limiters, divertor, plates and beam dumps.¹

The candidate materials considered for plasma side use where impurity generation occurs may be divided into low-Z, medium-Z, and high-Z materials. At low plasma edge temperatures (< 50 eV), several materials can be used, but high-Z materials such as W are predicted to have the greatest lifetimes. At higher edge temperatures (100-300 eV), both medium and high-Z materials are unacceptable due to excessive self-sputtering. The permissible plasma side materials are, therefore, confined to those whose self-sputtering coefficients do not exceed unity, thus limiting the choice of materials to atomic weights approximately that of SiC unless the edge temperature can be kept below 50 eV. Because candidate heat sink materials are copper or transition metal alloys, most suggestions for plasma side materials in high heat flux applications have involved low-Z coatings such as TiC or Be. Recent experience in TFTR with TiC coated poco-graphite limiters has shown, however, that severe problems can be associated with this approach to impurity control.²

The current lack of suitable plasma side materials encourages one to seek out alternative approaches that may provide more satisfactory solutions to this important problem area. One such approach to impurity control has involved an investigation of alloy systems which spontaneously form low-Z overlayers as a consequence of exposure to the fusion reactor environment.^{3,4} Several candidate systems for the production of such self-sustaining low-Z

overlayers have been identified and are being investigated from both a theoretical and experimental point of view. Alloys under investigation include Cu-Li, V-Al, W-Be, and Al-Li. While in all these cases, the low-Z component in the bulk is relatively dilute, typically less than 10 at.%, its equilibrium surface concentration can be expected to be greater than 90% under the conditions obtaining in a fusion reactor.

The key idea in the approach to impurity control outlined above is that surface segregation, which is thermodynamically driven by Gibbsian adsorption and kinetically enhanced in a radiation environment, can provide a self-regenerating low-Z surface by diffusion from the bulk. In principle, Gibbsian adsorption gives enrichment only for the very first layer of atoms with bulk alloy concentrations reestablished within one or two atomic layers from the surface. Although concentration profiles can be expected to be strongly modified in the presence of charged particle and neutron radiation fields, it is necessary to establish in the first instance the sputtering behavior of the material for a purely Gibbsian adsorption concentration profile. To be applicable in an actual machine, this approach to impurity control must provide in the first instance for a reduction in the sputtering yield of the medium-Z alloy component by about an order of magnitude. The question to be addressed then deals with the effect of a low-Z overlayer which is one monolayer in thickness on the sputtering yield of the higher-Z substrate on which it is adsorbed. We should note at the outset that this question has apparently not been posed in quite this form before and cannot as yet be answered in a definitive way. However, work done up to now suggests that strong reductions in substrate sputtering yields can be achieved as a result of monolayer coverages.

Again, for surface segregation to be a practical "coating" mechanism in fusion machine applications, the low-Z monolayers must be self-sustaining and

protective in the sense of lowering substrate sputtering yields by an order of magnitude. In turn, this means that the flux of sputtered atoms must originate essentially entirely in the first atomic layer. To be self-sustaining, surface segregation kinetics must be rapid enough to replenish material sputtered from the surface. There are two mechanisms which could bring this about. First, radiation-enhanced diffusion speeds up the process of surface segregation by several orders of magnitude. Second, if the sputtered flux consists primarily of secondary ions, a small negative potential on the target (-20 V), such as provided by the plasma sheath potential, is sufficient to return the ions to the surface thus reducing the sputtering yield.

It is desirable, therefore, that sputtered atoms originate in the very first layer of surface atoms, that the surface ionization coefficient is high in order to have large secondary ion fractions, and that the low-Z component of the alloy segregates very completely at the surface and does so rapidly in a radiation field. This paper discusses the theoretical and experimental evidence, particularly in the case of low energy sputtering (up to a few keV) which shows that more than 85% of all sputtered atoms originate in the surface layer. The implications of this finding for plasma side materials is considered.

Experimental²⁷ and theoretical³⁸ evidence for the kinetics of surface segregation and secondary ion emission of a particular alloy system, Cu-Li, is presented in other papers where it is shown that, under particle bombardment and in the presence of a small negative potential, a pure lithium overlayer can be maintained.

II. Effects of Gaseous Adsorbates on Sputtering Yields

The accurate determination of light ion sputtering yields of materials exposed to fusion plasmas has played a central role in evaluating the level of

impurities to be expected in fusion devices and reactors. The sputtering yields on which calculations of radiation losses from plasmas are based have been obtained from measurements on clean metal surfaces.⁵ It has become increasingly clear in recent years, however, that adsorbates, even at the monolayer level, can have important effects on sputtering yields particularly for light ion bombardment of metals. These effects have not been systematically explored nor have they been taken into account in calculations of expected plasma impurity concentrations. In the following, we wish to elucidate the nature of these effects, to delineate their theoretical basis, to explore the parametric influence of projectile, adsorbate and substrate mass, to describe changes in sputtering yields due to adsorbate geometry and to present the experimental evidence supporting the conclusions based on theoretical modeling.

Up to relatively recent times, quite insensitive methods have been used to determine sputtering yields defined as the mean number of atoms removed from the surface per incident ion. Most commonly, the weight loss of a target was measured after bombardment with very high ion fluences.⁶ In measurements of this sort where hundreds of monolayers had to be removed, it had already been shown that the sputtering yields measured for oxide covered surfaces,⁷⁻¹¹ as would be the case under conditions of poor vacuum,¹² may be lower than for clean surfaces.

Increases in sputtering yield are frequently observed in depth profiling after sputter cleaning a metal surface that had been exposed to the atmosphere.¹³ Thus, the sputtering yield of Fe has been found to increase after 10 keV Ar⁺ bombardment of well-oxidized 321 stainless steel at a dose corresponding to the removal of about 2×10^{16} atoms/cm².¹⁴ Effects such as these had generally been attributed either to changes in surface topography or to higher surface binding energies of oxygen with metal atoms.

The introduction of laser fluorescence spectroscopy to the study of the sputtering process has provided one with a sensitive method for following changes in sputtering yield in real time as a function of surface composition.^{15,16} Much of the work using this new method has been done in the "dynamic" dosing mode. In a series of experiments, Behrisch et al.¹⁷ measured sputtering yields of Fe for both H⁺ and D⁺ bombardment at 2 keV and He⁺ bombardment at 6 keV. LFS and weight loss measurements were employed for high fluence experiments in which the oxygen partial pressures in the vacuum chamber were adjusted so as to give a range of oxygen molecule to ion arrival rates of 10⁻³ to 10². Results for their H⁺ and D⁺ bombardments are shown in Fig. 1. Similar results have been obtained by Dullni et al. in "dynamic" dosing experiments of Ti with oxygen.¹⁸ Under these experimental conditions, it is not possible to determine the number of oxygen layers in the near surface region particularly since surface composition was not monitored. At the high ion fluences used, recoil implantation and ion beam mixing complicate the interpretation of the results, a fact which had been clearly recognized by these workers. Nonetheless, the results are striking in that the Fe sputtering yield, for example, changes by a factor of 15. Behrisch et al.¹⁷ discuss five contributory effects which can be summarized as: (1) changes in binding energy due to oxygen adsorption, (2) changes in binding energy due to topography; (3) "shadowing" by oxygen overlayers; (4) structural changes in the bombarded near surface region; and (5) development of surface structures such as blisters. In order to understand the profound effect of oxygen and other adsorbates in reducing substrate sputtering yields, it is clearly going to be necessary to assess the relative contribution of each of these factors.

Since the binding energy enters inversely in the sputtering yield formula, only unreasonably large changes in binding energy could explain the 15-fold decrease in Fe sputtering yield. Therefore, although factors (1) and

(2) can be expected to make some contribution to the observed effects, they cannot be the predominant causes. In order separately to assess factors 3-5, it is necessary to make sputter yield measurements which can be carried out with bombarding ion fluences so small as to minimize displacement damage, ion and recoil implantation as well as ion beam mixing. The recent development of "static" mode laser fluorescence as well as of multiphoton resonance ionization of sputtered atoms¹⁹ when coupled with surface Auger compositional analysis makes it possible to measure both ion-induced oxygen desorption cross sections and metal sputtering yields using pico-coulomb ion fluences. The effects of monolayer adsorbate coverages on sputtering yields can, therefore, be measured in sequential dosing experiments without changing the oxygen/metal ratio during a given data collection period.

On the basis of recently completed work¹⁶ on oxygen monolayers adsorbed on Ti metal, which will be more fully discussed below, one concludes that the ion fluences were too low in those experiments to rationalize the decreases in Ti sputtering yields due to oxygen absorption on the basis of surface structural changes. Assuming that the results found for the Ti-O system apply to the Fe-O system as well, one would conclude that factors (4) and (5) are not involved in the observed effects. One is left with factor (3) as mainly responsible for the reduction in sputtering yields observed by Behrisch et al. in the Fe-O system. Before inquiring into the reasonableness of this conclusion, and providing a quantitative interpretation of the results, we will summarize the experimental data for the Ti-O system mentioned above.

III. "Static Mode" Laser Fluorescence and Auger Spectroscopy Applied to the Study of Oxygen Monolayers on Titanium Metal.¹⁶

A systematic characterization of surface oxygen-metal reactions has shown that oxide-like sorption layers and "two-dimensional" oxides can form at room temperature on many metal surfaces.²⁰ The kinetics, mechanisms and structures of such layers can take many varied forms and the energetics for the formation of such layers appear to vary from metal to metal. Clearly, the details of the oxygen-metal bond influence many of the surface dependent properties.

In order to study the effect of monolayer and submonolayer coverages of oxygen on sputtering yields, we have developed the techniques of "static mode" laser fluorescence coupled with Auger spectroscopy and have applied the method to a study of Ti-metal surfaces interacting with oxygen. Details of the "static mode" laser fluorescence method have been described in the literature.^{15,16} Suffice it to say here that the principal innovation in the "static mode" LFS technique involves operating the ion source in a pulsed mode by application of a brief flat topped pulse (4 μ s duration), producing a 600 V potential difference across the deflection plate system of the ion gun, and resulting in a deflection of the 3 Kev ion beam about 6 mm at the Ti-target. The target was aligned so that the deflected beam reached the target center. During most of the 100 ms interval between laser pulses, the undeflected ion beam impacted the outer edge of the Ti target. This mode of operation minimizes sputtering during LFS data collection and has been shown to result in virtually unchanged O/Ti ratios during a single run. After measurements at a given O/Ti ratio have been completed, the ion beam is allowed to bombard the central region of the target continuously until the next desired O/Ti ratio is established and measured using the Auger monitoring system.

A dye laser (Molelectron MY34-DL16) was synchronized to fire 3 μ s after pulsing the ion beam. Broadband operation ($\sim 1 \text{ cm}^{-1}$ linewidth) was employed, with sufficient power to ensure a high saturation condition of the transitions

being excited. Details of the laser system and LFS techniques have been published elsewhere.^{15,16}

The Ti target was oxygen coated in a position facing an AES system, after sputter cleaning. The oxygen partial pressure ($\sim 10^{-6}$ Pa) was monitored with a quadrupole gas analyzer. In accordance with the high sticking coefficient for oxygen on titanium, one monolayer coverage was achieved at exposures of 1-2 L, while 5 L was sufficient to produce an AES signal corresponding to about 3 monolayers. Desorption of oxygen by the AES electron beam could be easily observed at coverages higher than two monolayers but could be kept to an acceptable rate by minimizing the electron beam current.

A. Nature of surface oxide layers and sputtering kinetics

In order to clarify the nature of oxygen bonding to titanium, which affects the sputtering yield, the kinetics of oxygen sputtering were investigated. The erosion of the oxygen near-surface layer by a steady beam of ions of current density J ions cm^{-2} can be described in terms of a cross-section σ for the desorption process:

$$\sigma = \frac{d(\ln y)}{dt} / J = S/n_0 \quad (1)$$

where S atoms ion^{-1} is the sputtering yield at one monolayer coverage, n_0 atoms cm^{-2} the area density for one monolayer, and y is a quantity proportional to actual surface coverage, $n(t)$ atoms cm^{-2} . Here we take for y the AES O/Ti signal ratio from the peak heights of the 510 eV oxygen and the 418 eV titanium lines in the differential Auger spectrum. While the sputtering process is not strictly describable by a cross section for independent ejection events, the approximation appears valid for low coverage.²¹⁻²³ In Fig. 2 where the O/Ti Auger ratio is plotted against time (for a beam current density

of $2 \times 10^4 \text{ Ar}^+ \text{ ions cm}^{-2} \text{ s}^{-1}$ at the monitoring position), four distinct regions, labelled A-D can be identified. The assignment of oxygen coverage values given in Table 1 is deduced from a model of the expected O/Ti Auger peak ratio as a function of coverage. As is discussed below, this is strongly supported by experimental evidence from other studies. Also given in Table 1 are the σ and S values calculated from Eq. (1) for a value of $n_0 = 1.474 \times 10^{15} \text{ atoms cm}^{-2}$.

A tightly bound layer corresponding to the D region of Fig. 2 has the lowest sputtering yield and has a transition to the C region at an O/Ti signal ratio of ~ 0.1 . A change in slope at this O/Ti ratio has been observed by Shih and Jona²⁴ and identified by them on the basis of LEED data as due to the formation of a 1/4 monolayer of oxygen. Later studies²⁵ confirm that the characteristic $p(2 \times 2)$ pattern seen in LEED is due to the presence of 1/4 monolayer of oxygen. The LEED results could not be used to differentiate between formation of an over or underlayer. We have shown that such information is obtainable from the sputtering results as discussed below.²⁶

B. Effect of oxygen adsorbates on Ti sputtering yield.

Experiments with LFS detection were performed on the sputtering of Ti atoms as a function of oxygen coverage. First, successive members of the a^3F_J , $J=2,3,4$ ground state multiplet were accessed and fluorescence detected at wavelengths selected from the $a^3F + z^3F^0$ system at $\sim 520 \text{ nm}$. The LFS signal was followed through diminishing oxygen coverage until essentially clean metal was indicated by Auger measurements. The relative normalization of the curves shown in Fig. 3 for the different fine-structure states was obtained in separate experiments on the clean metal target for each of the $J=2,3$, and 4 levels. Corrections for the different degeneracies, radiative lifetimes and branching ratios at the detection wavelength were applied. The

sum of the three ordinates at zero oxygen coverage was taken to be the total sputtering yield of Ti metal for 3 keV Ar⁺ (S = 1.1).^{11,28,29} Assumptions made in interpreting the data of Fig. 3 as Ti⁰ yields are that the velocity of the ejected Ti atom does not vary substantially with oxygen coverage or the state of the ejected species and that atoms sputtered in more highly excited electronic states or as ions constitute a negligible fraction of the total sputtered flux. Large errors are not expected but additional work is clearly required so as to be able fully to assess the effects of changing velocity, excited state and ion distributions.

) The salient result is that the Ti⁰ sputtering yield is a strongly decreasing function of oxygen coverage. It is lower by a factor of about six in the case of three monolayer oxygen coverage compared to a clean Ti metal surface. In order to understand the physical basis for these results, model calculations were performed with the TRIM code of Haggmark and Biersack,^{28,30} modified to include multiple layers and components for sputtering calculations. The best agreement between the data and the TRIM code calculations were obtained using a model in which the first two oxygen monolayers form underlayers. Interestingly, this situation was found by LEED to be the case for N₂ on Ti.²⁴ The two dimensional TiN structure bears a remarkable structural similarity to bulk TiN. It is tempting to speculate that oxygen monolayers on Ti form two dimensional oxides whose structure and bonding properties resemble bulk TiO and TiO₂.¹⁶ Oxygen overlayer formation occurs with the third oxygen layer which results in very large decreases in Ti yield.

IV. Depth of Origin of Sputtered Atoms

The "static mode" LFS experiments have shown for the first time that monolayer oxygen coverages can result in a decrease of substrate sputtering yields up to about an order of magnitude. One must now inquire whether this

result can be rationalized theoretically. Sputtering yield calculations have been done in recent years using a variety of computer codes^{28,30,31}. We have made extensive use of TRIM code calculations modified in such a way as to be able to include the effects of over and underlayer formation.¹⁶ For clean metal surfaces, TRIM calculations have given excellent agreement with experimentally determined values of sputtering yields. In addition, it is possible to determine the depth of origin of sputtered atoms using the TRIM code,³² and the results of calculations for D^+ at several energies on Cu and for 3 keV Ar^+ and He^+ on Ti are shown in Figs. 4 and 5. In the cases so far examined, the Monte Carlo calculations show that 80-90% of all sputtered atoms originate from the very first or surface layer. This appears to be generally true for most combinations of projectile and target masses and is relatively energy insensitive. A full documentation of these conclusions still remains to be made.

The results of TRIM calculations regarding the depth of origin of sputtered atoms have now been strikingly verified in a series of ingenious experiments by Dumke et al.³³ These workers first showed that ion scattering and Auger spectroscopy results are in agreement with theoretical expectations that the surface monolayer of a gallium-indium alloy containing 16.5% indium in the bulk is greater than 94% indium, while the next layer is only slightly enriched. They then report measured sputtering yields and angular distributions of sputtered atoms from both the solid and liquid phases of pure gallium and indium, and of gallium-indium eutectic alloy. These were obtained by Rutherford backscattering analysis of graphite collector foils. The sputtering of the liquid eutectic alloy by 15 keV Ar^+ results in a ratio of indium to gallium sputtering yields which is 28 times greater than would be expected from the target stoichiometry. Furthermore, the angular distribution of gallium is much more sharply peaked about the normal to the target surface than

the indium distribution. When the incident Ar^+ energy is increased to 25 keV, the gallium distribution broadens to the same shape as the indium distribution. With the exception of the sharp gallium distribution taken from the liquid eutectic at 15 keV, all angular distributions from liquid targets fit a $\cos^2\theta$ function. The sputtering yields from the eutectic allowed these workers to infer, in accord with theoretical expectations, that 85% of the sputtered atoms originate in the surface monolayer at 15 keV incident energy, while 70% do so at 25 keV.

V. Effects of Surface Segregated Layers on Sputtering Yields

More than 100 years ago Gibbs³⁴ showed that the surface of an alloy becomes enriched in the component that produces the lowest surface free energy. In simple situations where no major changes in chemical bonding are involved, and heats of solution or mixing are small, this generally is the component with the lowest surface energy in pure form.

This analysis has more recently been extended by several workers using the quasichemical, pair-wise model of bonding to express thermodynamic parameters.³⁵ If it is assumed that significant deviation from bulk composition is confined to one monolayer, which is reasonable in this model so long as the heat of mixing is small, then one can derive simple expressions for surface compositions and surface energies of solutions and alloys from the properties of the pure components. The work of Miedema has also been shown to predict the surface energies of a number of simple solutions quite accurately^{36,37} on the basis of a different model.

Calculations using models of this sort have recently been made by us for a series of substitutional solid solutions of Cu-Li, V-Al, and W-Be where the fraction of the minor components (Li, Al, and Be) were fixed at 4 at.%. From Fig. 6 it can be seen that the surface concentration of the minor component in

these alloys can reach very high values depending on the temperature. Thus, for the 4 at.% Cu-Li alloy system, the predicted surface concentration of Li is near 100% even at temperatures approaching the melting point of Cu. It is of interest now to inquire into the sputtering yield of Cu as a function of the number of Li overlayers. Calculations of this sort were made using the TRIM code with the assumption that the surface segregated Li forms in-layers in the sense of random substitution of Li for Cu in the surface layer until one monolayer is completed. Formation of the second Li-containing layer proceeds in the same fashion as the first.

From Fig. 7 it can be seen that the sputtering yield of Cu decreases from 0.26 for 2 keV He⁺ bombardment of clean Cu to 0.09 for an epitaxial Li overlayer which is one monolayer in thickness. At the level of two Li overlayers, the Cu yield is 0.02. The Li sputtering yield in the 1-2 monolayer regime is 0.20. For 200 eV He⁺ ions, the sputter yield calculations are shown in Fig. 8. Again at the one monolayer Li level, the Cu yield has decreased from 0.06 to 0.01 while at the two monolayer level, the Cu yield is virtually zero. The Li yield for 200 eV He⁺ ions varies essentially linearly with Li layer thickness and is 0.21 at the two Li monolayer thickness. The implications of these calculated results for applications of Cu-Li as a high heat flux plasmaside material are discussed below.

In Fig. 7 the sputtering yields with 2 keV He⁺ for a variety of plasma side materials are shown. In parentheses are given the atomic numbers (Z) of the elements. In the case of TiC, the number in parenthesis is the arithmetic mean of the atomic numbers of Ti and C. In the case of Cu-Li, the number in parenthesis is

$$\frac{S_{Cu}}{S_{Cu}+S_{Li}} \times \text{at. no. Cu} + \frac{S_{Li}}{S_{Cu}+S_{Li}} \times \text{at. no. Li}$$

appropriate for each He⁺ energy and Li layer thickness. It can be seen that on the basis of this comparison, the total sputter yield of Cu-Li at the one monolayer level for 2 keV He⁺ is lower than the sputter yield of graphite albeit the effective Z is somewhat higher (8 compared to 6). For 200 eV He⁺, the Cu-Li and Be sputter yields are almost the same while the effective Z for Cu-Li is close to 3 while that of Be is 4.

Another way of evaluating the possible utility of Cu-Li in fusion applications is to examine the effect of Li overlayers on the Cu self-sputtering coefficient. Extensive calculations using the REDEP code have recently shown³⁹ that a "runaway" condition occurs when the self-sputtering coefficient of Cu exceeds unity. This situation, which is reached for pure copper at plasma edge temperatures of ~ 30 eV, is pushed to ~ 150 eV in the case of a Li overlayer sputtering with 100% ion fraction and to 103 eV with 90% ion fraction. The very substantial increase in edge temperatures allowed with the Cu-Li system presents machine designers with an interesting new limiter or divertor candidate material.

The stability of Li overlayers produced in a self-sustaining fashion by surface segregation in a radiation environment is under study in our laboratory and in several collaborative experiments with other laboratories together with measurements of the effects of such overlayers on Cu substrate sputtering yields.

References

1. R. F. Mattas, D. L. Smith, and M. A. Abdou, J. Nucl. Mat., 122 & 123, 66-79 (1984).
2. J. L. Cecchi and the TFTR Group, Proc. 6th Int. Conf. on Plasma Surface Interactions in Controlled Fusion Devices, held at Nagoya University, Nagoya, Japan, May 1984.
3. D. M. Gruen, A. R. Krauss, M. H. Mendelsohn, and S. Susman, J. Nucl. Mat., 111 & 112, 831 (1982).
4. A. R. Krauss, D. M. Gruen, and A. B. DeWald, J. Nucl. Mat., 121, 398 (1984).
5. N. Matsunami et al., "Energy Dependence of the Yields of Ion-Induced Sputtering of Monatomic Solids," IPPJ-AM-32, Sept. 1983, Nagoya University, Nagoya, Japan.
6. R. Behrisch, ed. in "Topics in Applied Physics" (Springer, Berlin, 1980).
7. H. Schirwitz, Beitr. Plasmaphys. 2, 188 (1962).
8. W. O. Hofer and H. Liebl, in "Ion Beam Surface Layer Analysis," Vol. II. eds. O. Meyer, G. Linker and F. Kappler (Plenum, 1976) 659.
9. J. Hrbek, Thin Solid Films 42, 185 (1977).
10. W. O. Hofer and P. J. Martin, Appl. Phys. 16, 271 (1978).
11. W. O. Hofer, H. L. Bay, and P. J. Martin, J. Nucl. Mat., 76 & 77, 156 (1978).
12. O. C. Yonts and D. E. Harrison, J. Appl. Phys. 31, 1583 (1960).
13. J. W. Coburn, E. Taglauer, and E. Kay, J. Appl. Phys. 45, 1779 (1974).
14. A. Elbern, P. Mioduszeweki and E. Hintz, Proc. 7th Int. Vac. Cong. and 3rd Int. Conf. on Solid Surfaces (Vienna, 1977), 1433.
15. D. M. Gruen, M. J. Pellin, C. E. Young, M. H. Mendelsohn, and A. B. DeWald, Physica Scripta, T6, 42 (1983).

16. M. J. Pellin, C. E. Young, D. M. Gruen, Y. Aratono and A. B. DeWald, "Oxygen Underlayer Formation on Titanium by 'Static Mode' Laser and Auger Spectroscopy," Surf. Sci., in press.
17. R. Behrisch, J. Roth, J. Bohdanský, A. P. Martinelli, B. Schweer, D. Rusbüldt and E. Hintz, J. Nucl. Mat., 93 & 94, 645 (1980).
18. E. Dullni and E. Hintz, Verhandl. DPG. 16, 89 (1981); Phys. Lett. 88A 46 (1982).
19. M. J. Pellin, C. E. Young, W. F. Calaway, and D. M. Gruen, "Trace Surface Analysis with Pico-Coulomb Ion Fluences," Surf. Sci., in press.
20. E. Fromm and O. Mayer, Surf. Sci. 74, 259 (1978).
21. H. F. Winters and P. Sigmund, J. Appl. Phys. 45, 4760 (1974).
22. M. Braun, B. Emmoth, and I. Martinson, Physica Scripta 10, 133 (1974).
23. E. Taglauer, U. Beitat, G. Marin, and W. Heiland, J. Nucl. Mt. 63, 193 (1976); Surf. Sci. 63, 311 (1977).
24. H. D. Shih and F. Jona, Appl. Phys. 12, 311 (1977).
25. B. T. Jonker, J. F. Moran, and R. L. Park, Phys. Rev. 824, 2951 (1981).
26. M. J. Pellin, C. E. Young, M. H. Mendelsohn, D. M. Gruen, R. B. Wright, and A. B. DeWald, Proceedings of the 5th Int. Conf. on Plasma Surface Interactions in Controlled Fusion Devices, Gatlinburg, Tenn., May 1982.
27. A. R. Krauss, D. M. Gruen, N. Q. Lam, and A. B. DeWald, Proceedings, Sixth Int. Conf. on Plasma Surface Interactions in Controlled Fusion Devices, Nagoya, Japan, May 14-18, 1984.
28. J. P. Biersack and L. G. Haggmark, Nucl. Instr. Methods 174, 257 (1980).
29. P. Sigmund, Phys. Rev. 184, 383 (1969).
30. L. G. Haggmark, and J. P. Biersack, J. Nucl. Mat. 93 & 94, 664 (1980).
31. D. E. Harrison, P. W. Kelly, B. J. Garrison, and N. Winograd, Surf. Sci. 76, 311 (1978).

32. A. R. Krauss, D. M. Gruen, and A. B. DeWald, Proc. 19th Symp. on Engineering Problems of Fusion Research, Oct. 26-29, 1981, Chicago, IL.
33. M. F. Dumke, T. A. Tombrello, R. A. Weller, R. M. Honsley, and E. H. Cirlih, Surf. Sci. 124, 407 (1983).
34. J. W. Gibbs, Trans. Connecticut Acad. Sci. 3, 108 (1875/76).
35. F. L. Williams and D. Nason, Surf. Sci. 45, 377 (1974).
36. A. R. Miedema, Z. Metallkunde 69, 455 (1978).
37. A. R. Miedema and J. W. F. Darleijn, Surf. Sci. 95, 447 (1980).
38. A. R. Krauss, A. B. DeWald, D. M. Gruen, and N. Q. Lam, Proceedings, Workshop on Synergistic Effects in Surface Phenomena Related to Plasma-Wall Interactions, Nagoya, Japan, May 21-23, 1984.
39. J. Brooks, private communication.

Table 1. Sputtering yield data from erosion kinetics of O/Ti Auger
Signal using 3 keV Ar⁺.

Region	O/Ti at slope change	Coverage (monolayers)	S (atoms/ion)	σ (10^{-16}cm^2)
A	A-B = 0.92	>2	1.9	13.0
B	B-C = 0.39	1 - 2	0.35	2.4
C	C-D = 0.15	.25 - 1	0.20	1.4
D	—	0 - .25	0.11	0.7

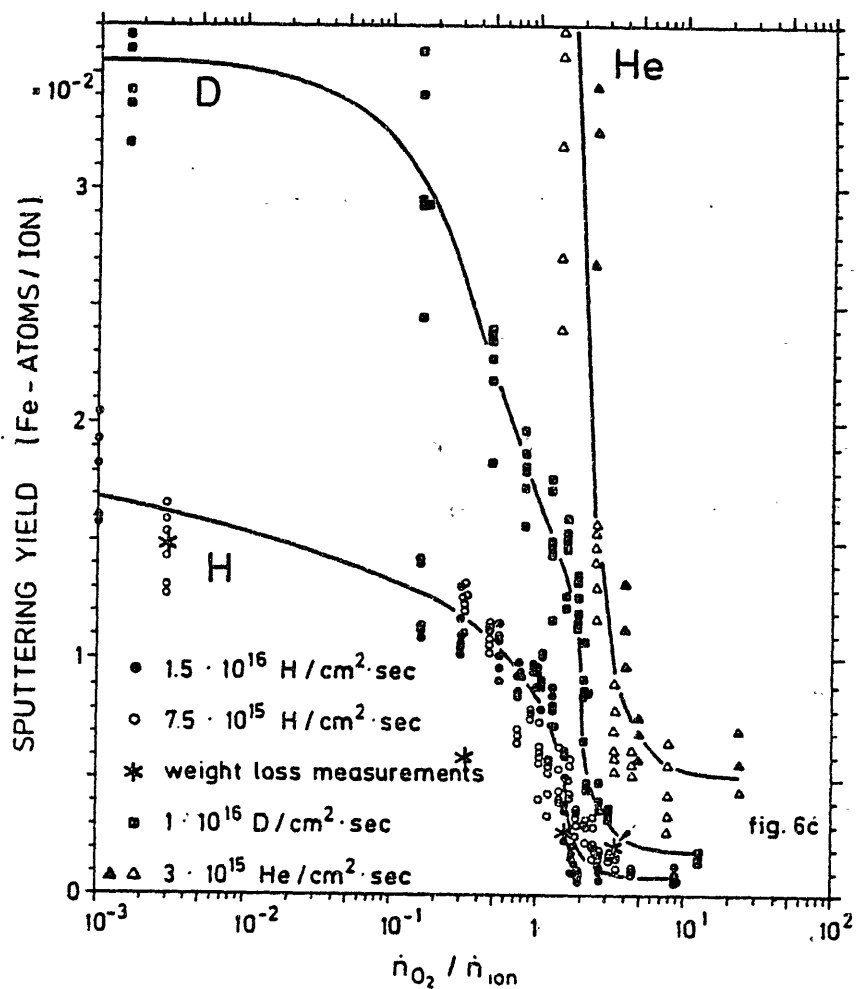


Fig. 1. High dose sputtering yields of polycrystalline Fe measured by LEFS as a function of the ratio between the oxygen molecule arrival rate on the surface \dot{n}_{O_2} and the ion arrival rate \dot{n}_{ion} for bombardment with 2 keV H and D ions and 6 keV He ions. The values indicated by the stars are measured by weight loss (from Ref. 17).

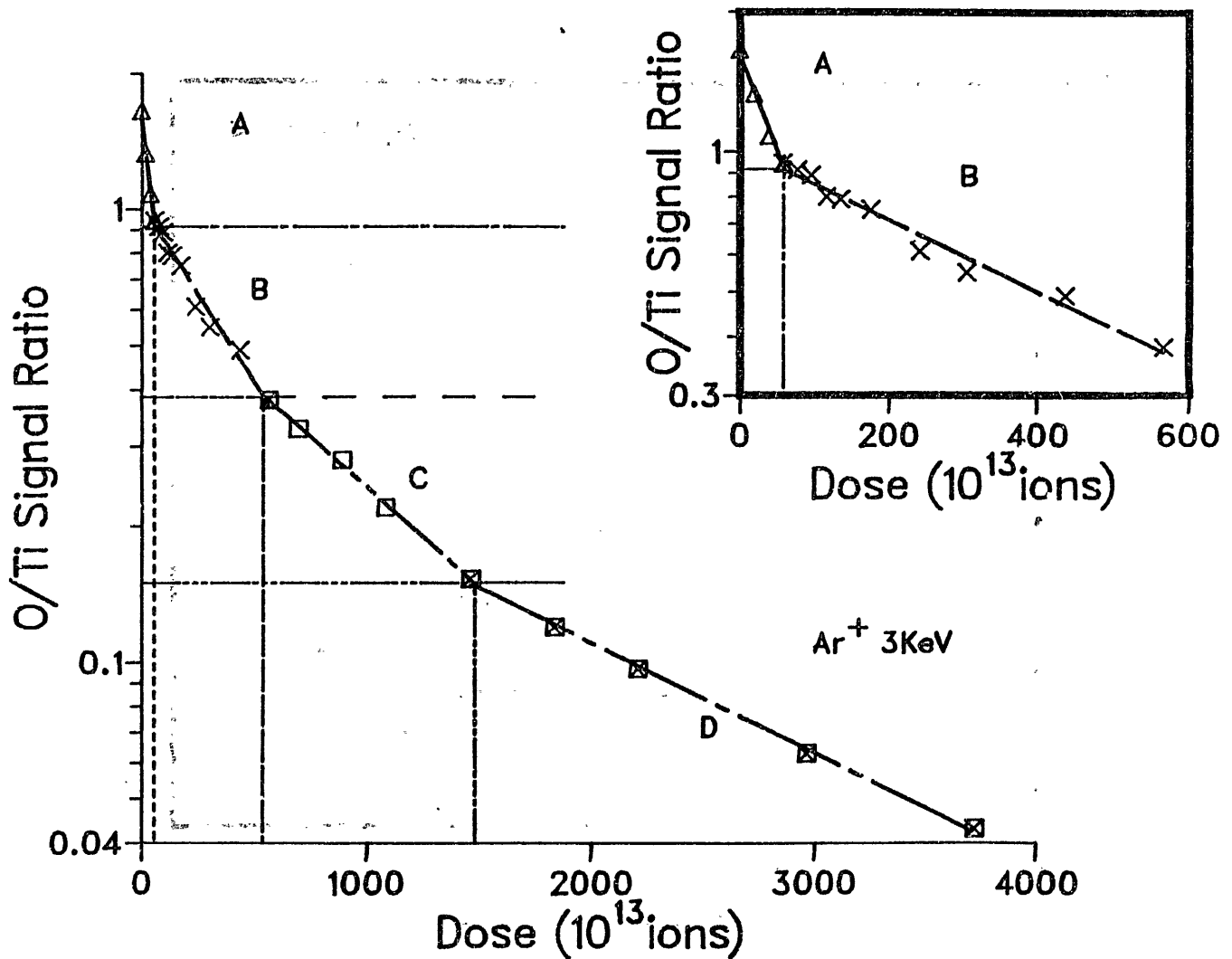


Fig. 2 Ion (3 keV Ar^+) induced oxygen erosion kinetics of a Ti target. The O/Ti Auger signal ratio is determined from the differential peak height of the oxygen KLL transition (512 eV) and the Ti LMV transition (418 eV). Four distinct erosion rates are observed (Table 1) with the fastest rate regions expanded in the insert.

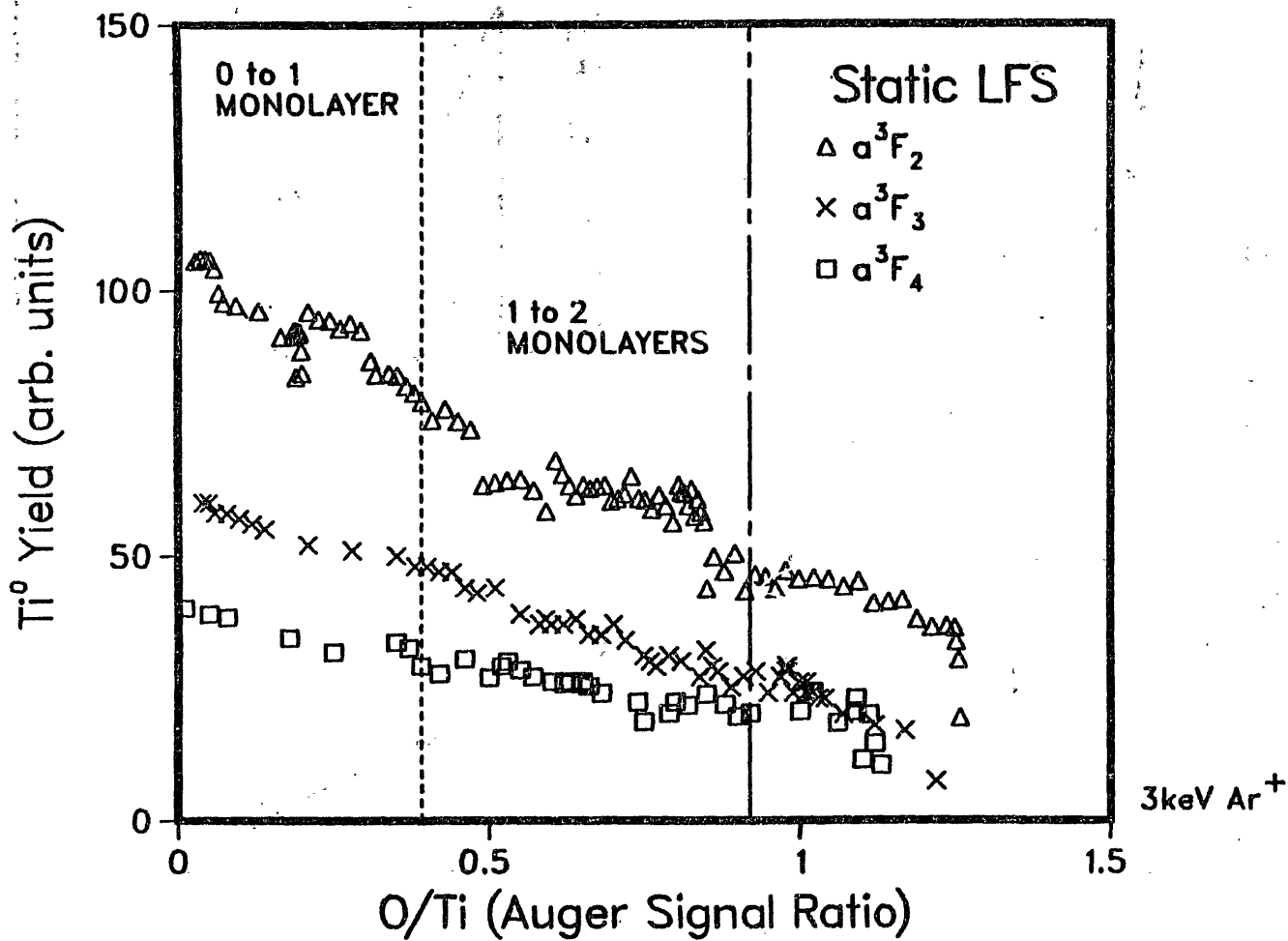


Fig. 3 LFS signal as a function of oxygen coverage for members of the Ti ground state multiplet. The primary ion was 3 keV Ar^+ .

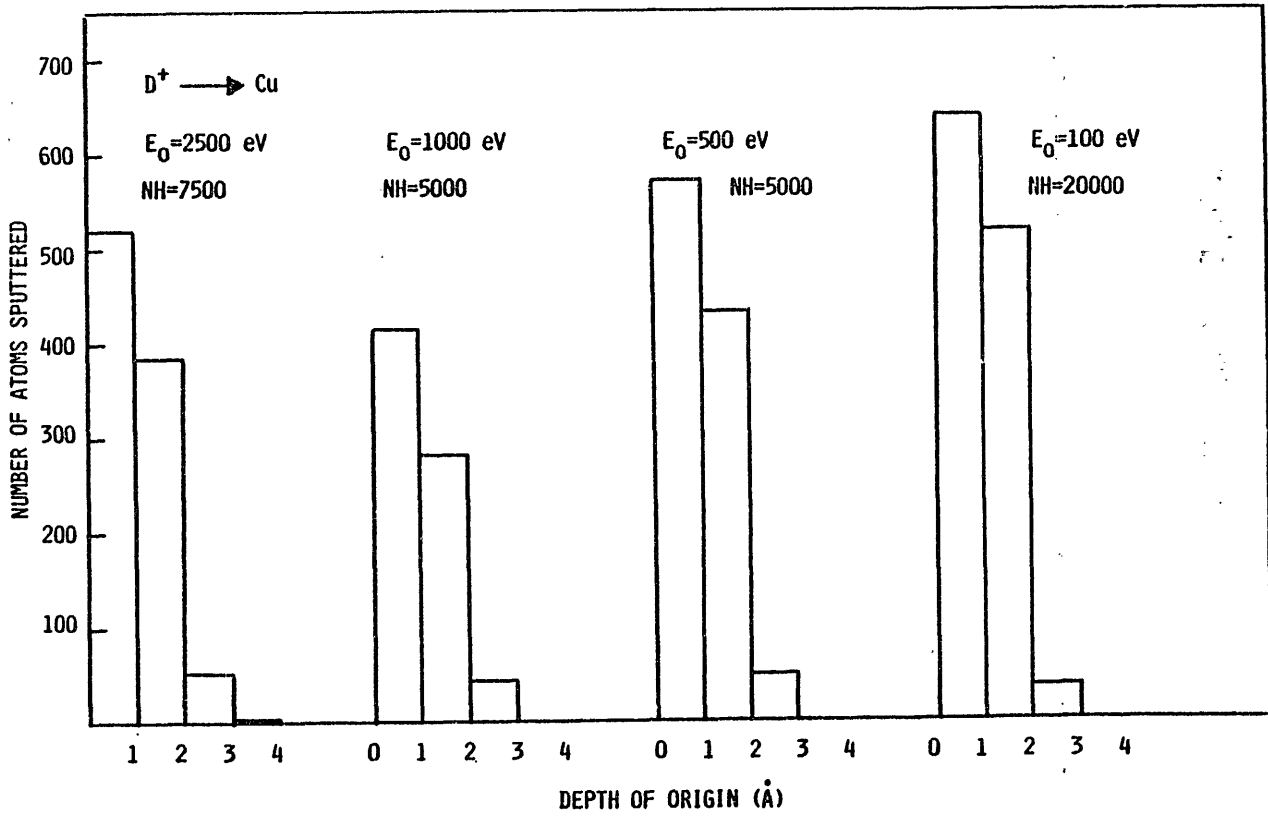


Fig. 4 Depth of origin of sputtered Cu atoms from a Cu target being bombarded by D⁺ at various energies. TRIM code calculations.

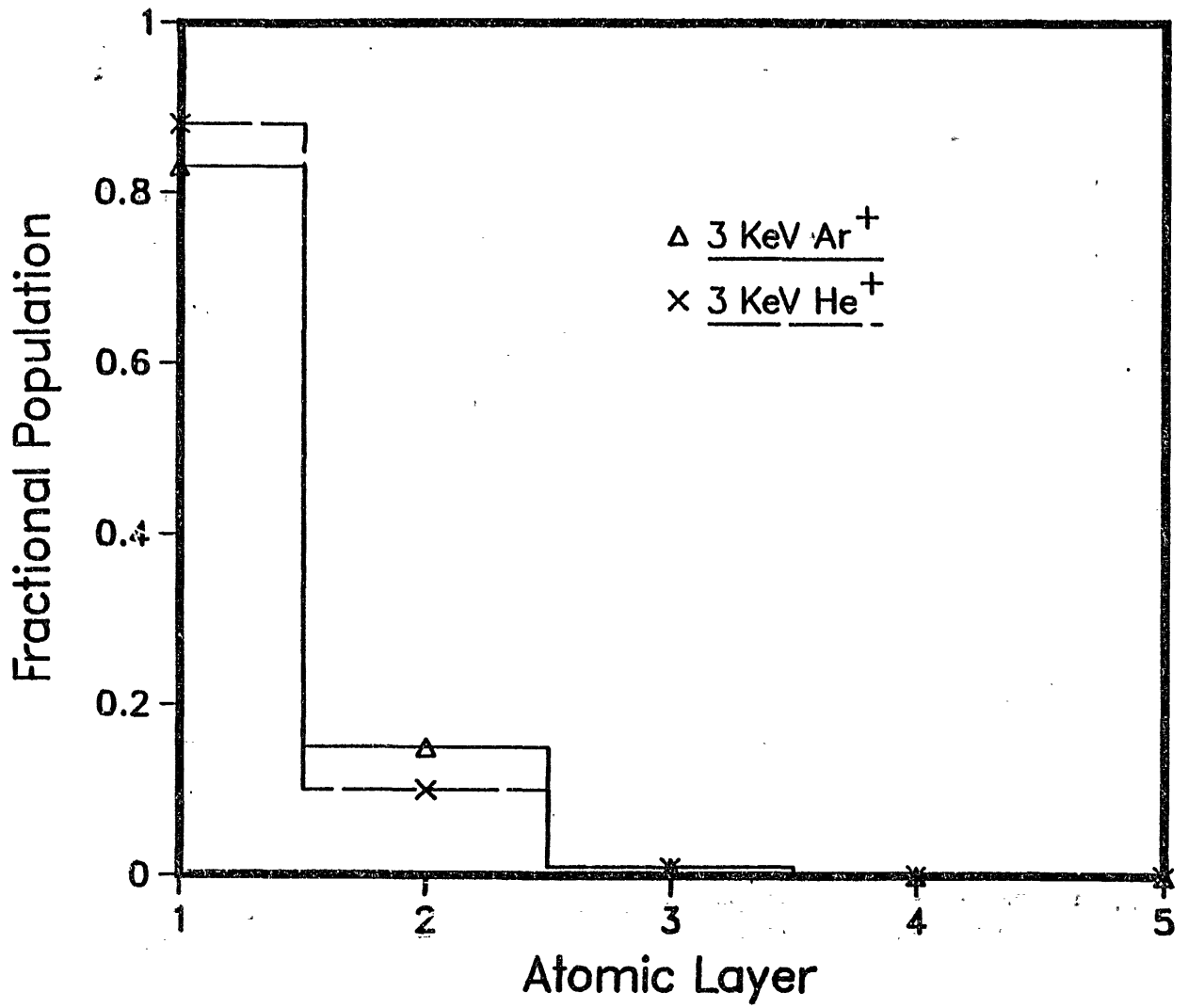


Fig. 5 TRIM code calculations showing the depth of origin of sputtered Ti atoms from a Ti surface following 3 keV Ar⁺ bombardment.

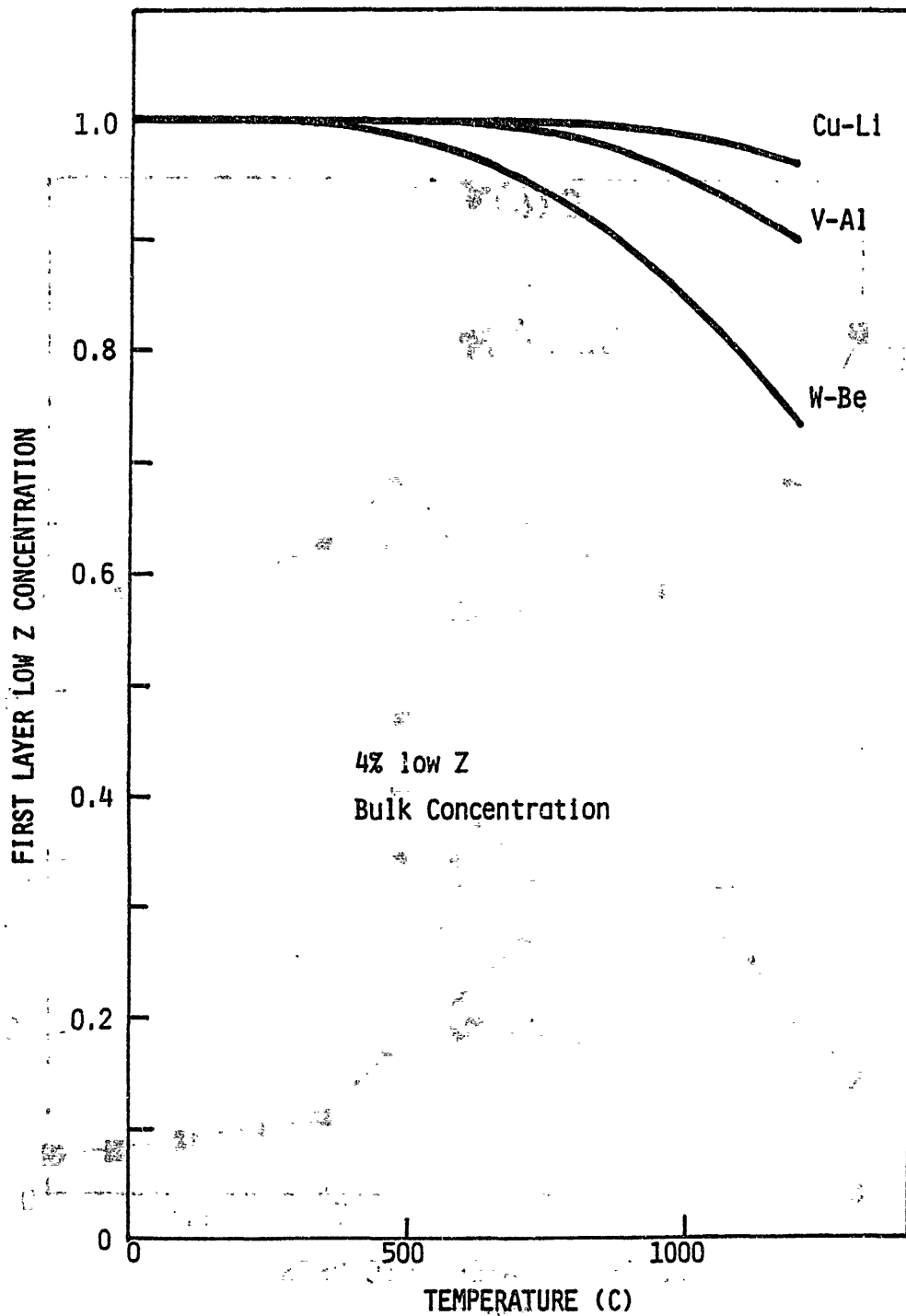


Fig. 6 Calculated first layer concentration (at.%) of the low-Z component of three binary alloys vs. temperature. The bulk composition of all three alloys is taken as 4 at.%, and the calculation is done in the Miedema model.

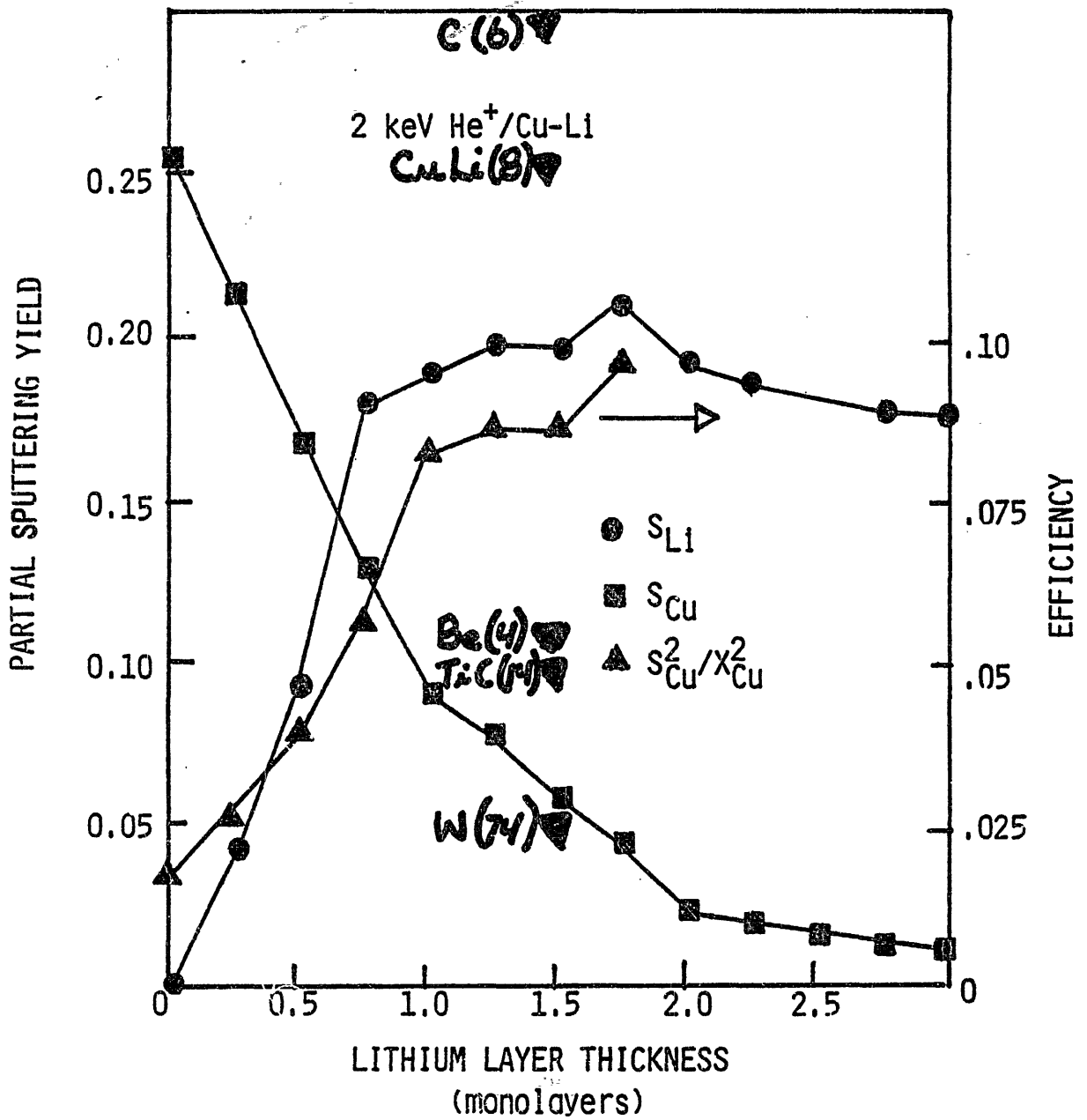


Fig. 7 Partial sputtering yields of Li and Cu from a Li-Cu alloy for 2 keV He⁺ bombardment. TRIM code calculations.

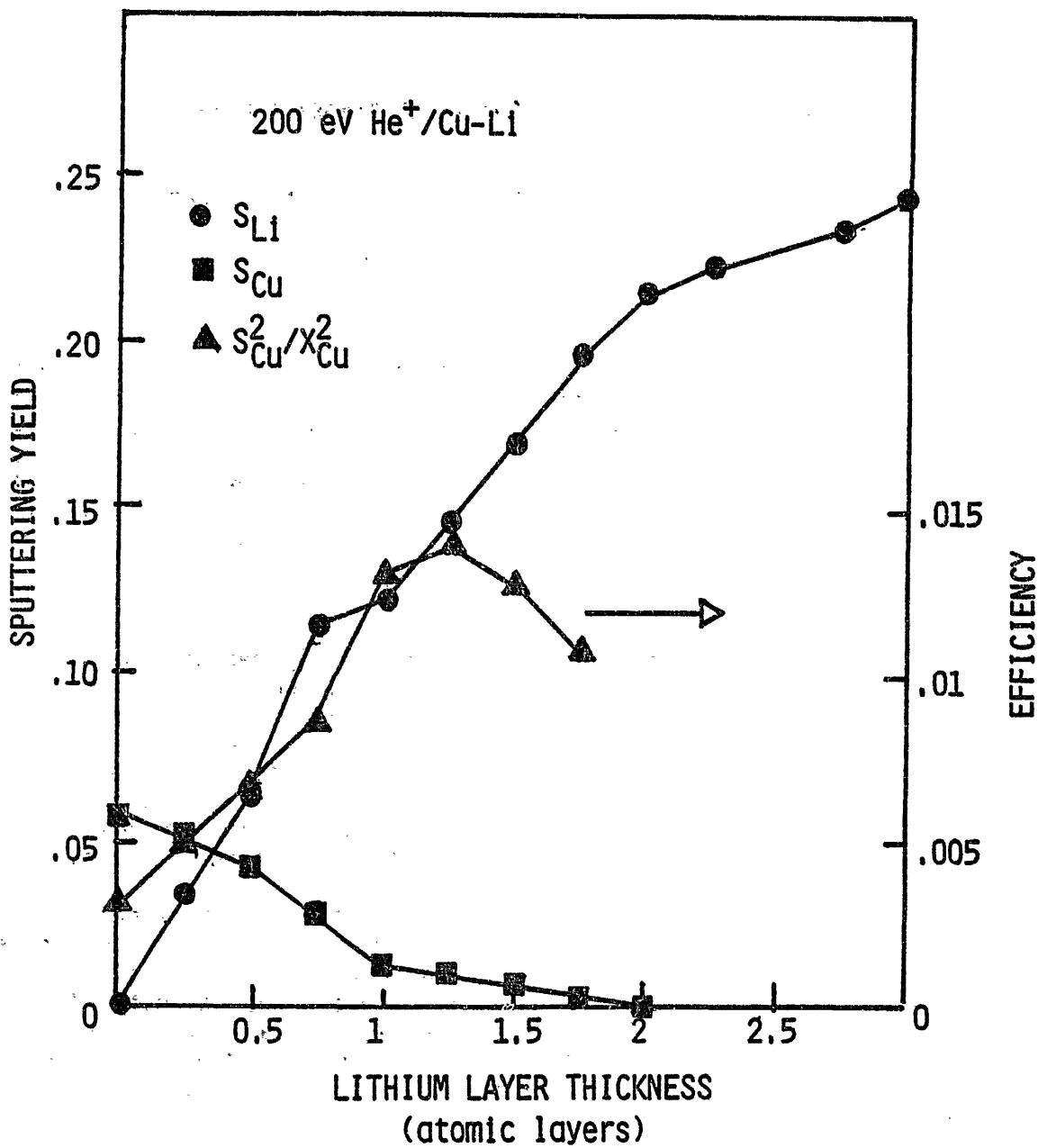


Fig. 8 Partial sputtering yields of Li and Cu from a Li-Cu alloy for 200 eV He⁺ bombardment. TRIM code calculations.

SYNERGISTIC SPUTTERING PROPERTIES OF BINARY ALLOYS

A. R. Krauss, A. B. DeWald,* D. M. Gruen and N. Q. Lam
Materials Science and Technology Division
Argonne National Laboratory
Argonne, IL 60439

We have found that dilute concentrations of lithium in copper produce surfaces which are nearly pure lithium when heated and subject to irradiation. In order to better understand the experimental results, we have modeled the Cu-Li system using a modified version of the TRIM computer code and an alloy segregation program developed by N. Q. Lam. The TRIM code calculates the sputtering yield and depth of origin of the sputtered atoms for materials in which the composition varies from one atomic layer to the next and the segregation program uses these sputtering yields to trace the evolution of the concentration profile.

The initial result of sputtering is to preferentially deplete the surface species. Continued irradiation, however, creates a subsurface region of high displacement damage. In the Cu-Li alloy, lithium moves very rapidly through this region, resulting in subsurface lithium enrichment. The enriched region broadens and eventually reaches the surface. The exact effect on the lithium concentration in the first two atomic layers depends on the temperature, damage profile, and particle flux. Results of the calculation are presented, along with a discussion of their implications for fusion reactor materials.

It is often assumed, when dealing with the sputtering of compounds and alloys, that each component has the same sputtering properties as the pure element, and that the sputtering rate of a given atomic species is, therefore, linear with atomic concentration. We have investigated the validity of this assumption in the context of dilute, highly segregating alloys proposed for fusion applications. It is found that as the concentration of a given element changes with time and from one atomic layer to the next, the sputtering yield also changes significantly.

*Georgia Institute of Technology, Atlanta, GA.

INTRODUCTION

One of the principal factors limiting the ultimate performance of magnetic fusion devices is the energy lost to atomic line radiation from plasma impurities arising from the erosion of structural components which face the plasma. Since the energy lost to line radiation increases very rapidly with the atomic number of the impurity atoms, it is especially important to limit the concentration of high-Z atoms in the plasma. Additionally, there is a serious structural problem associated with the use of high-Z materials facing the plasma: Sputtering, by both the D-T fuel and plasma impurities, is expected to be the dominant erosion mechanism in a fusion reactor. For most of the possible range of plasma parameters in which a fusion reactor would operate, even a very low concentration of high-Z plasma impurity would result in a self-sputtering cascade which would quickly destroy the structural components facing the plasma [1].

It is, therefore, desirable to use low-Z materials on all surfaces exposed to the plasma. The thermal, chemical, and mechanical properties of most low-Z materials are rather poor, dictating that they be used in the form of coatings deposited on, or bonded to, a structural substrate. However, the use of coatings results in a number of new problems related to the integrity of the interface, erosion-redeposition phenomena, and maintenance: Unless the coating is very thin or has a thermal expansion coefficient matched to that of the substrate, interface fracture is likely to occur as the result of thermal shock. Additionally, the bond is weakened as the result of accumulated gas and defects at the interface. Coatings such as titanium carbide used in current fusion devices are typically only 20 microns thick, and are subject to failure by microcracking and eventual spallation if the thickness exceeds 30-40 microns [2]. Erosion and redeposition processes may result in the transfer

of as much as 100 cm of limiter thickness per year [3], indicating that it is very likely to be impossible to maintain a stable coating thickness. Regions in which the coating is depleted may be replenished by in-situ deposition. This approach, however, adds an additional degree of complexity and does not help in regions in which the coating has become too thick to be structurally stable.

A novel approach to the production and maintenance of self-sustaining low-Z coatings [4] involves the use of alloys in which thermal and radiation-related segregation processes result in an overlayer consisting entirely of the low-Z component of the alloy. Several alloys based on fusion reactor candidate materials have been identified as theoretically capable of producing such an overlayer [5] (e.g. Cu-Li, W-Be, and V-Al). At thermodynamic equilibrium, the region which is expected to be enriched in the low-Z component is only one atomic layer thick. In a radiation environment however, a concentration profile of the low-Z component is expected, which may extend quite far into the subsurface region.

In order to be of practical use, the coating must: (1) form a reasonably complete low-Z overlayer, which is maintained for times at least comparable to the operating cycle of the fusion device, (2) be stable at the expected operating temperature of the substrate material, (3) significantly reduce both the light ion and self-sputtering of the high-Z alloy component, (4) have a long lifetime-to-depletion of the bulk inventory of the low-Z component. Additionally, the erosion rate of the low-Z alloy component must be low enough to prevent significant contamination of the plasma by the overlayer material, although the allowable level for low-Z atoms is relatively high [6].

Copper is frequently the material of choice for high heat flux applications. Because of its high sputtering yield, it is, however, unsuitable for

use as a plasma-side material. In this paper we discuss the use of copper-lithium alloy as a means of retaining the desirable features of copper while lowering both the erosion rate and the effective Z of impurities introduced into the plasma. Attempts to model the experimental results reveal a number of synergistic effects associated with the sputtering of binary alloys in a fusion reactor environment.

Cu-Li has been investigated both theoretically and experimentally, and it has been found that, at sputter-induced erosion rates comparable to those expected in a fusion reactor and temperatures appropriate to the use of copper as a limiter material, an alloy containing as little as 2.6 at.% Li quickly forms an overlayer consisting of nearly 100% lithium [5]. This overlayer is stable during extended irradiation at high temperature. Negligible reduction in bulk lithium concentration is observed after three week's sputtering at a rate of approximately 0.4 atomic layers per second and maintenance at a temperature of 430°C [7].

Calculations using the TRIM computer code to predict the copper and lithium sputtering yields indicate that, for a single atomic overlayer of lithium, the copper erosion is reduced by a factor of 4-6 relative to that of pure copper, depending on the mass and energy of the incident particle [7]. Similar results have been obtained experimentally [5]. Analysis of the near-surface lithium concentration by Auger electron spectroscopy indicates the presence of more than one atomic layer of lithium. Physical arguments based on the charge state of the sputtered lithium and the observed stability of the lithium overlayer at temperatures in excess of 400°C [7] dictate that the effective thickness of the lithium overlayer does not exceed 2 atomic layers. Calculated yields for the self-sputtering of copper from a pure copper surface and from copper covered with 1 and 1.5 atomic layers of lithium

are shown in Fig. 1. For comparison, the self-sputtering yield of tungsten is also shown. For impact energies in excess of 1 keV, the sputtering yield of tungsten exceeds unity, corresponding to the generation of a self-sputtering cascade which would quickly destroy the limiter. The impact energy depends on both the plasma edge temperature and the charge state of impurity atoms emanating from the edge region. For tungsten, an impact energy of 1 keV corresponds to an edge temperature of ~ 100 eV. For copper with a single lithium overlayer, the predicted kinetic energy corresponding to unity self-sputtering yield is 1400 eV, higher than for tungsten. If the lithium overlayer is as little as 1.5 monolayers thick, the self-sputtering window for Cu-Li is 3400 eV wide. Because the atomic number of the impurity influx would be reduced by a factor of 2.5 relative to that of tungsten, plasma performance would also be improved.

The TRIM calculations predict that the erosion rate of lithium from the Cu-Li alloy is comparable with the erosion rate of copper from pure copper. However, based on theoretical considerations and earlier experiments [8], it was anticipated that the lithium would be sputtered primarily as secondary ions. It has been shown that as a result of the electric potential gradient at the limiter of a tokamak, and the tangential toroidal magnetic field at the wall, the probability that a secondary ion will enter the plasma as an impurity is on the order of only a few parts per million [9,10]. The vast majority of the secondary ions are returned to the sputtered surface within ~ 100 μm of the point of origin. Laboratory experiments simulating the effect of the sheath potential at a tokamak limiter by applying a bias voltage to the sample and monitoring the surface composition during sputtering by means of Auger spectroscopy have shown that, for a temperature range of 140°C to 320°C , spanning the expected operating temperature range of a copper limiter in a fusion

reactor, the electric field completely suppresses the depletion of the lithium overlayer, as shown in Figs. 2 and 3.

The attainment of the conditions outlined above as necessary for the successful use of self-sustaining low-Z coatings have been demonstrated in the laboratory for dilute alloys of lithium in copper. The current work is a parametric modeling study aimed at elucidating the relevant properties affecting the sputtering of alloys in a fusion environment. It is directed specifically to an understanding of the experimental results observed for copper-lithium alloys [11] in terms of the time evolution and steady state of the lithium concentration profile.

THEORY

It was predicted by Gibbs [13] in 1875 that at thermodynamic equilibrium, the composition of the uppermost atomic layer of an alloy corresponds to a minimum in the surface free energy. It is only recently, however, that modern surface analysis techniques have been able to provide experimental confirmation [14]. It is predicted [15] that for a binary alloy, the concentrations C_A^1 and C_B^1 of atomic species A and B in the first atomic layer are given by

$$\frac{C_A^1}{C_B^1} = \frac{C_A^2}{C_B^2} \exp(-\Delta H_{\text{seg}}/kT) \quad (1)$$

where C_A^2 and C_B^2 are the second layer concentrations of A and B, and ΔH_{seg} is the segregation energy. The principal contribution to ΔH_{seg} results from minimization of the surface bond enthalpy, although lattice strain resulting from under- or oversized solute atoms also contributes to the segregation energy. A semi-empirical model due to Miedema [16] has been used with good success to calculate the segregation energy. A recent review by Chelikovsky

[17] summarizes the predictions of the Miedema model for a large number of solvent-solute combinations.

In most treatments, the quantities C_A^2 and C_B^2 in Eq. 1 are replaced by the bulk concentrations C_A and C_B , although it has been shown by Williams and Nason [18] that Gibbsian segregation is only approximately a first atomic layer phenomenon. In the present case, the slight difference between $C_{A,B}^2$ and $C_{A,B}$ is considered negligible in view of the radiation-related effects which have a much more pronounced effect on the solute concentration profile. These effects are: preferential sputtering, cascade mixing, radiation-enhanced diffusion, and radiation-induced segregation.

Preferential sputtering depletes the surface of solute atoms, A, at a rate which is proportional to the product of C_A^1 and S_A , the partial sputtering yield of A. For a process dominated by preferential sputtering, the surface composition is given by [19]:

$$\frac{C_A^1}{C_B^1} = \frac{C_A S_B}{C_B S_A} \quad (2)$$

Cascade mixing further acts to deplete the majority species at the surface by driving surface atoms into the bulk.

Solute atoms removed from the surface are replaced at a rate given by

$$\Omega J_A = -D_A \nabla C_A \quad (3)$$

where Ω is the atomic volume and J_A is the flux of A atoms across a plane parallel to the surface, ∇C_A is the solute concentration gradient, and D_A is the solute diffusion coefficient, given by

$$D_A = D_0 \exp(-\Delta H_{diff}/kT) \quad (4)$$

where ΔH_{diff} is the usual activation energy. Replenishment of solute atoms sputtered from the surface with atoms from the near-surface region results in an altered layer of thickness [20]

$$d \sim D_A/v \quad (5)$$

where v is the surface recession velocity. Morita, et al. [21] have determined the time required for the surface concentration to reach the steady state value given by Eq. (2):

$$\tau = \sigma_A \phi D_A / k_2 v^2 \quad (6)$$

where k_2 is a rate constant for segregation, ϕ is the ion flux and σ_A is the sputtering cross section for component A.

It should be noted that this formalism is not easy to apply since the quantity D_A is not flux-independent in a radiation environment. As a result of radiation-enhanced diffusion, the creation of mobile radiation-induced defects increases the flux of atoms diffusing along the solute concentration gradient by as much as several orders of magnitude, although the activation energy for diffusion is unchanged. Radiation-induced segregation, on the other hand, occurs when the solute atom motion is preferentially coupled to gradients in the defect concentrations. If solute-interstitial complexes are formed, the solute atoms are carried to the surface which acts as a sink for both vacancy and interstitial defects. If on the other hand, diffusion occurs by a vacancy migration process, radiation-induced segregation will act to

sweep solute atoms from the surface into the bulk. The relative values of the energies for solute migration via defects are, therefore, of extreme importance to the overall segregation behavior.

We have chosen to treat the interrelated phenomena of Gibbsian segregation, preferential sputtering, cascade mixing, radiation-enhanced diffusion and radiation-induced segregation via the Lam-Wiedersich model. We present here an outline of the model to illustrate the relevant parameters. More complete discussions are presented elsewhere [22,23]. The solid is divided into a number of layers of varying thickness; the first three layers are each one atomic layer thick. The net flux of solute atoms A between layers 1 and 2 is determined by

$$\Omega J_A = (v_A^{21} C_A C_B^1 - v_A^{12} C_A^1 C_B) \xi \quad (7)$$

where ξ is the atomic layer thickness, and

$$v_A^{12} = v_A^{21} \exp(\Delta H_{\text{seg}}/kT) \quad (8)$$

relates the inter-layer jump frequencies.

Displacement mixing is treated as a diffusion process in which the effective diffusion constants, D_A^* , D_B^* are equal and related to the nearest neighbor distance, λ , the depth-dependent DPA rate, K_0 , and the atomic mixing factor, n :

$$D_A^* = D_B^* = \lambda^2 K_0 n / 6 \quad (9)$$

Radiation-enhanced diffusion is also an activated diffusion process in which the diffusion coefficient is proportional to the defect concentration.

$$D_A = d_{AV} C_V + d_{Ai} C_i \quad (10)$$

where d_{AV} , d_{Ai} are the diffusivity coefficients for species A via vacancies and interstitials, respectively, and C_V , C_i are the vacancy and interstitial concentrations.

Radiation-induced segregation arises from a preferential coupling of the solute flux to vacancy and/or interstitial gradients:

$$J_A = -D_A \nabla C_A - C_A (d_{Ai} \nabla C_i - d_{AV} \nabla C_V). \quad (11)$$

The time dependence of solute, interstitial and vacancy concentrations, C_A , C_i , and C_V is expressed by a set of coupled differential equations [22].

It should be noted that the activation energies for vacancy and interstitial migration determine which mechanism is dominant in determining the solute flux and, as seen in Eq. 11, the two effects have opposite signs.

In general, the defect migration and formation energies are known in the pure metal but not in the alloy. Values of the heat of vacancy formation ΔH_f in copper, as determined by positron annihilation spectroscopy, range from 1.2 to 1.31 eV [24,25]. Both values have been used in the present work, as indicated in Table I. They give similar results in terms of the solute concentration profile. The value of the lithium migration energy ΔH_m in a largely copper matrix is not known and was considered as a parameter which was used to reproduce the incipient compound formation seen experimentally at temperatures

< 140°C. Other values for the vacancy and interstitial heats of formation and migration are listed in Table Ia.

RESULTS

Except as specifically noted, the results presented in this section were calculated using the parameters listed in Table I. The calculated time evolution of the solute concentration profile as a function of depth is shown in Fig. 4 for an alloy consisting of 2.6 at.% Li in Cu bombarded at 350°C. It is assumed that the sample is in thermodynamic equilibrium at $t=0$, the time that sputtering commences, and that the initial solute concentration profile corresponds to the equilibrated value given by Eq. 1 in the first atomic layer, and to the bulk concentration (2.6 at.%) everywhere else. The sample is bombarded by 3 keV Ar^+ at a flux of 3.1×10^{13} ions/cm²-s. This flux corresponds to a sputtering rate of 0.4 monolayers per second for pure copper, or roughly the sputtering rate anticipated for the limiter of a fusion reactor. The sputtering yield of copper in the alloy is taken as the value for pure copper while, for reasons to be explained below, the lithium sputtering yield is taken as 1/10 the elemental lithium value, 0.68. After only a few seconds have elapsed, the surface concentration of lithium has decreased significantly while subsurface lithium enrichment occurred within the first 50 Å. With increased sputtering time, the enriched region broadens and shifts to a greater depth. Eventually, the steady-state lithium concentration profile was obtained; the lithium concentration in the first layer increased to a large value, controlled by the sputtering yield ratio $S_{\text{Cu}}/S_{\text{Li}}$ (Eq. 2). The second layer lithium concentration is predicted to be significantly less than the first layer concentration, in accord with Eq. (1). It should be noted, however, that the formation of a compound phase, Cu_4Li occurs when the lithium

concentration exceeds ~18 at.% [27], and that the calculated profile is probably not accurate if the lithium concentration exceeds this value.

The behavior for 3 keV Ar⁺ sputtering of the first few atomic layers is shown more clearly in Fig. 5 which presents the time evolution of the lithium concentration at several selected depths. The copper and lithium sputtering yields are taken here as the elemental values. Figure 5a corresponds to a sample temperature of 350°C and Fig. 5b corresponds to sputtering at 140°C. The first three traces in Figs. 5a and 5b correspond to the lithium concentration at depths of 1, 2, and 5 atomic layers. The fourth trace corresponds to the depth at which the greatest subsurface lithium enrichment occurs at steady state, i.e., long sputtering times. This depth represents the 23rd atomic layer at 350°C and the 17th layer at 140°C. Initially, dominant radiation-induced segregation leads to a strong lithium depletion in the first layer and lithium enrichment in the subsurface peak damage region. After only 0.1 seconds of sputtering time, the second layer lithium concentration has already noticeably increased. With increasing time, the peak of the lithium-enriched region moved deeper into the bulk. Eventually, as a result of preferential sputtering the surface lithium concentration increases to the steady-state value.

This value of the first layer lithium concentration is determined by Eq. (2) and is independent of temperature. Because a larger value was assumed for the lithium sputtering yield in Fig. 5, the steady-state value of the first layer lithium concentration is smaller than the value shown in Fig. 4 (13.5% instead of 60%). Because the diffusion coefficient is temperature-dependent, the width of the Li-enriched region and maximum accumulation at a given depth vary with temperature. At low temperature the maximum subsurface concentration may be high enough to result in Cu₄Li compound precipitation. For the

calculation at 140°C, the values of ΔH_m and ΔH_f shown in Table I were chosen to show incipient precipitation at a depth of 17 atomic layers, in accord with experiment [12]. At higher temperatures (e.g. 350°C), the concentration profile broadens and the lithium concentration at a given depth decreases. In agreement with experiment, no compound precipitation is predicted at this temperature.

So far we have used two different values for the lithium partial sputtering yield without giving justification. This point is addressed here. The partial sputtering yields of alloy components are not in general equal to the values corresponding to the pure element. TRIM calculations have shown [8] that for a compound material, the composition of the immediate environment strongly affects the sputtering cross section of any given component. The calculations presented so far are not self-consistent in that the partial sputtering yields are assumed constant, although not necessarily equal to the elemental values. In the example of a thin layer of light atoms on a heavier substrate, the substrate produces a high reflectivity for the incident projectile and provides an efficient mechanism for direction of momentum away from the surface. Consequently, it is calculated that a monolayer of Li on Cu has a higher sputtering yield than pure lithium, in spite of the fact that the Li-Cu bond is stronger than the Li-Li bond. Figure 6 shows the reflection coefficient, lithium partial sputtering yield, and sputtering cross section for lithium atoms sputtered from the first atomic layer of a hypothetical structure in which successive atomic layers are filled with lithium. As the lithium layer increases in thickness, the reflection coefficient decreases. Since lithium is added, the lithium sputtering yield increases up to a thickness of two monolayers, but the sputtering cross section for lithium atoms in the first atomic layer decreases. Since the sputtered atoms all

originate in the first two atomic layers, increasing the lithium thickness beyond two layers, merely decreases the efficiency with which the projectile momentum is directed away from the surface, and the lithium sputtering yield decreases. Since we anticipate on the basis of Figs. 4 and 5 that the composition in the first few atomic layers will change drastically with time, significant variation of the sputtering yields is expected. For purposes of comparison with Fig. 5, Fig. 7 shows a self-consistent calculation using the partial sputtering yield values predicted by TRIM as the composition profile changes. The subsurface solute concentration profile is almost the same as that of Fig. 5b, but the first and second layer lithium concentrations are lower. In particular, the second layer does not show the initial increase in Li concentration.

An additional mechanism of perhaps even greater significance comes into play in a fusion environment. It is expected [26] and has been demonstrated experimentally [7,12] that a significant fraction of the lithium sputtered from the copper substrate is in the form of secondary ions. These atoms are promptly returned to the surface by the sheath potential and make no contribution to the erosion. The net effect is as if the sputtering yield had been reduced by an amount corresponding to the fraction of atoms which are sputtered as neutrals [11]. The effect on the concentration profile for bombardment of Cu-2.6 at.% Li by 500 eV deuterons is shown in Fig. 8 for assumed secondary ion fractions (β^+) of 0%, 50%, 90% and 98%. Since a high secondary ion fraction is equivalent to a low sputtering yield, the first layer lithium concentration increases with β^+ to the value determined by Eq. (1). For high secondary ion fractions, the calculated first layer lithium concentration reaches ~80%. Because of the low effective sputtering yield, lithium accumulates in the sub-surface region, forming an altered layer which becomes

increasingly broader and more lithium-enriched. Again, these results are indicative of the fundamental processes, but are not quantitatively accurate once compound precipitation occurs. According to Old and Trevena [27], lithium tends to diffuse out of a region in which Cu_4Li formation has occurred rather than accumulate to greater levels. Consequently, it is to be expected that the first and second layer lithium concentrations at steady state are higher and the subsurface concentration is lower than shown in Fig. 8.

The width of the lithium-enriched region at steady state depends not only on the charge state of the sputtered solute atoms, but also on the mass and energy of the incident projectile via the displacement profile, K_0 . Figure 9 shows the calculated DPA profiles in copper for 3 keV Ar^+ and 3 keV D^+ bombardment. Ar^+ bombardment is similar to medium mass self-sputtering in a fusion device. The anticipated impact energy is approximately $10 T_e$, where T_e is the plasma edge temperature. For light ion sputtering, the impact energy is closer to T_e . For self-sputtering, the DPA profile is peaked very near the surface. At the same energy, the DPA profile resulting from D^+ impact is much broader, although the peak damage rate is much lower per incident ion. Even at 500 eV, an energy more appropriate for light ion sputtering, the DPA profile for D^+ impact is much broader than for self-sputtering, as shown in Fig. 10a.

It is anticipated that heavy impurity atoms will strike the limiter at near-normal incidence, but for light atom sputtering, the angle of incidence will be close to 60° [28]. The resulting DPA profile will be peaked much closer to the surface as shown in Fig. 10b. This effect has not yet been incorporated into our calculations, but it is to be expected that the near surface lithium concentration will increase as a result.

Figure 11 illustrates the resulting solute concentration profiles for 3 keV Ar⁺ and D⁺ bombardment. In order to investigate the effect of the DPA profile, a higher flux ($2.3 \times 10^{15} \text{ cm}^{-2} \text{ sec}^{-1}$) has been assumed here for deuteron bombardment in order to produce the same peak DPA rate as for the argon bombardment. The sharply peaked argon DPA profile produces a region about 350 Å wide which is strongly lithium-enriched. Deuteron bombardment produces a thicker altered layer and exhibits less near-surface lithium enrichment.

Figure 12 exhibits an additional synergistic effect which is not as yet treated in a self-consistent manner. By comparison with Fig. 9a, it can be seen that the DPA profile depends strongly on the composition of the target as well as the mass and energy of the projectile. As the composition profile changes with irradiation time, the DPA profile, which affects the evolution of the solute concentration profile, also changes.

DISCUSSION AND SUMMARY

It is unlikely that first wall and limiter structures of a tokamak reactor will consist of elemental metals. Even if they were initially single component materials, plasma mixing will result in a mixture of materials -- the so-called "tokamakium" -- at the plasma interface. The sputtering properties of mixed materials may be quite different from the properties observed for any one of the components. It has been demonstrated [29], for example, that the angular distribution of light atoms sputtered from a heavy substrate is peaked strongly in the forward direction.

On the other hand, multi-component materials which are initially homogeneous will cease to be uniform in a fusion environment. The altered spatial

distribution of the components will in turn strongly affect the plasma-surface interaction that is responsible for the mixing and redistribution processes.

It has been calculated that a coating only 1-2 monolayers thick almost eliminates the sputtering of the underlying material. Such layers have been produced in the laboratory and evidence of reduced substrate sputtering has been obtained for several materials [5,30]. In the case of lithium overlayers on copper, experiments indicate that substantially complete layers may be maintained during 3 keV Ar⁺ sputtering at a flux of 70 $\mu\text{A}/\text{cm}^2$ and temperatures greater than 260°C. In the presence of electric and magnetic field conditions expected to prevail in a fusion environment, the minimum temperature is lowered to < 140°C.

Calculations carried out in an attempt to understand the experimental results show an initial solute depletion in the first few atom layers and an enrichment in the subsurface region, as a consequence of radiation-induced segregation, and an eventual increase in the near-surface concentrations toward steady state. The steady state value of the first layer concentration is determined by the preferential sputtering process. However, changes in the effective partial sputtering yields, as a result of the altered near-surface composition profile, the inhibition of lithium erosion associated with a high secondary ion fraction and the effect of the sheath potential, strongly alter first layer solute concentration and the steady-state composition profile.

The experimentally observed increase in the apparent steady-state-surface lithium concentration as the temperature is raised is not predicted by the calculation. However, the calculation is based on the assumption of a solid solution. At high lithium concentrations, the formation of the Cu₄Li phase renders this assumption invalid. The probable effect of compound formation

would be to broaden the lithium-enriched region and raise the lithium surface concentration.

The displacement profile plays a key role in determining the solute concentration profile via radiation-induced segregation. The DPA profile, however, is strongly sensitive to the mass, kinetic energy, angle of incidence of the projectile, and the solute concentration profile.

The treatment used here has been only partly self-consistent but suffices to demonstrate a variety of synergistic effects in the sputtering of alloys in a fusion environment. Some of these effects will no doubt represent problems in the design of future fusion reactors, while others may present opportunities for the creation of self-sustaining coatings which are tailored to requirements of fusion reactor operation.

TABLE Ia: INPUT PARAMETERS

FIGURE	4,11a	5a	5b	7	8	11b
Li bulk conc. (at. fraction)	.026	.026	.026	.026	.026	.026
Temperature (°C)	350	350	140	140	140	350
Projectile	Ar	Ar	Ar	Ar	D	D
Impact Energy (eV)	3000	3000	3000	3000	500	3000
Flux (ions/cm ² -sec)	3.1×10^{13}	3.1×10^{13}	3.1×10^{13}	3.1×10^{13}	1.1×10^{16}	2.3×10^{15}
Peak Damage Rate (DPA/sec)	.075	.075	.075	.075	1.0	.075
ΔH_{seg} (eV)	-.65	-.65	-.65	-.65	-.65	-.65
Cu ΔH_V^f (eV)	1.20	1.31	1.31	1.20	1.20	1.20
Cu ΔH_i^f (eV)	3.34	3.34	3.34	3.34	3.34	3.34
Cu ΔH_V^m (eV)	0.82	0.76	0.76	0.82	0.82	0.82
Cu ΔH_i^m (eV)	0.12	0.12	0.12	0.12	0.12	0.12
Li ΔH_V^f (eV)	0.85	0.34	0.34	0.72	0.85	0.85
Li ΔH_V^m (eV)	0.70	0.67	0.67	0.59	0.70	0.70
Li ΔH_i^m (eV)	0.12	0.12	0.12	0.12	0.12	0.12
C_V	1.7×10^{-9}	3.1×10^{-10}	3.4×10^{-17}	2.4×10^{-14}	2.2×10^{-14}	1.7×10^{-9}
C_i	8.8×10^{-28}	1.7×10^{-18}	2.0×10^{-30}	1.6×10^{-41}	1.6×10^{-41}	8.8×10^{-28}
v^{av} (sec ⁻¹)	8.0×10^7	1.9×10^8	4.5×10^4	2.3×10^6	1.1×10^5	8.0×10^7
v^{ai} (sec ⁻¹)	5.7×10^{11}	5.4×10^{11}	1.2×10^{11}	1.9×10^{11}	1.9×10^{11}	5.7×10^{11}
v^{bv} (sec ⁻¹)	8.7×10^6	3.6×10^7	2.8×10^3	3.7×10^3	3.7×10^3	8.7×10^6
v^{bi} (sec ⁻¹)	5.7×10^{11}	5.4×10^{11}	1.2×10^{11}	1.9×10^{11}	1.9×10^{11}	5.7×10^{11}

TABLE Ib: OUTPUT VALUES

FIGURE	4,11a	5a	5b	7	8 ($\beta^+ = .98$)	11b
Li yield* S_{Li}	0.68	0.68	0.68	2.44	0.68	0.68
Cy yield* S_{Cu}	3.98	3.98	3.98	4.05	3.98	3.98
C_a^1 (steady state)	0.59	0.135	0.135	0.04	0.77	0.143
C_a^2 (steady state)	0.30	0.030	0.027	0.0030	0.38	0.0016
C_a^{max} subsurface (steady state)	0.66	0.115	0.17	0.21	0.91	0.086

* $S_{Li,Cu} = Y_{Li,Cu} / C_{Li,Cu}^1$, where $Y_{Li,Cu}$ is the number of sputtered atoms per incident ion.

REFERENCES

1. C. C. Boley, J. N. Brooks, and Y. Kim. Argonne National Laboratory Fusion Power Report ANL-FPP-TM-171 (1983).
2. U. Cecchi, Proc. 6th Intl. Conf. on Plasma-Surface Interactions, May 14-18, 1984, Nagoya, Japan, J. Nucl. Mater. (in press).
3. J. Brooks and M. Kaminsky, Proc. 5th Intl. Conf. on Solid Surfaces. Sept. 26 - Oct. 1, 1983, Madrid, Spain, J. Nucl. Mater. (in press).
4. A. R. Krauss and D. M. Gruen, J. Nucl. Mater. 85 & 86 (1979) 1179.
L. E. Rehn, P. R. Okamoto, D. I. Potter, and H. Wiedersich, *ibid*, p.1139,
5. A. R. Krauss, D. M. Gruen, and A. B. DeWald, Proc. Symp. on Energy Removal and Particle Control in Fusion Devices, Princeton NJ, July 26-29, 1983, J. Nucl. Mater., 121 (1984) 398.
6. Argonne National Laboratory Fusion Power Report ANL/CTR/TM-47.
7. A. R. Krauss, D. M. Gruen, N. Q. Lam and A. B. DeWald, Proc. 6th Intl. Conf. on Plasma-Surface Interactions, Nagoya, Japan, May 14-18, 1984, J. Nucl. Mater. (in press).
8. D. M. Gruen, A. R. Krauss and M. J. Pellin, Proc. Workshop on Synergistic Effects in Surface Phenomena Related to Plasma-Wall Interactions, Nagoya, May 21-23, 1984 (to be pub. in Radiation Effects).
9. A. R. Krauss and D. M. Gruen, J. Nucl. Mater. 93 & 94 (1980), 686.
10. A. R. Krauss and D. M. Gruen, J. Nucl. Mater. 103 & 104 (1981), 239.
11. A. B. DeWald, J. N. Davidson, A. R. Krauss and D. M. Gruen, J. Nucl. Mater. 111 & 112 (1982), 448.
12. A. R. Krauss, D. M. Gruen, and M. Venugopalan, Proc. 3rd Conf. on Fusion Reactor Materials, Sept 19-22, 1983, Albuquerque, NM, J. Nucl. Mater. 122 & 123 (1984) 1425.

13. J. W. Gibbs, Trans. Connecticut Acad. Sci. 3 (1875/76) 108.
14. M. L. Tarng and G. K. Wehner, J. Appl. Phys. 42 (1971) 2449.
15. P. Wynblatt and R. C. Ku, Surf. Sci. 65 (1977) 511.
16. A. R. Miedema, Z. Metallkund 69 (1978) 455.
17. J. R. Chelikowsky, Surf. Sci. Lett. 139 (1984) L197.
18. F. L. Williams and D. Nason, Surf. Sci. 45 (1974) 377.
19. H. Wiedersich, H. H. Andersen, N. Q. Lam, H. W. Pickering, and L. E. Rehn in Surface Modification and Alloying, J. M. Poate and G. Foti, eds., Plenum, NY (1983).
20. N. Itoh and K. Morita, Rad. Eff. 80 (1984) 163.
21. K. Morita, H. Ohno, M. Takami, and N. Itoh, Proc. Workshop on Synergistic Effects in Surface Phenomena Related to Plasma-Wall Interactions, Nagoya, May 21-23, 1984.
22. N. Q. Lam and H. Wiedersich, J. Nucl. Mater. 103 & 104 (1981) 433.
23. N. Q. Lam and H. Wiedersich, Rad. Eff. Lett. 67 (1982) 107.
24. R. W. Siegel in Positron Annihilation, P. G. Coleman, S. C. Sharma, and L. M. Diana, eds., North Holland (1982).
25. J. L. Campbell, C. W. Schulte, and R. R. Gingerich, J. Nucl. Mater. 69 & 70 (1978) 609.
26. S. K. Allison and M. Kamegai, Rev. Sci. Inst. 32 (1961) 1090.
27. C. F. Old & P. Trevena, Metal Sci. 15 (1981) 281.
28. R. Chodura, J. Nucl. Mater. 111 & 112 (1982) 420 and A. B. DeWald, A. W. Bailey, and J. Brooks (in preparation).
29. S. Ichimura, H. Shimizu, H. Murakami, and Y. Ishida, Proc. 6th Intl. Conf. on Plasma-Surface Interactions, Nagoya, May 14-18, 1984 (submitted to J. Nucl. Mater.).

30. R. Behrisch, J. Roth, J. Bohdanský, A. P. Martinelli, B. Schweer, D. Rusbüldt, and E. Hintz, *J. Nucl. Mater.* 93 & 94 (1980) 645.
31. W. Klemm and B. Volavsek, *Z. Anorg. Allg. Chemie.* 296 (1958) 184.

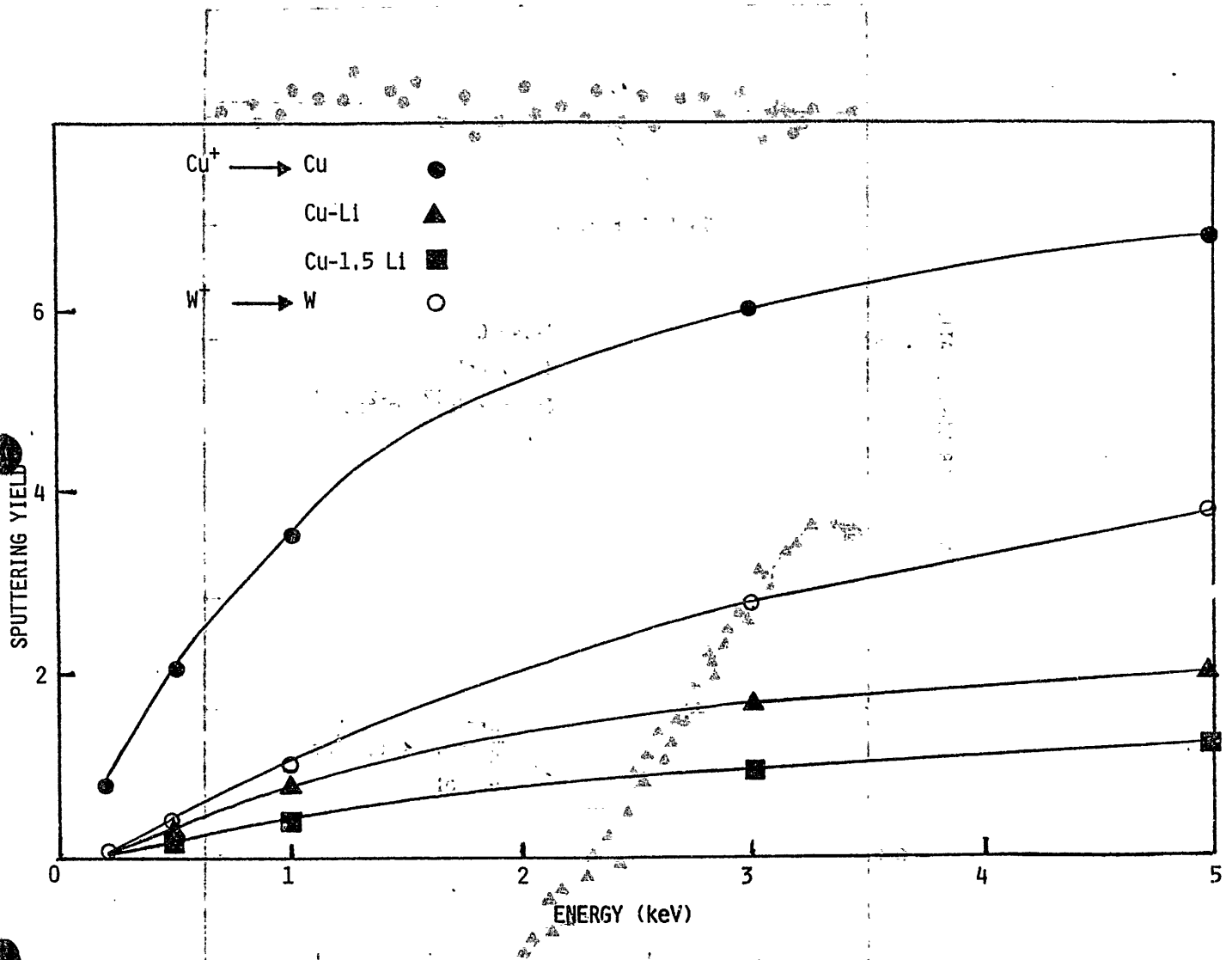


Fig. 1. Self-sputtering yields for W^+ incident on W. (O) and Cu^+ incident on Cu (●), Cu + 1 monolayer Li (▲), and Cu + 1.5 monolayers Li (■). The atomic radius of Li is taken to be the same as that of Cu, in accord with the X-ray diffraction data of Klemm and Volavsek [31].

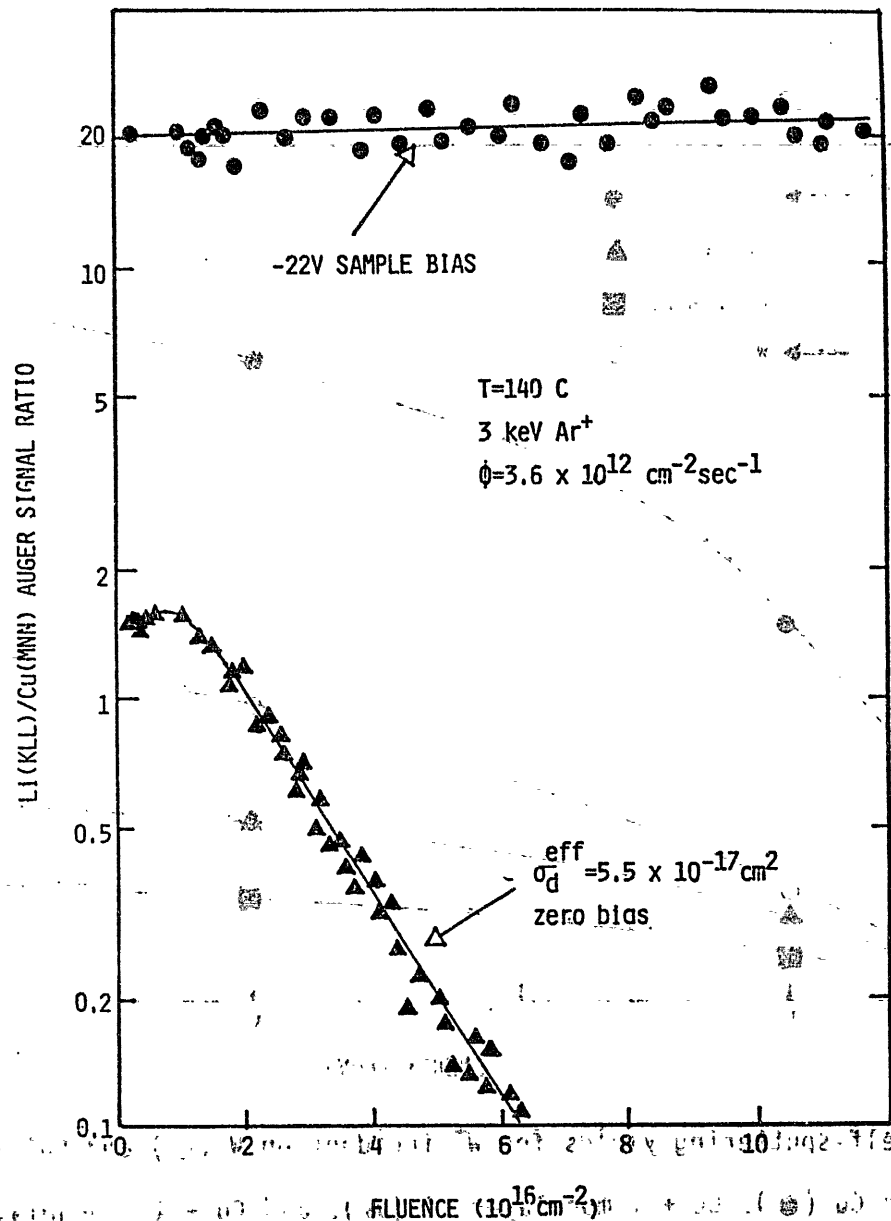


Fig. 12. Experimental measurement of Li(KLL)/Cu(MNN) Auger signal ratio at 140°C vs. fluence during sputtering by 3 keV Ar⁺ at a flux of 3.6 x 10¹² ions/cm²-sec. The two traces represent the effective desorption cross section for sputtering in a field-free (▲) and non-field-free (●) environment. The latter trace demonstrates the maintenance of a lithium overlayer under reactor-like conditions.

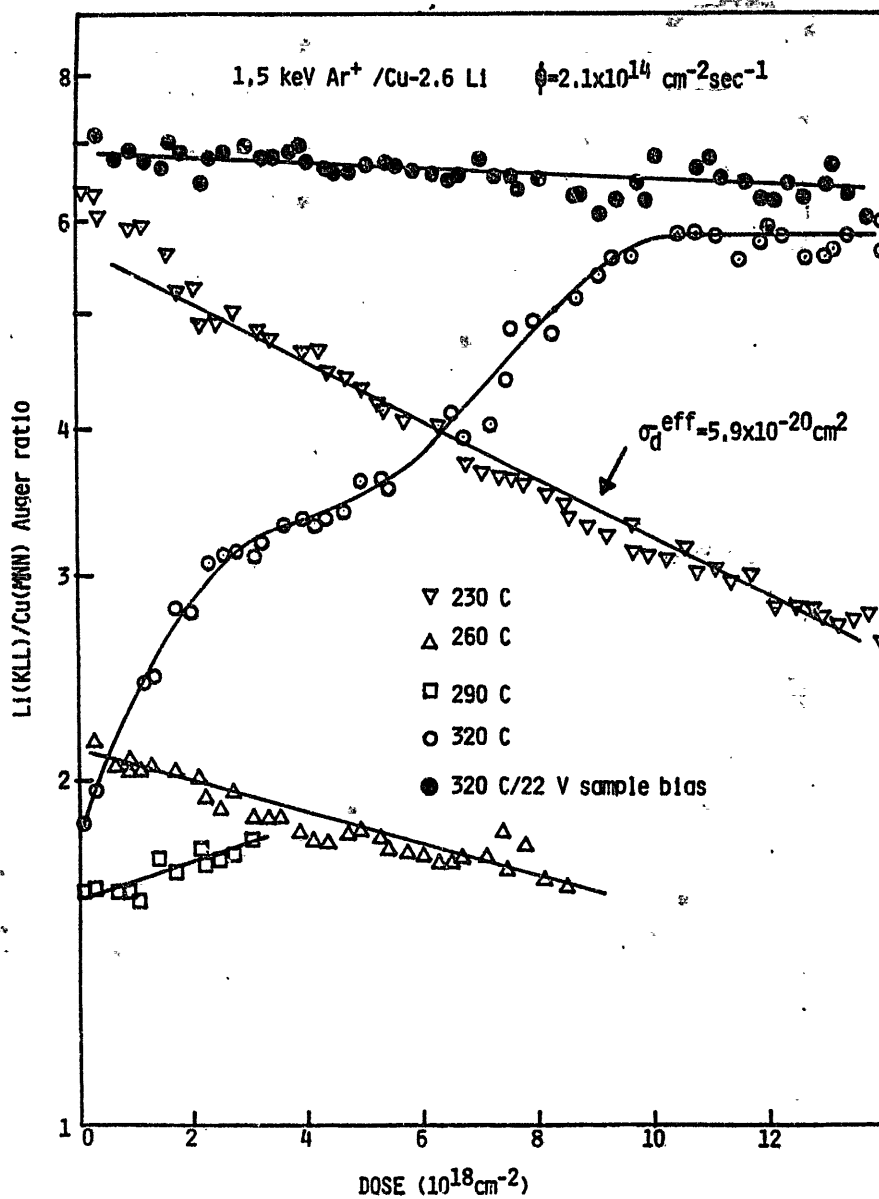


Fig 3. Experimental measurement of Li(KLL)/Cu(MNN) Auger signal ratio at temperatures of 190°C, 230°C, 260°C, 290°C, and 320°C vs. fluence during sputtering by 3 keV Ar⁺ at a flux of 3.1×10^{13} ions/cm²-sec. The data for 320°C show a strong reduction in the lithium depletion rate when a 22 V potential is applied to the sample.

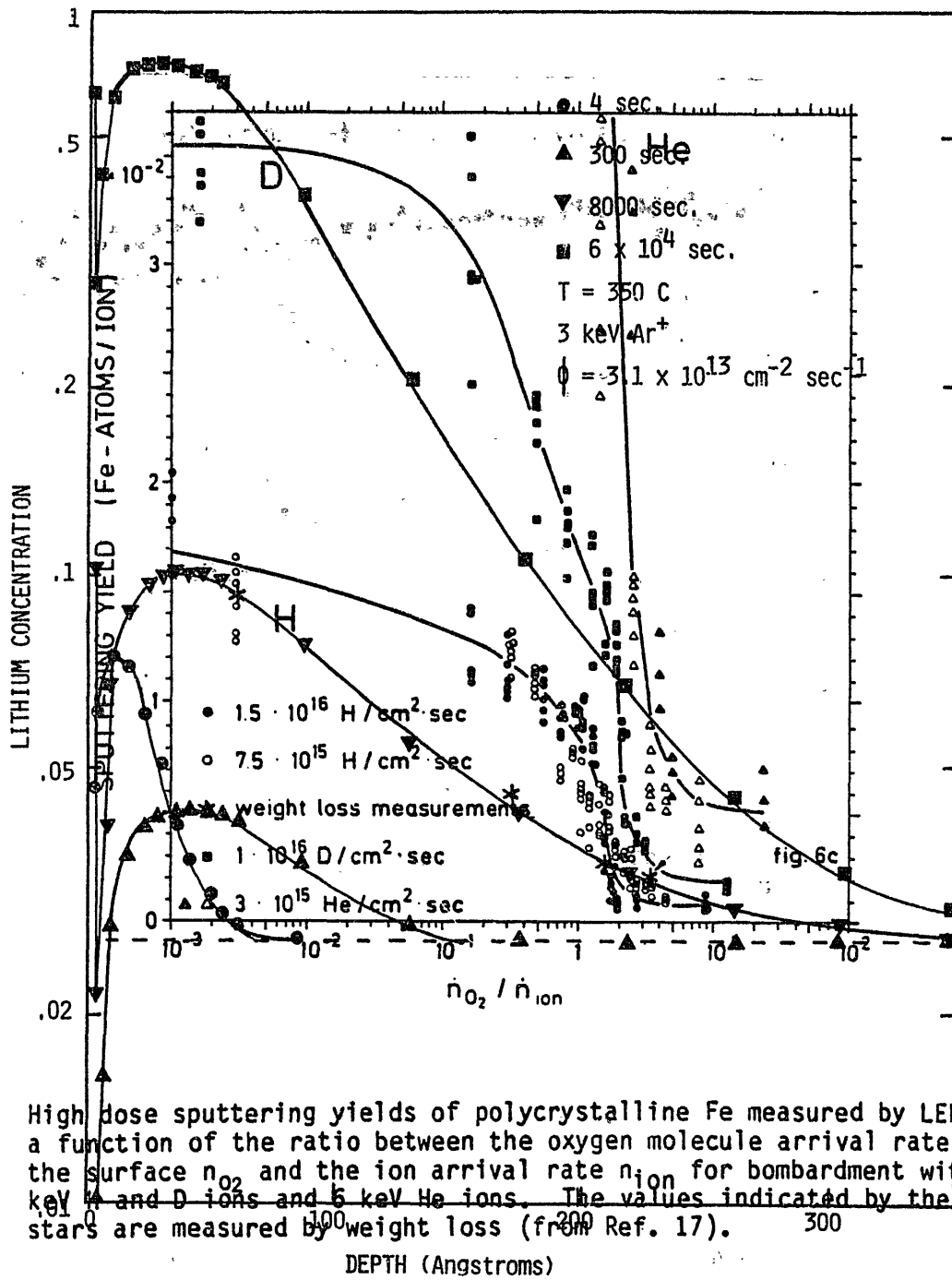


Fig. 1. High dose sputtering yields of polycrystalline Fe measured by LEIS as a function of the ratio between the oxygen molecule arrival rate on the surface n_{O_2} and the ion arrival rate n_{ion} for bombardment with 2 keV H and D ions and 6 keV He ions. The values indicated by the stars are measured by weight loss (from Ref. 17).

Fig. 4. Solute concentration profile as a function of time for 3 keV Ar⁺ bombardment of Cu-2.6 at.% Li. The first layer and subsurface region are Li enriched, but the second atomic layer is lithium depleted.

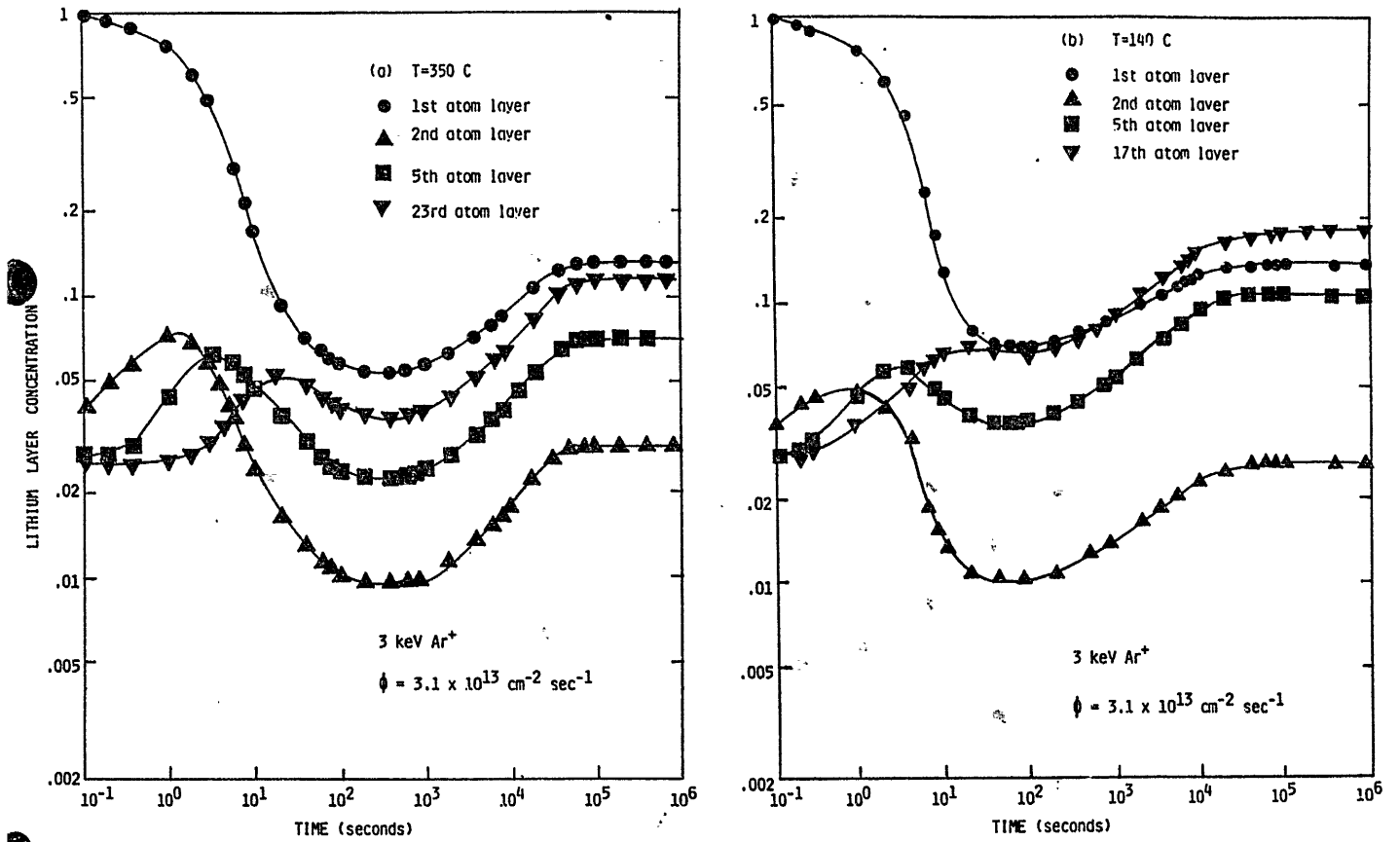


Fig. 5. Time evolution of solute concentration at various depths for 3 keV Ar⁺ bombardment of Cu-2.6 at.% Li at 350°C (5a) and 140°C (5b). Elemental values were used for Cu and Li partial sputtering yields.

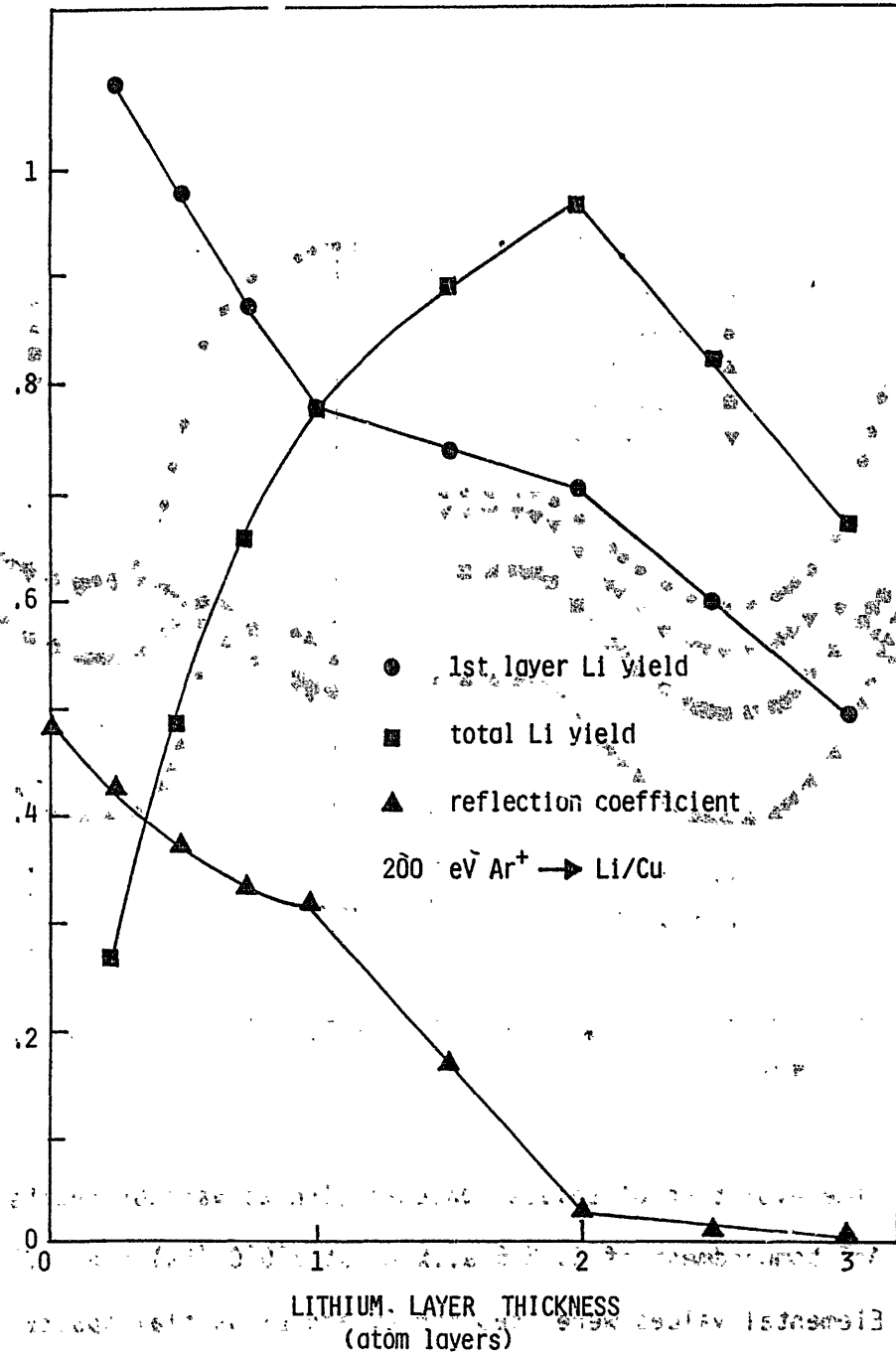


Fig. 6. Reflection coefficient (▲), Li partial sputtering yield for the first atomic layer (●), and total Li sputtering yield (■) as a function of lithium layer thickness for 200 eV Ar⁺ incident on Cu with a Li overlayer.

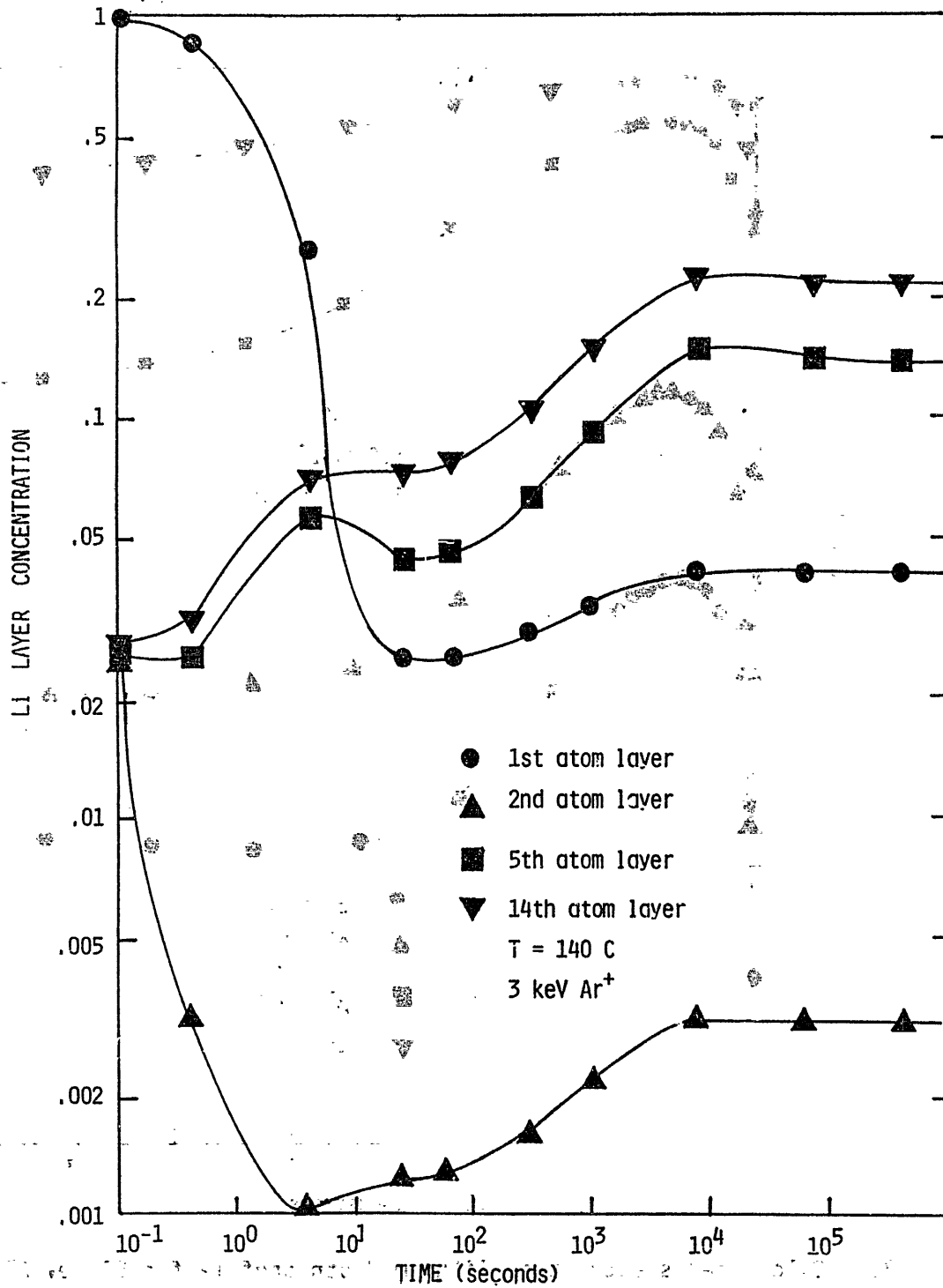


Fig. 7. Time evolution of solute concentration at various depths for 3 keV Ar⁺ bombardment of Cu-2.6 at.% Li at 140°C. Copper and lithium self-sputtering yields were calculated self-consistently by TRIM. The resulting concentration values in the first and second atomic layers are lower than found in Fig. 5.

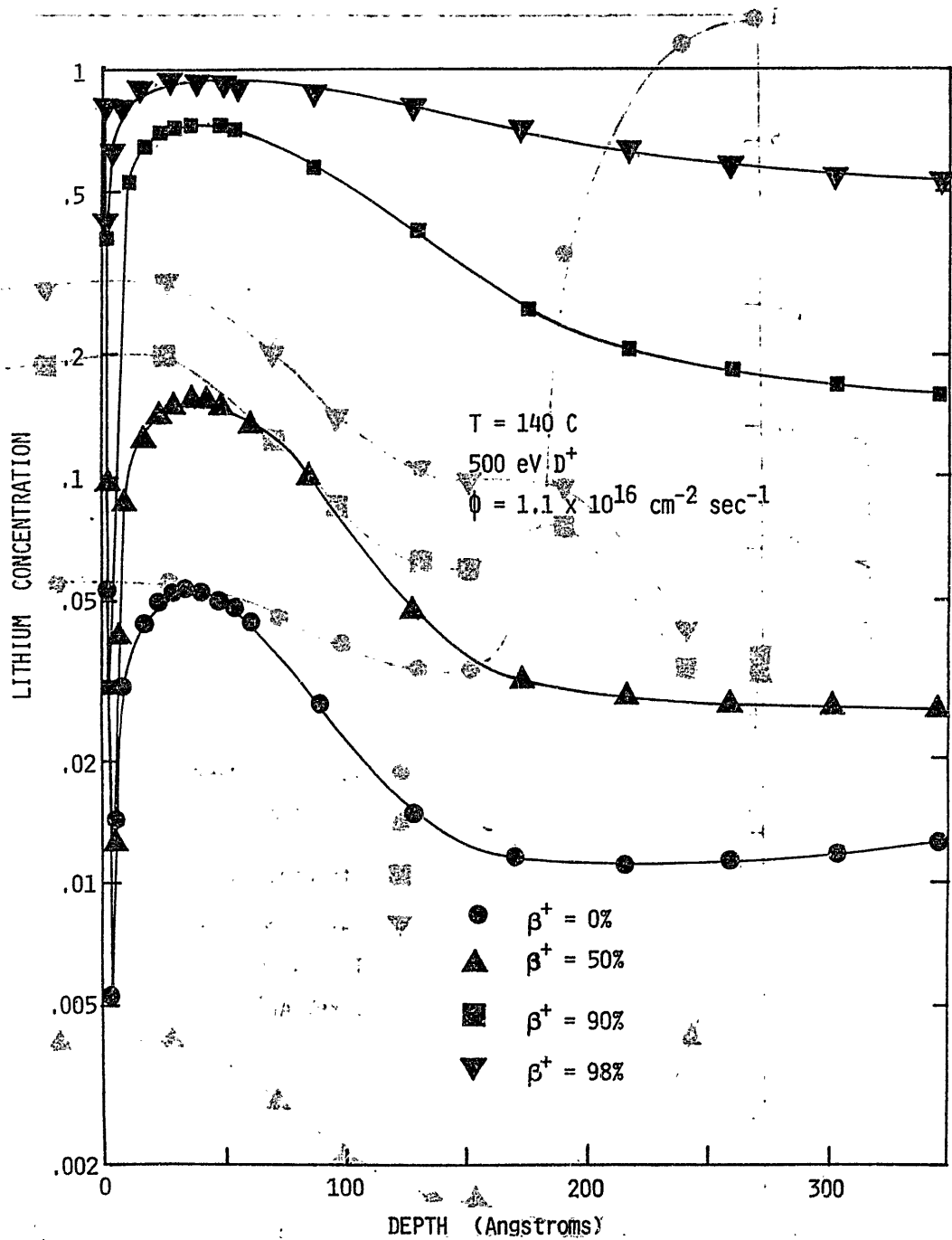


Fig. 8. Calculated steady state lithium depth profile for 500 eV D^+ bombardment of Cu-2.6 at.% Li, assuming values of 0, 0.5, 0.9, and 0.98 for the secondary ion fraction of the sputtered lithium atoms. As the secondary ion fraction increases, the subsurface lithium concentration increases and the Li-enriched region broadens.

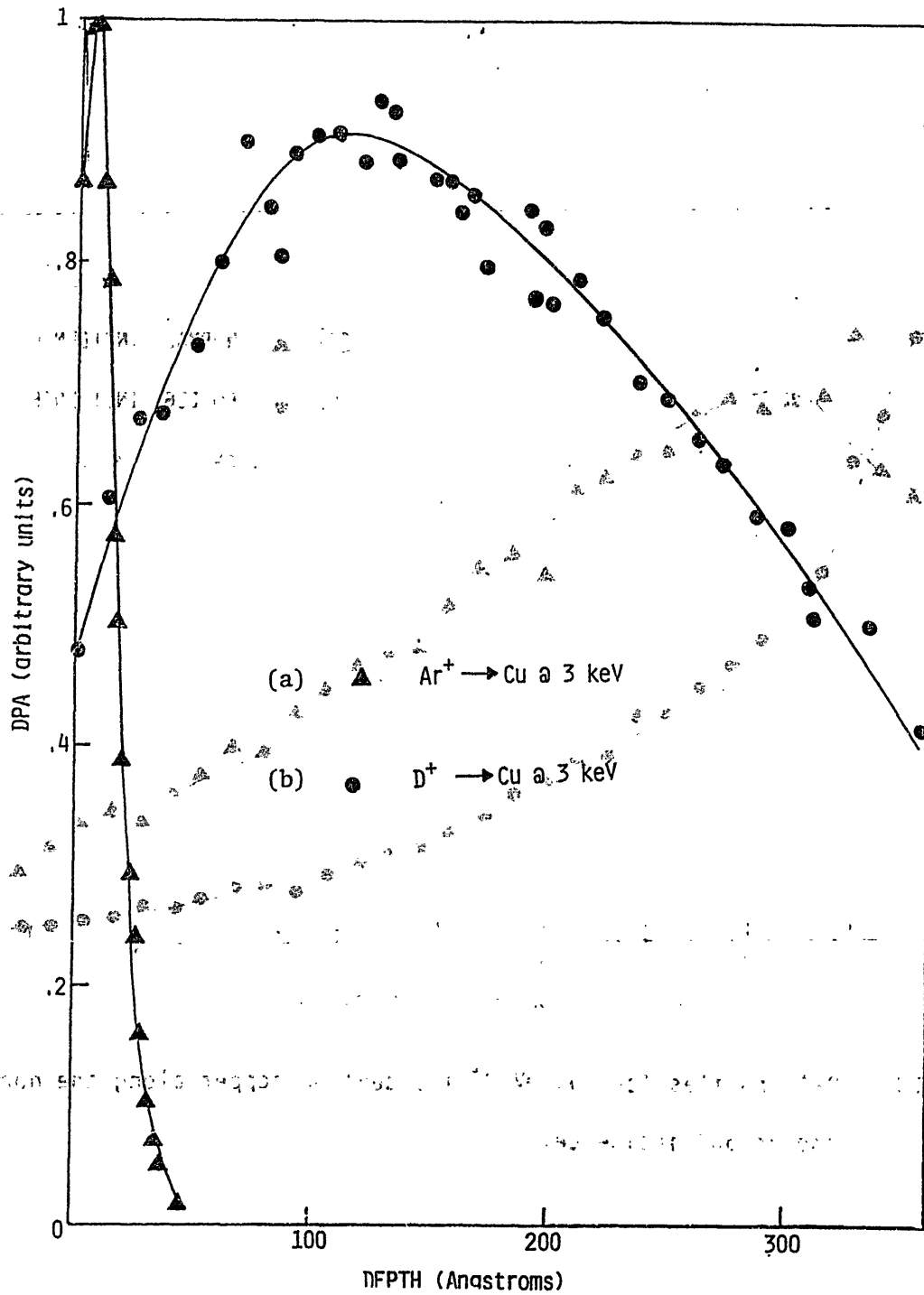


Fig. 9. DPA profiles for 3 keV Ar⁺ (9a) and D⁺ (9b) bombardment of Cu.

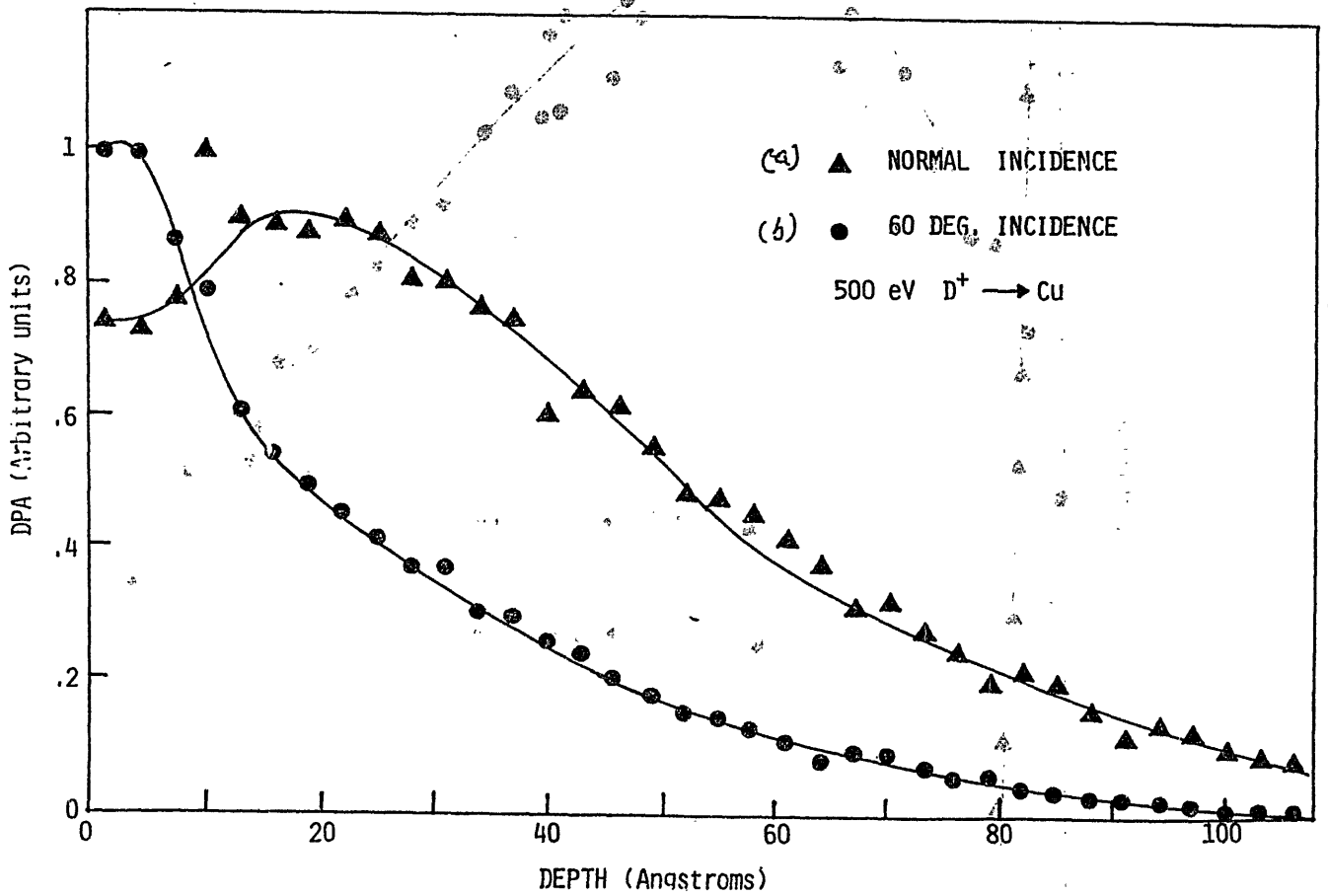


Fig. 10. DPA profiles for 500 eV D⁺ incident on copper along the normal (0°) and at 60° incidence.

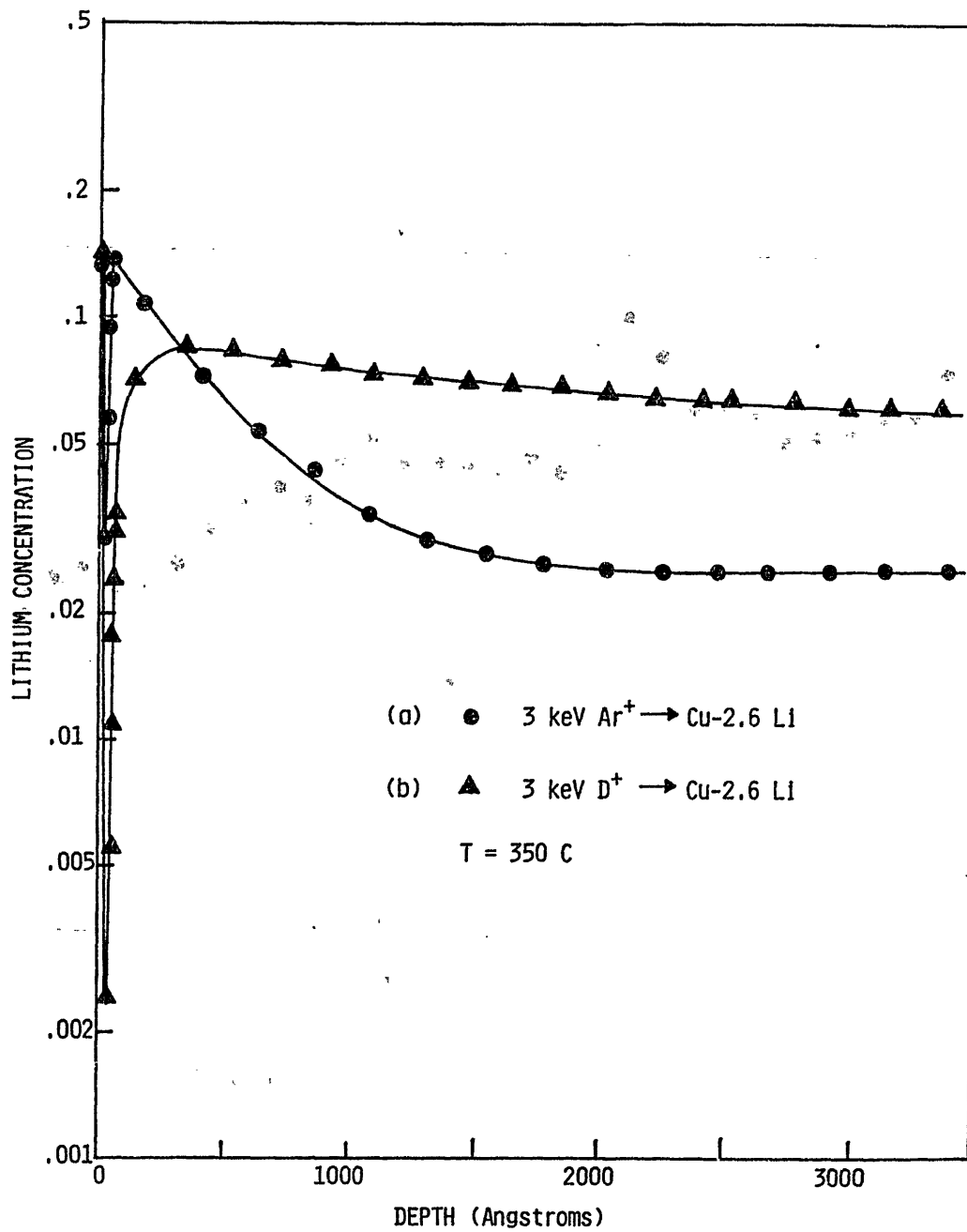


Fig. 11. Lithium concentration profiles corresponding to Figs. 9a and 9b.

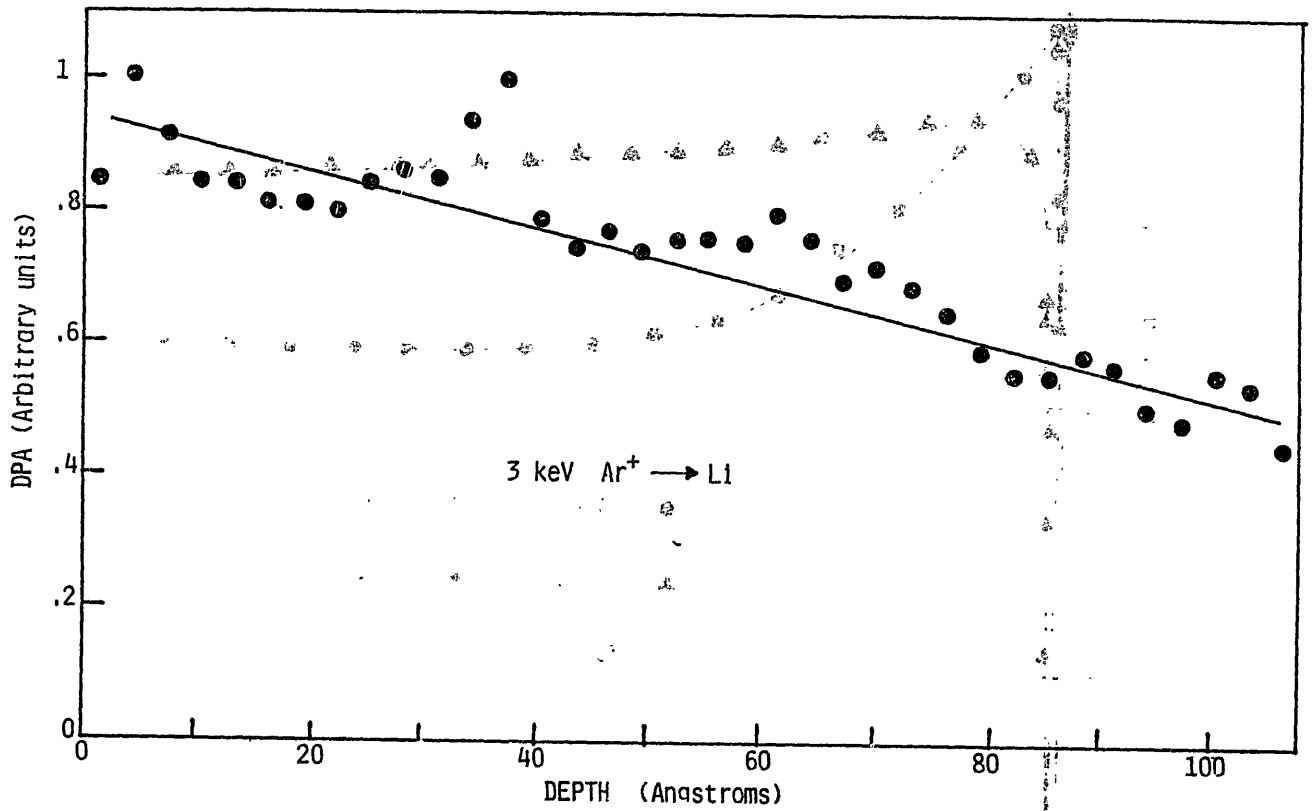


Fig. 12 DPA profile for 3 keV Ar⁺ bombardment of Li.

PROGRAM OF THE WORKSHOP
ON
SYNERGISTIC EFFECTS IN SURFACE PHENOMENA
RELATED TO PLASMA-WALL INTERACTIONS

May 21-23, 1984,
Auditorium, IPP, Nagoya University

Monday, 21. May

- 9:00- 9:20 Registration
- 9:20- 9:30 Opening
- 9:30-12:30 Morning Session: Synergistic Effects in Fusion Machine
(R. A. Langley, Chairman)
- Review talk: R. Behrisch, Synergistic Effects in
Plasma Surface Interaction
- 14:00-17:30 Afternoon Session: Synergisms on Hydrogen Recycling
(S. Imoto, Chairman)
- Review talk: B. L. Doyle, Theory of Steady State
Hydrogen Transport in Solids
- Review talk: F. Waelbroeck, Synergisms Involving
Hydrogen Recycling
- 18:00-20:00 Party

Tuesday, 22. May

- 9:00-12:30 Morning Session: Synergisms on Surface Erosion
(J. Bohdanský, Chairman)
- Review talk: O. Auciello, Synergisms in Materials
Erosion Due to Multispecies Impact
- Review talk: A. R. Krauss, Synergistic Sputtering
Properties of Binary Alloys
- 14:00-17:30 Afternoon Session: Desorption and Surface Composition
(W. O. Hofer, Chairman)
- Review talk: D. M. Gruen, Effect of Surface Coverage
and Composition on Desorption and
Related Phenomena

Wednesday, 23. May

- 9:00-12:00 Morning Session: Summary
(C. Ferro and K. Kamada, Co-Chairman)
- Summary talks: R. A. Langley, S. Imoto, J. Bohdanský,
W. O. Hofer

List of Participants

Auciello, O.
Institute of Aerospace Studies
University of Toronto
4925 Dufferin Street Downsview Ontario M3H 5T6, Canada

Bauder, U.H.
Institut fuer Grundlagen der Elektrotechnik
Techn. Universitaet Muenchen
Arcisstr. 21, 8000 Muenchen 2, FRG

Behrisch, R.
Max-Planck-Institut
fuer Plasmaphysik
D-8046 Garching Muenchen, FRG

Betz, G.
Institut fuer Allgemeine Physik
Technische Universitaet Vienna
A-1040 Vienna Karlsplatz 13, Austria

Bohdansky, J.
Max-Planck-Institut
fuer Plasmaphysik
D-8046 Garching, FRG

Brooks, J.N.
Fusion Power Program
Argonne National Lab.
9700 South Cass Avenue, Argonne, Ill. 60439, USA

Budny, R.
Plasma Physics Laboratory
Princeton University
Princeton, NJ 08544, USA

Cohen, S.A.
Plasma Physics Lab.
Princeton University
P.O. Box 451 Princeton, NJ 08544, USA

Downing, J.N.
Los Alamos National Lab.
P.O. Box 1663
M.S. K 303, Los Alamos, New Mexico 87545, USA

Doyle, B.L.
Sandia National Lab.
P.O. Box 5800
Albuquerque, NM 87185, USA

Dylla, H.F.
Plasma Physics Lab.
Princeton University
P.O. Box 451, Princeton, NJ 08544, USA

Ertl, K.
Max-Planck-Institut
fuer Plasmaphysik
D-8046 Garching, FRG

Eshita, T.
Department of Engineering
Nagoya University
Nagoya 464, Japan

Ferro, C.
Associazione EURATOM-ENEA Sulla Fusion-Centro
Ricerche Energia Frascati
C.P.65-00044 Frascati, Rome, Italy

Franconi, E.
Associazione EURATOM-ENEA Sulla Fusion-Centro
Ricerche Energia Frascati
C.P.65-00044 Frascati, Rome, Italy

Furuyama, Y.
Dept. Nuclear Engineering
Osaka University
Osaka 565, Japan

Grosman, A.
Association EURATOM-CEA sur la Fusion
Boite Postale n 6
Fontenay-aux-Roses, France

Gruen, D.M.
Fusion Power Program, Argonne National Laboratory
9700 South Cass Avenue, Argonne,
Illinois 60439, USA

Haasz, A.A.
Institute of Aerospace
University of Toronto
4925 Dufferin Street, Downsview, Ontario M3H 5T6, Canada

Hamamoto, M.
Department of Energy Engineering
Oita University
Oita 870-11, Japan

Hasuyama, H.
Dept. of Energy Conversion Engineering,
Kyushu University
6-1, Kasuga-Koen, Kasuga-shi, Fukuoka 816, Japan

Hofer, W.O.
Institut fuer Grenzflaechen und
Vakuumphysik der Kernforschung, Juelich GMBH
Postfach 1913, D-5170 Juelich, FRG

Hopkins, G.R.
GA Technologies, Inc.,
P.O.Box 81608
San Diego, CA 92138, USA

Horino, Y.
Department of Engineering
Nagoya University
Nagoya 464, Japan

Hsu, W.L.
Sandia National Laboratories
Livermore
California 94550, USA

Husinsky, W.
Institut fuer Allgemeine Physik
Technischen Universitaet Wien
A-1040 Wien, Karlsplatz 13, Austria

Ichimura, S.
Electro Technical Laboratory
Sakura-mura
Ibaraki 305, Japan

Imoto, S.
Faculty of Engineering
Osaka University
Osaka 565, Japan

Itoh, N.
Department of Crystalline Materials Science
Nagoya University
Nagoya 464, Japan

Kamada, K.
Institute of Plasma Physics
Nagoya University
Nagoya 464, Japan

Katiyar, V.K.
Department of Mathematics
University of Roorkee
Roorkee-247667, U.P., India

Krauss, A.R.
Materials Science and Technology Division
Argonne National Lab.
Argonne, Il. 60439, USA

Langley, R.A.
Fusion Energy Division
Oak Ridge National Lab.
P.O.Box Y, Oak Ridge, TN37830, USA

Li, Z.G.
Southwestern Institute Physics
P.O. Box 15
Leshan, Sichuan, The People[s Republic of China

Manos, D.M.
Plasma Physics Lab.
Princeton University
P.O.Box 451, Princeton, NJ 08544, USA

Maruse, S.
Department of Electronic Engineering
Nagoya University
Nagoya 464, Japan

Matsunami, N.
Department of Nuclear Engineering
Nagoya University
Nagoya 464, Japan

McCracken, G.M.
UKAEA
Culham lab.
Abingdon, Oxon OX 14 3DB, UK

Miyahara,A.
Institute of Plasma Physics
Nagoya University
Nagoya 464, Japan

Miyake,M.
Department of Nuclear Engineering
Osaka University
Suita 565, Japan

Morita,K.
Department of Crystalline Materials Science
Nagoya University
Nagoya 464, Japan

Mosser,A.
Laboratoire de Cristallographie
E.R.A. 7 du C.N.R.S.
4, rue Blaise Pascal, 67000 Strasbourg, France

Muraoka,K.
Department of Energy Conversion
Kyushu University
Fukuoka 816, Japan

Nagai,S.
Osaka Laboratory for Radiation Chemistry,
JAERI
Osaka 572, Japan

Nagata,S.
Department of Nuclear Engineering
Tohoku University
Sendai 980, Japan

Namba,T.
Department of Nuclear Engineering
University of Tokyo
Tokyo 113, Japan

Nishikawa,M.
Mitsubishi Atomic Power Industries Inc.
4-1 Shibakoen 2
Minato-ku Tokyo 104, Japan

Ohno,K.
Department of Engineering
Nagoya University
Nagoya 464, Japan

Okada,M.
National Research Institute
for Metals
Ibaraki 305, Japan

Oku,T.
Department of Engineering
Nagoya University
Nagoya 464, Japan

Petravic,M.
Plasma Physics Lab.
Princeton University
P.O. Box 451, Princeton, NJ 08544, USA

Roberto, J.B.
Oak Ridge National Lab.
P.O. Box Y
Oak Ridge, TN 37830, USA

Roosendaal, H.E.
North-Holland Physics Publishing Co.
P.O. Box 103, 1000 AC
Amsterdam, Netherland

Roth, J.
Max-Planck-Institut fuer Plasmaphysik
D-8046
Garching, FRG

Sagara, A.
Institute of Plasma Physics
Nagoya university
Nagoya 464, Japan

Saidoh, M.
Japan Atomic Energy Research Institute
Tokai-mura
Ibaraki 319-11, Japan

Sakai, H.
RIKEN
The Institute of Physical and Chemical Research
Wako-shi 351, Japan

Sato, Kentaro
Miyagi National College of Technology
Natori
Miyagi 981-12, Japan

Sestaro, A.
Association EURATOM-ENEA
CRE Frascati
C.P. 65, 00044 Frascati, Rome, Italy

Shikama, T.
National Research Institute
for Metals
Ibaraki 305, Japan

Shimizu, H.
Electrotechnical Laboratory
Sakura-mura
Ibaraki 305, Japan

Shimizu, R.
Department of Applied Physics
Osaka University
Osaka 565, Japan

Stangeby, P.C.
University of Toronto
Institute of Aerospace Studies
4925 Dufferin Street, Downsview, Ontario M3H 5T6, Canada

Sugisaki, M.
Department of Nuclear Engineering
Kyushu University
Fukuoka 812, Japan

Sukenobu,S.
Energy Science and Technology Lab.
Toshiba R & D Center
Kawasaki 210, Japan

Taglauer,E.
Max-Planck-Institut
fuer Plasmaphysik
D-8046 Garching,FRG

Tanabe,T.
Faculty of Engineering
Osaka University
Osaka 565, Japan

Tawara,H.
Institute of Plasma Physics
Nagoya University
Nagoys 464, Japan

Terreault,B.
Universite du Quebec
Centre de L'Energie INRS
CP 1020, Verannes Quebec J0L 2p0,Canada

Tomita,M.
Dept. Nuclear Engineering
Kyoto Unuversity
Kyoto 606, Japan

Vernickel,H.
Max-Planck-Institut fuer
Plasmaphysik
D-8046 Garching,FRG

Vietzke,E.
Nuclear Research Center
Institut fuer Plasmaphysik Kernforschung
Juelich GMBH, Postfach 1913 D-5170 Juelich,FRG

Waelbroeck,F.
Institut fuer Plasmaphysik Kernforschung
Juelich GMBH
Postfach 1913 D-5170 Juelich,FRG

Winter,J.
Institut fuer Plasmaphysik Kernforschung
Juelich GMBH
Postfach 1913 D-5170 Jue'lich,FRG

Yamada,R.
Japan Atomic Energy Research Institute
Tokai-mura
Ibaraki 319-11,Japan

Yamaguchi,S.
Dept. Nuclear Engineering
Tohoku University
Sendai 980, Japan

Yamamura, Y.
Applied Physics Department
Okayama University of Science
Okayama 700, Japan

Yamanaka, S.
Department of Nuclear Engineering
Osaka University
Osaka 565, Japan

Yamashita, K.
Institute of Inorganic Chemistry
University of Zurich
8057 Zurich, Switzerland

Yamawaki, M.
Faculty of Engineering
University of Tokyo
Tokyo 113, Japan

Zhu, Y.
Southwestern Institute of Physics
P.O. Box 15 Leshan
Sichuan, The People's Republic of China

LIST OF IPPJ-AM REPORTS

- IPPJ-AM-1* "Cross Sections for Charge Transfer of Hydrogen Beams in Gases and Vapors in the Energy Range 10 eV–10 keV"
H. Tawara (1977) [Published in Atomic Data and Nuclear Data Tables 22, 491 (1978)]
- IPPJ-AM-2* "Ionization and Excitation of Ions by Electron Impact –Review of Empirical Formulae–"
T. Kato (1977)
- IPPJ-AM-3 "Grotrian Diagrams of Highly Ionized Iron FeVIII-FeXXVI"
K. Mori, M. Otsuka and T. Kato (1977) [Published in Atomic Data and Nuclear Data Tables 23, 196 (1979)]
- IPPJ-AM-4 "Atomic Processes in Hot Plasmas and X-Ray Emission"
T. Kato (1978)
- IPPJ-AM-5* "Charge Transfer between a Proton and a Heavy Metal Atom"
S. Hiraide, Y. Kigoshi and M. Matsuzawa (1978)
- IPPJ-AM-6* "Free-Free Transition in a Plasma –Review of Cross Sections and Spectra–"
T. Kato and H. Narumi (1978)
- IPPJ-AM-7* "Bibliography on Electron Collisions with Atomic Positive Ions: 1940 Through 1977"
K. Takayanagi and T. Iwai (1978)
- IPPJ-AM-8 "Semi-Empirical Cross Sections and Rate Coefficients for Excitation and Ionization by Electron Collision and Photoionization of Helium"
T. Fujimoto (1978)
- IPPJ-AM-9 "Charge Changing Cross Sections for Heavy-Particle Collisions in the Energy Range from 0.1 eV to 10 MeV I. Incidence of He, Li, Be, B and Their Ions"
Kazuhiko Okuno (1978)
- IPPJ-AM-10 "Charge Changing Cross Sections for Heavy-Particle Collisions in the Energy Range from 0.1 eV to 10 MeV II. Incidence of C, N, O and Their Ions"
Kazuhiko Okuno (1978)
- IPPJ-AM-11 "Charge Changing Cross Sections for Heavy-Particle Collisions in the Energy Range from 0.1 eV to 10 MeV III. Incidence of F, Ne, Na and Their Ions"
Kazuhiko Okuno (1978)
- IPPJ-AM-12* "Electron Impact Excitation of Positive Ions Calculated in the Coulomb-Born Approximation –A Data List and Comparative Survey–"
S. Nakazaki and T. Hashino (1979)
- IPPJ-AM-13 "Atomic Processes in Fusion Plasmas – Proceedings of the Nagoya Seminar on Atomic Processes in Fusion Plasmas Sept. 5-7, 1979"
Ed. by Y. Itikawa and T. Kato (1979)
- IPPJ-AM-14 "Energy Dependence of Sputtering Yields of Monatomic Solids"
N. Matsunami, Y. Yamamura, Y. Itikawa, N. Itoh, Y. Kazumata, S. Miyagawa, K. Morita and R. Shimizu (1980)

- IPPJ-AM-15 "Cross Sections for Charge Transfer Collisions Involving Hydrogen Atoms"
Y. Kaneko, T. Arikawa, Y. Itikawa, T. Iwai, T. Kato, M. Matsuzawa,
Y. Nakai, K. Okuno, H. Ryufuku, H. Tawara and T. Watanabe (1980)
- IPPJ-AM-16 "Two-Centre Coulomb Phaseshifts and Radial Functions"
H. Nakamura and H. Takagi (1980)
- IPPJ-AM-17 "Empirical Formulas for Ionization Cross Section of Atomic Ions for
Electron Collisions –Critical Review with Compilation of Experimental
Data–"
Y. Itikawa and T. Kato (1981)
- IPPJ-AM-18 "Data on the Backscattering Coefficients of Light Ions from Solids"
T. Tabata, R. Ito, Y. Itikawa, N. Itoh and K. Morita (1981)
- IPPJ-AM-19 "Recommended Values of Transport Cross Sections for Fast Collision and
Total Collision Cross Section for Electrons in Atomic and Molecular Gases"
M. Hayashi (1981)
- IPPJ-AM-20 "Electron Capture and Loss Cross Sections for Collisions between Heavy
Ions and Hydrogen Molecules"
Y. Kaneko, Y. Itikawa, T. Iwai, T. Kato, Y. Nakai, K. Okuno and H. Tawara
(1981)
- IPPJ-AM-21 "Surface Data for Fusion Devices – Proceedings of the U.S.–Japan Work-
shop on Surface Data Review Dec. 14-18, 1981"
Ed. by N. Itoh and E.W. Thomas (1982)
- IPPJ-AM-22 "Desorption and Related Phenomena Relevant to Fusion Devices"
Ed. by A. Koma (1982)
- IPPJ-AM-23 "Dielectronic Recombination of Hydrogenic Ions"
T. Fujimoto, T. Kato and Y. Nakamura (1982)
- IPPJ-AM-24 "Bibliography on Electron Collisions with Atomic Positive Ions: 1978
Through 1982 (Supplement to IPPJ-AM-7)"
Y. Itikawa (1982)
- IPPJ-AM-25 "Bibliography on Ionization and Charge Transfer Processes in Ion-Ion
Collision"
H. Tawara (1983)
- IPPJ-AM-26 "Angular Dependence of Sputtering Yields of Monatomic Solids"
Y. Yamamura, Y. Itikawa and N. Itoh (1983)
- IPPJ-AM-27 "Recommended Data on Excitation of Carbon and Oxygen Ions by Electron
Collisions"
Y. Itikawa, S. Hara, T. Kato, S. Nakazaki, M.S. Pindzola and D.H. Crandall
(1983)
- IPPJ-AM-28 "Electron Capture and Loss Cross Sections for Collisions Between Heavy
Ions and Hydrogen Molecules (Up-dated version of IPPJ-AM-20)
H. Tawara, T. Kato and Y. Nakai (1983)

- IPPJ-AM-29 "Bibliography on Atomic Processes in Hot Dense Plasmas"
T. Kato, J. Hama, T. Kagawa, S. Karashima, N. Miyanaga, H. Tawara, N. Yamaguchi, K. Yamamoto and K. Yonei (1983)
- IPPJ-AM-30 "Cross Sections for Charge Transfers of Highly Ionized Ions in Hydrogen Atoms (Up-dated version of IPPJ-AM-15)"
H. Tawara, T. Kato and Y. Nakai (1983)
- IPPJ-AM-31 "Atomic Processes in Hot Dense Plasmas"
T. Kagawa, T. Kato, T. Watanabe and S. Karashima (1983)
- IPPJ-AM-32 "Energy Dependence of the Yields of Ion-Induced Sputtering of Monatomic Solids"
N. Matsunami, Y. Yamamura, Y. Itikawa, N. Itoh, Y. Kazumata, S. Miyagawa, K. Morita, R. Shimizu and H. Tawara (1983)
- IPPJ-AM-33 "Proceedings on Symposium on Atomic Collision Data for Diagnostics and Modelling of Fusion Plasmas, Aug. 29 – 30, 1983"
Ed. by H. Tawara (1983)
- IPPJ-AM-34 "Dependence of the Backscattering Coefficients of Light Ions upon Angle of Incidence"
T. Tabata, R. Ito, Y. Itikawa, N. Itoh, K. Morita and H. Tawara (1984)
- IPPJ-AM-35 "Proceedings of Workshop on Synergistic Effects in Surface Phenomena Related to Plasma-Wall Interactions, May 21 – 23, 1984"
Ed. by N. Itoh, K. Kamada and H. Tawara (1984)

Available upon request to Research Information Center, Institute of Plasma Physics, Nagoya University, Nagoya 464, Japan, except for the reports noted with*.